# TOWARDS A TRI-LEAFLET POLYURETHANE HEART VALVE PROSTHESIS

Tom G Mackay

A thesis submitted in partial fulfillment of the requirements for the degree of PhD in the Bioengineering Unit, University of Strathclyde, 1992.

## Abstract

Given the poor durability of bioprosthetic heart valves and thrombogenicity of mechanical valves, recent attention has been directed towards synthetic leaflet valves. The work of this thesis forms part of a project to develop a tri-leaflet polyurethane heart valve prosthesis. Two aspects have been addressed: *in vitro* valve function and durability test methods, and fabrication techniques for polyurethane valves.

Existing *in vitro* valve testing facilities, comprising a hydrodynamic function tester (pulse duplicator) and accelerated fatigue testers, have been upgraded. An improved data acquisition system combined with a computerised control system has been developed for the pulse duplicator. The new system allows valve function to be more efficiently and reliably assessed, and also provides a means for characterising the pulse duplicator and its transducers. Accelerated fatigue testing facilities have been similarly enhanced by the introduction of a computerised data acquisition system.

In order to exploit the design potential offered by the use of a synthetic material, an integrated CAD/CAM system has been developed for producing sculptured valve formers. Such formers have been incorporated into injection moulding tools for tri-leaflet polyurethane valves. Polyurethane valves have been moulded, but to date not with sufficiently thin leaflets: the required leaflet thickness (< 150 $\mu$m) results in a mould cavity which presents an enormous resistance to flow in the injection moulding process. However, a finite element-based mathematical model has been used to simulate the flow of molten polyurethane into the mould cavity and initial results suggest that it should indeed be possible to injection mould a polyurethane valve and a practicable means of achieving this has been identified.

The sculptured formers incorporated into the

injection moulding tools have also been used to create dip moulded tri-leaflet polyurethane valves. These dip moulded valves, though difficult to produce consistently, function reasonably well in the pulse duplicator and accelerated fatigue tests are in progress.

## Acknowledgements

I would like to acknowledge the support and counsel provided by my supervisor Dr AC Fisher, and my former supervisor Dr RA Black. I wish to thank Professor DJ Wheatley for his encouragement and guidance, and Miss MM Tolland for her assistance. I am grateful to Dr GM Bernacca and Dr J Hykin for advice and help with scientific matters, to Mr W Morton and Mr J Morrison for their technical support, and to the Department of Medical Illustrations at the Glasgow Royal Infirmary for their services. My thanks are also due to Dr H Mackie of The National Centre for Prosthetics and Orthotics for his assistance in using the Deckel FP4NC milling machine, and to Mr W Barr of the Department of Production Engineering in providing the Peco 15MR injection moulding machine. I am greatly indebted to the staff of IBM (UK) Ltd at Greenock for their encouragement and the provision of an injection moulding tool. I am similarly indebted to Mr C Hindle and Dr C Geddes of the Department of Applied Chemical & Physical Sciences (Polymer Technology Group), Napier University, for their support and assistance with all aspects of injection moulding.

This project was funded by the British Heart Foundation to whom I am most grateful.

## Work Carried Out by the Author

For the course of this project the author was based at the Department of Cardiac Surgery, Glasgow Royal Infirmary. The techniques outlined in Chapter 4 for measuring the frequency responses of transducers on the pulse duplicator and determining the aortic input impedance of the pulse duplicator were developed by the author. The computer software for the valve testing facilities, as discussed in Chapter 5, was written by the author. The prototype injection moulding tools described in Chapter 8 (figs 8.9 & 8.12) were designed and machined by the author, using numerical code generated by the author's CAD/CAM system and a Deckel FP4NC milling machine at The National Centre for Prosthetics and Orthotics, University of Strathclyde. The mouldings generated using these tools were produced by the author using moulding machines at the Department of Cardiac Surgery, Glasgow Royal Infirmary (figs 8.10 & 8.11) and at the Department of Production Engineering, University of Strathclyde (figs 8.13 & 8.15). The 'IBM moulding tool', as described in Chapter 9 (figs 9.1 & 9.2), resulted from a collaborative effort. The author designed the valve whereas the tool itself (steel platen housing, runner system, ejection mechanism etc) was designed by the design team at IBM (UK) Ltd, Greenock, in close consultation with the author. The machining code for the valve leaflet surfaces on the IBM tool was generated by the author, and the actual machining was carried out by the workshop staff at IBM (UK) Ltd, Greenock, to the author's specification. The mouldings produced from the IBM tool (fig 9.9) were generated at the Department of Applied Chemical & Physical Sciences, Napier University, with the assistance of Mr C Hindle. The dip moulded polyurethane valves described in Chapter 9 (fig 9.9) were fabricated and tested by the author at the Department of Cardiac Surgery, Glasgow Royal Infirmary. The MOLDFLOW

computer simulations of the injection moulding process described in Chapter 10 were carried out at the Department of Applied Chemical & Physical Sciences, Napier University, under the supervision of Mr C Hindle.

# Table of Contents

# Index of Figures

## Index of Tables

# Chapter 1. Introduction

In the UK approximately 5000 artificial heart valves are implanted annually into patients suffering from valvular heart disease. Those patients receiving mechanical prostheses face a lifetime of anticoagulation therapy, while recipients of bioprostheses may reasonably expect to return to hospital after a period of years for a repeat operation.

It is a testament to the highly efficient design of the natural heart valves that, despite over 30 years of research and development, their performance has yet to be even closely matched by the best available prosthetic valves. Though, of course, native valves have the inherent advantage of incorporating fibroblasts for growth and repair, and 30 years is an insignificant period in human evolutionary time scales.

Given the thrombogenicity of mechanical valves and the poor durability of biological valves, new materials and designs are currently being investigated. In particular, tri-leaflet polyurethane valves represent a promising configuration: the tri-leaflet central-flow design is intrinsically good haemodynamically and polyurethane is a tough, flexible and reasonably biocompatible material. Additionally, new applications for prosthetic valves are being found in prosthetic blood pumping devices, such as left ventricular assist devices, artificial hearts, and more recently skeletal muscle ventricles. Devices such as these may favour the use of polyurethane valves.

The Department of Cardiac Surgery at the Glasgow Royal Infirmary has previously taken the development of a bovine pericardial prosthetic valve from the drawing board, through *in vitro* function and durability testing and evaluation in animal models, to clinical use (Fisher & Wheatley, 1987). The work of this thesis builds logically on from this earlier experience, and relates to

the development of a tri-leaflet polyurethane valve.

The aims of this study were twofold: existing *in vitro* valve testing facilities were to be upgraded, and fabrication procedures appropriate to the production of tri-leaflet polyurethane valves were to be investigated.

The existing *in vitro* valve testing facilities comprise a hydrodynamic function tester (pulse duplicator), in which the principal features of flow through the left side of the heart and systemic circulation are approximately re-created, and also accelerated fatigue testers which are used to evaluate valve durability. Improvements were to be made to data acquisition procedures and computerised control systems were to be introduced.

One of the several advantages of using a synthetic valve material rather than a material derived from animals is that there are a range of well-established fabrication techniques available. In particular, injection moulding represents a highly attractive means of producing prosthetic heart valves, in terms of ability to realise complex designs, quality control, as well as economy. The process of injection moulding has recently become increasingly sophisticated. CAD/CAM (computer-aided design/computer-aided manufacture) systems are now commonly employed to construct highly complex moulding tools with great precision; software packages, based on finite element analysis, are available which can be used to simulate the flow of molten plastic into moulding tools, and thus allow tool designs and processing conditions to be optimized; and computerized control systems have been introduced into the moulding machines themselves. These latest technological aids were to be utilised in order to explore the prospects for injection moulding a polyurethane valve.

The pulse duplicator and accelerated fatigue testing facilities were successfully enhanced; the data acquisition and control software which were developed are

now used in routine valve evaluations. A CAD/CAM system was developed in order to construct injection moulding tools for tri-leaflet polyurethane valves. These tools were used to mould valves, but as yet valves have not been injection moulded with sufficiently thin leaflets. However, a mathematical model of the injection moulding process was used to identify a means by which valves could be successfully moulded. The sculptured leaflet formers incorporated in the injection moulding tools were used to produce dip moulded polyurethane valves; these valves function reasonably well in the pulse duplicator and accelerated fatigue tests are in progress.

# Chapter 2. Native and Prosthetic Heart Valves

## 2.1 Native heart valves: Structure, function and failure

Four non-return valves are central to the function of the heart: two atrioventricular valves, the mitral and tricuspid; and two ventriculoarterial valves, the aortic and pulmonary. The atrioventricular valves maintain unidirectional flow from the low-pressure priming chambers (left and right atria) to the high-pressure pumping chambers (left and right ventricles), while the ventriculoarterial valves similarly ensure unidirectional flow from the ventricles to the systemic and pulmonary circulations.

The valves consist of thin, pliable leaflets which are composed mainly of collagen and elastin fibres embedded within a mucopolysaccharide ground substance. The leaflets attach to fibrous annuli encircling the respective orifices. Each of the ventriculoarterial valves is constructed from three semilunar-shaped leaflets. In the case of the atrioventricular valves, the mitral valve has two leaflets while the tri-cuspid has three; additionally, the atrioventricular valve leaflets are tethered by fibrous chordae tendineae to papillary muscles within the ventricles (fig 2.1).

Maintenance of unidirectional flow is achieved chiefly through the passive response of the leaflets to pressure gradients across them, though contraction of the papillary muscles prevents prolapse of the atrioventricular valves under the large pressure generated during ventricular contraction (systole).

Healthy valves present no measurable resistance to forward flow nor do they leak when closed. However, their function can be impaired by disease. A chronic fibrosing reaction in valve leaflets, which gives rise to stenotic or regurgitant valves, can be secondary to rheumatic fever. Although less common nowadays in this country,

Figure 2.1 Left heart anatomy (from Wheatley, 1986)

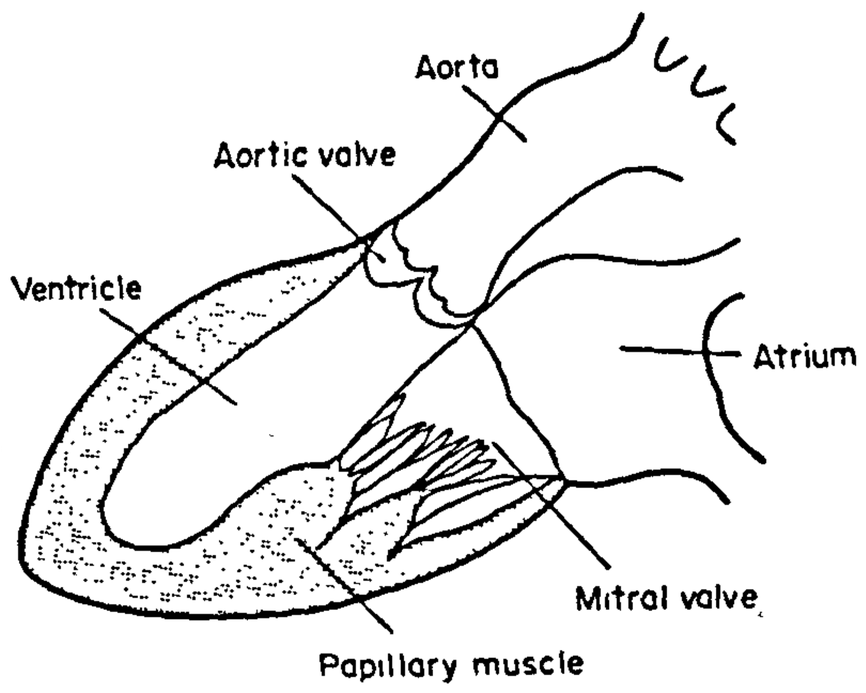

rheumatic heart disease remains prevalent in overseas countries with poorer standards of public health and limited access to antibiotics. Valve stenosis may also be caused by chronic leaflet calcification or congenital abnormalities such as the bicuspid aortic valve. Infective endocarditis can cause rapid valve degeneration, usually in valves which are already abnormal, and results in leaflet tears and perforations.

The pathophysiological effects of valvular stenosis and regurgitation are similar. Pulmonary congestion and oedema are associated with mitral valve disease whereas left ventricular hypertrophy, which may ultimately result in ventricular failure, is associated with aortic valve disease. Aortic regurgitation results in a rapid drop in diastolic arterial pressure and can be readily detected (Wheatley, 1986).

Valve function may be clinically assessed by a variety of techniques including listening to heart sounds, radiography, echocardiography, cardiac catheterization, and nuclear imaging.

## 2.2 Prosthetic Heart Valves

The implantation of prosthetic valves became a practical treatment for valvular heart disease in the 1960's, following the development of the cardiopulmonary bypass apparatus. Valve replacement surgery is now a well established procedure with over 50,000 prostheses implanted annually in the USA and approximately 5000 in the UK (Collins, 1991). Two general categories of prosthetic valve have evolved: mechanical and biological.

### 2.2.1 Mechanical Valves

Three types of mechanical valve are in current use: caged-ball, tilting disc and bileaflet.

Caged-ball valves, such as the Starr-Edwards (fig

2.2), were the first type of mechanical valve to be implanted. The Starr-Edwards valve has been modified over the years, through changing the poppet material from the original lipid-absorbing silicone rubber and covering the struts to reduce thrombogenicity. Such valves, though durable, are inherently obstructive to flow and poor haemodynamically.

Tilting disc valves, such as the Björk-Shiley and Omniscience (fig 2.3), offer less resistance to flow and a lower profile height than caged-ball valves. Various mechanisms for pivoting and retaining the slim disc occluder have been designed. The Björk-Shiley valve has evolved through many changes in occluder material, shape, and opening angle.

Bileaflet valves, such as the St Jude (fig 2.4), generate a more uniform flow field than the tilting disc valves. The St Jude valve has an all-pyrolitic carbon construction and is widely used.

All mechanical valves are associated with problems of thromboembolism and haemolysis, and patients require indefinite anticoagulation therapy. Three factors contribute to these problems: the use of synthetic materials which do not have adequate blood compatibility; the valve designs generate highly disturbed or turbulent flow fields as well as regions of flow stasis (Hasenkam *et al*, 1988c); and the rigid occluding mechanisms may directly damage blood components. Generally, mechanical valves are durable. Occasional failures arise from mechanical defects or biological processes such as a build up of host tissue or thrombus on the valve. The failure of Björk-Shiley convexo-concave valves due to strut fracture, though relatively rare compared with the incidence of thromboembolic complications, continues to generate media interest and public anxiety. Approximately 86,000 convexo-concave valves were implanted worldwide between 1979 and 1986; as of November 1991, a total of

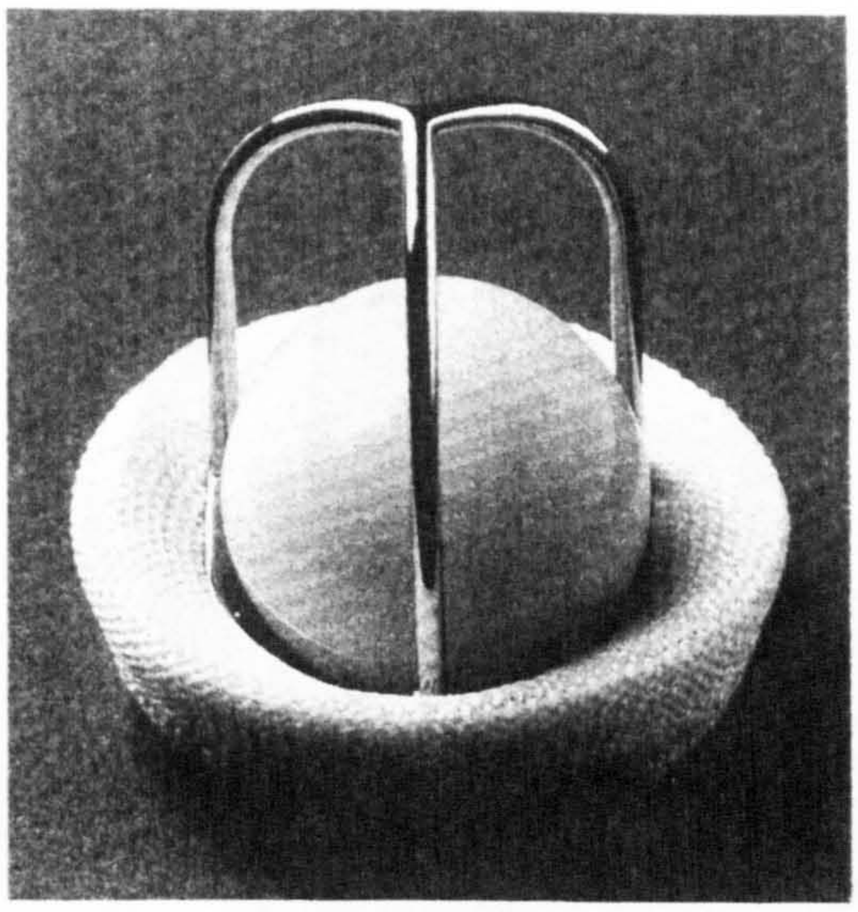

Figure 2.2 Caged-ball valve

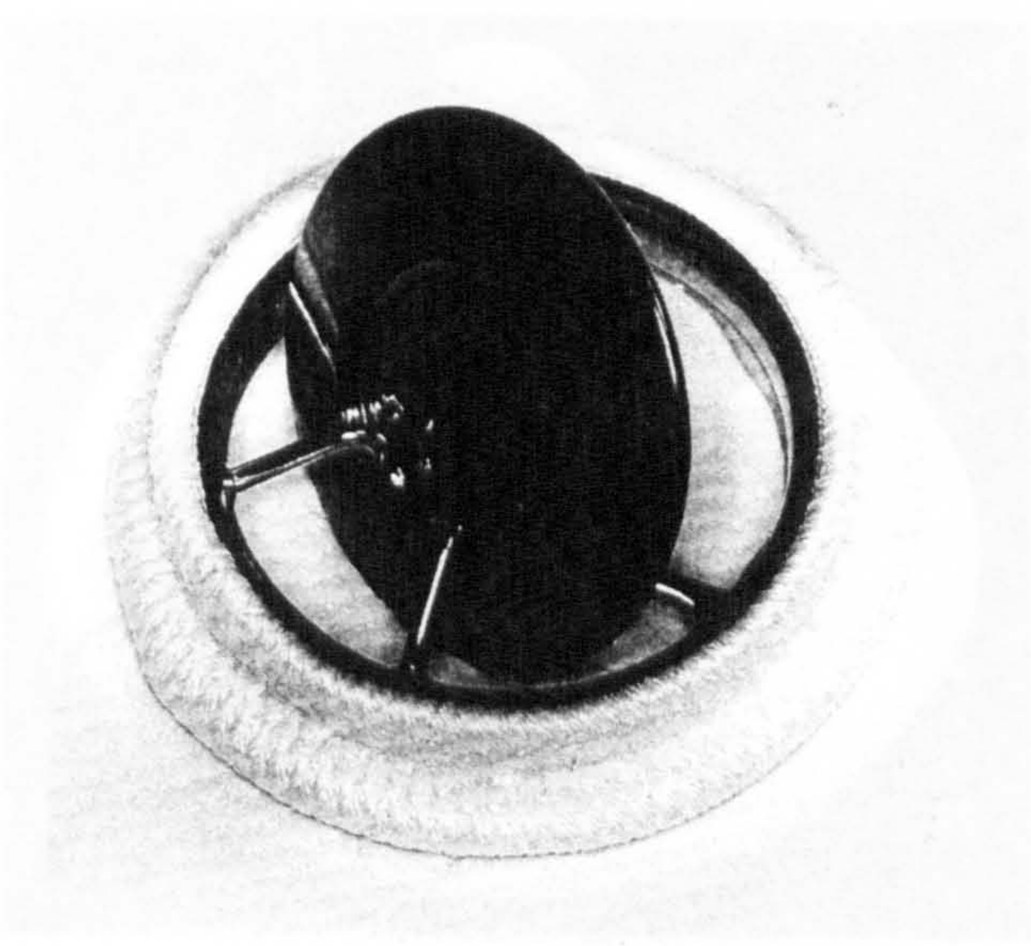

Figure 2.3 Tilting disc valve

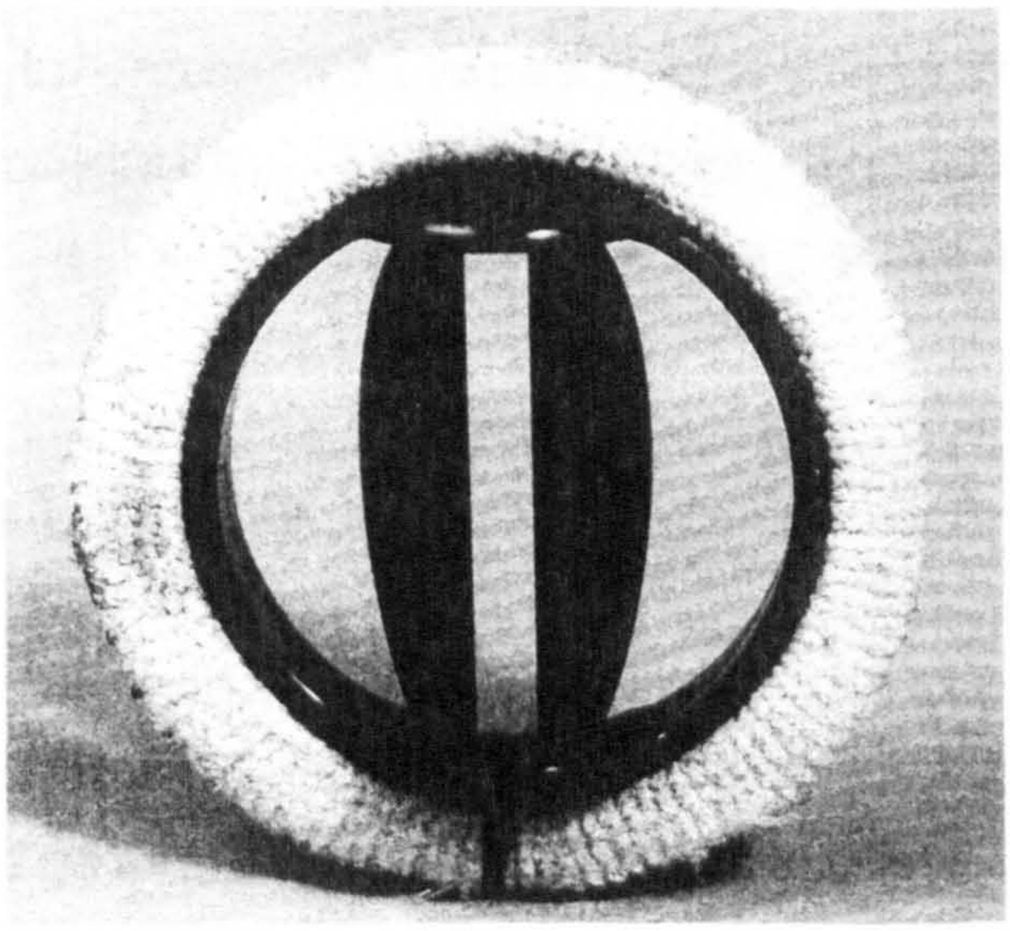

Figure 2.4 Bi-leaflet mechanical valve

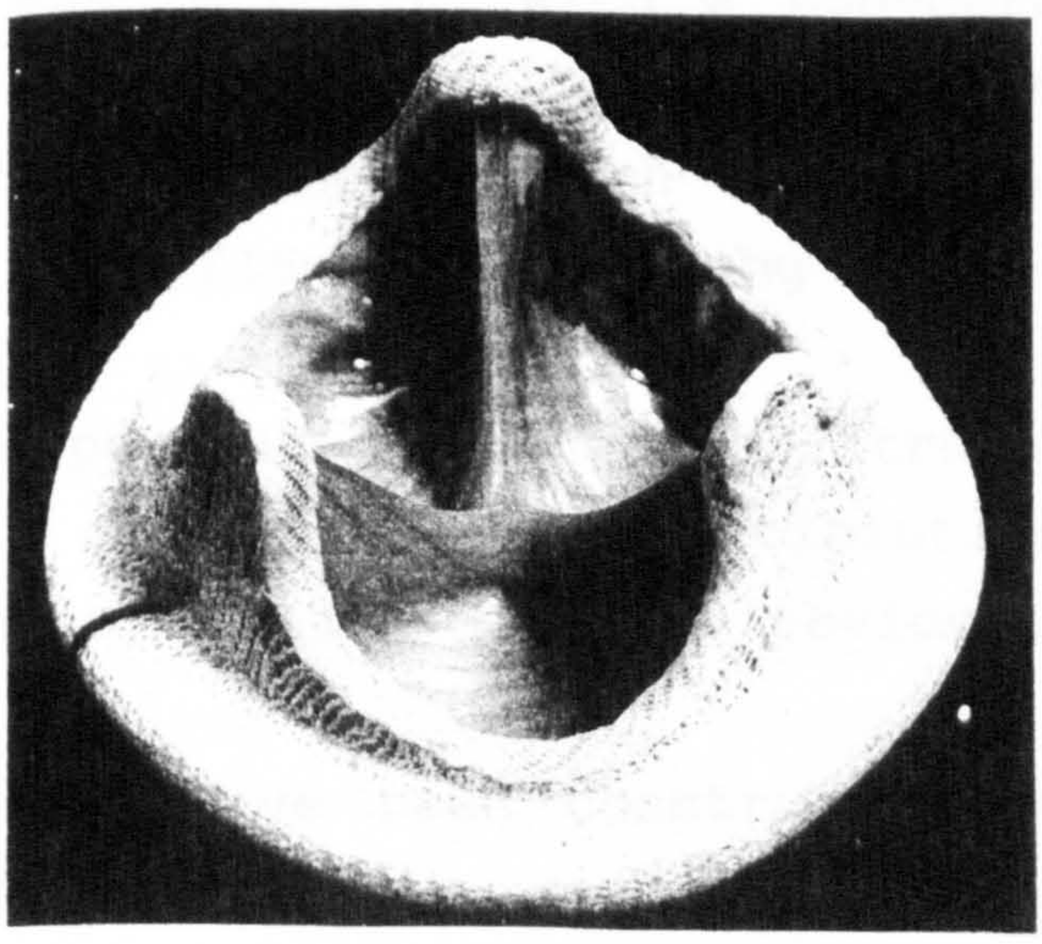

Figure 2.5 Porcine bioprosthetic valve

466 fractures had been reported, of which 320 resulted in fatalities (Collins, 1991). In order to avoid welds which may give rise to such failures, the latest Björk-Shiley model, the Monostrut, incorporates an occluder-housing machined from a single continuous piece of titanium alloy.

### 2.2.2 Biological Valves

The most commonly used bioprosthesis derives from the porcine aortic valve (fig 2.5). Porcine valves are mounted onto frames to assist insertion and fixed in glutaraldehyde to reduce antigenicity. Unfortunately, the frames reduce the available orifice area and fixation stiffens the leaflets. Consequently, porcine bioprostheses, and particularly the smaller sizes, are mildly stenotic. However, over the years, improvements in their haemodynamic function have been effected: by replacing the right coronary leaflet, which incorporates an inflexible muscle shelf, with a non-coronary leaflet from another valve (Wright, 1979); and introducing low pressure fixation methods which result in a greater degree of leaflet flexibility being retained (Broom & Thompson, 1979).

As well as porcine aortic valves, transplanted human aortic valves, sterilized with antibiotics, have been employed. However, their usage is obviously limited by supply.

Bioprostheses have been constructed using leaflets cut from collagenous sheets, such as bovine pericardium, with the leaflets mounted onto three-pronged stents. Early bovine pericardial valves displayed relatively poor durability owing to the leaflets abrading against the frames and tearing. The Glasgow pericardial valve provided a non-abrasive contact between the leaflets and frame by incorporating a frame covered in smooth pericardium; consequently, a superior *in vitro* durability

was demonstrated (fig 2.6, Fisher & Wheatley, 1987).

Biological valves have a lower attendant risk of thromboembolism than mechanical valves, and recipients do not generally require long-term anticoagulation. They are, however, prone to chronic calcification and tissue failure (fig 2.7). Sites of calcium deposits tend to coincide with regions of stress concentration in the leaflets; the underlying mechanisms, while under investigation, have yet to be elucidated (Bernacca *et al*, 1992b).

### 2.2.3 Current Status

While neither mechanical nor biological prostheses are ideal, they do represent a vastly preferred alternative to untreated valvular disease. In terms of survival with the original valve prosthesis intact, the clinical outcomes for patients implanted with biological prostheses are similar to those for patients with mechanical valves plus anticoagulation up to the first 5 years. Thereafter, advantage shifts to the more durable mechanical valves, albeit with a higher associated risk of bleeding complications (Bloomfield *et al*, 1991). Bioprostheses are generally favoured for elderly patients and those for whom anticoagulation is especially problematic.

The evolution of prosthetic heart valves looks set to continue. In particular, less thrombogenic materials are required for mechanical valves, along with improved designs to create less flow disturbance and stasis. For bioprostheses, greater durability may arise from fixation procedures or other chemical treatments which enhance mechanical properties and inhibit calcification, combined with designs that reduce leaflet stress concentrations.

Given the limitations of existing mechanical and biological valves, alternative solutions are being

Figure 2.6 Bovine pericardial bioprosthetic valve

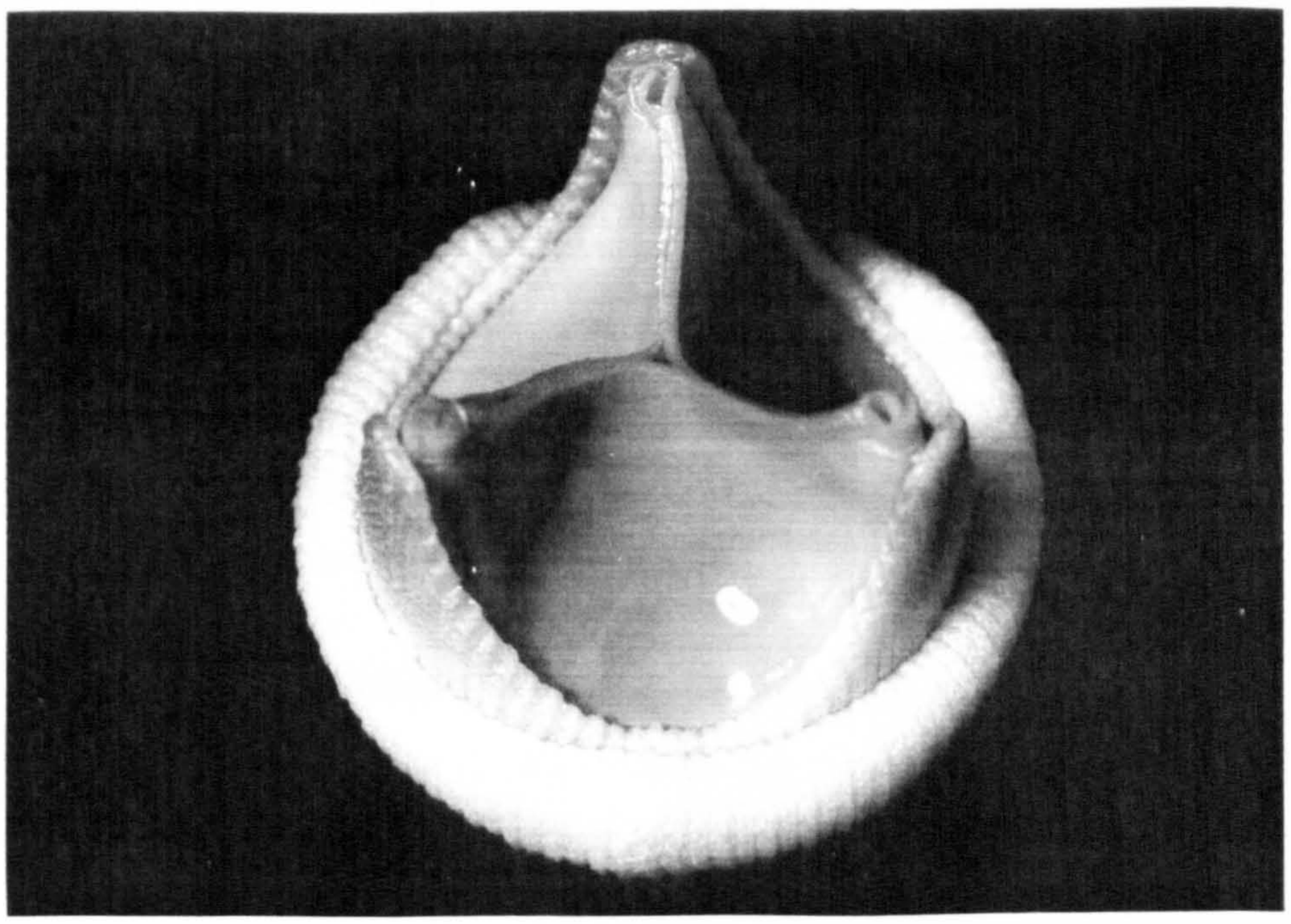

Figure 2.7 Heavily calcified (explanted) bioprosthesis

pursued. All mechanical valve designs incorporate occluding mechanisms which partially obstruct forward flow and ultimately limit the potential for reducing flow disturbance. From a fluid mechanical point of view, the central-flow design of bioprosthetic valves is inherently better. However, there is only a limited range of material properties and design options available for valves constructed from biological materials. Therefore, the possibilities of a central-flow type valve constructed from synthetic materials would appear worthy of investigation. Tri-leaflet synthetic valves have demonstrated promising *in vitro* performances, but to date they have performed rather poorly in animal trials owing to problems relating to calcification and thrombus formation (Jansen *et al*, 1991).

# Chapter 3. Fluid Mechanical Considerations

## 3.1 Introduction

The study of heart valve fluid mechanics has a long history, being an interest of Leonardo da Vinci in the early sixteenth century. While research in this field considerably predates the introduction of valve replacement surgery, the need to design prosthetic valves has provided the impetus for more recent study.

Owing to anatomical and physiological differences, the flow fields surrounding the atrioventricular and ventriculoarterial valves are rather dissimilar; in the proceeding sections 3.2 and 3.3 the flows associated with the mitral and aortic valves are considered in turn. Flow downstream from the aortic valve and the possibility of ensuing turbulence are discussed in sections 3.4 and 3.5. The flow disturbance created by prosthetic valves is the subject of section 3.6. Sections 3.7 and 3.8 close this chapter with a consideration of 2 commonly used methods of assessing valve hydraulic performance: associated pressure-flow relations and energy losses.

## 3.2 Mitral Valve

Consider the normal motion of the mitral valve in the cardiac cycle (Yellin, 1983). After the aortic valve closes, the left ventricle relaxes isovolumetrically until the pressure within it falls below that in the atrium (fig 3.1). Under the action of this pressure gradient, the mitral valve opens and the ventricle starts to fill rapidly as it continues to relax. Following relaxation the ventricle behaves as a passively compliant chamber, mitral flow decreases exponentially as the atrial and ventricular pressures equilibrate, and the valve leaflets move towards closure. The pressure gradient and accelerating flow are then re-established by

Figure 3.1 Pressures and flows in the left heart
(from Yellin, 1983)

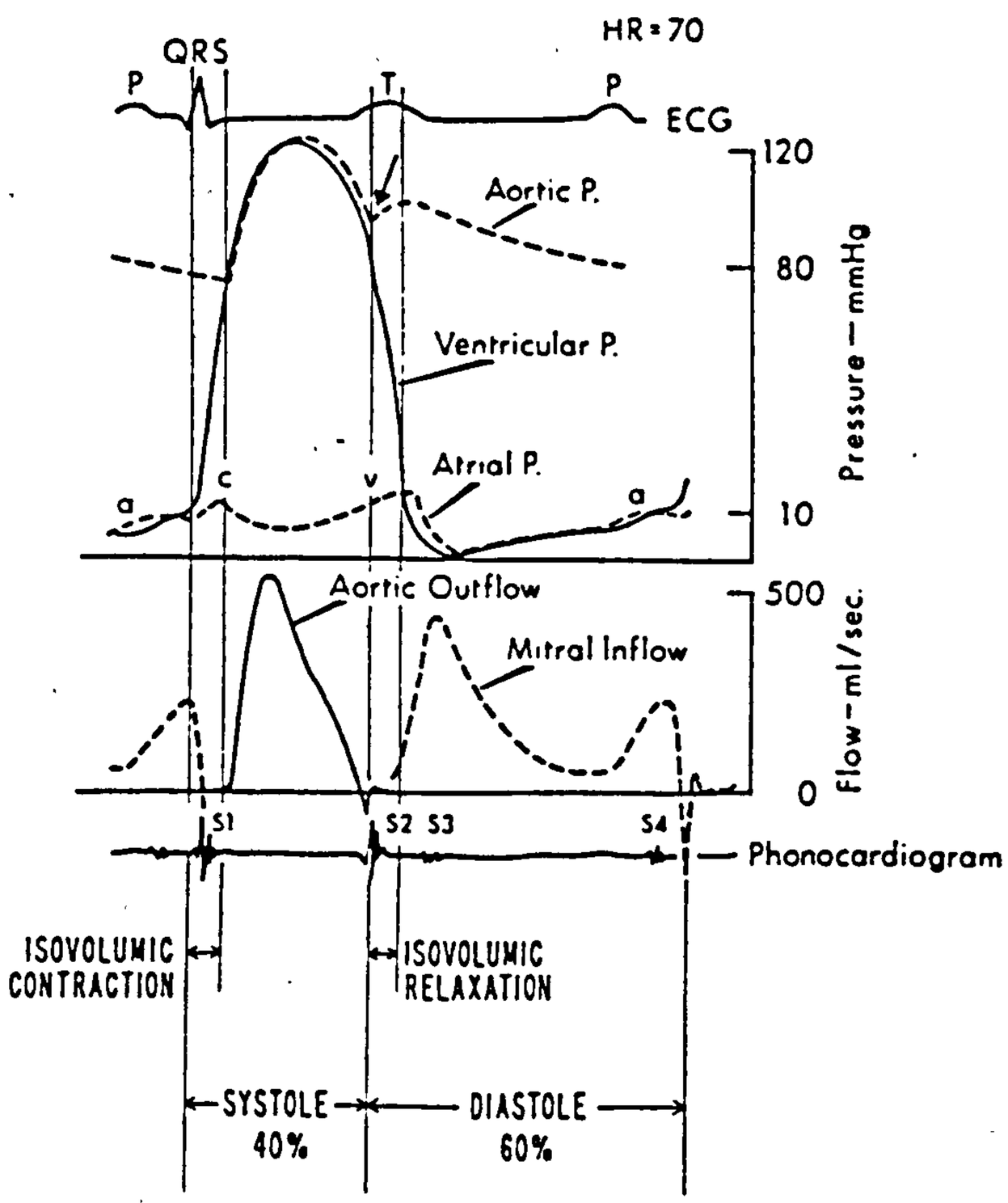

left atrial contraction and the valve is again fully opened. With the atrium relaxing and the mitral valve still open, the left ventricle begins its contraction. The pressure gradient rapidly reverses and the mitral valve closes with little or no reverse flow. The large ventricular pressure pushes the mitral valve leaflets towards the atrium until the chordae tendineae prevent further displacement. Note that this elastic displacement of the sealed valve would result in a velocity probe recording a pulse of reverse flow.

The mechanism of valve closure, in particular, the process by which the leaflets close whilst maintaining forward flow, has been the subject of much contemplation. An early study by Henderson & Johnson (1912) resulted in the 'breaking of the jet' idea: the decelerating jet of mitral flow produces a region of low pressure in its wake, surrounding fluid is drawn into the wake and pushes the leaflets together. A mechanism based on the thrust produced by a large ring vortex was put forward by Bellhouse & Bellhouse (1969b) and Bellhouse (1972a). They proposed that the incoming mitral flow jet struck the apex of the ventricle and spread upwards and outwards behind the valve leaflets generating a vortex which tended to close the valve; they supported their theory with qualitative, *in vitro* flow visualisation studies. Further, Bellhouse (1972b) later suggested that the adverse axial pressure gradient associated with decelerating flow also contributed to valve closure (and was equivalent to the "breaking of the jet" idea of Henderson & Johnson). More recently, Reul *et al* (1981), similarly using flow visualisation but with a more realistic model than that of Bellhouse, disputed the vortex theory and argued that the negative pressure gradient alone brought about valve closure with no reverse flow. Reul *et al* observed large vortices forming in their model ventricle during early diastole and believed that these may have contributed to the mid-

diastolic partial valve closure which occurs prior to atrial contraction, but these vortices had decayed away before end-diastolic valve closure. Again based on *in vitro* flow visualisation, Lee & Talbot (1979), in agreement with Reul *et al*, found that mitral valve closure depends chiefly upon the fluid motion passing between the valve cusps rather than the ventricular geometry; they also pointed out that there is vorticity associated with the decelerating mitral flow jet which may contribute to valve closure, but these are not the vortices associated with the large scale motion of fluid towards the apex and up the ventricular walls (as proposed by Bellhouse).

The preceding studies were based on flow patterns observed in model left ventricles; *in vivo* flow details are much more difficult to obtain. Taylor & Wade (1973), using angiography and direct flow visualisation (using an endoscope and temporarily replacing the blood with a transparent medium), observed stable vortices within canine and ovine left ventricles. More recently, with the same techniques, secondary vortices have been observed in association with the chordae (Malcolm & Taylor, 1989). Velocities with considerable high frequency content have been recorded with hot-film velocity probes inside equine ventricles (Nerem *et al*, 1974). Also, Hwang *et al* (1977) reported turbulent flow downstream from a healthy human mitral valve *in vitro*; however, the ventricular geometry and compliance were not simulated. Flow disturbances measured with hot-film velocity probes may, in part, be due to the probes themselves: Nerem *et al* used a catheter-tip velocity probe (diameter 3 mm) taped to a pressure transducer, and Hwang *et al* used 2 orthogonally orientated hot-film probes (each 2.2 mm long). More recently, using Doppler ultrasound techniques, Jones *et al* (1986) observed large scale, non-turbulent motion of blood towards the ventricular apex and up the walls towards the outflow tract in sheep.

Analytically, the fluid mechanical situation in the left ventricle is highly complex, i.e. unsteady flow of a non-newtonian fluid within a contractile chamber of changing complex geometry. Bellhouse (1972a) proposed a mathematical model based on the assumption of 1-dimensional inviscid flow through the mitral valve and vortex flow in the ventricle. Lee & Talbot (1979) extended Bellhouse's model by introducing viscous effects and assuming a constant kinetic energy density within the ventricle (rather than a vortex); their model was successful in predicting mitral valve motion from measured trans-valvular flow, for a rigid leaflet valve. A numerical solution to the 2-dimensional Navier-Stokes equations for viscous flow, appropriate to the mitral valve and left atrium and ventricle, has been presented by Peskin (1982). The fluid boundary is based on the cardiac anatomy and has approximately physiological contractile properties (McQueen *et al*, 1982); the model is limited to rather low Reynolds numbers however. The results suggest that vortices are indeed involved in the valve closure mechanism; vortices are shed from the tips of the valve leaflets and grow during flow deceleration. The model also implies that efficient valve closure (and vortex formation) is dependent on there being some tension in the chordae tendineae during diastole (to prevent the leaflets from opening too far); this is contrary to the *in vitro* observations of Bellhouse (1972a) and Lee & Talbot (1982). A similar numerical simulation has recently been undertaken by Schoephoerster & Chandran (1990).

## 3.3 Aortic Valve

Consider the normal motion of the aortic valve in the cardiac cycle (Laniado *et al*, 1976; Thubrikar *et al*, 1977; van Steenhoven *et al*, 1981). Following ventricular isovolumetric contraction, the valve opens rapidly to

create an approximately circular aperture. With aortic flow still accelerating, the valve leaflets start to move inwards; the gradual reduction in orifice area continues throughout mid-systole resulting in a more triangular-shaped orifice. The valve closes with little, or no, reverse flow while aortic flow decelerates under an adverse pressure gradient. The diameter of the aortic-sinus region increases substantially from diastole to systole (Brewer *et al*, 1976 & 1977), and the outward movement of valve commissures under increasing ventricular pressure may assist in valve opening (Thubrikar *et al*, 1979). Note that, as with the mitral valve, a pseudo-regurgitation would be recorded with velocity/flow probe at the end of systole due to displacement of the sealed aortic valve towards the ventricle.

Discussions over the mechanism of aortic valve closure are similar to those in the case of the mitral valve. Bellhouse & Bellhouse (1968) and Bellhouse (1972b) proposed that vortices in the sinuses of Valsalva (3 pouches in the aortic wall behind the valve leaflets), as well as the adverse pressure gradient associated with decelerating flow, contributed to efficient valve closure. Vortex formation, they suggested, arose from the valve leaflets projecting slightly into the sinuses and thus directing part of the systolic flow into the sinuses; the vortices persist after peak systole and produce a thrust which pushes the leaflets together. Additionally, they argued that these sinus vortices were responsible for holding the valve leaflets in a steady position throughout mid-systole. However, as Talukder *et al* (1977) pointed out, after a rapid opening the aortic valve leaflets move away from the sinuses and present a near triangular orifice (Robel, 1972); sinus vortices, they proposed, would be generated during the decelerating systolic flow phase but these would be secondary to the reversed pressure gradient. Furthermore, Talukder and

colleagues used a model aortic root with removable sinuses to show that efficient closure of a synthetic tri-leaflet valve was not dependent on the presence of sinuses, a view shared by Schramm *et al* (1982) but contrary to the observations of Bellhouse & Bellhouse (1968) and van Steenhoven & van Dongen (1979), made in similar studies. The disagreement may be due to the differences in model geometry and compliance and aortic flow reproduction.

Mathematical descriptions of simplified aortic valve flow have been offered. Bellhouse & Talbot (1969) and Bellhouse (1969) used a model with 1-dimensional flow through the valve and vortex flow in the sinuses to predict the aortic wall pressure distribution from the measured peak aortic flow velocity; simplifying the model greatly by ignoring the effects of the moving leaflet and retaining a stagnation point at the sinus ridge was found to give similar results (Bellhouse, 1972b). Van Steenhoven & van Dongen (1979) assumed a constant sinus pressure and rigid valve leaflets for their 1-dimensional model; from measured flow velocities, the leaflet positions during closure were determined numerically. Using a 2-dimensional experimental model, they observed a marked difference in sinus vortex behaviour and valve closure at higher deceleration rates. Hung (1983) presented a numerical solution for inviscid axisymmetric flow during early systole; given Bellhouse & Talbot's data for valve opening area as a function of time, the corresponding pressure and velocity fields were calculated. Hung's model was particularly sensitive to the shape and velocity of the opening leaflets. Swanson & Clark (1973) developed an approximate method for calculating the displacements of a 2-dimensional valve leaflet during opening. By assuming that the leaflets offered no resistance to flow and similarly that the fluid in the sinuses offered no resistance to the leaflet motion, they calculated leaflet displacements simply by

integrating, with respect to time, an assumed accelerating velocity profile for flow at the base of the aorta.

## 3.4 Aorta

The thoracic aorta presents a complex flow boundary to blood ejected from the left ventricle, i.e. a compliant, twisting, tapering U-tube with side branches. The flow pattern has been studied in a replica human aortic arch with hot-film anemometry and flow visualisation (Yearwood & Chandran, 1984), in dogs using hot-film anemometry (Seed & Wood, 1971; Clark & Schultz, 1973; Paulsen & Hasenkam, 1983) and Doppler ultrasound (Farthing & Peronneau, 1979), and more recently hot-film anemometry has been used in the human ascending aorta (Paulsen *et al*, 1988). Systolic velocity profiles in the ascending aorta were observed to be relatively flat and slightly skewed; the direction and magnitude of the skew varied spatially and temporally. The skew in the proximal ascending aorta towards the left-anterior wall is thought to be due to the relative aorta-ventricle alignment and/or the pattern of contraction. Progressing up to the aortic arch, the axial velocity profile skews towards the inner wall of the bend under the influence of a centripetal pressure gradient. The boundary layer on the inner wall of the aortic arch separates such that in the descending aorta the core of irrotational flow is confined to the region nearest the outer wall and the region nearest the inner wall is occupied with a region of complex rotational fluid motion. As the aortic valve closes, the slower moving fluid near the inner wall reverses direction under the adverse pressure gradient whereas fluid near the outer wall maintains a slow forward motion; throughout diastole the rotational flow diffuses and dissipates.

The authors cited in the previous paragraph,

studying canine aortic flow using hot-film anemometry, also observed varying degrees of flow disturbance or turbulence. Seed & Wood (1971) remarked upon low frequency disturbances in their velocity measurements made at the proximal ascending aorta but not at the distal, and in one experiment turbulence was seen extending to the descending aorta; Clark & Schultz, 1973, and Paulsen & Hasenkam, 1983, reported similar findings. However, the degree of turbulence or disturbance was not quantified (or defined). A study to quantify flow disturbances in the human aorta was undertaken by Stein & Sabbah (1976) using a catheter-tip hot-film velocity probe. For 6 patients with healthy aortic valves and normal cardiac output, 'disturbed' velocity profiles were recorded immediately above the aortic valve but the disturbance did not extend as far as the mid-ascending aorta. One patient with a normal aortic valve and high cardiac output exhibited turbulent ascending aortic flow. For patients with aortic insufficiency and stenosis, turbulent velocity profiles were recorded throughout the ascending aorta and into the innominate artery; the turbulent energy density in these cases, calculated as the mean square of the fluctuating velocity component, was an order of magnitude greater than for those patients with normal valves. The magnitude of turbulence appeared to be related to peak velocity, supported in a later study showing a lesser degree of disturbance for the pulmonary valve (Stein *et al*, 1979). Turbulence calculations were based on velocity fluctuations in the axial direction only. The difference between 'disturbed' and turbulent flow is not clearly defined; the distinction as used by Stein & Sabbah is consistent with a definition based on turbulent energy density. In the context of arterial blood flow, Yellin (1966) chose to describe transient velocity fluctuations which decay as they propagate downstream as disturbed flow and reserved turbulence for self-preserving, random distortions. Note

that the effect the hot-film velocity probe has on the transition from laminar to turbulent or disturbed flow is unclear. At low Reynolds numbers the presence of a small probe may have an insignificant effect but near to critical Reynolds numbers this might not be the case. Stein & Sabbah used a catheter of diameter 1 mm. A subsequent *in vitro* study, using non-invasive laser Doppler anemometry downstream from highly stenotic human aortic valves (orifice area 0.2 and 0.3 $cm^2$), found levels of turbulence similar to those reported *in vivo* (Stein *et al*, 1982).

## 3.5 Turbulent Flow

It is probable that aortic blood flow in healthy individuals is not generally turbulent, but may be subject to transient disturbances during flow deceleration. This seems reasonable taking the view that the cardiovascular system has evolved into an optimally-efficient means of transporting blood, since turbulent flow has higher associated energy losses than laminar flow. Furthermore, turbulence has been implicated in a number of disorders of the vascular system, as recently reviewed by Stein & Sabbah (1990). Turbulent stresses can initiate thrombus formation by damaging or destroying blood corpuscles or through endothelial deterioration. For an exposure time of 1-10 milliseconds, i.e. a typical time for a blood cell to pass through a valve, the threshold shear stress level for lysis of both red blood cells and platelets is approximately 200-400 $Nm^{-2}$; the threshold shear stress level has been found to decrease logarithmically with increasing exposure time (Tillman *et al*, 1984). Subsequent deposition of stress-activated platelets and thrombi on valve surfaces may lead to increased valvular stenosis (and so to increased turbulence). Turbulence may also play a role in the creation of poststenotic dilation, the progression of

atherosclerosis, and in the production of ejection murmurs. Note that, as well as turbulent flow, flow stagnation is also believed to promote thrombus formation (Yoganathan *et al*, 1978).

It is well established that an obstruction in the aortic root, be it a pathological aortic valve or a prosthesis, increases the likelihood of turbulent flow downstream. However, the criteria for the transition to turbulence in the complex cardiovascular environment are not well established. Young (1979) reviewed results from a number of experiments investigating the development of turbulence in steady flow through various types of constriction; the trend revealed was an inverse relation between critical Reynolds number and degree of stenosis. The basis for the transition in steady flow through uniform pipes, the Reynolds number, applied to unsteady flow (calculated from the mean, instantaneous, or peak velocity) is not sufficient as it contains no information pertaining to the unsteadiness of the flow or the obstruction geometry. Yellin (1966) attempted to characterise the transition for pulsatile pipe flow by introducing a *relaxation time*; the dimensionless relaxation time is defined for a sinusoidal flow imposed on a steady flow, as illustrated in figure 3.2. Yellin argues that viscous dissipation of transient disturbances occurs while the Reynolds number is below its critical value, and therefore turbulence is less likely to develop the longer the time spent at sub-critical Reynolds numbers and the greater the depth of penetration into the region of sub-critical Reynolds number. Supporting experimental evidence demonstrated the relative stability of low frequency, large amplitude flows; however, the ratio of oscillating flow component to mean flow component was considerably smaller than is the case in aortic flow. Nerem & Seed (1972) arrived at a different conclusion from Yellin; they suggested that the

Figure 3.2 Definition of relaxation time
(after Yellin, 1966)

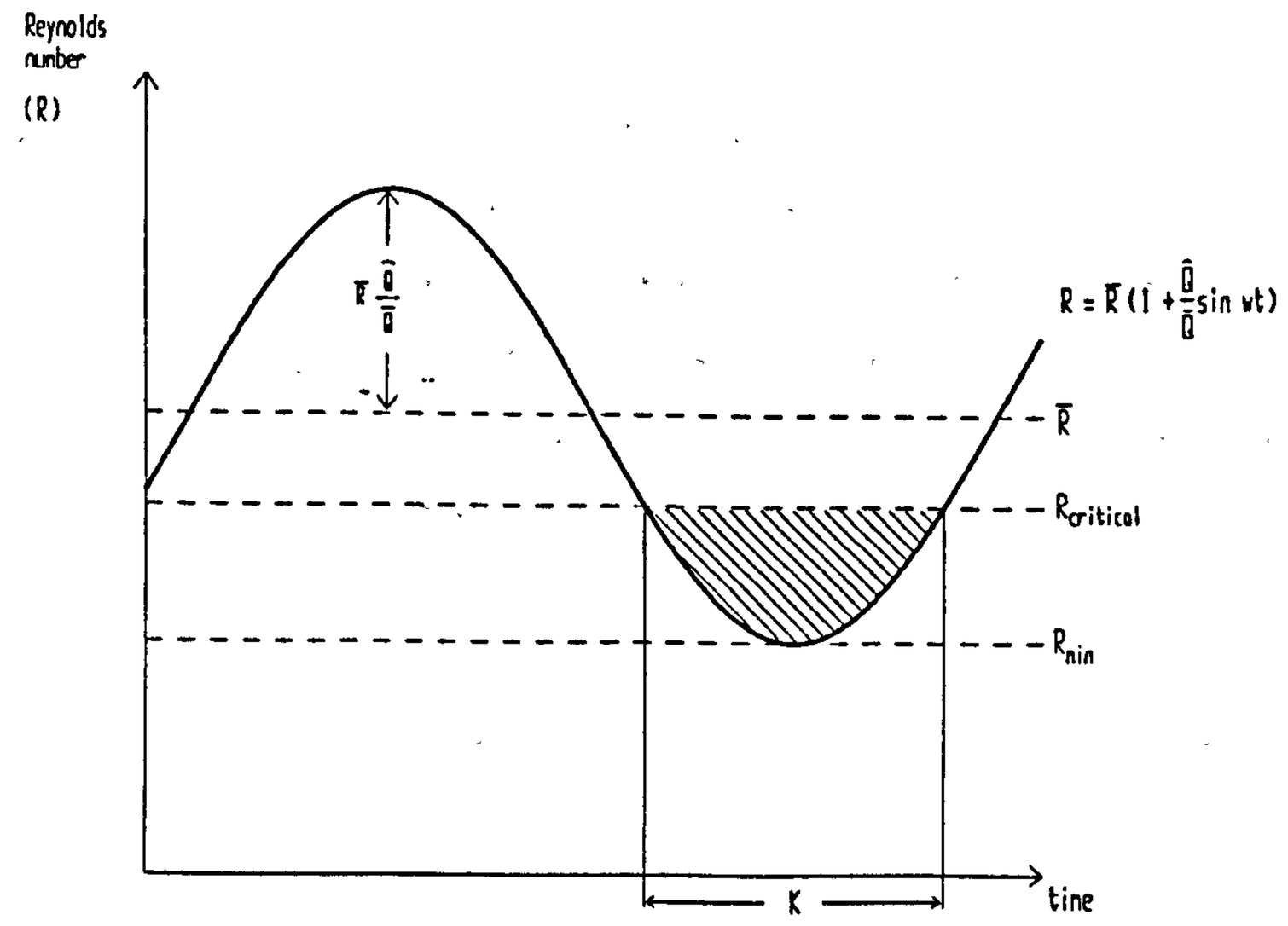


For sinusoidal flow through pipe, radius r, with viscosity $\nu$, then:

$$\text{Relaxtion time} = \frac{K\nu}{2r^2}(R_{critical} - R_{min})$$

approximately given by shaded area

likelihood of turbulent flow was increased at lower frequencies but their experimental evidence, from hot-film velocity measurements in dogs, was not convincing.

The propagation of turbulence in a uniform tube, downstream from a valve-like nozzle, in single-pulse flow was studied by Clark (1980). At the onset of flow, he observed a laminar shear layer, extending from the nozzle, rapidly roll up to create a forward propagating ring vortex. Disturbances in the shear layer were observed prior to the vortex reaching the tube wall; as flow re-attached to the wall, turbulence extended across the entire cross-section and progressively dissipated as it passed downstream. By the end of the flow pulse, turbulent mixing had resulted in fluid 'particles' from the jet region (i.e. fluid which had passed through the nozzle within the duration of the pulse) invading the re-circulating region between the jet and the tube wall. Using a combination of flow visualization and hot-film anemometry, Clark demonstrated that the occurrence of turbulence in a single flow pulse is associated with fluid 'particles' that have passed through the nozzle within the duration of that pulse; smaller nozzle orifices were associated with greater downstream turbulence penetration.

Turbulent flow, as observed downstream from stenoses both *in vitro* and *in vivo*, usually begins close to the instant of peak flow, becomes more intense during flow deceleration and damps out before the next cycle begins (Young, 1979). Notice that the abrupt increase in cross-sectional area immediately downstream of a stenotic valve need not be the only origin of flow disturbance in the ascending aorta: valve leaflets projecting into the flow, fluttering leaflets, or surface roughness may also contribute (Sabbah & Stein, 1979). Further, there is the possibility of ventricular disturbances created during the diastolic filling period being carried into the aortic root in systole. The constrictive nature of

prosthetic heart valves, and the occluding mechanisms of mechanical valves in particular, are obvious sources of aortic flow disturbance, as will be discussed in the next section.

## 3.6 Prosthetic Valves

The design, material properties, and mechanics of prosthetic valves, especially mechanical valves, are rather different from those of the native heart valves, and therefore it is not surprising to find considerable differences in their associated fluid mechanics. In general, prostheses generate less uniform flow fields with higher degrees of turbulent stresses.

The fluid mechanics of prosthetic valves have been studied extensively *in vitro* and to a lesser extent in animal models and humans. Detailed non-invasive study in humans awaits the development and application of appropriate measuring techniques (eg magnetic resonance imaging may be suitable). The complex *in vivo* conditions are difficult to accurately reproduce and all *in vitro* investigations involve some degree of compromise, generally in terms of model geometry and impedance, flow generation, and fluid rheology. Furthermore, there is considerable variation in apparatus and testing protocols between different investigators which makes comparison of results difficult. In this context, note a recent detailed study of velocity fields and turbulent stresses associated with a range of prosthetic valves, undertaken both *in vitro* and *in vivo*, including humans, utilising the same measurement procedure (Hasenkam *et al*, 1987 & 1988a,b,c,d; Paulsen *et al*, 1988a,b).

Before considering the flow characteristics of specific valve types, it is worth considering the experimental techniques used to investigate them and the methods used to quantify turbulent flow.

### 3.6.1 Experimental techniques

Several experimental techniques have been used in the study of prosthetic valve flow. Flow visualisation techniques are effective in highlighting areas of turbulence, vorticity, and stagnation, and they have the benefit of simultaneously illuminating the flow field over a wide area. *In vitro* flow visualisation has been utilised downstream of aortic prostheses (Wieting *et al*, 1969; Olin, 1971; Wright & Temple, 1977; Schramm *et al*, 1982; Tindale *et al*, 1982; Chandran *et al*, 1983) and mitral prostheses (Wright & Temple, 1977; Dellsperger & Wieting, 1978; Chandran *et al*, 1989b). Note that flow visualisation is commonly used as a qualitative method, but if the tracer particles can be generated at a controlled rate, as in hydrogen bubble visualisation, velocity information can be extracted (Lichtenstein *et al*, 1986); alternatively, flow velocities can be estimated from particle streak lengths measured from photographs (Wieting *et al*, 1969).

Hot-film anemometry is an attractive quantitative method of measuring flow velocities in that it can be used both *in vitro* and *in vivo*. However, it is an invasive technique and determining flow directionality is a problem. It has been applied to the *in vitro* study of aortic mechanical valves in steady flow (Figliola & Mueller, 1981; Hasenkam *et al*, 1987 & 1988a) and pulsatile flow (Hasenkam *et al*, 1988b,c) as well as aortic bioprosthetic and mechanical valves in pigs (Hasenkam *et al*, 1988d) and aortic mechanical valves in humans (Paulsen *et al*, 1988a). Flush-mounted hot-film velocity probes have been used for wall shear stress measurements in the vicinity of aortic mechanical prostheses (Tillman *et al*, 1984).

A widely used *in vitro* technique for measuring flow velocities downstream from prosthetic valves is laser Doppler anemometry (LDA). The popularity of LDA stems

from its associated high frequency response, spatial resolution, potential for simultaneous measurement of 2 orthogonal velocity components at a point, and freedom from calibration. However, LDA is not suitable for use *in vivo*. Flows associated with mechanical valves (Figliola & Meuller, 1981; Bruss *et al*, 1983; Chandran *et al*, 1985a,b), biological valves ( Chandran *et al*, 1984; Reul *et al*, 1985; Walburn *et al*, 1985;), or both (Phillips *et al*, 1980; Yoganathan *et al*, 1986; Hanle *et al*, 1989) have been studied in the aortic position using LDA; flows through prosthetic valves in the mitral position have received rather less attention (Woo & Yoganathan, 1986; Schoephoerster & Chandran, 1991). Note that LDA has also been used with synthetic tri-leaflet valves both in the aortic (Woo *et al*, 1983; Herold *et al*, 1987; Chandran *et al*, 1989a; Einav *et al*, 1990) and in the mitral (Schoephoester & Chandran, 1991) position. The similar technique of Doppler ultrasound anemometry has been used for 2-dimensional velocity measurements downstream from mechanical prostheses in an model elastic aorta (Farahifar *et al*, 1985).

### 3.6.2 Quantification of turbulent stress

Consider a turbulent flow of instantaneous velocity $U_i$, which is given by the sum of a mean component $U_i$ and a random turbulent component $u_i$:

$$U_i = \overline{U_i} + u_i \qquad (3.1)$$

For an incompressible, newtonian fluid of dynamic viscosity $\mu$ and density $\rho$, the stress on a fluid element is given by (Hinze, 1959):

$$T_{ij} = -\overline{p}\delta_{ij} + \mu(\partial\overline{U_i}/\partial x_j + \partial\overline{U_j}/\partial x_i) - \rho u_i u_j \qquad (3.2)$$

where p is the pressure, $\delta$ is the Kronecker delta,

the overscore represents a mean value, and subscripts represent orthogonal directions. The turbulence terms, $\rho\overline{u_i u_j}$, are known as Reynolds normal (i=j) and shear (i≠j) stresses (RNS and RSS).

In the context of damage to blood elements, presumably shearing stresses are the more relevant. Further, laminar shear stresses, $\mu(\partial\overline{U}_i/\partial x_j + \partial\overline{U}_j/\partial x_i)$, have been shown to be considerably smaller than turbulent stresses downstream of mechanical prostheses in steady flow (Hasenkam, 1988a). (Note that this study did not include measurements of wall shear stress.) The problem with calculating RSS is that 2 orthogonal velocity components need to be measured simultaneously. This has been achieved with '2-dimensional' LDA (Walburn *et al*, 1985; Yoganathan *et al*, 1986; Chandran *et al*, 1989a; Nygaard *et al*, 1990;). Attempts have also been made using 2 orthogonal hot-film velocity probes, but this technique has an inherent poor spatial resolution (Hwang *et al*, 1977; Figliola & Mueller, 1981). A recent LDA study by Nygaard *et al* (1990) demonstrated that RSS = 0.5 RNS downstream of a mechanical and a porcine valve, for a range of physiological flow conditions. The RSS were calculated for planes ±45° to the flow axis. This result justifies the assumptions of others (Phillips *et al*, 1980) and suggests that it may be possible to estimate *in vivo* RSS from axial velocity measurements.

### 3.6.3 Flow characteristics

There are some general trends common to a number of experimental studies (those cited in section 3.6.1). All prosthetic valves create disturbed flow; maximum turbulent shear stress levels are at least close to the maximum level sustainable by blood corpuscles. An impression of the valve structure can be recognized in the measured velocity profiles; this is particularly clear when velocity profiles are given across the entire

flow cross section (Hasenkam *et al*, 1987; Hanle *et al*, 1989). For example, the 3 orifices of the St Jude bi-leaflet valve can be seen as 3 peaks in the measured velocity profile. Regions of higher turbulent stress tend to be in regions of higher velocity gradient. Steady flow velocity measurements are reasonably representative of those at peak pulsatile flow. Although turbulence damps out within a few diameters length downstream from the valve, the velocity field some considerable distance further downstream is determined by the valve type and orientation: as far as the mid-aortic arch for the aortic valve (Chandran *et al*, 1985a,b; Farahifar *et al*, 1985), and the entire left ventricle for the mitral valve (Chandran *et al*, 1989). There is qualitative agreement between *in vitro* and *in vivo* results (Jones *et al*, 1986; Hasenkam *et al*, 1988c,d).

Tilting disc valves such the Björk-Shiley family and the Medtronic-Hall (formerly Hall-Kaster) create highly skewed velocity fields with the highest velocities centred over the major orifice. A region of relatively slow moving fluid over the minor orifice correlates with areas of thrombus deposition and tissue overgrowth observed in explanted valves (Yoganathan *et al*, 1978). The convex-concave Björk-Shiley valve produces a less skewed velocity field, with smaller associated turbulent stresses, than the standard flat disc model, for the same opening angle (Hasenkam, 1988b,c). In the Björk-Shiley valve there is a narrow annular gap between the closed disc and the housing ring, there are particularly high shear stresses (up to 500 $Nm^{-2}$) associated with reverse flow through this annulus (Tillmann *et al*, 1984). The bi-leaflet St Jude valve creates a rather more uniform velocity field than the tilting disc valves; regions of high velocity are observed over the 3 orifices and lower velocity areas shadow the hinges and occluders. Relatively flat, but turbulent, velocity profiles with spherical depressions in the central region are

associated with caged-ball valves (Starr-Edwards and Smeloff-Cutter). Tri-leaflet pericardial and porcine valves produce quite different velocity fields from the mechanical valves; flows are jet-like, frequently skewed, with porcine valves tending to create more eccentric jets with higher associated velocities. Synthetic tri-leaflet valve flows are qualitatively similar to those for bioprostheses.

A mathematical description of pulsatile flow through prosthetic valves at physiological Reynolds numbers, such that the transition to turbulent flow is incorporated, has not been realised as yet. The 2-dimensional model used by Peskin (1982), described earlier in section 3.2, has been applied to mechanical prostheses in the mitral position, but only at low Reynolds numbers. The 2-dimensional steady flow model for aortic mechanical prostheses described by Idelsohn *et al* (1985) could accommodate Reynolds numbers up to 2000; although the transition to turbulence was not modelled, the predicted velocity fields were in qualitative agreement with *in vitro* observations. A steady turbulent flow model, applied to axisymmetric flow through a tri-leaflet prosthesis, has been developed by Stevenson *et al* (1985); the velocity fields and levels of turbulent shear stress were similar to those found *in vitro*.

## 3.7 Pressure-Flow Relations

All prosthetic heart valves present some degree of obstruction to the flow through them. Clearly the degree of stenosis depends on the particular valve design and mechanics, but even in the ideal case in which the valve occluder(s) or leaflet(s) present no resistance at all to the fluid motion there is still a flow restriction due the valve housing and sewing ring. The pressure drop across an obstruction can be investigated experimentally and, in simple cases, may be amenable to mathematical

analysis.

### 3.7.1 Theoretical considerations

Consider, for example, flow through the stenotic aortic valve (fig 3.3). Fluid which is accelerated through the region of stenosis during ejection emerges as a high velocity jet as it encounters an abrupt expansion in area. A region of rotational flow is created between the separated jet and the aortic wall and turbulent mixing occurs. Further downstream, flow re-attaches to the wall and turbulence extends across the entire aortic cross-section (Clark, 1976a).

Following the analysis presented by Clark (1978) and referring to figure 3.3, for an inertia dominated flow with a flat velocity profile and thin boundary layer, the equation of motion for a circular elemental disc of width $\delta x$ and radius r is:

$$-\partial p/\partial x\ [\pi r^2 \delta x] - \tau_x 2\pi r \delta x = \rho \pi r^2 \delta x\ (\partial u/\partial t + u \partial u/\partial x) \quad (3.3)$$

or

$$-\partial p/\partial x - 2\tau_x/r = \rho(\partial u/\partial t + u \partial u/\partial x) \quad (3.4)$$

where p is pressure, u is velocity, $\rho$ is fluid density, and $\tau_x$ is a generalised viscous shear stress at the wall. In words, equation (3.3) states that the pressure force minus the frictional force is equal to the elemental disc mass multiplied by the temporal and spatial accelerations. The effects of fluid compressibility and gravity have been ignored: the range of pressures encountered in the cardiovascular system are sufficiently low that blood is effectively incompressible and the effect of gravity may be eliminated by imposing a horizontal orientation. Integrating equation (3.4) by

Figure 3.3 Schematic flow through aortic valve

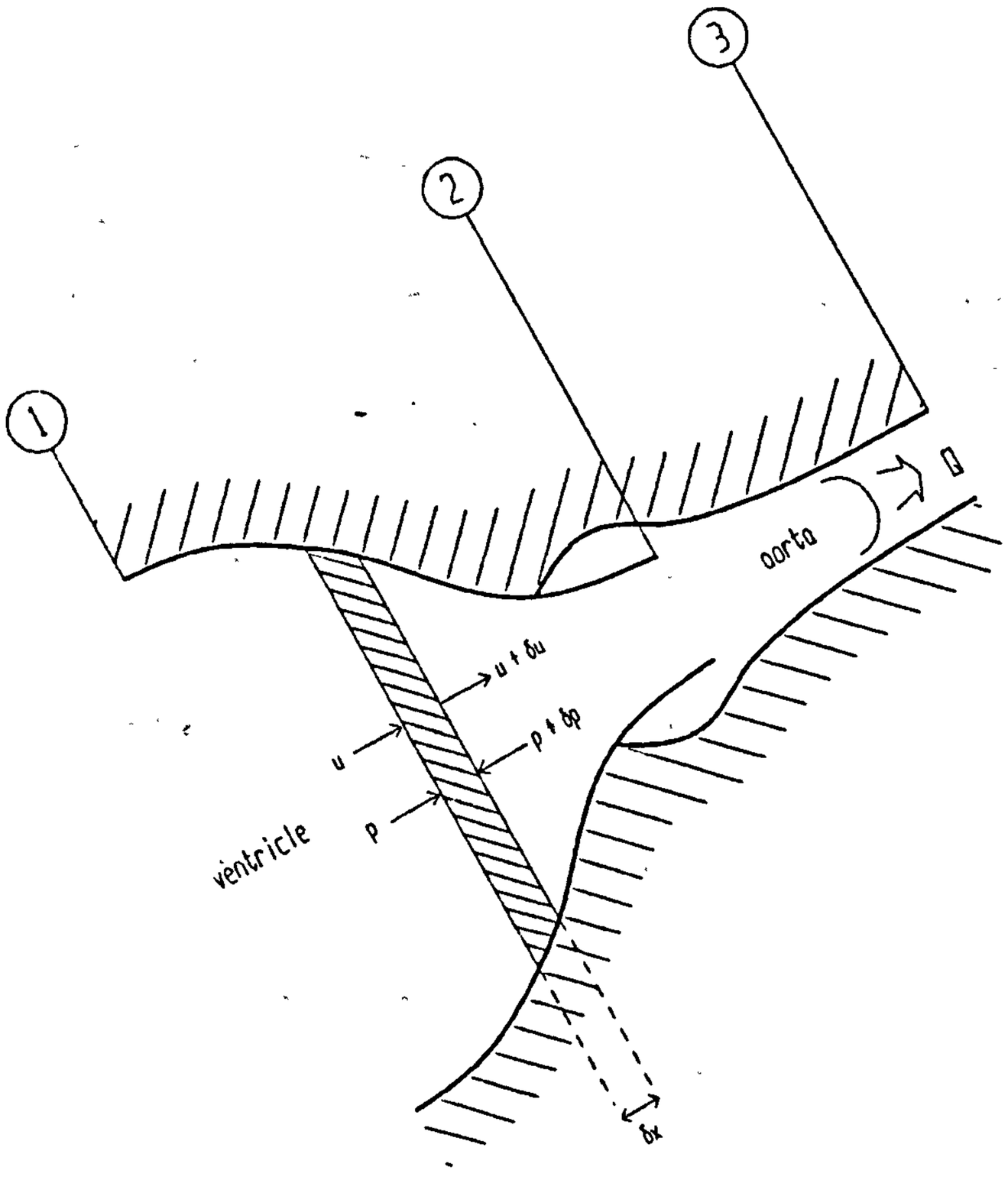

parts, from position 1 upstream of the valve to position 2 at the valve tip, gives:

$$p_1 - p_2 - \int_1^2 2\tau_x/r \, dx = \rho \int_1^2 \partial u/\partial t \, dx + \tfrac{1}{2}\rho(u_2^2 - u_1^2) \qquad (3.5)$$

If it is now assumed that the system has rigid walls then, at all x locations, the flow rate Q is given by $Q = uA$, where $A = \pi r^2$. Thus:

$$p_1 - p_2 - \int_1^2 2\tau_x/r \, dx =$$

$$\rho dQ/dt \int_1^2 1/A \, dx + (\rho Q^2/2A_2^2)[1 - A_2^2/A_1^2] \qquad (3.6)$$

The frictional term is determined by the particular nature of the flow and fluid, and the wall geometry and texture, and is therefore difficult to evaluate. However, frictional losses may be incorporated into a valve coefficient $C_d$, defined for steady flow by:

$$C_d = \left[ \frac{p_1` - p_2`}{p_1 - p_2} \right]^{\frac{1}{2}} \qquad (3.7)$$

where the prime denotes the ideal pressure that would be measured in the absence of friction. Note that $C_d$ implicitly includes the effects of a changing velocity profile from points 1 to 2. If the convective acceleration term is large compared to the local acceleration term, then the pressure drop may be expressed as:

$$p_1 - p_2 = \rho/2(Q/A_2C_d)^2[1-(A_2/A_1)^2] + \rho dQ/dt \int_1^2 1/A dx \qquad (3.8)$$

i.e. the pressure drop is given by the sum of a convective acceleration term due to the increasing fluid kinetic energy and a local acceleration term. For a sinusoidal flow, the pressure drop leads the flow by an

amount proportional to the relative size of the local acceleration term. If, instead of a rounded entrance nozzle, as illustrated in figure 3.3, the obstruction takes the form of a thin plate orifice, as would be the case for a mechanical prosthesis, then the acceleration region is extended a short distance beyond the orifice to a position known as the *vena contracta*. Here the fluid jet has its minimum area, $A_c$, which, by convention, is related to $A_2$ by a coefficient of contraction, $C_c$: $A_c = C_cA_2$. Likewise, it is usual to relate the ideal frictionless velocity at the vena contracta, $u_{c'}$, to the actual velocity, $u_c$, by introducing a coefficient of velocity, $C_v$: $u_c = C_vu_{c'}$. Thus, for steady flow, equation (3.8) can be re-written:

$$p_1 - p_c = \rho/2\ (Q/C_vC_cA_2)^2[1 - (C_cA_2/A_1)^2] \qquad (3.9)$$

If $A_1 >> A_2$, and taking $C_d = C_cC_v$, then equation (3.9) becomes the standard orifice meter equation (Massey, 1983):

$$p_1 - p_c = \frac{\rho Q^2}{2C_d^2A_2^2} \qquad (3.10)$$

The region immediately downstream of the valve is complicated by the presence of separated flow and turbulence. If position 3 (fig 3.3) is taken to be far enough downstream that flow is again approximately one-dimensional, then momentum conservation gives:

$$(p_2-p_3)A_3 - \int_{A_w}\tau_x dA = \rho(Q_3u_3 - Q_2u_2) + \rho d/dt[\int_{V_{2,3}} u\ dV] \qquad (3.11)$$

where $\tau$ is again the wall shear stress, $A_w$ is the aortic wall area bounded between positions 2 and 3, and $V_{2,3}$ is the volume enclosed by $A_2$, $A_3$ and $A_w$. That is, the pressure force minus the wall frictional force is equal to the rate of momentum flux plus the rate of

change of momentum within $V_{2,3}$. For a rigid aorta this becomes:

$$p_2 - p_3 = \rho u_3^2(1 - A_3/A_2) + (\rho/A_3)\,d/dt\left[\int_{V_{2,3}} u\ dV\right] + 1/A_3\int_{A_w}\tau_x dA \qquad (3.12)$$

The presence of turbulence means that momentum is continually being exchanged within $V_{2,3}$ even in the absence of large scale unsteady flow. To simplify matters, the rate of change of momentum term may be approximated by:

$$(\rho/A_3)\,d/dt\left[\int_{V_{2,3}} u\ dV\right] = (\rho l/A_3)\,dQ/dt + \int_{V_{2,3}} L(Q)\ dV \qquad (3.13)$$

where l is the distance between points 2 and 3, and L(Q) represents the turbulent losses. As before, provided the local acceleration term is relatively small, the combined wall and turbulent losses may be incorporated into a loss coefficient $C_t$ and equation (3.12) can now be expressed as:

$$p_2 - p_3 = (\rho u_3^2/C_t^2)[1 - A_3/A_2] + (\rho l/A_3)\,dQ/dt \qquad (3.14)$$

Note that for $A_3 > A_2$ the convective acceleration contribution is negative thus predicting an increase in pressure due to the recovery of kinetic energy. Combining equations (3.8) and (3.14) gives an expression for the overall pressure drop:

$$p_1 - p_3 = \rho Q^2\{(1/2A_2^2C_d^2)[1 - (A_2/A_1)^2] + (1/A_3^2C_t^2)[1 - A_3/A_2]\} + \rho\,dQ/dt\left\{\int_1^2 1/A\ dx + 1/A_3\right\} \qquad (3.15)$$

or

$$p_1 - p_3 = K_1\{\ Q^2/C_o^2\ \} + K_2\ \{\ dQ/dt\ \} \qquad (3.16)$$

where $K_1$, $K_2$ are constants and $C_o$ is an overall loss coefficient. Note that the unsteady term in equation (3.16) can be eliminated by averaging over the period of forward flow:

$$\overline{p_1 - p_3} = K_1\{ \overline{Q^2}/C_o^2 \} \qquad (3.17)$$

or by considering the pressure drop at peak flow:

$$(p_1 - p_3)_{Q_{max}} = K_1\{ Q_{max}^2/C_o^2 \} \qquad (3.18)$$

Equations (3.17) and (3.18) predict the same pressure drop as for the equivalent steady flow.

### 3.7.2 Experimental observations

The preceding analysis is based upon that given by Clark (1978); similar arguments have been expressed and experimentally investigated by numerous others. In particular, fixed apertures rather than valves have been used for experimental corroboration. Clark (1976b) used tapered nozzles to simulate aortic stenosis *in vitro* and found good agreement between measured pressure drops and those predicted by equations (3.8) and (3.14). In particular, the unsteady term in equation (3.8) was found to be negligibly small for severe stenosis ($A_2/A_1 = 1/16$) and the use of a steady flow coefficient $C_d$ in equation (3.8) was validated. In a similar study using thin plate orifices, Yellin & Peskin (1977) found that pressure drops for unsteady and equivalent steady flows measured between positions 1 and 3 were characterised by the same loss coefficient $C_o$, validating equation (3.16).

Application of the orifice meter equation (3.10) to heart valves was proposed by Gorlin & Gorlin (1951). They suggested that stenotic valve areas could be calculated from measurements of pressure drop and cardiac output, provided a discharge coefficient was known:

$$\text{valve area} = \frac{\overline{Q} \text{ through valve}}{C_d \cdot CF \cdot \sqrt{(\overline{\Delta p} \text{ across valve})}} \qquad (3.19)$$

where CF is a unit conversion factor. The error introduced from using mean rather than root mean square (RMS) flow (eqn 3.17) has been widely reported (Clark 1976a; Gabbay *et al*, 1978; Tindale & Trowbridge, 1986) and can be corrected if the shape of the flow waveform is known. Gabbay *et al* (1978) proposed using a modification of the Gorlin equation (3.19) to calculate an *effective* orifice area (EOA), which could be used to characterize a valve's hydrodynamic performance. The EOA is given by the valve area as calculated by the Gorlin equation (3.19) but with an assumed discharge coefficient of 1 and root mean square flow instead of mean flow:

$$\text{EOA } (cm^2) = \frac{Q_{RMS}}{51.6 \cdot \sqrt{(\overline{\Delta p})}} \qquad (3.20)$$

where $Q_{RMS}$ is measured in millilitres per second and the pressure in millimetres of mercury. Alternatively, EOA's can be calculated from the flow and pressure drop at the instant of peak flow (Aaslid *et al*, 1975). The EOA description of valve proficiency has been adopted by several investigators (Walker *et al*, 1980; Yoganathan *et al*, 1983; Fisher, 1986; Schoephoerster & Chandran, 1989). Note that the orifice meter equation (3.10) requires $A_1 >> A_2$ and the downstream pressure to be measured at the vena contracta, therefore a calculated EOA is not a measurable area unless the valve has a discharge coefficient of approximately 1 and the measurement criteria are met (Tindale & Trowbridge, 1986).

The Gorlins' method was to be applied to patients undergoing cardiac catheterization. For eleven natural mitral valves, Gorlin & Gorlin (1951) found that

calculated areas agreed with measured areas (at postmortem or intraoperatively) to within 0.2 $cm^2$ (mean calculated area = 0.75 $cm^2$). A discharge coefficient of 0.6 was used, based on a postmortem area measurement. Although these early results were encouraging, they did not conclusively justify the general application of an equation based on steady flow through a fixed orifice to non-return valves in pulsatile flow; this has been the subject of many subsequent *in vitro* and *in vivo* investigations. The Gorlin equation (3.19) has been widely used; however, its use has not been without controversy and interest in this area has recently been revived (Carrabello, 1987; Gorlin, 1987).

The pressure-flow relations for heart valves have been studied extensively *in vitro*. Results from early investigations were in broad agreement with equation (3.16), but more recently inconsistencies have been revealed. Roschke (1973) reviewed some early experimental results for steady flow through mechanical valves: pressure drops were approximately proportional to steady flow squared. Viggers *et al* (1967) found a linear relationship between pressure drop at peak flow and peak flow squared for pulsatile flow through mechanical valves, consistent with equation (3.18). Gentle (1977 & 1978) found for mechanical valves, the same parabolic relationship between pressure drop and steady flow as that between mean pressure drop and mean squared pulsatile flow, in agreement with equation (3.17); however, the average flow was calculated over the period of forward pressure, which may have resulted in a small error if the local acceleration terms were sufficiently large. A comprehensive study of mechanical and bioprosthetic valves undertaken by Gabbay *et al* (1978a) showed that both peak flow and RMS flow gave consistent characterisations of the pressure drop across valves in pulsatile flow, and these results were in agreement with those from steady flow. Further validation of steady and

pulsatile flow equivalence was provided by Yoganathan *et al* (1979) who showed that, for pulsatile flow through mechanical valves, the mean systolic pressure drop is given by the equivalent steady flow pressure drop. Additionally, Scotten *et al* (1981) found that their mean pressure drop against root mean square pulsatile flow data for Björk-Shiley prostheses showed good correlation with equivalent steady flow results published by Aberg & Henze (1979). The study of Scotten *et al* is particularly interesting because for a range of mechanical valves they found that the mean pressure drops were proportional to $(Q_{RMS})^c$ where c ranged from 1.55 to 2.13 (this point will be discussed later). Scotten *et al* also found exponent c = 1.84 for a reference orifice (6.6 $cm^2$) which is contrary to the earlier results of Clark (1976b) and Yellin & Peskin (1977).

As well as the ability to predict pulsatile pressure drops from steady flow data, the apparent steady/pulsatile flow equivalence has a second important implication: the energy associated with opening the valve is either negligibly small or is elastically recovered when the valve closes. In this context, it is worth emphasizing that the above citations involving prosthetic heart valves, with the exception of the Gabbay *et al* (1978a) were based on studies which used mechanical valves. The energy required to open, for example, a heavily calcified explanted bioprostheses is significant and obviously much greater than that required for a tilting disc valve. In an extensive study of bioprostheses, Wright (1979) reported that measured steady flow pressure drops were on average 19% less than the equivalent pulsatile flow pressure drops. However, the comparison was made using the mean pulsatile flow rather than RMS pulsatile flow. Wright used a sinusoidally reciprocating pump; presuming a sinusoidal flow was produced, the mean flow data can be converted to root mean flow by multiplying by 1.11 (for a ½ sine wave:

$Q_{RMS}$ = 1.11 $Q_{mean}$). This correction factor brings the steady flow data into approximate agreement with the pulsatile flow data. Wright also commented upon the variable way in which bioprosthetic valves open; specifically, he found that the minimum peak pulsatile flow required for the third leaflet to open varied widely, even for valves of the same construction, both for porcine and bovine pericardial valves. In general, pericardial valves opened more readily than porcine valves.

Variations in valve orifice areas with flow have been studied for steady and pulsatile flow. An increase in tri-leaflet valve orifice area with increasing steady flow has been widely described (Thomson & Barratt-Boyes, 1977; Tindale *et al*, 1982; Yoganathan *et al*, 1983; Reul *et al*, 1985). As a consequence, Tindale *et al* (1982) found that the steady flow pressure drop across porcine and pericardial valves was proportional not to $Q^2$ but to $Q^c$, where c ranged from 1.51 to 1.86 (cf. Scotten *et al*, 1981). In the same experiment, Tindale *et al* found that exponent c was approximately 2 for a range of mechanical valves under steady flow; Bruss *et al* (1983) arrived at the same result.

In pulsatile flow, ideal valves open and close rapidly with minimal energy loss and are wide open for much of the duration of forward flow; thus applying the fixed orifice equation (3.16) may well be a suitable approximation. The applicability of equation (3.16) then depends upon how quickly the valve opens and closes and, once open, how insensitive the open area is to increasing pulsatile flow. *In vitro* studies by Walker *et al* (1980) and Chandran *et al* (1986) indicate that for the duration of forward flow porcine and pericardial valves spend approximately 5% of the time opening and 2-3 times longer closing; van Steenhoven *et al* (1981) reported similar findings studying canine aortic valves *in vivo*. For the period between opening and closing, the data of Chandran

*et al* depict a fairly constant orifice area whereas the measurements of Walker *et al* were performed in the mitral position and consequently show a semi-closure and re-opening of the valve due to simulated atrial contraction. Furthermore, the Chandran *et al* results indicate that both valve types (porcine and pericardial) take relatively longer to close at higher heart rates. Yoganathan *et al* (1983) commented on pericardial valves opening more quickly than porcine valves, in corroboration with data from Wright (1979), but this is not obvious from the results of Chandran *et al*. Whether pericardial valves open faster than porcine valves will, of course, depend to some degree upon the specific valve construction. Notice that these observations have been made *in vitro* using unimplanted valves; it is to be expected that, for example, stiff explanted valves would spend a proportionately longer time opening and closing. Further, the valve areas quoted in these studies are the planimetered areas measured from photographs or video images. In general, and in particular for porcine valves, the measured open area may be a superposition of different planes and could give rise to an underestimate of the area 'seen' by the fluid (Tindale *et al*, 1982). Also note that mechanical valves close faster and later in the flow cycle than bioprostheses (van Steenhoven *et al*, 1982).

There are contradictory reports concerning the variation in maximum open valve area with cardiac output (or 'pulse duplicator output'). Increasing areas for pericardial and porcine valves (Stein & Munter, 1971; Yoganathan *et al*, 1983; Chambers *et al*, 1989) as well as polyurethane valves (Schoephoerster & Chandran, 1989) have been observed, but approximately constant areas have also been reported both for pericardial and porcine bioprostheses (Gabbay *et al*, 1979; Walker *et al*, 1979; Walker *et al*, 1980; Cannon *et al*, 1985) and synthetic leaflet valves (Woo *et al*, 1983). Stein & Munter, 1971,

using a roentgenographic technique, found that human aortic valve orifice areas were dependent on cardiac output. A recent comprehensive study demonstrated an increase in explanted human aortic valve area with cardiac output, and for a range of bioprostheses, both unimplanted and explanted, some valves opened fully at low flow rates while others opened progressively with increasing pulsatile flow; furthermore, different stroke volume/heart rate combinations with the same cardiac output resulted in differing orifice areas (Cochrane *et al*, 1991).

A valve orifice area which increases with pulsatile flow would result in the mean pressure drop being proportional to $Q_{RMS}$ raised to a power less than 2 and the calculated area (EOA or Gorlin) increasing with $Q_{RMS}$. Measuring the pressure drop across porcine bioprostheses in patients undergoing catheterization, Ubago *et al* (1980) reported an increasing calculated (Gorlin) area with increasing flow and suggested this may be due to the valve orifice area increasing. Subsequent *in vitro* studies found a good correlation between the measured increase in orifice area and that predicted by the Gorlin equation (Chambers *et al*, 1989; Cochrane *et al*, 1991). (Note that Ubago applied the Gorlin equation at three time intervals within the diastolic period (early, mid, and late) in order to get a range of flow values; using this method, unlike equations (3.19) and (3.20), the local acceleration contributions to the pressure drop are not eliminated and may lead to inaccuracies). However, similar increases in calculated areas have been reported in cases where the bioprosthetic orifice area has remained approximately constant (Gabbay *et al*, 1978b; Cannon *et al*, 1985); furthermore, mechanical valves have shown the same tendency (Gabbay *et al*, 1979; Köhler *et al*, 1981; Scotten *et al*, 1981; Swanson, 1984a). Schoephoerster & Chandran (1989) found that the measured increase in orifice area with flow for a pericardial and

a polyurethane valve correlated well with the calculated increase if the discharge coefficient was assumed to be a linear function of flow; mechanical valve orifice areas remained constant when measured over the physiological range of cardiac output and, as for the tri-leaflet valves, taking the discharge coefficient to be a linear function of flow resulted in a consistent calculated area. Interestingly, the discharge coefficients of the mechanical valves were more dependent on the flow than were the tri-leaflet valve discharge coefficients. It is well known that for low Reynolds numbers, where viscous effects are more prominent, nozzle discharge coefficients are functions of Reynolds number (Rivas & Shapiro, 1954). Steady flow experiments have demonstrated this dependency of discharge coefficient upon flow for fixed nozzles simulating aortic valves (Clark, 1976a) and for prosthetic valves (Akutsu *et al*, 1980). Gabbay *et al* (1979) suggested that these viscous effects were the likely explanation for their earlier reported increase in calculated bioprosthesis area with flow. That viscous effects are small is indirectly confirmed by several investigators reporting the insensitivity of measured pressure drops across valves to the viscosity of the test medium (Olin, 1971; Yellin & Peskin, 1975; Swanson & Clark, 1977b; Wright, 1979; Scotten *et al*, 1979; Yoganathan *et al*, 1979; van Steenhoven & Veenstra, 1982; Swanson, 1984b; Chandran *et al*, 1986; Carey & Herman, 1989).

A second explanation for the increase in calculated EOA with pulsatile flow concerns the mechanisms of energy loss downstream of the valve. In equation (3.16), all the flow losses associated with the valve are lumped together in a single factor which is assumed to be proportional to $Q^2$, as is the case for fully developed turbulent flow in pipes. However, depending on the specific construction of the valve and its surroundings, as well as the location of the pressure transducer(s), the predominant loss

mechanism may not be that of fully developed turbulence but perhaps some degree of developing or decaying turbulence; thus, in the exponential relationship between pressure drop and flow, the exponent may be less than 2 (Swanson, 1984a). Indeed, Swanson, 1984b, suggested using the measured exponent as a turbulence index. In this context, it is interesting to consider the apparently anomalous results of Cannon *et al* (1985). Using a porcine bioprostheses with a diaphragm snare 0.5 cm downstream to simulate stenosis, they found good agreement between calculated (Gorlin) orifice areas and measured areas over the range of physiological pulsatile flow, provided the discharge coefficient was a linear function of the root mean pressure drop. Their data suggested that the pressure drop was a linear function of flow, as is the case for fully developed laminar pipe flow. Perhaps these results reflect some coupling effect between the valve and snare.

To summarise, the pressure drop across mechanical and tri-leaflet valves is given by:

$$\text{pressure drop} = \text{constant} \cdot Q^{c} \qquad (3.21)$$

where exponent c lies between 1.5 and 2 depending on the particular valve and the particular testing environment (and in the case of pulsatile flow, Q is either peak or mean, and the pressure drop likewise). For ideal inviscid fluid and irrotational flow, there would only be a pressure drop if the flow cross sectional area decreased, in which case the exponent would equal 2. In a real fluid, the exponent would also equal 2 if the dominating energy loss mechanism was that of fully developed turbulence; however, if there were significant viscous losses, either at the valve or downstream, then the exponent would be less than 2. A flow dependent orifice area would also tend to reduce the size of the exponent.

As well as slightly variable pressure-flow

relations, different investigators have also reported varying absolute magnitudes for valvular pressure drops. In a review article by Swanson (1984a) pressure drops for the same valve, as measured by different investigators, were observed to vary by up to a factor of five. This was attributed to differences in pulse duplicator geometry and placement of pressure transducers. The pressure recovery predicted in equation (3.14) has been observed in steady flow (Clark, 1976a; Akutsu *et al*, 1980; Schramm *et al*, 1982; Tindale *et al*, 1982; Bruss *et al*, 1983;) and pulsatile flow (Clark, 1976b; Fisher *et al*, 1986a; Fisher & Wheatley, 1988); Clark, 1976b also observed pressure recovery downstream of an induced aortic stenosis in a dog. This phenomenon is clearly a source for discrepancies between pressure drops measured by different investigators. Note that the relatively sophisticated numerical analysis of diastolic flow entering the left ventricle, presented by Peskin (1982) (re section 3.2), also demonstrated a pressure recovery effect.

The preceding discussion has concentrated on the pressure-flow relations averaged over the period of forward flow, which eliminates the effects of local inertia. The effect of local inertia, in particular its effect on the relative pressure-flow phase, as predicted by equation (3.16), has been demonstrated *in vitro* (Yellin & Peskin, 1975; Clark 1976b) and *in vivo* (Clark, 1978; Pasipoularides *et al*, 1984). Clark (1978) attributed discrepancies between measurements made in dogs and theory (eqn 3.16) to the effects of aortic compliance. Tindale & Trowbridge (1983) derived an expression similar to equation (3.16) which included the effect of some aortic compliance; the 'resistive' term ($K_1Q^2/C_o^2$ in equation (3.16)) was not given explicitly but taken from steady flow measurements. The predicted pressure waveforms are in good agreement with those measured for mechanical and bioprosthetic valves, with

the exception that the measured pressure trace shows an initial spike on valve opening.

As has been previously stated, the lack of standardization in hydrodynamic valve testing makes comparison of results from different investigators difficult. However, there have been a number of comparative studies in which several valve types have been evaluated under identical conditions (Gabbay *et al*, 1978; Yoganathan *et al*, 1979; Walker *et al*, 1980; Tindale *et al*, 1982; Fisher *et al*, 1986b; Reul *et al*, 1986; Herold *et al*, 1987). In these studies, tilting disc prostheses consistently show the lowest mean and peak pressure drops, pericardial tri-leaflet valves have similar or slightly higher associated pressure drops. Porcine valves are generally more impedimental than pericardial valves, with pressure drops similar to caged ball valves. Larger pressure gradients are observed across smaller valve sizes, small porcine valves being particularly obstructive (Gabbay *et al*, 1978). The polyurethane tri-leaflet valve developed by Herold *et al* (1987) had an associated pressure gradient which lay in the upper range for pericardial valves and in the lower range for porcine valves; the pressure drop was shown to be highly sensitive to changes in leaflet thickness.

## 3.8 Energy Loss

The obstructive nature of prosthetic heart valves makes for a less energy efficient transfer of fluid across them. The dissipation of mechanical energy may be attributed to the fluid viscosity and to inelastic deformations of the valve.

After Clark (1979), consider again flow through the stenotic aortic valve (fig 3.3). As before, the effect of gravity and fluid compressibility are ignored. Thus, for region S, consisting of the ventricular wall area, $A_V$, and the aortic valve orifice area, $A_2$, the rate of change

in volume, V, is given by the net volumetric flow rate:

$$\int_S \mathbf{v}\cdot\mathbf{n}\ ds = -d/dt \int_V dV \qquad (3.22)$$

where **v** is the velocity vector and **n** is the outward pointing unit vector normal to surface element ds. Energy conservation gives:

$$\rho d/dt[\int_V (v^2/2)\ dV] = \int_S pv\cdot\mathbf{n}\ ds - \rho\int_S (v^2/2)\mathbf{v}\cdot\mathbf{n}\ ds - \epsilon \qquad (3.23)$$

where p is pressure, $\rho$ is fluid density and $\epsilon$ is the rate of energy dissipation. In words, the rate at which kinetic energy changes within region S is equal to the rate at which work is done on (or by) the boundary S minus the rate at which kinetic energy flows out of (or into) S and minus the rate of energy dissipation (power loss).

If the flow across $A_2$ is taken to have an approximately flat velocity profile then the flow work term in equation (3.23) may be expressed as:

$$\int_S pv\cdot\mathbf{n}\ ds = \int_{A_V} pv\cdot\mathbf{n}\ ds - p_2A_2v_2 \qquad (3.24)$$

or using the conservation of volume (eqn 3.22):

$$\int_S pv\cdot\mathbf{n}\ ds = Q_2(p_1 - p_2) \qquad (3.25)$$

where an averaged pressure $p_1$ is defined:

$$p_1 = \int_{A_V} pv\cdot\mathbf{n}\ ds\ /\ dV/dt \qquad (3.26)$$

Under the same approximation, the kinetic energy flux term in equation (3.23) becomes:

$$\rho\int_S (v^2/2)\mathbf{v}\cdot\mathbf{n}\ ds = \rho(v_2^2/2)Q_2 - \rho(v_1^2/2)Q_1 \qquad (3.27)$$

The rate of change of kinetic energy term on the left hand side of energy balance equation (3.23) can be simplified if a rigid-walled system is assumed:

$$\rho d/dt[\int_V (v^2/2)\ dV] = \rho Q(dQ/dt)\int_1^2 1/A\ dx \qquad (3.28)$$

Thus, the rate of energy dissipation may be expressed:

$$\epsilon = Q\{\ p_1 - p_2 + \rho(v_2^2/2)[(A_2/A_1)^2 - 1]$$
$$- \rho(dQ/dt)\int_1^2 1/A\ dx\ \} \qquad (3.29)$$

Some insight into the energy loss may be achieved by re-introducing the nozzle discharge coefficient, $C_d$, to eliminate the pressure difference from equation (3.29). Recalling equation (3.8), that the pressure drop across a valve equals the sum of a convective acceleration term ($K_1Q^2$) and a local acceleration term ($K_2dQ/dt$); substituting into equation (3.29) yields:

$$\epsilon = Q\{\ (\rho v_2^2/2C_d^2)[1 - (A_2/A_1)^2] + \rho(dQ/dt)\int_1^2 1/A\ dx +$$
$$\rho(v_2^2/2)[(A_2/A_1)^2 - 1] - \rho(dQ/dt)\int_1^2 1/A\ dx\ \} \qquad (3.30)$$

which simplifies to:

$$\epsilon\ /\ \rho Q(v_2^2/2) = (1/C_d^2 - 1)[1 - (A_2/A_1)^2] \qquad (3.31)$$

and is plotted in figure 3.4. Note the increase in energy loss for a smaller relative orifice area and that for a typical stenosis, say $A_2/A_1 = 0.25$ with $C_d = 0.9$, the power loss is approximately one quarter of the output kinetic energy flux.

Figure 3.4 Relative power loss for a rigid nozzle

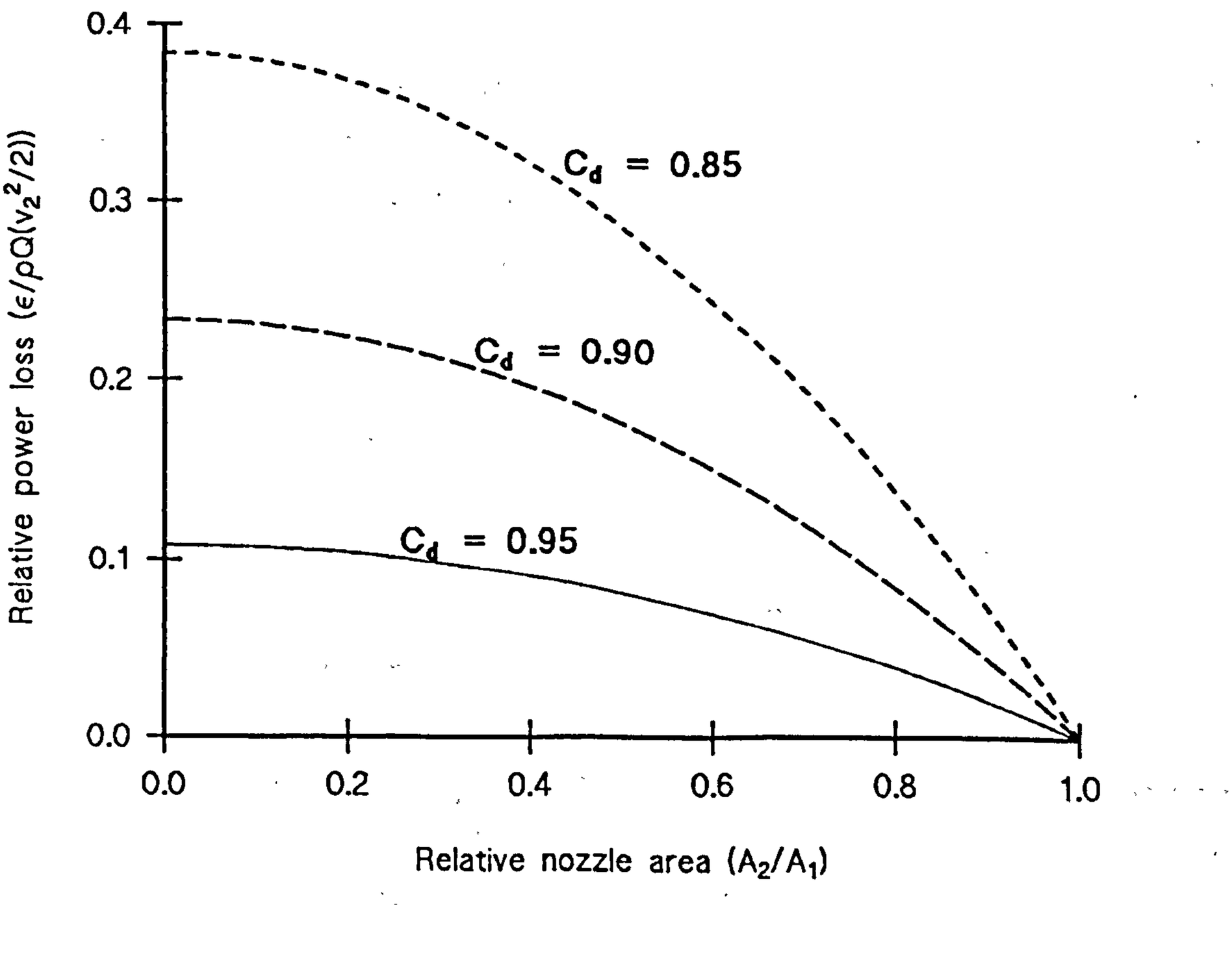

Integrating the energy rate equation (3.29) over the systolic period eliminates the unsteady term and gives the associated energy loss, for small $(A_2/A_1)^2$, as:

$$\int_{sys} \epsilon \, dt = \int_{sys} Q(p_1 - p_2) \, dt - \int_{sys} \rho Q(v_2^2/2) \, dt \qquad (3.32)$$

i.e. the difference between the flow work and the output kinetic energy. Likewise, integrating over the period of regurgitation or leakage also eliminates the unsteady term and gives the corresponding energy loss.

A more general derivation of the energy loss equation (3.32) has been published by Leefe & Gentle (1987). Clark (1979) extended the preceding analysis downstream to the region of turbulent losses, between positions 2 and 3 (fig 3.3). He showed that the downstream power loss was given by an expression of the same form as equation (3.29); i.e. rate of energy loss equals rate of flow work minus kinetic energy flux and an unsteady term which can be eliminated by integration.

The calculation of energy losses associated with forward and reverse flow provides a means of characterising a valve's hydrodynamic efficiency. In so doing, both systolic and diastolic performances can be directly compared and the overall valve performance may be gauged by a single parameter. This method has been adopted by a number of investigators (Gilbert *et al*, 1970; Olin, 1971; Viggers, 1972; Swanson, 1984; Walker *et al*, 1984; Knott *et al*, 1988). Energy losses are often calculated with the kinetic energy term in equation (3.32) neglected (Reul *et al*, 1972; Mohnhaupt *et al*, 1975; Fisher & Wheatley, 1988). For the aortic valve this gives an overestimate of the energy loss as some of the kinetic energy is recovered downstream (Clark 1979); in the case of the mitral valve, the kinetic energy flux is dissipated in the ventricle and the flow work represents the true energy loss. Likewise in reverse flow, the

kinetic energy flux is dissipated in the ventricle or atrium and can be neglected.

It is important to note the confusion that may occur in interpreting energy losses when there is significant reverse flow through either the mitral or aortic valve. For example, in the case of reverse flow through the aortic valve, there is a direct energy loss associated with the fluid passing backwards through the aortic valve. However, if, in order to maintain a constant net ventricular output, the ventricular stroke volume increases then there will also be a systolic energy loss associated with the retrograde fluid. On the other hand, if the ventricular stroke volume remains constant, then there will be a reduction in the diastolic energy loss across the mitral valve. In particular, Fisher & Wheatley (1988) pointed out that their calculated aortic valve energy losses during closing regurgitation were small because of the small pressure gradient throughout that period, however the additional energy loss associated with the increased ventricular stroke volume would be much larger (for a constant cardiac output).

# Chapter 4. Valve Function and Durability Testing

## 4.1 Introduction

The *in vitro* evaluation of hydrodynamic performance and durability plays an indispensable role in the development of new heart valve prostheses. Detailed comparisons can be made between different valve designs under identical conditions. Clearly, there are limitations to *in vitro* testing: the complex fluid mechanical environment of the cardiovascular system can only be rather crudely approximated *in vitro*, and the biological effects even less so. Nevertheless, *in vitro* systems are convenient, more amenable to a detailed study of the mechanical factors influencing valve performance, and only on the basis of satisfactory *in vitro* performance can animal trials be justified.

This chapter concerns the hydrodynamic function and durability testing facilities available at the Glasgow Royal Infirmary (GRI); these facilities being typical of those used at other centres.

## 4.2 Hydrodynamic Function Tests

Before attempting to simulate physiological flow through heart valves, the pumping characteristics of the left ventricle and the arterial input impedance must be considered.

The heart is a pump (or rather a pair of pumps in series) of variable stroke volume and frequency, producing uni-directional periodic flow. The volume of blood ejected from the left ventricle is determined by the contractility and end-diastolic length of ventricular muscle fibres as well as the arterial input impedance; in turn, these factors along with the heart rate are controlled by complex neural and biochemical means. In an engineering environment, fluid pumps (or by analogy,

electrical generators) are commonly characterised in terms of a pressure-flow (or voltage-current) relationship. In particular, the idea of rating a source by its output impedance has been applied to the left ventricle. Elzinga & Westerhof (1979) studied the effect of different arterial loads on isolated de-nervated cat hearts. Their data reveals that the ventricular output impedance and the arterial input impedance are of the same order of magnitude and the ventricle can be considered neither as a pure flow nor pure pressure source: as cardiac output increases the output impedance also increases and the pump becomes more like a constant flow source. Notice that in going from rest to exercise, human cardiac output can increase by a factor of 5 or more (by increasing heart rate and to a lesser extent stroke volume) and this is accompanied by only a relatively modest increase in systolic arterial blood pressure. This suggests that the heart effectively operates with a relatively low output impedance (Ganong, 1981).

A variety of electro-mechanical and pneumatic pumps have been used in pulse duplicators. Electro-mechanical pumps used range from sinusoidally-reciprocating piston pumps (Wright, 1979) to those which use shaped-cams (Martin & Black, 1976; Gentle, 1978; Scotten *et al*, 1979), spring-biasing (Martin & Black, 1976; Swanson & Clark, 1977a; Arabia *et al*, 1989) or electronic means (Martin *et al*, 1981; Scotten *et al*, 1983; Leefe *et al*, 1986; Knott *et al*, 1988) to create a more physiological flow. Some investigators use servo-control mechanisms to enable the ventricular volume-time relations to be pre-set (Martin *et al*, 1981; Scotten *et al*, 1983; Leefe *et al*, 1986) while others include some compliance in the pump mechanism (Martin & Black, 1976; Knott *et al*, 1988). Pneumatic pumps have been used to control the ventricular pressure-time relations (Wieting *et al*, 1969; Black, 1973; Mohnhaupt, 1975; Cornhill, 1977; Yoganathan *et al*,

1979; Köhler *et al*, 1981; Cannon *et al*, 1985; Chandran *et al*, 1989). A range of ventricular geometries and compliances have been used: rigid cylindrical chambers (Wieting *et al*, 1969; Swanson & Clark, 1977a; Gabbay *et al*, 1978; Tindale & Trowbridge, 1983; Woo & Yoganathan, 1986; Arabia *et al*, 1989), flexible cylindrical chambers (Olin, 1971; Köhler *et al*, 1981), rigid ventricle-shaped chambers (Wright, 1979; Chandran *et al*, 1989b), and flexible ventricle-shaped chambers (Black, 1973; Cornhill, 1977; Scotten *et al*, 1979; Reul, 1983; Cannon *et al*, 1985). Note that Gabbay *et al* (1981) when comparing results from 2 pulse duplicators, one with a rigid and the other a flexible ventricular chamber, found little difference in calculated EOA's.

Westerhof *et al* (1971) demonstrated that the input impedance of the systemic arterial tree can be simulated with a lumped capacitance-resistance model. Their hydraulic model consisted of a lumped series resistance (characteristic) connected to a parallel combination of lumped capacitance (*windkessel*) and resistance (peripheral). Most pulse duplicators are based on this model; deviations include, for example, the use of a distributed capacitance (Swanson & Clark, 1977a; Arabia *et al*, 1989), the use of 2 lumped capacitances (Martin & Black, 1976), and the omission of an explicit characteristic resistance (Yoganathan *et al*, 1979; Cochrane *et al*, 1991). Note that the characteristic resistance, which is much smaller than the peripheral resistance, is effectively the high frequency resistance. Compliant aortic roots have been incorporated into pulse duplicators (Scotten *et al*, 1979; Reul, 1983), but this makes measurement of flow through the aortic valve more difficult and the effect on the pressure drop across the aortic valve is small (Tindale & Trowbridge, 1983).

Flow measurement in pulse duplicators, usually involving electromagnetic flow meters, is problematic. Axisymmetric flow is necessary to give an accurate

measurement which implies that the probe should not be used in the vicinity of curving or abruptly changing geometry, while locating the probe in a uniform pipe several diameters long may introduce undesirable inertial effects (McDonald, 1974). Also, if compliant chambers separate the valve under investigation from the flow probe then instantaneous flow through the valve cannot be directly measured.

The fluid media used in pulse duplicators usually either matches approximately the blood density (eg saline) or the blood density and viscosity (eg glycerol solution). As was remarked in the previous chapter, there have been several reports of measured valvular pressure drops being insensitive to the fluid viscosity (Olin, 1971; Yellin & Peskin, 1975; Swanson & Clark, 1977b; Scotten *et al*, 1979; Yoganathan *et al*, 1979; van Steenhoven & Veenstra, 1982; Swanson, 1984b), and it has been suggested that exposure to glycerol solution has a deleterious effect on bioprosthetic valve leaflets (Wright, 1979). However, more recent studies by Chandran *et al* (1986) and Carey & Herman (1989) revealed no change in bioprosthesis hydrodynamic performance with increased exposure to glycerol solution. Furthermore, Chandran *et al*, and Carey & Herman, in comparing results between saline and glycerol solution filled pulse duplicators, observed small, and reversible, differences in valvular pressure drop and valve leaflets generally moving more slowly in the more viscous fluid; however, note that the effects were small, somewhat variable, and based on only 2 and 3 valves respectively. Lewis & Macleod (1983) used a mixture of cow's milk and rennet in their pulse duplicator and found milk clots forming on mechanical valves in locations similar to those in which thrombi are deposited *in vivo*; they proposed using this test fluid as a means of comparing the thrombogenicity of different valve designs.

In addition to testing with pulsatile flow, steady

flow testing is widely used (Aberg & Henze, 1979; Yoganathan *et al*, 1979; Tindale *et al*, 1982; Reul, 1983); such studies require less sophisticated apparatus and are useful as an initial indicator of valvular pressure drop.

## 4.3 The GRI Pulse Duplicator

The GRI pulse duplicator has been described in detail elsewhere (Fisher, 1986; Fisher *et al*, 1986a) and is shown schematically in figure 4.1. The updated data acquisition and computer control software is described in the following chapter.

Briefly, pulsatile flow is generated with a servo-controlled positive displacement pump (Scotten *et al*, 1983). The pump input signal is selected from a choice of 4 pump velocity waveforms generated by an IBM PC. The velocity waveforms incorporate the main features of the cardiac cycle: decreasing diastolic period with increasing heart rate, asymmetric systolic flow waveform, and end-diastolic atrial contraction (fig 4.2). Atrial, ventricular and aortic test chambers are axisymmetric (with the exception of 3 aortic sinuses), rigid and transparent, and allow good visibility of both the mitral and aortic valve outflow aspects. The systemic circulation is represented by a parallel combination of lumped capacitance (trapped volume of air) and resistance (cross-clamp). Valves can be tested in either the mitral or aortic position; a Björk-Shiley plano-convex valve is usually mounted in the position not under investigation. The pulse duplicator can be easily converted for steady flow measurements, by the inclusion of a roller pump between the compliance chamber and the atrial reservoir.

As indicated in figure 4.2, the standard testing conditions, as used routinely for the hydrodynamic evaluation of explanted valves, range from stroke volume 60 ml, 60 beats per minute to stroke volume 80 ml, 120

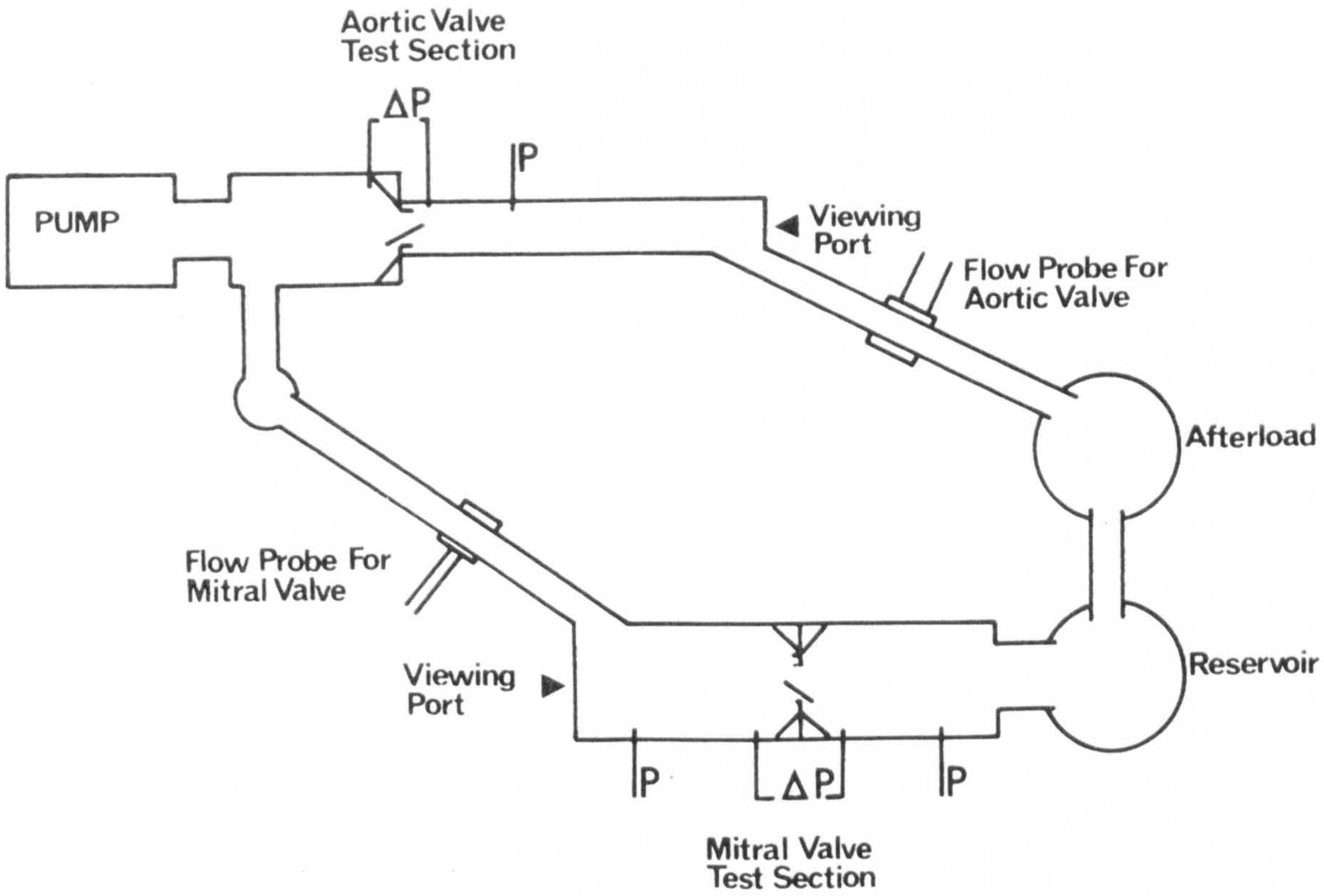


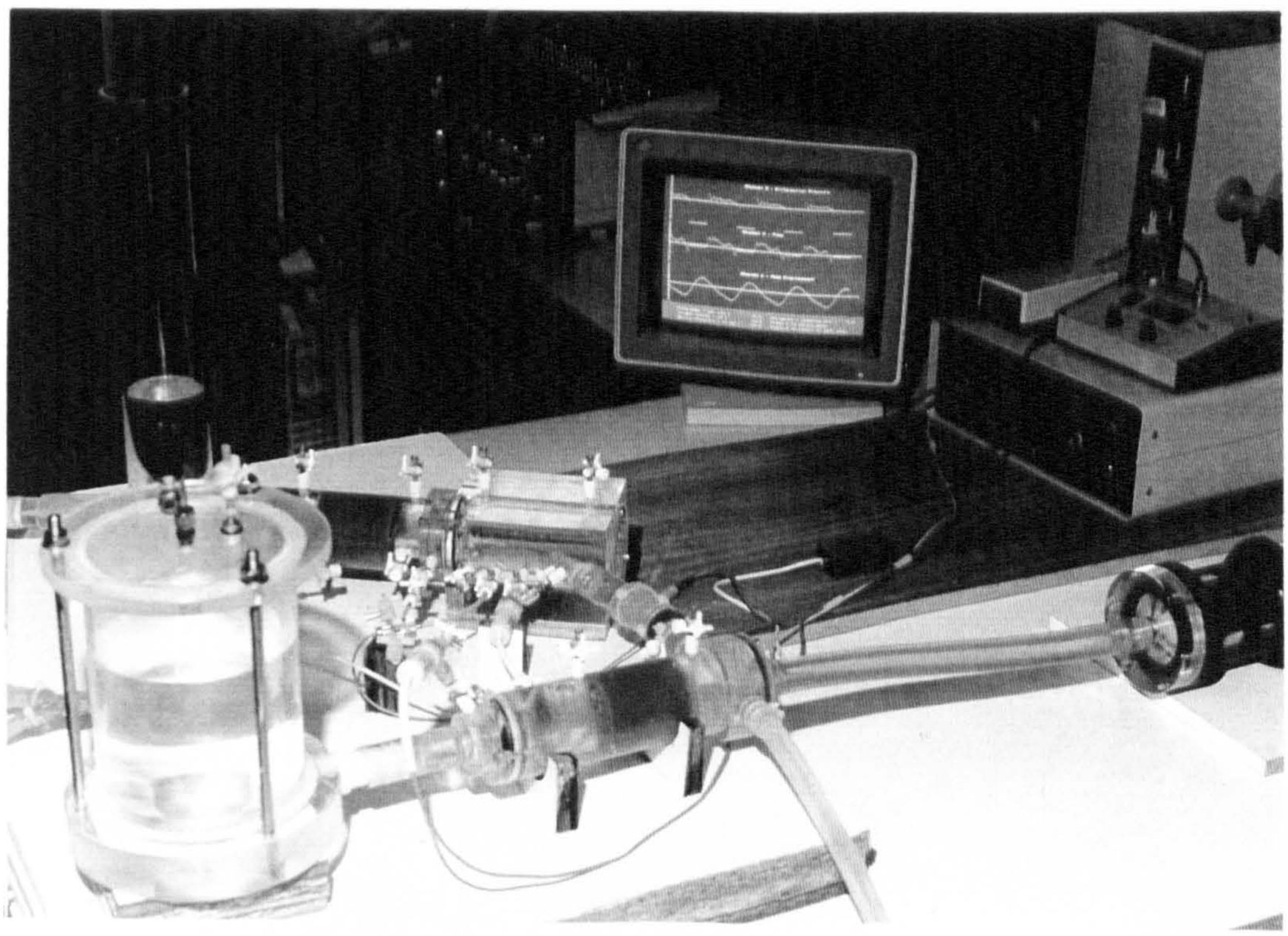

Figure 4.1 The GRI pulse duplicator

Figure 4.2 Pump velocity waveforms and standard testing conditions

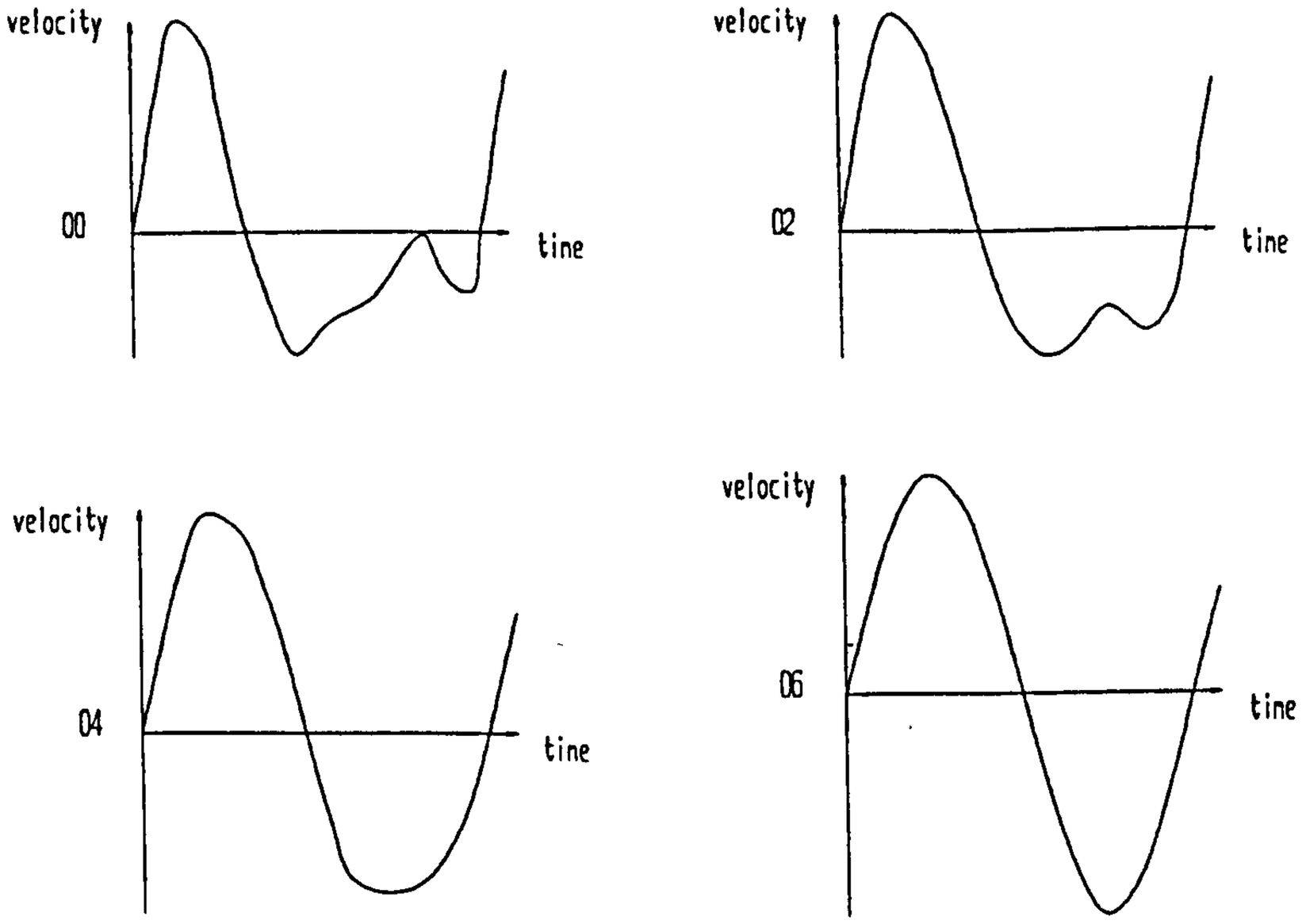


Standard testing conditions:

| | Waveform | Beats per minute | Stroke volume (ml) |
|---|---|---|---|
| A | 02 | 60 | 60 |
| B | 02 | 70 | 70 |
| C | 02 | 80 | 80 |
| D | 04 | 100 | 80 |
| E | 06 | 120 | 80 |

with mean aortic pressure of 95 mm Hg in all cases

beats per minute, i.e. equivalent to cardiac output of 3.6 to 9.6 litres per minute. Throughout this range, a mean aortic pressure of 95 mm Hg [12.5 kPa] is maintained by adjusting the variable peripheral resistance. (Referring to figure 4.2, note that, in order to maintain consistency with a previous testing protocol, waveform 00 is not incorporated in the standard testing conditions). The servo-controlled pump acts as a pure flow generator in the sense that, at a given test setting, the same forward flow waveform is generated irrespective of the nature of the valve under investigation, but the pump also effectively operates in a constant pressure mode in that, for a given valve, the mean aortic pressure is constant irrespective of 'cardiac output'. Notice that although mean aortic pressure is maintained at a constant value with increasing 'cardiac output', peak systolic aortic pressure increases and minimum diastolic aortic pressure remains relatively unchanged, which is similar to the physiological response (Ganong, 1981).

## 4.4 Instrumentation

Valve movements can be recorded either using a video camera (Panasonic AI) or with synchronised flash photography. The video camera system allows still frames to be viewed at 20 millisecond intervals. For synchronised flash photography, the data acquisition program generates a trigger signal for an electronic flash gun (a stroboscope is actually used) with a user-defined time delay; the time delay can be any integral multiple of the analog-digital sampling period, typically 1 millisecond. There are valve viewing ports downstream of both the aortic and mitral valves.

There are 7 transducers monitoring the GRI pulse duplicator. Pressures in the aortic, atrial and ventricular chambers are recorded using wall-mounted blood pressure transducers (Elcomatic EM751), while a

differential transducer (Gaeltec 3CT special) measures the pressure drop across the valve under investigation. The pressure signals are amplified and offset (Elcomatic EM724) to provide suitable input for the data acquisition system. Flow downstream from the mitral or aortic valve is measured using an electromagnetic flow meter (Gould Statham SP2201) with a cannulating type flow probe, 26 mm in diameter. The pump has 2 in-built transducers for monitoring the piston displacement and velocity.

The pressure transducers are calibrated with a static head of mercury or oil. The flow transducer calibration is checked by connecting the probe directly to the pump by a short length of rigid tubing and comparing the flow signal with the pump displacement or velocity signal. The pump has a facility for calibrating its displacement transducer by entering a known displacement step. The transducer zeros are checked immediately prior to each test run.

### 4.4.1 Flow meter frequency response

The data acquisition software has procedures for analysing the harmonic composition of averaged transducer waveforms. This facility has been used to look at the frequency response of the electromagnetic flow meter. As when checking the flow meter gain, the pump was directly coupled to the flow probe. A square wave, from a signal generator, was used as the pump velocity input signal and the flow meter response was compared with the pump tachometer output (or the differentiated pump displacement signal). The measured relative amplitude and phase are plotted as functions of frequency in figure 4.3; for comparison, a typical flow waveform and associated energy spectrum measured downstream from a Björk-Shiley plano-convex valve are shown in figure 4.4.

The amplitude response falls to -3 dB at approximately 10 Hz and is greater than -6 dB at

Figure 4.3 Flow meter frequency response

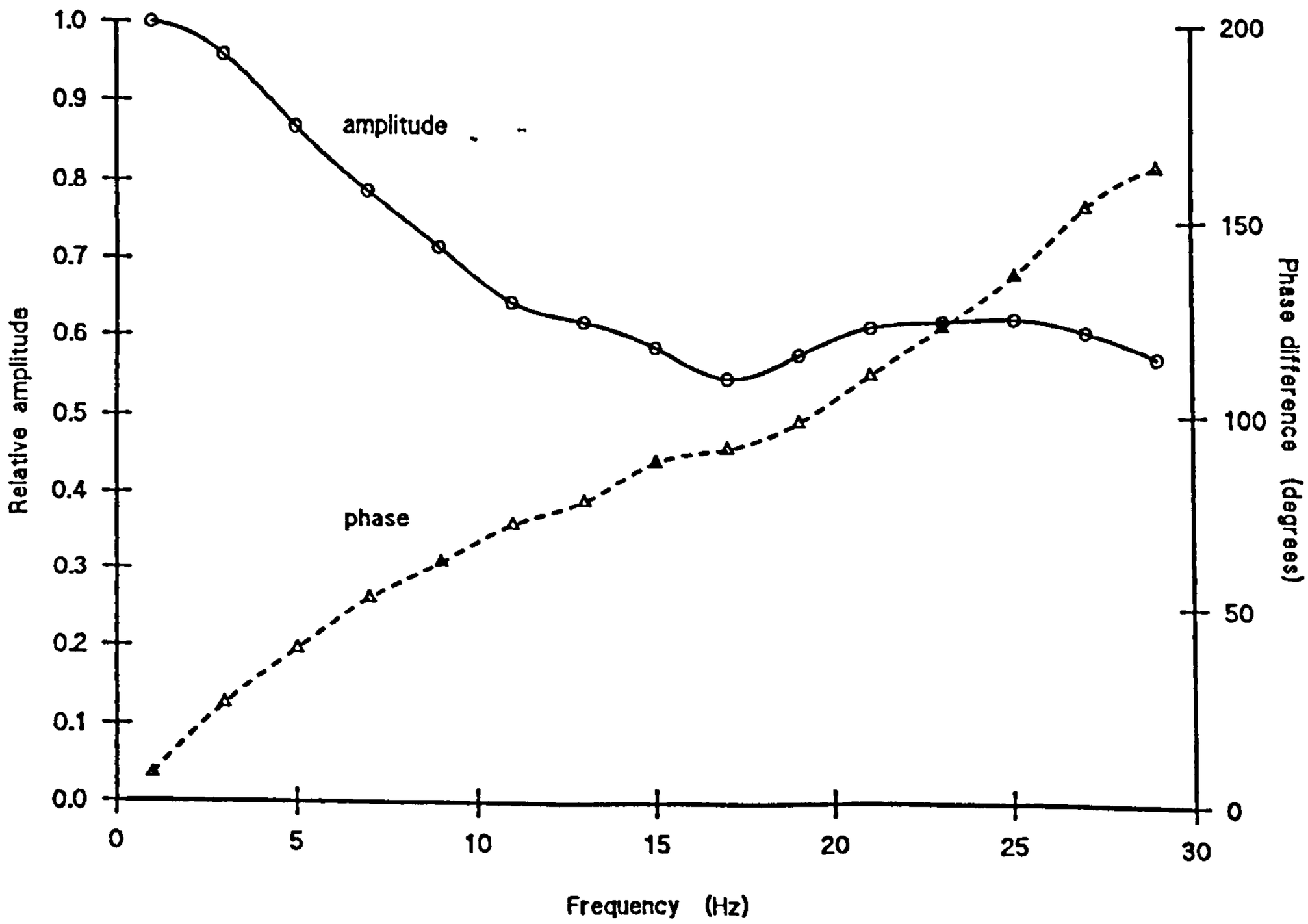

**Figure 4.4 Typical (mitral) flow waveform and associated power distribution for tilting disc valve**

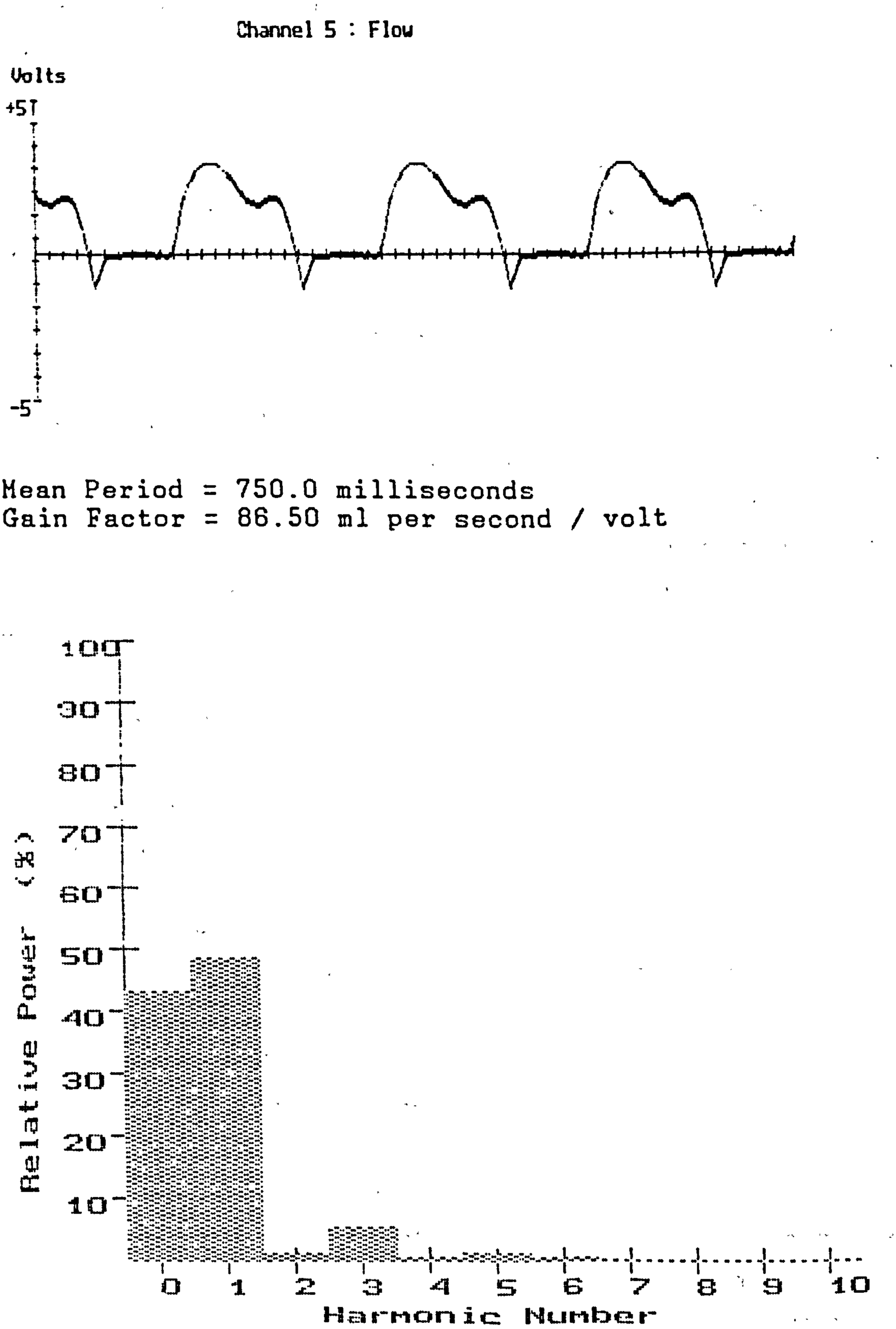

frequencies up to 30 Hz. Typically, 99% of the energy associated with the flow signal is contained within the first 8 harmonics, similar to the case in humans (Nichols *et al*, 1977). Thus, the flow meter amplitude response was considered to be adequate. However, the approximately linear phase shift with frequency is more significant. As can be seen in figure 4.3, the first harmonic of the flow meter signal lags that of the pump signal by approximately 7°; this has been accounted for in the data acquisition software by advancing the averaged flow waveform in time by the appropriate amount.

The frequency response measured with the flow probe *in situ* (i.e. downstream from a fixed-open valve port in the pulse duplicator, with the other valve port blocked off) was slightly different due to capacitive effects in the fluid circuit between the pump piston and the probe. In particular, it is difficult to remove small air pockets which tend to gather in the flow straightener section (a honeycomb of straws) upstream from the aortic valve.

### 4.4.2 Pressure transducer frequency response

A sinusoidal fluid pressure generator, similar to that described by Foreman & Hutchison (1970) was used to measure the frequency response of the pulse duplicator pressure transducing system. The transducing system includes a column of fluid which separates the pressure transducer diaphragm from the site of pressure measurement, and it is this length of fluid which limits the system response. The pressure generator comprises a sealed fluid chamber closed at one end by an acetate diaphragm; an electromagnetic vibration generator (Ling 201), driven by a 30 watt power amplifier with sinusoidal input of variable frequency and magnitude, is attached to the diaphragm (fig 4.5). The amplifier input was manually adjusted to generate constant amplitude pressure

Figure 4.5 Schematic variable-frequency sinusoidal pressure generator

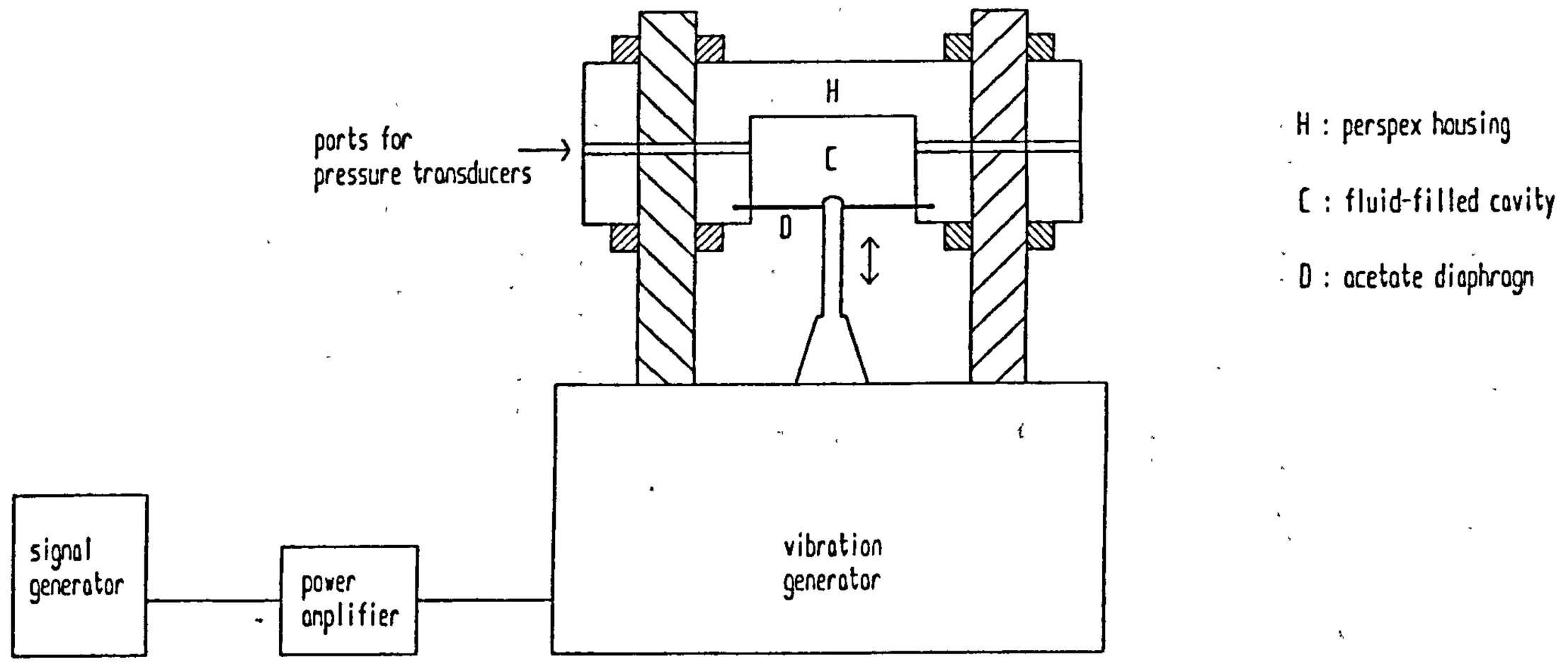

oscillations, as measured on a reference pressure transducer, over a range of frequencies. The pressure transducer under investigation was connected to the fluid chamber using the same connectors as used in the pulse duplicator. A catheter tip pressure transducer (Gaeltec 16CT or Millar Mikro Tip PC-350A), located at the site of wall pressure measurement, was used as the reference transducer. The relative magnitude and phase frequency response was read off an oscilloscope.

At frequencies up to 150 Hz, the Elcomatic transducing system (transducer diaphragm enclosed within a hemispherical rigid dome, connected to the fluid chamber via a 3-way tap) behaves like a simple harmonic oscillator with a single degree of freedom, implying that the transducer diaphragm behaves as a massless linear spring and represents the lumped compliance of the system. All 3 transducers had resonant frequencies above 100 Hz; a typical response is shown in figure 4.6.

The free vibration frequency of such a hydraulic system, with transducer diaphragm stiffness E (change in pressure per unit change in volume, Newton·metres$^{-5}$) can be calculated from (Clark, 1985):

$$f_o = (1/2\pi)(E/I)^{1/2} \qquad (4.1)$$

where I is the total fluid *inertance* between the transducer diaphragm and the measuring site. For a fluid tube with radius r which varies along its length l, the inertance is given by:

$$I = (\rho/\pi) \int_0^l 1/r^2 \, dx \qquad (4.2)$$

where x is the distance along the tube axis and $\rho$ is the fluid density. An order of magnitude calculation, based on equation 4.1, results in a resonance frequency of the same order as that found experimentally; a more

Figure 4.6 Ventricular pressure transducer frequency response

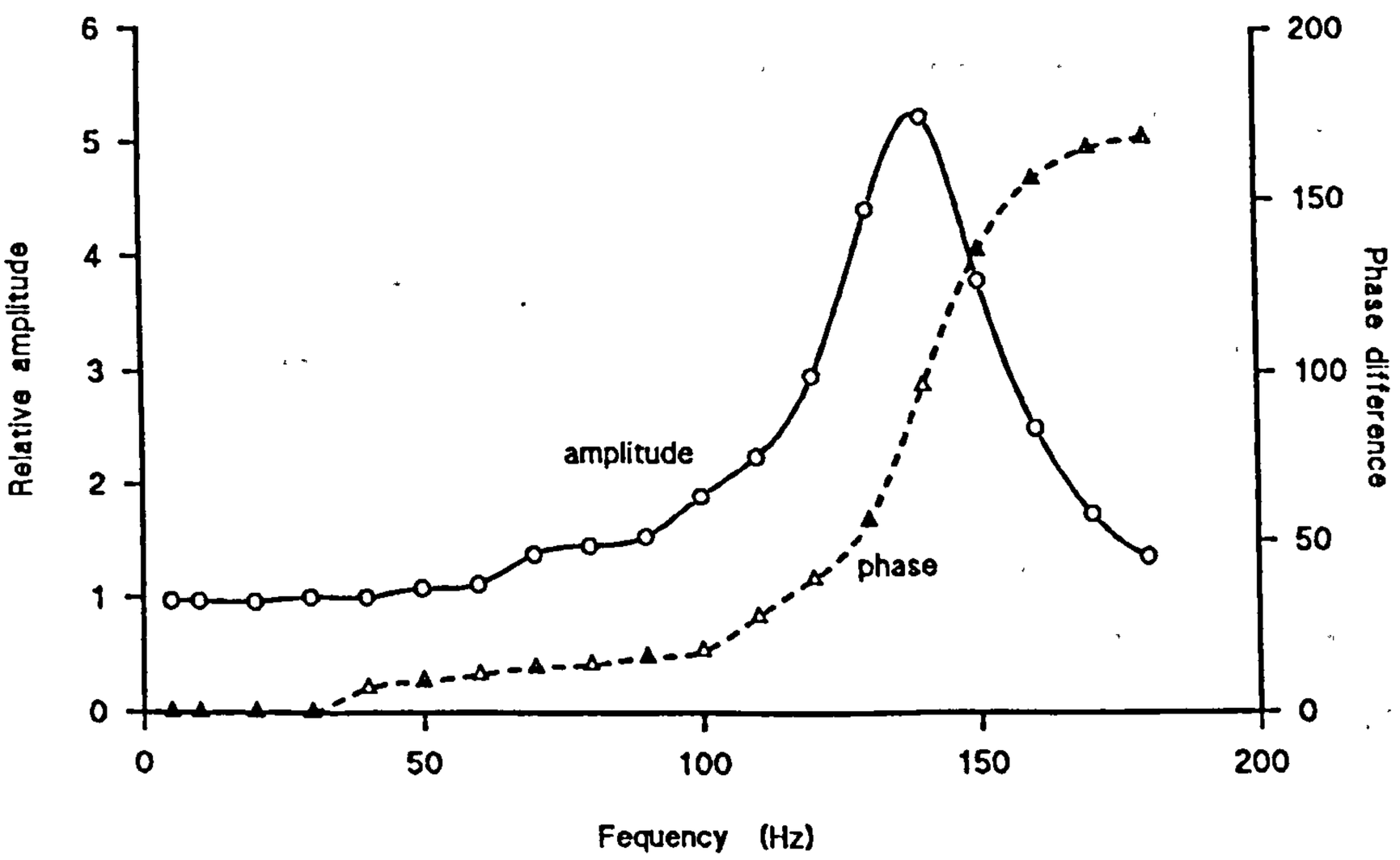

precise calculation is not justified since the transducer diaphragm stiffness is unknown. (The manufacturer quotes a volume displacement of < 0.003 $mm^3$ per 100 mm Hg [13.2 kPa], however the transducers were several years old and it not known how the diaphragm stiffness varies with age and use).

The frequency response measurements were found to be particularly sensitive to air bubbles accidentally entrapped in the system. The column of fluid coupling the transducer to the measuring site has several abrupt changes in cross-sectional area along its length and it is tricky to remove all the air bubbles. By deliberately introducing an air bubble, of approximate radius 1 millimetre, the resonance frequency fell from 120 Hz to 55 Hz. For the abiabatic expansion-contraction of an air bubble, the pressure-volume relation is $pV^{1.4}$ = constant, and the bubble stiffness is given by $dp/dV = 1.4p/V$, which at atmospheric pressure is $3.3 \times 10^{13}$ $Nm^{-5}$. This is considerably smaller than the stiffness of the transducer diaphragm (0.003 $mm^3$ per 100 mm Hg [13.2 kPa] is equivalent to a stiffness of $4.4 \times 10^{15}$ $Nm^{-5}$).

The differential pressure transducing system comprises a transducer diaphragm, each side of which is connected to the pressure measuring site by a length of stiff plastic tubing and a 3-way tap. To measure its frequency response, one arm of the transducer was connected to the pressure generator and the other was left open to atmospheric pressure. The response up to 180 Hz is shown in figure 4.7. The transducer response did not show resonance in this frequency range, but both the amplitude and phase increased approximately linearly with increasing frequency. Note the break in the graph around 90 Hz. This is because at 90 ± 10 Hz the response was nonlinear; that is to say, for a sinusoidal pressure input the transducer output signal was a rather distorted sine wave. Also, above 150 Hz the output signal was a rather skewed sine wave. The nonlinearities may be due to

Figure 4.7 Differential pressure transducer frequency response

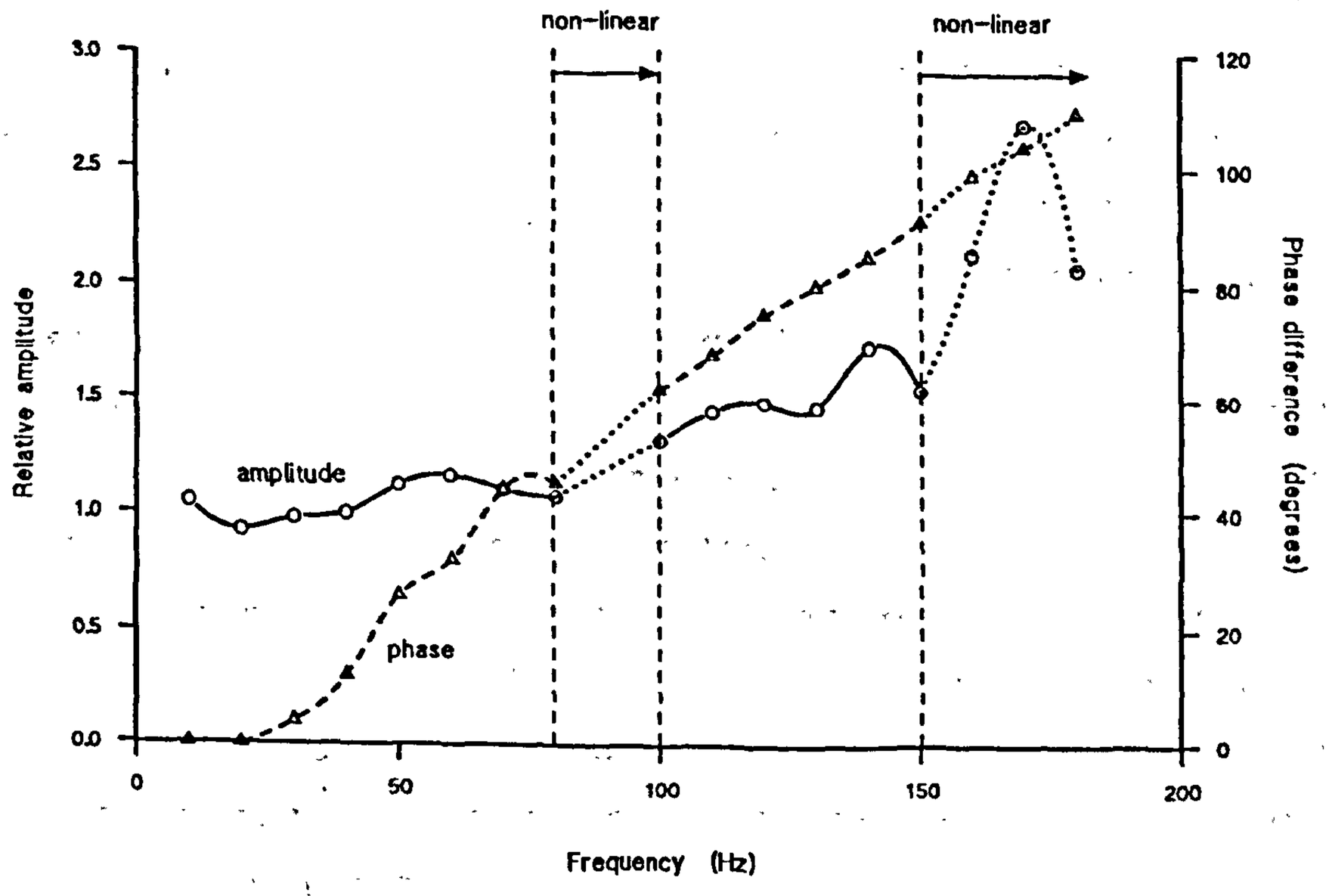

some dynamic interference with the other transducer arm or, perhaps, due to compliance associated with the plastic tubing of the transducer arm. As the length of tubing separating the transducer diaphragm and the pressure measurement site increases, so the effects of distributed compliance increase, the system behaves less like a lumped compliance model and nonlinear behaviour is introduced (Clark, 1985).

A typical, averaged ventricular pressure waveform and its associated energy spectrum, measured in the pulse duplicator with mechanical valves in both the mitral and aortic positions, are shown in figure 4.8. Typically, more than 99% of the energy associated with the pulse duplicator pressure signals is contained within the first 20 harmonics. Patel *et al* (1965) found a similar result in humans. On this basis, the frequency responses of the transducers are adequate and further signal processing in the data acquisition software is not necessary.

The pressure transducer frequency response was also investigated *in situ*, by a method similar to that used for the flow meter, with the catheter tip transducer, rather than the pump tachometer, acting as the reference. The catheter tip transducer was located at the point of wall pressure measurement and the pressure signals were recorded with the pulse duplicator operating in one of its standard testing modes. In an attempt to excite as many harmonics as possible, a range of pump velocity input waveform shapes were tried (square wave, triangular wave, etc), but the standard waveforms were found to be equally effective. The data acquisition software calculated the harmonic compositions of the catheter tip and pulse duplicator pressure transducers; by comparing the signals, frequency responses similar to those obtained by the pressure generator method were found. However, the magnitudes of the higher harmonics are very small and above 100 Hz they begin to merge with the background noise. Also, nonlinearities associated with

**Figure 4.8 Typical ventricular pressure waveform and associated power distribution for tilting disc valve**

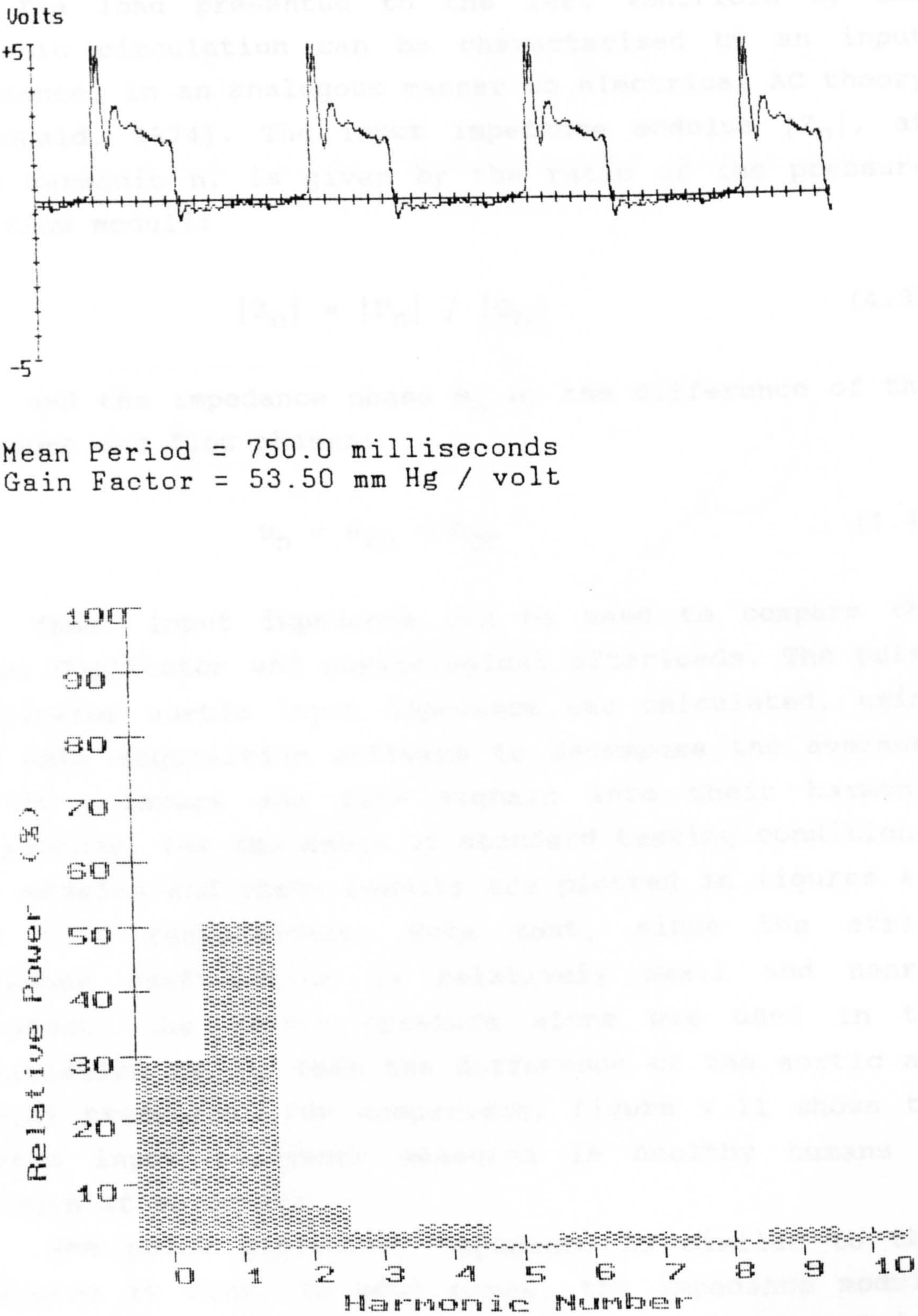

the differential transducer are not exposed with this method. Therefore, it was concluded that the pressure generator method was better.

## 4.5 Aortic Input Impedance

The load presented to the left ventricle by the systemic circulation can be characterised by an input impedance, in an analogous manner to electrical AC theory (McDonald, 1974). The input impedance modulus $|Z_n|$, at each harmonic n, is given by the ratio of the pressure and flow moduli:

$$|Z_n| = |P_n| \; / \; |Q_n| \qquad (4.3)$$

and the impedance phase $\theta_n$ by the difference of the pressure and flow phases:

$$\theta_n = \theta_{Pn} - \theta_{Qn} \qquad (4.4)$$

Thus, input impedance can be used to compare the pulse duplicator and physiological afterloads. The pulse duplicator aortic input impedance was calculated, using the data acquisition software to decompose the averaged aortic pressure and flow signals into their harmonic components, for the range of standard testing conditions. The modulus and phase results are plotted in figures 4.9 and 4.10 respectively. Note that, since the atrial pressure contribution is relatively small and nearly constant, the aortic pressure alone was used in the calculation rather than the difference of the aortic and atrial pressures. For comparison, figure 4.11 shows the aortic input impedance measured in healthy humans by Nichols *et al* (1977).

The pulse duplicator impedance is similar to that measured *in vivo*. In both cases, the impedance modulus drops abruptly from a large value at dc to a minimum

Figure 4.9 Aortic input impedance (amplitude) for GRI pulse duplicator

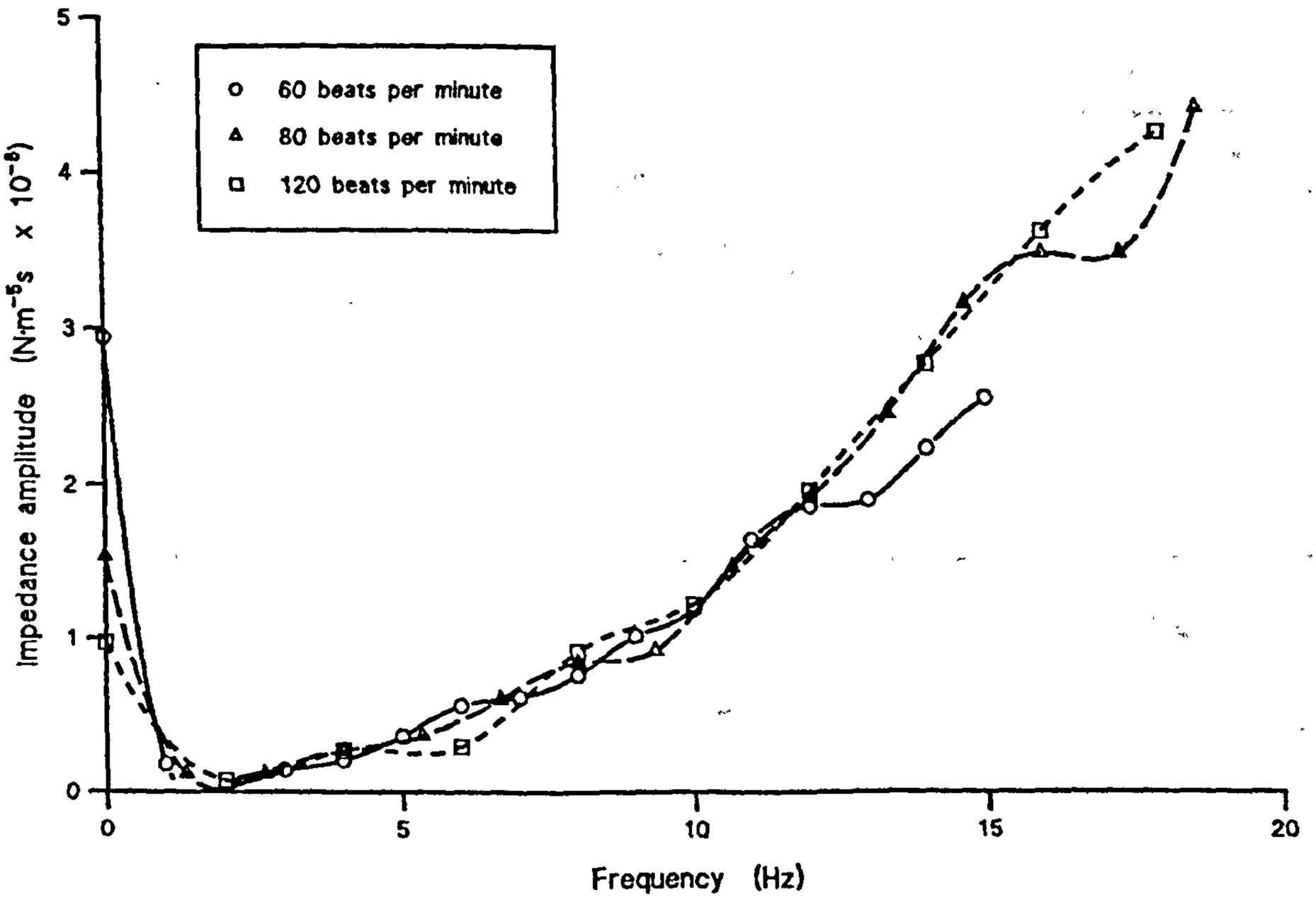

Figure 4.10 Aortic input impedance (phase) for GRI pulse duplicator

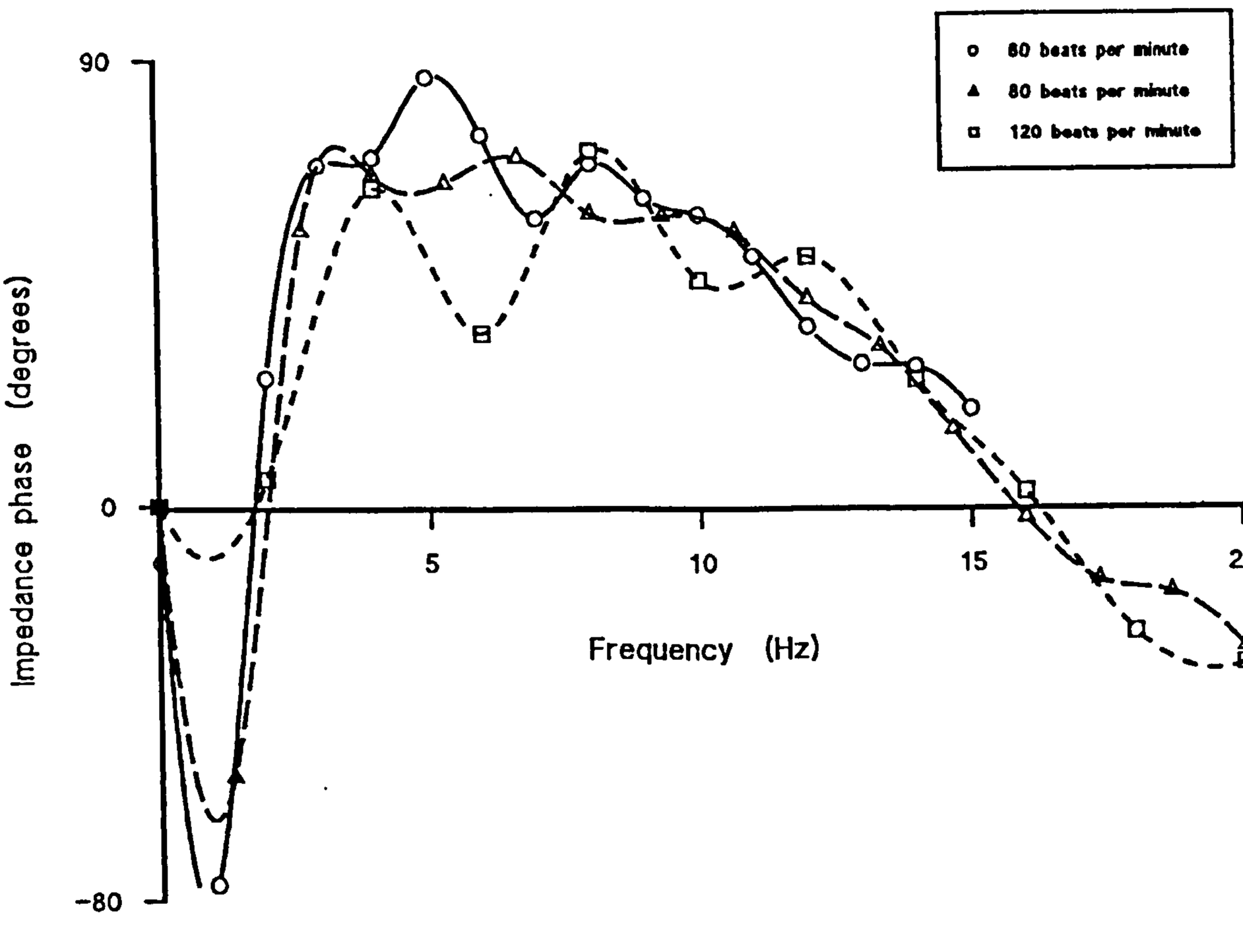

Figure 4.11 Mean aortic input impedance of 5 healthy humans (from Nichols *et al*, 1977)

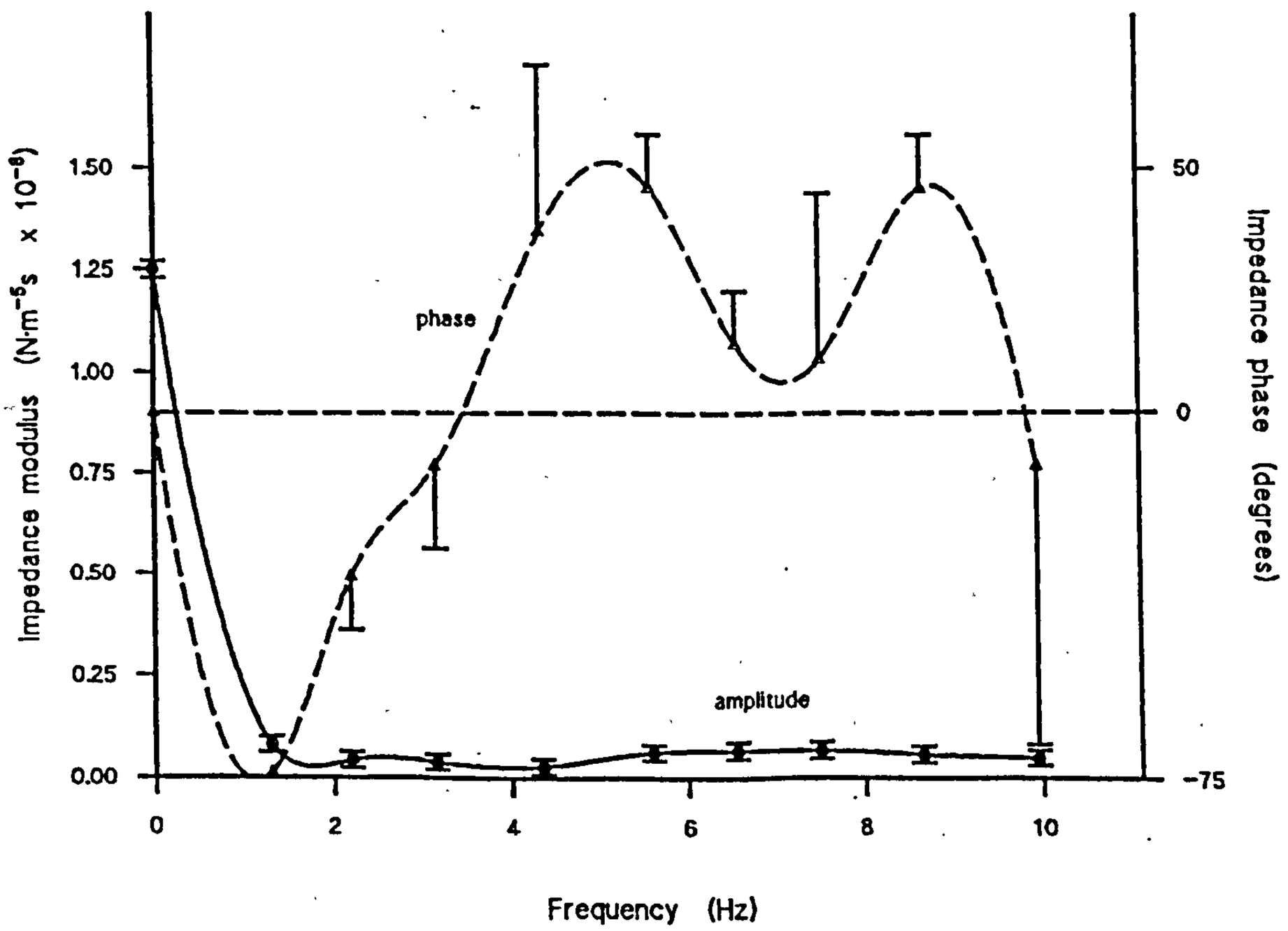

value and then proceeds to increase slowly, and the impedance phase is initially negative (flow leading the pressure) and increases to become positive, crossing zero in the vicinity of the modulus minimum. The pulse duplicator modulus minimum occurs at a lower frequency and is rather more pronounced than is the case *in vivo*, correspondingly the gradient of the impedance phase at the zero cross-over is much larger for the pulse duplicator. This discrepancy probably results from the greater fluid inertia in the *in vitro* model (the volume of fluid enclosed within the ventricular chamber of the pulse duplicator is approximately 800 ml). At low frequencies the capacitive effects of the arterial walls (*windkessel*) dominate the impedance response, as the frequency increases the fluid inertial effects become more important. The impedance modulus (and phase to a lesser extent) measured in the pulse duplicator varied only slightly with 'cardiac output' (figs 4.9 & 4.10). The decrease in 0 Hz impedance modulus with increasing 'cardiac output' reflects the changes made in peripheral resistance in order to maintain a mean aortic pressure of 95 mm Hg [12.5 kPa]. That the impedance moduli (other than the 0 Hz term) are rather insensitive to 'cardiac output' suggests the impedance is dominated by reactive components.

There are few reports in the literature of pulse duplicator aortic input impedance; presumably, most investigators settle for a qualitative inspection of the flow and pressure signals in order to establish how well the model represents the physiological environment (Scotten *et al*, 1979). Westerhof *et al* (1971) and Cornhill (1977) used similar 3-parameter afterload models and both reported calculated input impedances consistent with *in vivo* data. Also, Martin & Black (1976) calculated input impedance moduli for their afterload with 2 lumped capacitances and found good agreement with *in vivo* results. The input impedances calculated by these authors

are a closer match to the physiological response than are those presented in figures 4.9 & 4.10, probably because of less fluid inertia in their pulse duplicators.

## 4.6 Accelerated Fatigue Testing

The durability of flexible leaflet valves is of major concern, however *in vitro* fatigue testing has received relatively little attention in the literature as compared with hydrodynamic characterisations of valves. The time scales involved necessitate accelerated fatigue testing as a practicable means of assessing valve durability *in vitro*. Accelerated fatiguing of strips of leaflet material alone has been performed (Broom, 1978; Hayashi, 1987), but such results are difficult to interpret in terms of valve durability due to the complex loading and displacements involved in opening and closing a valve. A variety of whole valve accelerated fatigue testers have been used, most involve high-frequency pulsing of fluid through stationary valves (Clark *et al*, 1978; Chetta & Lloyd, 1980; Reul, 1983; Gabbay *et al*, 1984 & 1988). Note that Yu *et al* (1987) have proposed 2 accelerated fatigue tests in which they attempt to consider the effects of mechanical loading on the closed valve separately from the open valve: the first test involves pulsing air (0-450 mm Hg [0-59.2 kPa], at 20-40 Hz) against the outflow aspect of a closed valve, while in the second a high pressure air jet is directed through an open valve from the inflow side causing the valve to flutter at 1000-1500 Hz.

The system used at the GRI, and other centres (Nugent *et al*, 1984), is the commercially available Rowan Ash accelerated fatigue tester (Black, 1973; Martin *et al*, 1980). An electromagnetic vibrator, driven by a power amplifier of variable sinusoidal frequency and magnitude output, oscillates up to 6 valves through stationary columns of fluid; a valve compartment is shown in figure

4.12. Pushing the valve upwards closes the valve and forces fluid around the recirculation tube, the valve then opens when pulled downwards. Valve displacement can be adjusted by altering the amplifier output to allow full opening of the valves, the closing pressure can then be set by adjusting the variable resistance on the recirculation tube. The pressure drop across the valve is measured with a differential transducer (Gaeltec 3CT special), the frequency response of which was discussed in section 4.4.2. A computerised data acquisition system, described in the following chapter, displays the 'raw' or averaged pressure signal; the averaged waveform may then be filtered if desired. A typical averaged differential pressure waveform and its associated energy spectrum are shown in figure 4.13. (Note that figure 4.13 shows 3 identical averaged waveforms and the apparent 'noise' is actually standard deviation error bars drawn at each averaged point, as described in Chapter 5). From the distribution of energies, it can be seen that the transducer has an adequate frequency response for this application (fig 4.7). Valve motion can be directly visualized with a stroboscope triggered by the Rowan Ash drive unit; alternatively, the stroboscope can be triggered (single flash) by the data acquisition system to allow valve photography.

As with valve function tests, there is considerable variation in test apparatus and methods. For example, Clark *et al* (1978) ran their fatigue tester at 37°C whereas others operate at room temperature. Hayashi (1987) has shown that dynamic stress relaxation in polyurethane can increase by 15% upon increasing the ambient temperature from 24 to 37°C. Reul (1983) uses a glycerol solution as the test fluid whereas others use a glutaraldehyde solution. Clark *et al* (1978) reported no difference in cycles to wear for mechanical valves fatigued in water and in a solution with viscosity similar to blood, but Mohri *et al* (1973) found that using

Figure 4.12 Schematic valve compartment in fatigue tester

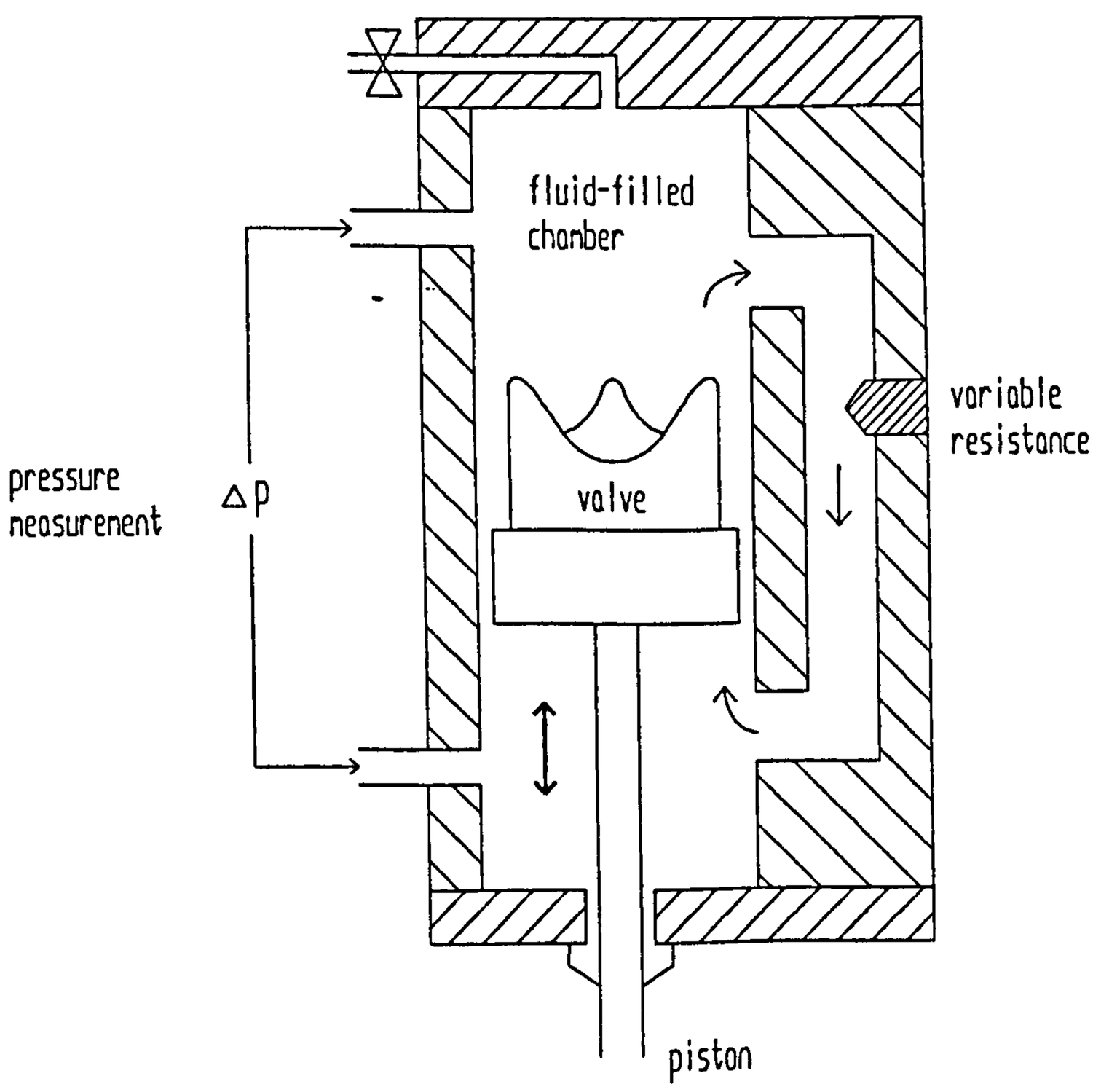

Figure 4.13 Typical differential pressure waveform and associated power distribution for tri-leaflet polyurethane valve in fatigue tester

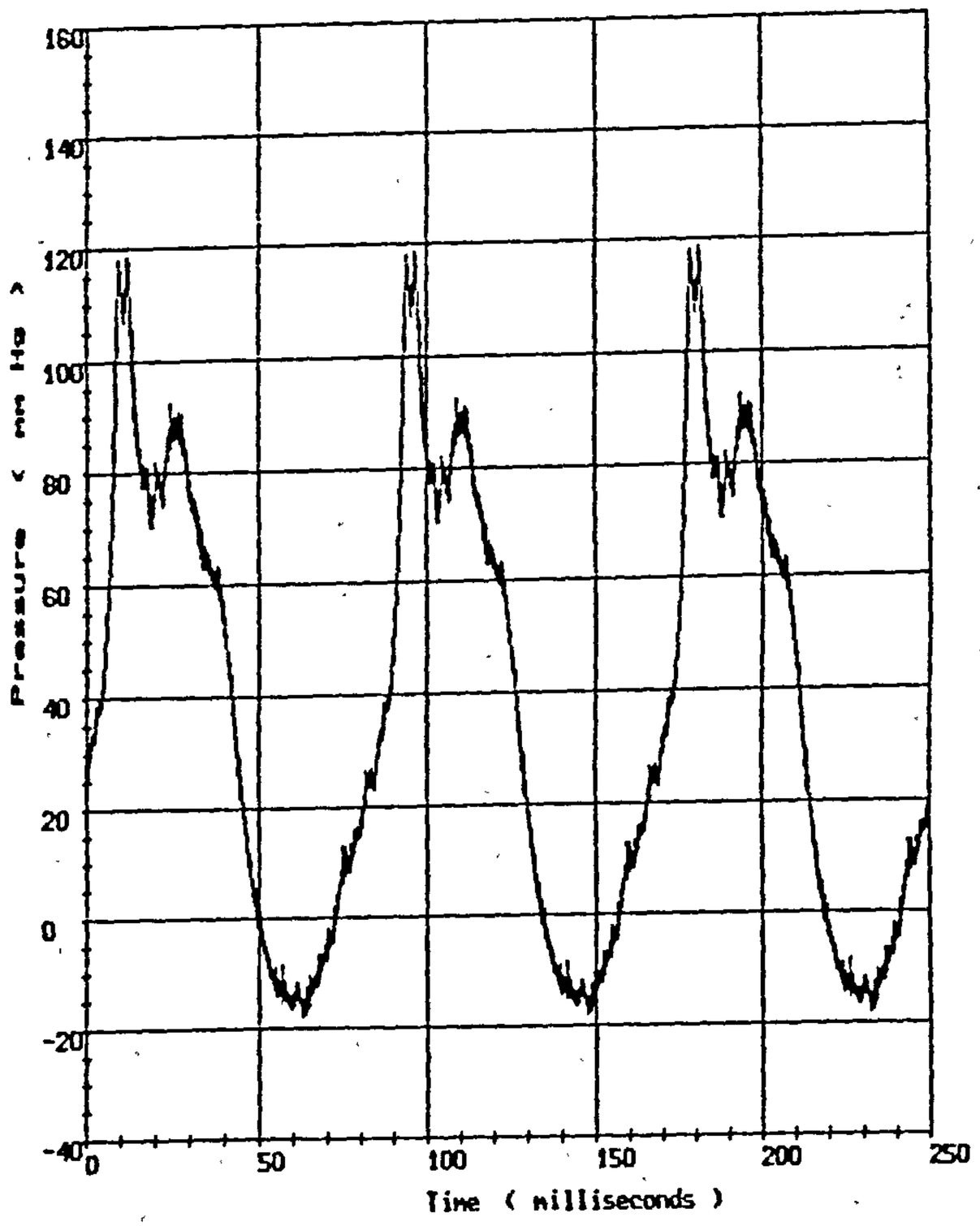


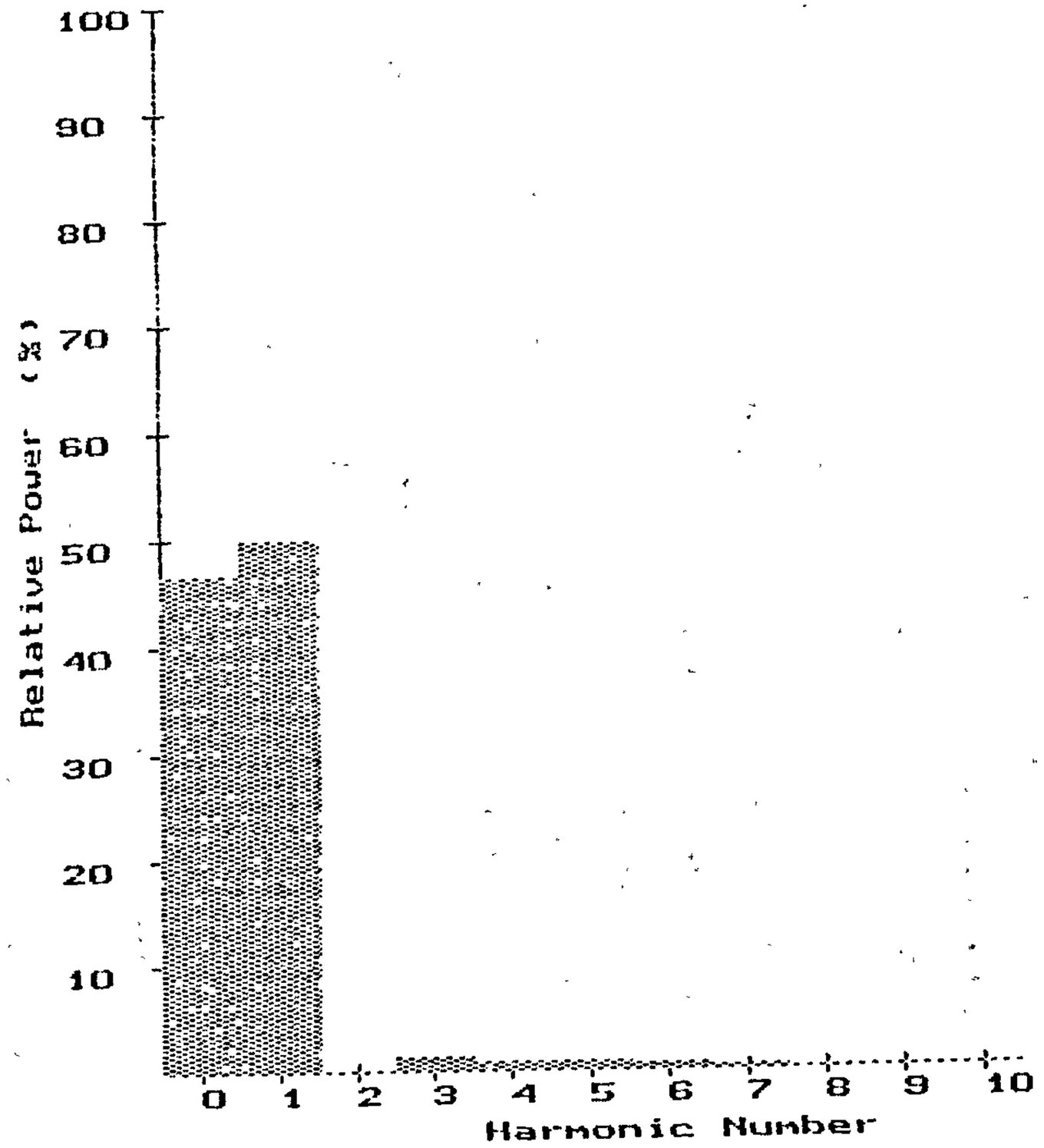

a more viscous fluid for their fatigue tests increased the durability of their synthetic leaflet valves. Comparing polyurethane strips fatigued in saline and a cholesterol-lipid solution, Hayashi (1987) found 13% more dynamic stress relaxation with the cholesterol-lipid solution. A range of operating frequencies have been used; presumably the highest frequency at which the valve fully opens and closes is used in each case. Black (1973) achieved a maximum rate of 125 Hz with synthetic leaflet valves, but lower frequencies are more usual: 12 Hz (Reul, 1983; Wheatley *et al*, 1987), 13 Hz (Nugent *et al*, 1984), 17 Hz (Mohri *et al*, 1973), 20 Hz (Martin *et al*, 1980), 21 Hz (Chetta & Lloyd, 1980), 23 Hz (Gabbay *et al*, 1988), 30 Hz (Gabbay *et al*, 1984), 33-35 Hz (Mohri *et al*, 1973; Clark *et al*, 1978). Broom (1977) found little difference in load/extension curves for fixed mitral valve tissue cyclically loaded at 1 Hz and 35 Hz, but Hayashi (1987) found that polyurethane cycled at 0.8 Hz showed 25% more dynamic stress relaxation than when cycled at 5 Hz. Also, valve leaflet motion is rather different at accelerated rates from that at physiological rates (Wheatley *et al*, 1987). Gabbay *et al* (1984) reported that lowering the test rate from 30 Hz to 17 Hz resulted in pericardial valves lasting 2-3 times longer before failing; similar behaviour was displayed by the prototype silicone rubber valves of Mohri *et al* (1973). Clearly, there is a necessity to standardize accelerated fatigue testing procedures to allow meaningful comparisons to be made.

The prediction of *in vivo* durability from *in vitro* accelerated fatigue lifetimes is rather speculative since biological, as well as mechanical, factors determine how quickly a valve fails. Further, the valvular displacements and loading at high frequencies may not be representative of those at physiological rates. After Nugent *et al* (1984), the most useful applications of accelerated fatigue testing are: identification of modes

of mechanical failure; isolation of design, material or manufacturing flaws; and comparison of different valve types under identical conditions. Several investigators have described failure modes induced by accelerated fatigue testing which are similar to those found *in vivo*, particularly for pericardial valves. Such a failure mode is the leaflet tearing in the vicinity of the commissures, along the line of the frame edge; the tear may be caused by the leaflet abrading against the cloth-covered frame (Gabbay *et al*, 1984 & 1988; Wheatley *et al*, 1987), stress concentrations associated with the holding suture at the commissures (Trowbridge *et al*, 1988), and the compressive forces associated with bending (Broom, 1978). Based upon the results of accelerated fatigue testing and the examination of failure modes in explanted valves, Fisher & Wheatley (1987) were able to design a pericardial bioprosthesis with improved durability. The Glasgow valve incorporated a pericardium-covered inner frame which reduced leaflet abrasion and bending stresses along the frame edge.

Although similar patterns of failure have been observed in fatigue tested valves and explanted valves, the number of cycles required to cause failure are generally longer *in vivo* than *in vitro*. Wheatley *et al* (1987) suggested that the effects of abrasion are lessened *in vivo* due to host tissue ingrowth observed on cloth-covered frames; Gabbay *et al* (1988) did not find such tissue ingrowth. Trowbridge *et al* (1988) compared the extensibilities of unimplanted and implanted fixed pericardial tissue and found the implanted tissue considerably stiffer and thicker. On this basis they proposed that *in vitro* accelerated fatigue testing might overestimate *in vivo* durability of bioprostheses, but this suggestion is at variance with the reported findings.

As well as host tissue ingrowth, a number of biological factors influence bioprosthesis durability *in*

*vivo*, the most prominent being leaflet calcification. A recent innovation by Bernacca *et al* (1992a) offers the potential for including the effects of calcification in accelerated fatigue testing. Bernacca *et al* demonstrated *in vitro* calcification of pericardial valves in accelerated fatigue tests, using salt solutions with physiological concentrations of calcium and phosphate as the test medium. The mechanism of the calcification and its rate of proliferation may not be the same as in the physiological environment, but calcium deposits were observed in similar locations as found in explanted valves and this method could be most useful in a comparative study of valve durability.

## 4.8 Summary

The methods used for the *in vitro* evaluation of valve function and durability at the GRI have been described. They represent a compromise between a detailed simulation of the complex physiological environment and what is practicable. The pulse duplicator is capable of reproducing near physiological volumetric flows and reflects the principal features of the arterial input impedance. Accelerated fatigue testing is performed with the commercially available Rowan Ash tester which can provide a useful indicator of valve durability in response to cyclic mechanical loading. These testing facilities are most useful in comparative studies between different valve types; absolute evaluations should be interpreted with caution.

# Chapter 5. Software for Valve Testing

## 5.1 Introduction

In recent years, digital computers have been used increasingly in both the laboratory and clinical assessments of prosthetic heart valves. Advances in technology have facilitated improved methods of data acquisition and computerized control systems.

Early pulse duplicators relied on oscilloscopes and chart recorders to monitor pressure and flow signals (Olin, 1971; Reul *et al*, 1972; Black, 1973). Mean values, effective orifice areas (EOA's), or energy losses were found using analog computation methods (Swanson & Clark, 1977a; Wright, 1979; Yoganathan, 1979) or, alternatively, pressure and flow signals were manually digitised and the calculations performed electronically (Gabbay *et al*, 1978). More recently, computerised data acquisition systems have been used with pulse duplicators (Mohnhaupt *et al*, 1975; Walker *et al*, 1983; Chandran *et al*, 1984; Yoganathan *et al*, 1984; Reul *et al*, 1986; Arabia *et al*, 1989), fatigue testers (Nugent *et al*, 1984), and in the study of valve haemodynamics (Murgo *et al*, 1977; Kawachi *et al*, 1985; Paulsen *et al*, 1988a).

Progressing from passive data acquisition, in the pulse duplicators described by Martin *et al* (1981) and Leefe *et al* (1986), the computer also provides the input signal for the velocity servo-system driving the pump piston. This development, to a computer-controlled closed system, is potentially very powerful. Perhaps a closer approximation to the ventricular pumping action may be achieved by using the pressure and flow signals in feedback loops to control piston movements.

This chapter describes software which was developed to enhance existing valve testing facilities: the GRI pulse duplicator and the Rowan Ash fatigue tester. The previous pulse duplicator software (MacDonald *et al*,

1986), which performed a data acquisition function based on an Apple II micro-computer with an 8-bit analog-digital converter (ADC), has been replaced by an improved system. The new system performs similar data acquisition tasks but with an increased ADC bit resolution, increased graphics resolution, and operates much faster. Additionally, digital filtering methods have been introduced. The new system incorporates a digital-analog converter (DAC) which is used to enable the computer to provide the input velocity waveform for the pump; the pump input signal was previously generated by a programmable waveform generator (Fisher *et al*, 1986). This feature allows greater flexibility in selecting pump velocity waveforms. The new system further uses the DAC to synchronise valve photography with flow or pressure signals. The new pulse duplicator data acquisition program has also been adapted for use on the Rowan Ash accelerated fatigue tester.

## 5.2 Specifications

Two programs have been developed : PULSEDUP performs data acquisition and controls the pump and photography timing on the pulse duplicator, and FATIGUE similarly carries out data acquisition and controls photography timing with the fatigue tester. The programs are based around a specific ADC/DAC board (PC-30A, Amplicon LiveLine Ltd.) and should run on any IBM PC or compatible, with VGA graphics, running DOS 3.30 or later; the pulse duplicator presently operates with a Dell 210 PC. The procedures used for generating graphical printouts are specific to the Epson LX-800 dot matrix printer. Both programs have been written entirely in Borland Turbo Pascal 5.0; the executable code for PULSEDUP occupies 112 kilobytes and FATIGUE 54 kilobytes.

The ADC/DAC board provides 16 input channels for a 12-bit ADC, and 4 DAC's : two 12-bit and two 8-bit. A

schematic outline of features relevant to PULSEDUP and FATIGUE is given in figure 5.1. Briefly, a 16 channel multiplexer connects the selected analog channel, via a sample and hold device, to the 12-bit ADC. The ADC is controlled through three 8-bit ports on a programmable peripheral interface (PPI). Sampling is initiated by an interrupt signal, generated on interrupt request line 5, by the PPI. Sampling frequency is selected by programming an on-board timer chip; the timer uses two 16-bit down counters, connected in cascade. The input timing signal has the frequency of the board bus (which is the computer bus frequency divided by 4) and signals are output to the sample and hold device at the programmed sampling frequency. Further details can be found in the board manual. The computer responds to the interrupt request by transferring control to an interrupt service procedure; these can be declared within Turbo Pascal 5.0 using the 'interrupt' directive, without the need for assembly language routines. The general format used in PULSEDUP and FATIGUE for calling interrupt service procedures is given in figure 5.2; such a format is used on every occasion the computer inputs or outputs values using the ADC/DAC board.

## 5.3 Pulse Duplicator Software : PULSEDUP

The requirements made of PULSEDUP are as follows :

(1) Monitor seven transducer signals from the pulse duplicator (3 direct pressures : aortic, atrial, and ventricular; a differential pressure; an aortic or mitral flow signal; pump velocity and displacement signals). Display these signals graphically in real-time and allow their zero and gain values to be checked and/or adjusted.

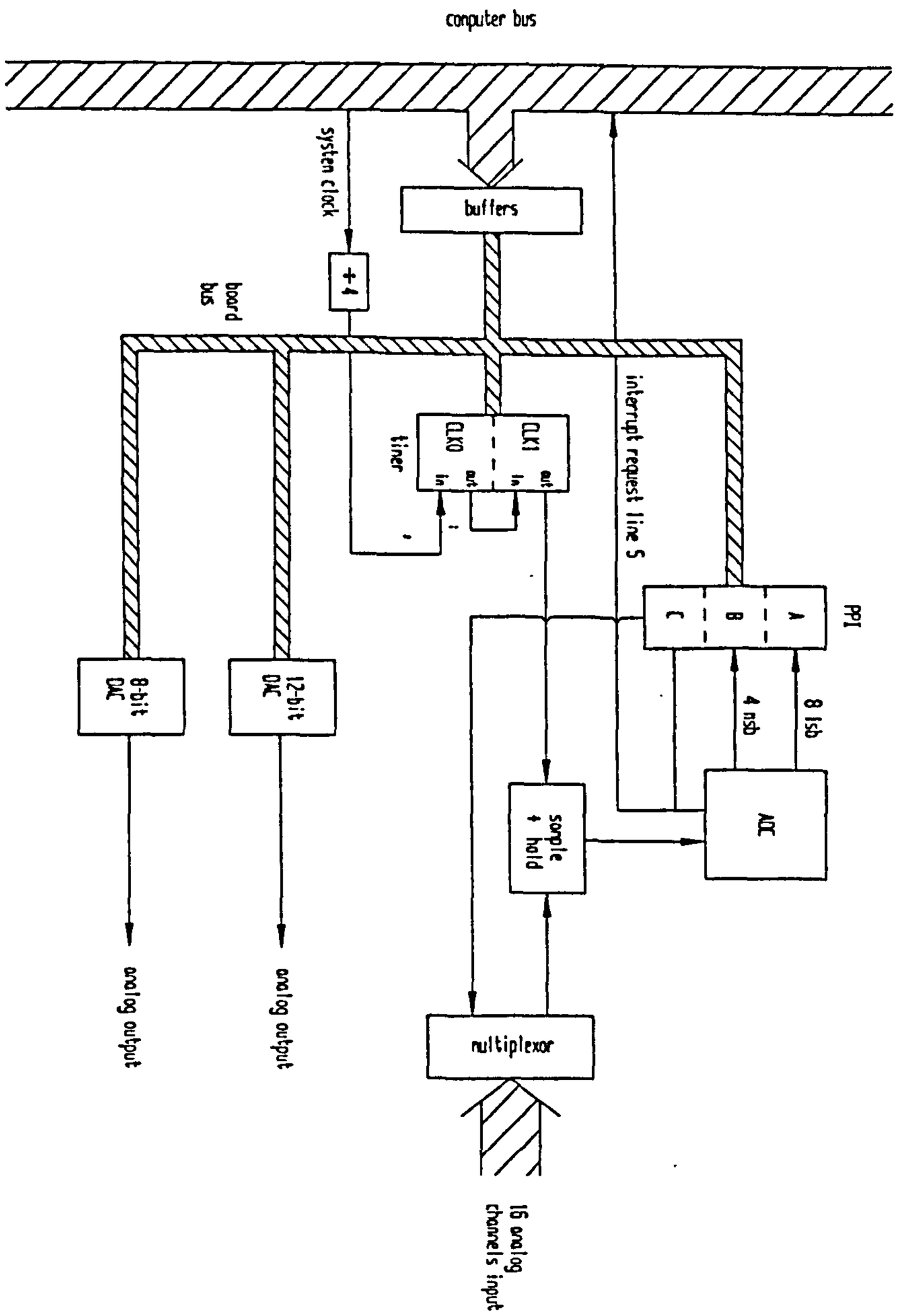


Figure 5.1 Schematic ADC/DAC board

Figure 5.2 General format for calling interrupt procedures as used in PULSEDUP and FATIGUE

```
VAR  vector   :  pointer;

     GetIntVec($0d,vector);      { returns the address of
                                   interrupt vector $0d
                                   in vector }

     SetIntVec($0d,@interrupt_5);

                                 { points interrupt vector
                                   $0d to the address of
                                   the interrupt handler
                                   PROC. INTERRUPT_5 }

     Disable_IRQ(0);             { user-defined procedure to
                                   disable the internal
                                   clock interrupt }

     Enable_IRQ(5);              { user-defined procedure to
                                   enable interrupt
                                   request line 5 }


{ PROC. INTERRUPT_5 called when interrupt request
  reaches CPU }


     Disable_IRQ(5);             { disables interrupt request
                                   line 5 }

     Enable_IRQ(0);              { enables internal clock
                                   interrupt }

     SetIntVec($0d,vector);      { points interrupt vector
                                   $0d back to its original
                                   address }
```

(2) Provide the pump velocity signal for the servo-system controlling the pump piston, whilst displaying any 3 of the 7 input signals graphically in real-time.

(3) Provide a trigger signal, at a user-defined instant in the valve's cycle of opening and closing, to initiate valve photography.

(4) Collect data from the seven transducers over a period of time, calculate the average waveforms, and save these on disc.

(5) From the averaged waveforms, calculate the mean pressure difference, the mean and root mean square flows, the volume of fluid displaced, the energy loss and the EOA's, for various time intervals in the cycle.

(6) Display the averaged waveforms and provide graphical printouts of them.

(7) Allow the averaged waveforms to be digitally filtered; the filtered waveforms should be saved on disc to allow their re-input for (5) and (6).

Requirements (1),(4),(5) and (6) are common to the previous data acquisition program.

PULSEDUP can be considered as the sum of four discrete sub-programs: CALIBRATION, DATA ACQUIRE, CALCULATIONS and VIEW DATA; these correspond to modes selectable from a menu. An outline of their inter-communications is given in figure 5.3, and a brief description of each follows.

Figure 5.3 Inter-communications within pulse duplicator software (PULSEDUP)

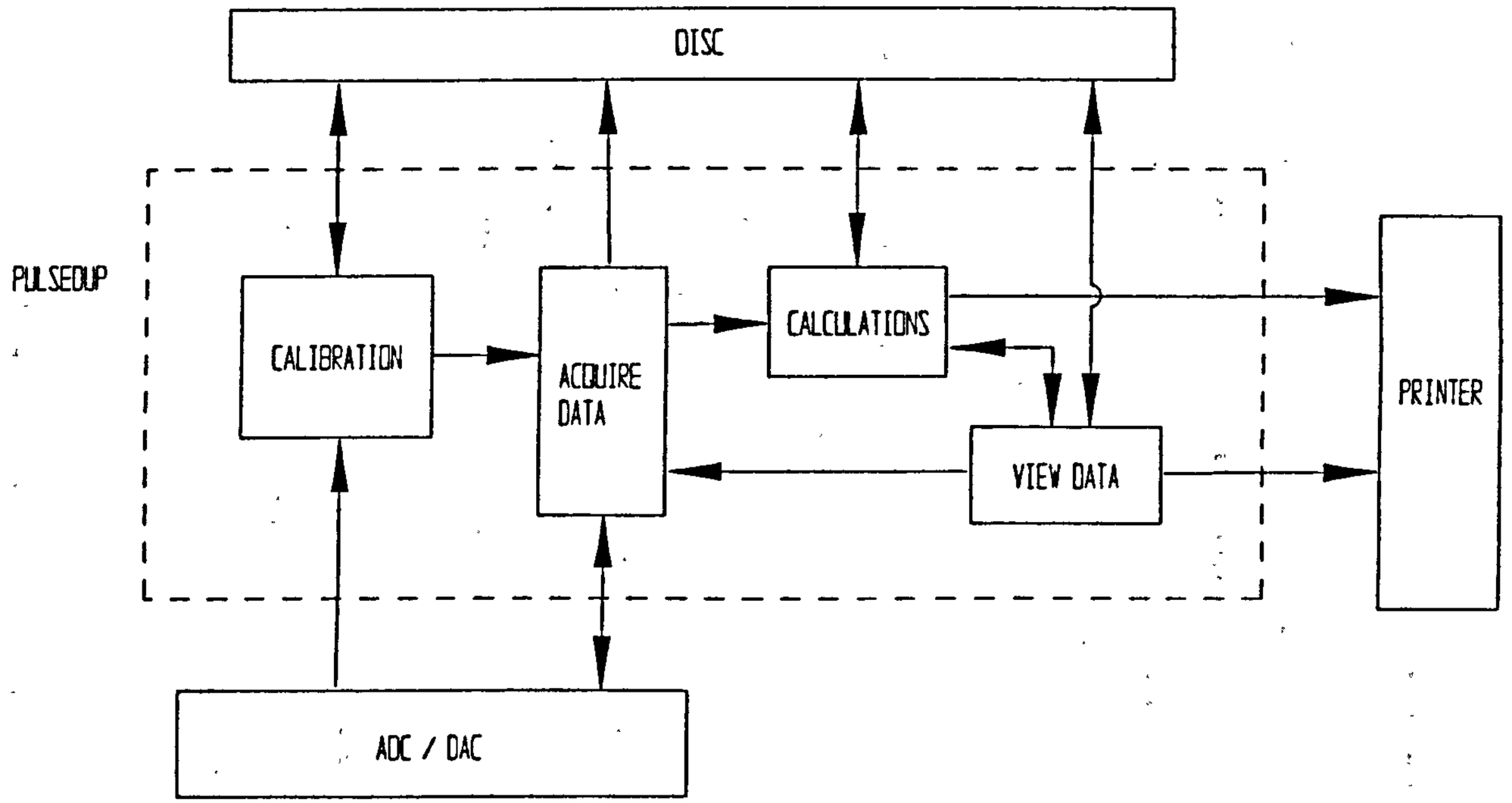

### 5.3.1 CALIBRATION

This mode is concerned with the configuration of PULSEDUP. The sub-program begins by reading a configuration file from disc. This file contains the default values for each transducer zero and gain, and the ADC/DAC sampling frequency; these defaults were set in a previous run of PULSEDUP. Any changes to these values can be saved on disc to become the default values for the next run.

The transducer zeros are checked by displaying the signal value while the pulse duplicator is at rest, and gains are checked by applying known inputs to transducers, as described in Chapter 4. The ADC/DAC sampling frequency is adjusted by programming the on-board timer chip. PULSEDUP has been designed to operate with sampling frequencies in the range 800 to 2000 Hz; frequencies outwith this range may give rise to problems. Regardless of the sampling rate, DATA ACQUIRE always samples 28000 data points (56 kilobytes); increasing the sampling frequency increases the number of points per waveform but reduces the number of waveforms to be averaged over. The value normally used is 1400 Hz (i.e. 200 Hz per channel), the same value as used by the previous system. Note that the ADC sampling frequency is also the frequency at which the pump velocity data is output. CALIBRATION mode also allows the time axis scale to be set for the graphical display of waveforms.

### 5.3.2 DATA ACQUIRE

This mode is concerned with generating the pump velocity signal whilst displaying graphically the input signals in real-time; generating a signal to initiate valve photography; acquiring data over a period of time; and the subsequent averaging and saving of data to disc.

When appropriately selected, any 3 of the 7 input

signals are displayed as graphs, in real-time. Also displayed, along with the graphs, are mean values for the pump frequency (and its standard deviation), pump stroke volume, and aortic pressure; these enable standard test conditions to be established in the pulse duplicator. Once the required settings of frequency, stroke volume and mean aortic pressure have been attained and have stabilized, the user can prompt PULSEDUP to save the incoming data. Unlike the previous system, the real-time graphical display is maintained as the data to be saved is acquired. In total 28000 points (56 kilobytes) are saved, 4000 per channel. The mean period and its standard deviation is found for the pump displacement signal; this is done by finding the zero cross-over points. The pump displacement signal is best suited for this as it only crosses zero twice per wavelength under all standard testing conditions. The 7 transducer signals are then averaged over this mean period. The averaged waveforms, along with the standard deviations at each point on the waveform, can then be saved on disc. The transducer zero and gain values and the sampling frequency are saved with the averaged data; these are required for subsequent calculations. The data is stored in a readable ASCII text format.

The output pump velocity waveform is selected from a choice of 4, as described in Chapter 4. Each waveform is stored on disc, digitised into 100 points; the appropriate file is read when selected. An output waveform frequency must also be selected; the range offered is 30 to 150 beats per minute. A pump velocity value is sent to the DAC every time a value is read from the ADC; this requires the velocity waveform to be digitised into (sampling frequency ÷ velocity waveform frequency) number of points. This is achieved by fitting a free cubic spline interpolant through the 100 points. That is, a cubic polynomial is defined between each 2 adjacent points such that the polynomial matches the

original waveform at the 2 points, and neighbouring polynomials have the same first and second derivative at each point. Formally, given the velocity waveform F defined on [1,100] and a set of points, $1 = X_1 < X_2 < \ldots < X_{100} = 100$, the free cubic spline interpolant, S, for F is a function satisfying :

(1) S is a cubic polynomial, denoted $S_j$, on the subinterval $[X_j, X_{j+1}]$ for each $j = 1,2,\ldots,100$;
(2) $S(X_j) = F(X_j)$ for each $j = 1,2,..,100$;
(3) $S_{j+1}(X_{j+1}) = S_j(X_{j+1})$ for each $j = 1,2,\ldots,99$;
(4) $S'_{j+1}(X_{j+1}) = S'_j(X_{j+1})$ for each $j = 1,2,\ldots,99$;
(5) $S''_{j+1}(X_{j+1}) = S''_j(X_{j+1})$ for each $j = 1,2,\ldots,99$;
(6) $S''(X_1) = S''(X_{100}) = 0$ (Free Boundary);

The cubic spline procedure used in PULSEDUP was taken from Turbo Pascal Numerical Methods Toolbox 4.0; the algorithm is described in detail in Burden & Faires (1985).

The interpolated points are calculated and stored in an array before any data is sent to the DAC. When the pump velocity values are being output, they are simply read out of the array; i.e. there is no real-time interpolation.

A 12-bit bi-polar DAC is used. Note that PULSEDUP can also be run with a programmable waveform generator providing the pump velocity signal.

Similar procedures of averaging and interpolation were used to originally create the 100-point pump velocity waveform files. The waveforms were derived from signals produced by the previously used programmable waveform generator. The ADC was used to sample the generator output over a period of time, an average period was found by looking for the zero cross-over points, and averaged waveforms calculated. The cubic spline procedure was used to fit 100 equally spaced points through each waveform.

DATA ACQUIRE mode also has an option for providing a trigger signal to initiate photography. The time delay for the trigger signal is user-defined and can be any integer multiple of the sampling period; i.e. any integer multiple of 0.5 to 1.25 milliseconds. The origin for the time delay is taken as the instant the pump displacement signal crosses zero, going from positive to negative. Once the user sets the desired delay, PULSEDUP monitors the pump displacement signal until the zero cross-over occurs, the program then monitors the flow signal (by default) whilst counting down the selected number of sampling periods. The trigger signal is sent to one of the 8-bit DACs. A graphical representation, showing the flow signal (by default) at the instant of sending the signal, is displayed and can be printed (fig 5.4). In CALCULATIONS mode the relative timings of the averaged pump displacement, pressure and flow waveforms are given, thus allowing the instant the trigger signal was sent to be cross-referenced to any of the flow or pressure waveforms.

### 5.3.3 CALCULATIONS

In this mode mean pressure differences, mean and root mean square flows, volumes displaced through the valve, EOA's and energy losses are calculated for the averaged data. The data may come directly from DATA ACQUIRE or may be read in from a file on disc, created by an earlier run of DATA ACQUIRE or VIEW DATA.

The average flow and differential pressure signals are plotted on the screen. They are optionally plotted with or without error bars; the error bars are drawn as twice the size of the standard deviation at each point. Vertical cursors are placed at 5 points in time: beginning of forward flow (point 1), beginning of forward

Figure 5.4 Flow meter trace (volts vs time) at instant of sending photography trigger signal

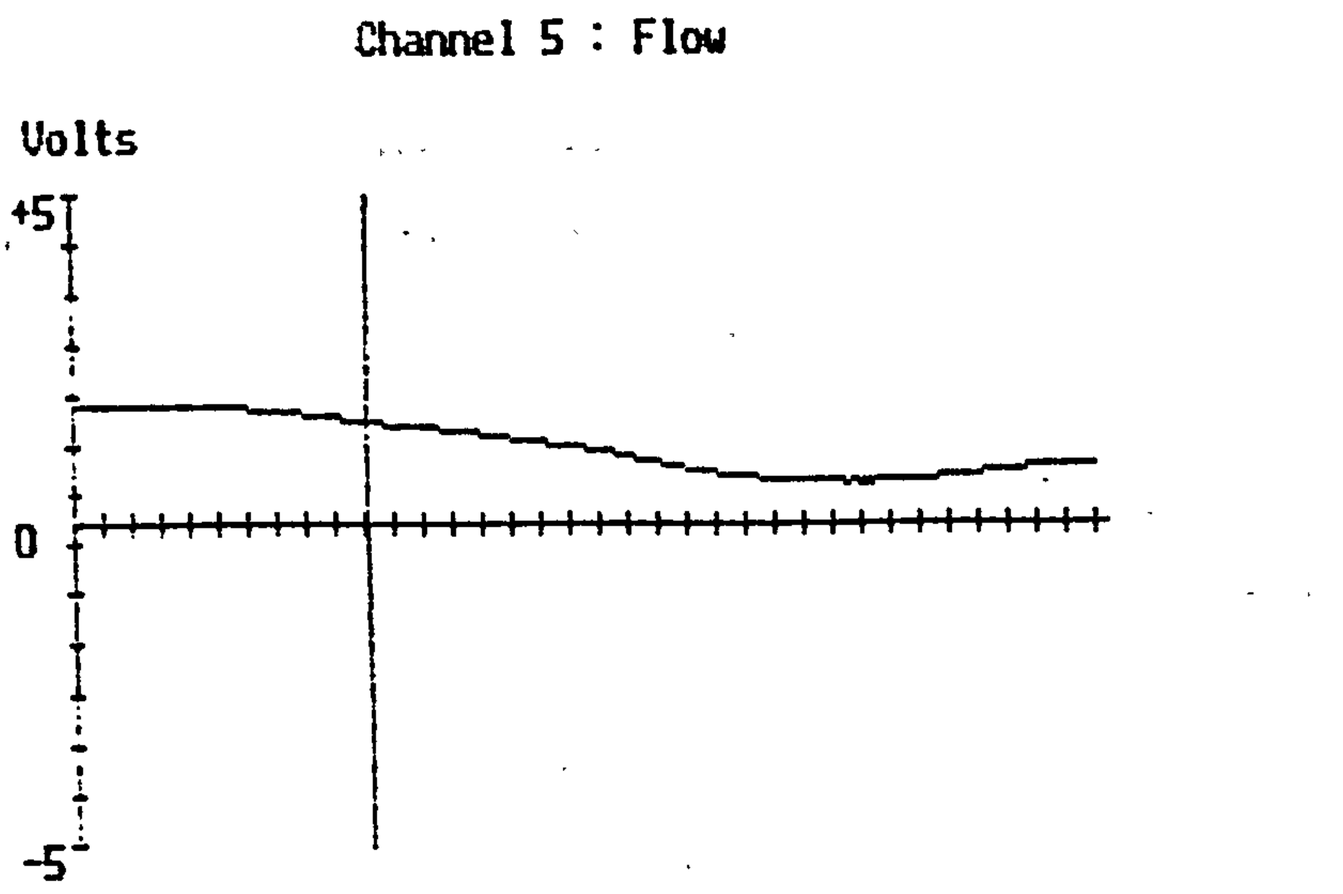


Delay of 100 sampling cycles i.e. 71.4 milliseconds

Flow = 189.26 ml per second

pressure (point 2), end of forward pressure (point 3), end of forward flow (point 4) and start of leakage flow (point 5). The times define the intervals used in the subsequent calculations. Additionally, peak forward flow and peak forward pressure are identified by horizontal cursors. The cursor positions are confirmed or re-set by the user.

An estimate of the overall deviation on each input signal is found by calculating the mean of the standard deviations for each channel. Times, in milliseconds, are calculated for the various user-set intervals. Volumes displaced through the valve during forward flow (points 1 to 4), closing regurgitant flow (points 4 to 5) and leakage flow (points 5 to 1) are found by integrating the flow waveform. For 4 intervals during forward flow (points 1 to 4, 2 to 3, 2 to 4, and 1 to 3), the mean pressure difference, mean and root mean square flow, and EOA are calculated. The EOA at peak forward flow and pressure is found. Finally, energy losses associated with flow through the valve are calculated for each of the 5 intervals. For the interval of forward pressure (points 2 to 3), the differential pressure signal is used in the calculation; for the other intervals, the large reverse pressure is outwith the differential pressure range so the difference of the 2 direct pressure measurements, on either side of the valve, is used.

Results of the calculations may be saved on disc and/or printed. An example calculations file is reproduced in Appendix 1.

### 5.3.4 VIEW DATA

VIEW DATA provides a means for viewing and filtering the averaged data waveforms. As in CALCULATIONS, the data may be input directly from DATA ACQUIRE (or CALCULATIONS) or be read in from a file on disc.

The user selects one of the 7 averaged waveforms to

be displayed; as in CALCULATIONS, error bars are optionally displayed. Further options allow the graph to be printed and/or the waveform to be filtered. The filtering process removes unwanted high frequency components by performing a Fourier analysis. That is, for a periodic waveform y(t) of period T, such that:

$$y(t) = \tfrac{1}{2}A_0 + \sum_{n=1}^{\infty}[A_n\cos(2\pi nt/T) + B_n\sin(2\pi nt/T)] \qquad (5.1)$$

the Fourier coefficients $A_n$ and $B_n$ are calculated from the digitised waveform $y_m$ of number points P using:

$$A_n \approx 2/P \sum_{m=0}^{P-1} y_m\cos(2\pi nm/P) \qquad (5.2a)$$

$$B_n \approx 2/P \sum_{m=0}^{P-1} y_m\sin(2\pi nm/P) \qquad (5.2b)$$

The number of harmonics to be included is user-defined from the range 1 to 20, and the Fourier coefficients can be saved on disc. A power distribution is calculated using Parseval's formula. That is, for periodic y(t), the associated mean power is proportional to:

$$\overline{y^2} = 1/T \int_0^T y(t)^2\,dt = (\tfrac{1}{2}A_0)^2 + \sum_{n=1}^{\infty} \tfrac{1}{2}(A_n^2 + B_n^2) \qquad (5.3)$$

The power distribution may be plotted on screen or printed (see figs 4.4 & 4.8). The power components are normalised with the mean square value of the original waveform. The filtered waveform is generated by a direct Fourier synthesis of the specified number of harmonics (eqn 5.1): the magnitude and phase of the harmonic components are not scaled or shifted. The exception is the flow waveform which is advanced by 20 milliseconds to account for the flow meter frequency response, as

discussed in Chapter 4. The user can choose to save the filtered waveform on disc and re-input the data to CALCULATIONS or VIEW DATA. The filtering routines were validated during the software development by introducing waveforms of known harmonic composition as test inputs.

## 5.4 Fatigue Tester Software : FATIGUE

The software for the fatigue tester has been derived from PULSEDUP, with many procedures in common. The requirements for FATIGUE are :

(1) Display on a graph the differential pressure signal and allow the transducer zero and gain values to be checked and re-set.

(2) Sample the pressure signal over a period of time and graphically display the resulting averaged pressure waveform.

(3) Filter the averaged pressure waveform.

(4) Generate a trigger signal to initiate valve photography, with a user-specified delay.

The checking and re-setting of the transducer zero and gain values is carried out in exactly the same way as in PULSEDUP, with default values being read from and written to a configuration file on disc. The display of the 'raw' differential pressure signal proceeds in a slightly different manner. Since the waveform frequency is an order of magnitude higher than in PULSEDUP, the sampling frequency is correspondingly higher, at 2000 Hz. At this frequency there is not enough time to display the waveform in real-time; instead 600 consecutive values are sampled then displayed on screen. The user can opt to repeat the sampling or print the graph.

In acquiring data to find an averaged waveform, 2 signals are sampled: the differential pressure and the stroboscope trigger signal produced by the Rowan Ash drive unit. Sampling is at 4000 Hz, 2000 Hz per channel, and of duration 1 second, giving 200 points per wavelength for a fatigue tester running at 10 Hz. The mean period is found by looking for zero cross-over points on the stroboscope signal; the pressure signal is subsequently averaged over this period. A graph of the averaged pressure waveform is displayed and may be printed. As in PULSEDUP, the waveform is optionally displayed with error bars, twice the size of the standard deviation at the each point.

The user may select to filter the averaged pressure waveform. Filtering proceeds by carrying out a Fourier analysis over a user-specified number of harmonics, the range offered is 1 to 20. Parseval's formula (eqn 5.1) is used to calculate a power distribution and power components are normalised by the mean square of the original averaged waveform; results are displayed and may be printed. The filtered waveform is calculated by a Fourier synthesis of the Fourier coefficients, and again the results are displayed and may be printed.

As an illustration, differential pressure waveforms for a dip moulded polyurethane valve are reproduced in figures 5.5 to 5.9. The figures respectively show the 'raw' pressure trace (fig 5.5), the averaged pressure waveform with error bars (fig 5.6), the power distribution for the averaged pressure waveform (fig 5.7), and the filtered averaged waveforms constructed by the Fourier synthesis of the first 5 (fig 5.8) and 10 (fig 5.9) harmonic components.

Analogous to PULSEDUP, FATIGUE also provides an option for generating a photography trigger signal. The trigger time delay is user-defined and can be any integer

Figure 5.5
'Raw' differential pressure trace
from accelerated fatigue tester

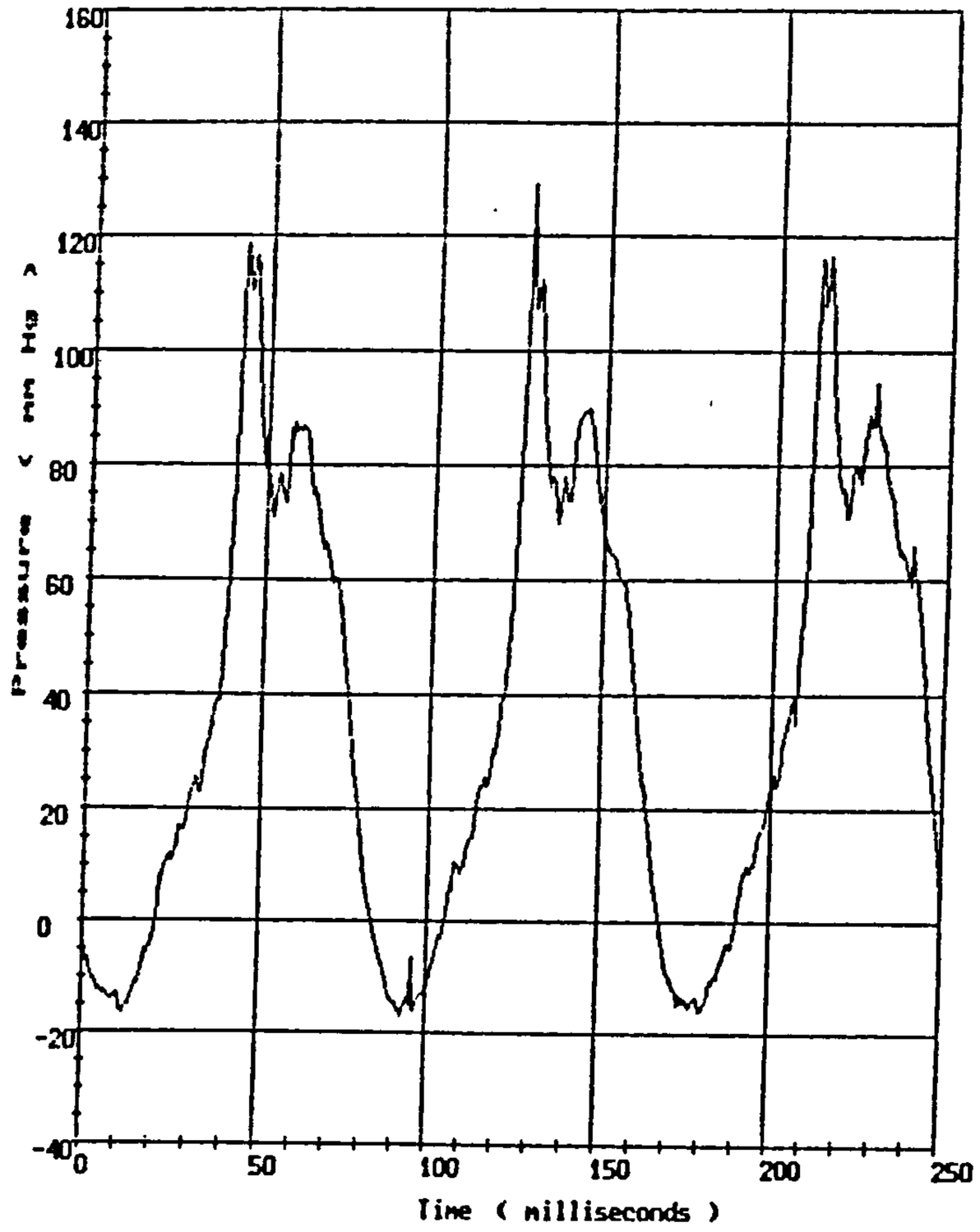


Figure 5.6
Averaged differential pressure waveform
from accelerated fatigue tester

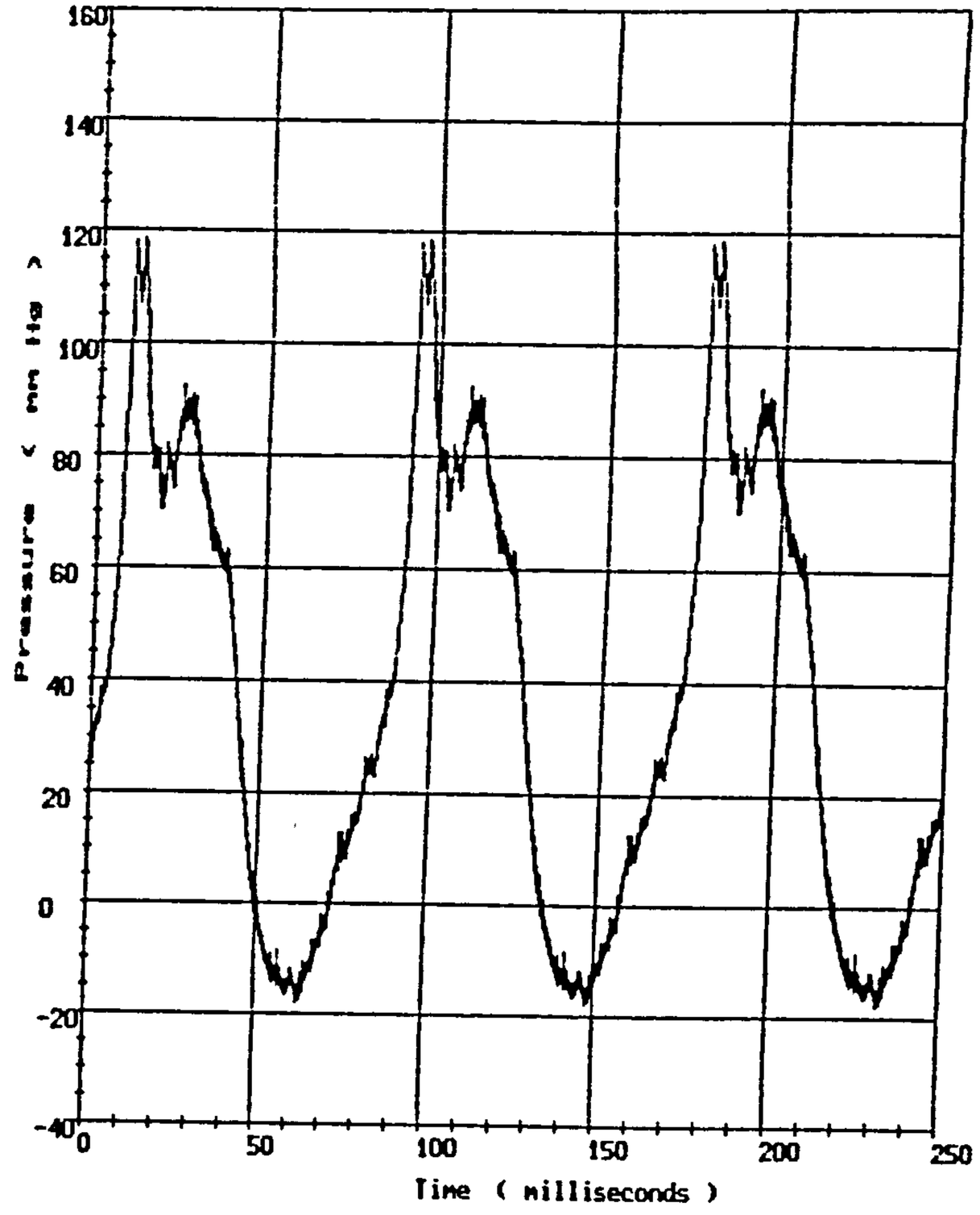

Figure 5.7 Power distribution for averaged differential pressure waveform

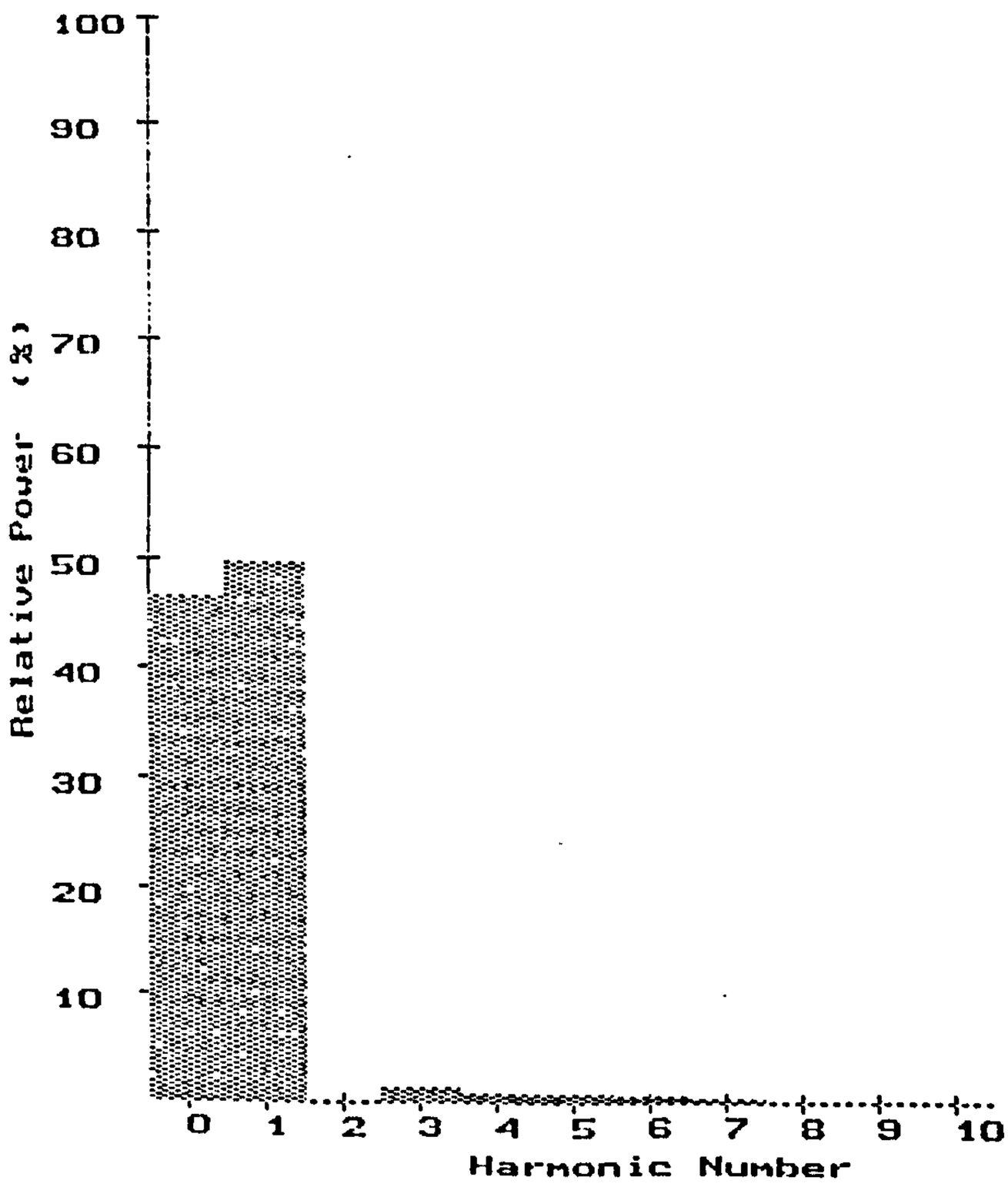

Figure 5.8
Filtered differential pressure waveform
- 5 harmonics

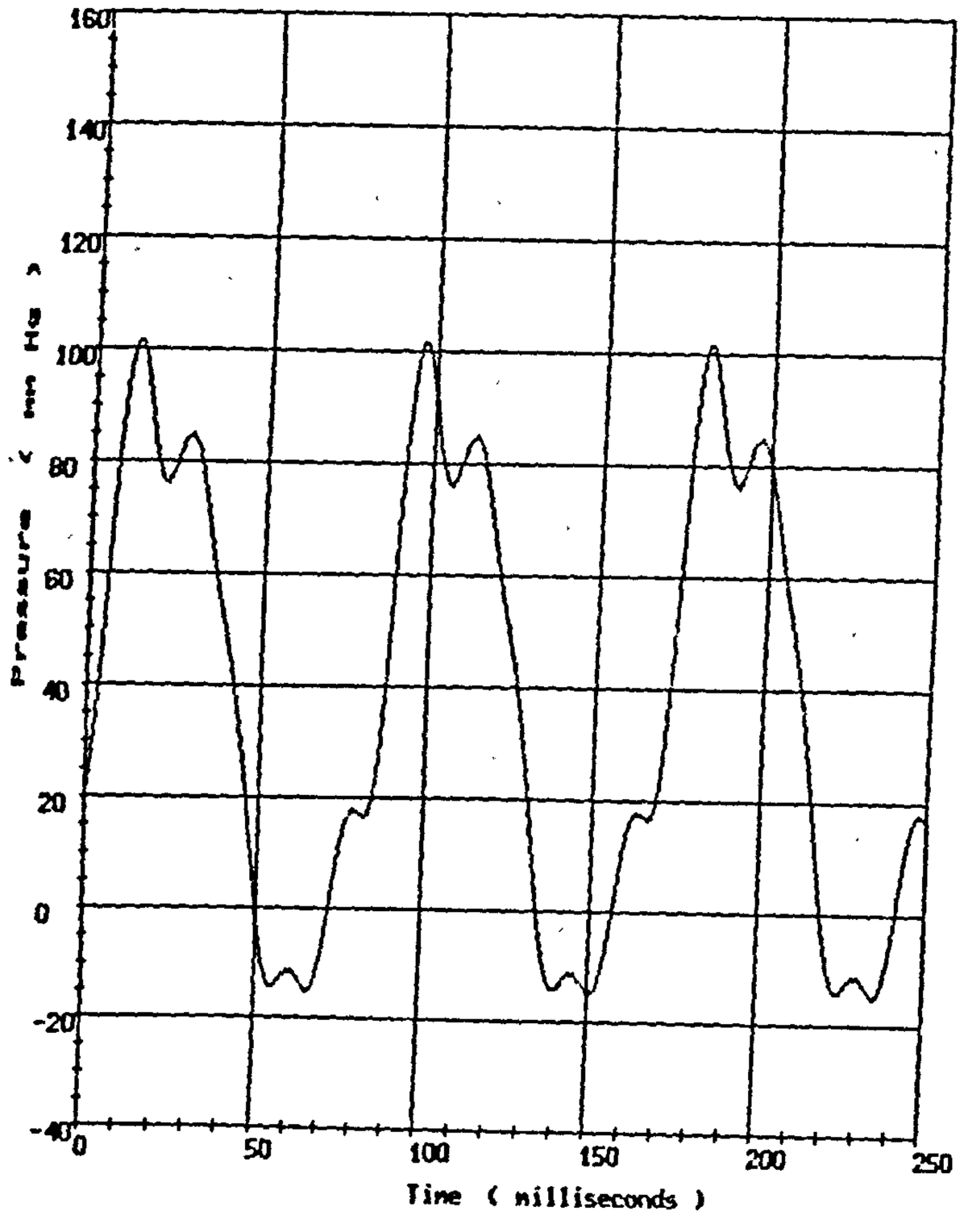


Figure 5.9
Filtered differential pressure waveform
- 10 harmonics

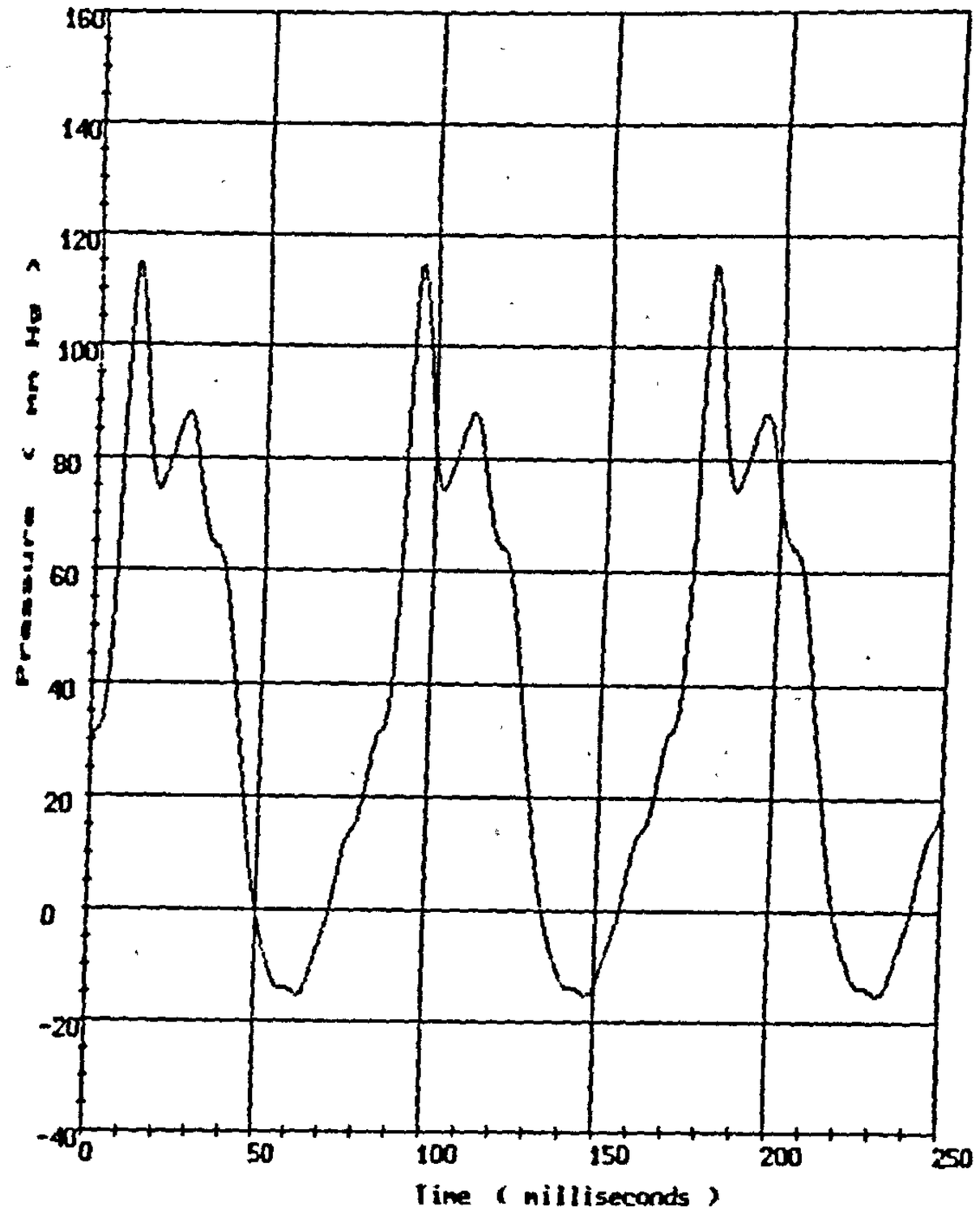

multiple of the sampling period (in this case 0.5 milliseconds). The origin for the time delay is the instant the stroboscope signal falls from >+5 volts to 0 volts; this is also the instant the stroboscope itself triggers on. Thus, the delay can be set relative to the instant in the valve cycle which is illuminated by the stroboscope. Once the desired delay has been set, the stroboscope signal is monitored until the cross-over occurs, and then the program counts down the specified number of sampling periods. The trigger signal is output to one of the 8-bit DAC's.

## 5.5 Discussion

The software described in this chapter represents an enhancement of the existing valve testing equipment. A comparison of features common to PULSEDUP and the previous system reveals several advantages in favour of PULSEDUP. The ADC bit resolution has increased from 8 to 12; the overall operating speed has increased by a factor of approximately 3 (the previous system took approximately 15 minutes to carry out a cycle of acquiring and averaging data, performing calculations and printing graphs whereas PULSEDUP takes approximately 4 to 5 minutes to complete the same cycle); and the graphics resolution has approximately doubled.

The development, from a data acquisition system to an integrated system in which the computer both controls the input and monitors the output, has significant implications. At the moment, PULSEDUP generates only those waveforms previously produced by the programmable waveform generator, however, the system could easily be extended to include a much wider range of waveforms. Further, such a computerised closed system has the potential for transforming the pulse duplicator from a flow generator to a pressure generator, by using a pressure transducer signal, rather than the pump velocity

signal, to control the pump servo-system. Possibly, a combination of pump velocity and pressure signals could be incorporated in the servo-system to better simulate physiological flow conditions.

To calculate the pump velocity waveform, PULSEDUP uses a cubic spline procedure to interpolate between 100 points; the calculated waveform is described by (sampling frequency ÷ velocity waveform frequency) number of points, typically 1400 points. A similar method is described by Leefe *et al* (1986) in which the pump waveform is described by a 25-term Fourier series sampled at 1024 points. Cochrane *et al* (1991) describe a DAC system in which the pump waveform is represented by a 7-element piecewise linear function, discontinuities being smoothed out by mechanical damping in the pump.

The photography trigger signal, generated by PULSEDUP, can be delayed by an integer multiple of 0.5 to 1.25 milliseconds. This time resolution is much better than the 20 milliseconds offered by the video camera system which is also used to visualise valve movements; the quality of image produced by the 35 mm camera is also better than that provided by the video still frame facility. The time resolution is similar to that achieved in high-speed cinematography (Rainer *et al*, 1978; Chandran *et al*, 1986). In comparison with this technique, the PULSEDUP system has the advantage of being inexpensive and the ability to directly refer the timings of the images produced to times on the pressure and flow waveforms. The principal drawback with the PULSEDUP technique is that consecutive images of a valve opening or closing originate from different valve cycles; photographs are taken after the pulse duplicator has reached a steady state but a valve may not open and close in precisely the same way in each opening/closing cycle. A similar procedure for valve photography has been described by Yoganathan *et al* (1983) in which a camera is synchronised with a timer on the pulse duplicator; Arabia

*et al* (1989) describe a method equivalent to that of PULSEDUP, in which the camera is triggered through a DAC on the data acquisition computer.

The option in PULSEDUP for filtering the averaged waveforms is useful for removing unwanted high frequency components. Also, the ability to decompose an averaged waveform into its harmonic constituents is utilised in the determination of transducer frequency responses and in the calculation of aortic input impedance, as described in Chapter 4.

The introduction of a data acquisition system to the fatigue tester brings with it several advantages over the previous system of displaying an analog-filtered differential pressure signal on an oscilloscope (Fisher *et al*, 1986). Specifically, the computer monitor is much larger than a typical oscilloscope screen, thus pressure tracings can be seen in greater detail; FATIGUE can display averaged pressure waveforms, perform digital filtering, and generate a photography trigger signal. Note that the particular differential pressure transducer used with FATIGUE has an approximately flat frequency response over the range of relevant frequencies (0 - 150 Hz), thus Fourier coefficients in the filtering procedure are not scaled. However, a transducer with a much more complicated frequency response could also be catered for. A frequency response waveform could be stored on disc, and in an analogous fashion to the pump velocity waveforms in PULSEDUP, the cubic spline interpolation procedure could be used to find frequency scaling factors at the various harmonic frequencies. Also, note that the filtering procedure in FATIGUE does not phase shift any harmonic components. The differential pressure transducer phase shift is approximately linear with frequency over the relevant range, thus the measured waveform has an overall time delay but the correct shape.

# Chapter 6. Valve Design Considerations

## 6.1 Introduction

The designs of bioprosthetic valves in current clinical use, and most prototype flexible leaflet valves made from synthetic materials, are based on the 3-leaflet configuration of the natural aortic valve. The central-flow design with an unobstructed open orifice is less likely to give rise to downstream flow disturbances and concomitant trauma. In contrast, the problems of thrombus formation and haemolysis associated with mechanical valves are, at least in part, attributable to their occluding mechanisms which partially obstruct the open valve orifice area. The principal limitations of central-flow bioprostheses are their unsatisfactory long-term durability and function, with leaflet tears and calcification being the prominent failure modes (Fisher *et al*, 1989). A greater understanding of the mechanics involved in valve function may give rise to modified valve designs and/or fixation procedures which result in enhanced *in vivo* performances. Although the link between tissue calcification and mechanical factors has not been clarified, it is likely that an improvement in mechanical durability will also reduce the propensity for calcification. Hitherto, improvements in valve design have generally resulted from an experimental trial and error approach, however, the ever increasing availability of high-powered computing resources raises hope for a theoretically-optimized valve design. The scope for improving bioprosthesis design is, of course, ultimately limited by what can be practicably achieved with the biological tissue; there is an argument for considering a synthetic leaflet valve for which a wider range of design options, material properties (both mechanical and chemical), and manufacturing techniques are available.

In this chapter the mechanical aspects of valve

design will be discussed and the arguments for contemplating a synthetic leaflet valve put forward. Before dealing with these matters it is important to consider the design and mechanical characteristics of the 'ideal' valve which tri-leaflet prostheses attempt to emulate: the native aortic valve.

## 6.2 The Natural Aortic Valve

The native aortic valve consists of 3 thin flaps suspended from the aortic root; the leaflets respond passively to flow conditions, offering minimal resistance to forward flow and preventing reverse flow during diastole. At the attachment of each leaflet to the aortic wall there is a U-shaped arch of fibrocartilaginous tissue; behind each leaflet the aortic wall bulges outwards forming 3 pouches (*sinuses of Valsalva*, fig 6.1).

The outflow leaflet surface has a characteristic folded appearance with corrugations running circumferentially, whereas the inflow surface is relatively smooth. Leaflet thickness varies greatly across the surface, being thinnest in the leaflet belly (Clark & Finke, 1974); there are differing reports of relative thickness for the coaptational part of the leaflet (Broom & Christie, 1982) but agreement on a localized thick spot at the centre of the free edge (*nodulus Aranti*). The non-coapting leaflet surface is generally taken to have a cylindrical geometry with an inclination angle of 20-30° to the valve base (Robel, 1972; Swanson & Clark, 1974; Butterfield *et al*, 1991); the geometry has also been described as paraboloid of revolution (Mercer *et al*, 1973) and elliptic paraboloid (Hamid *et al*, 1986). The fibrocartilaginous arches at the leaflet attachment have been variously described as parabolic (Mercer *et al*, 1973) and elliptical (Swanson &

Figure 6.1 Construction of aortic valve (from Sauren *et al*, 1980)

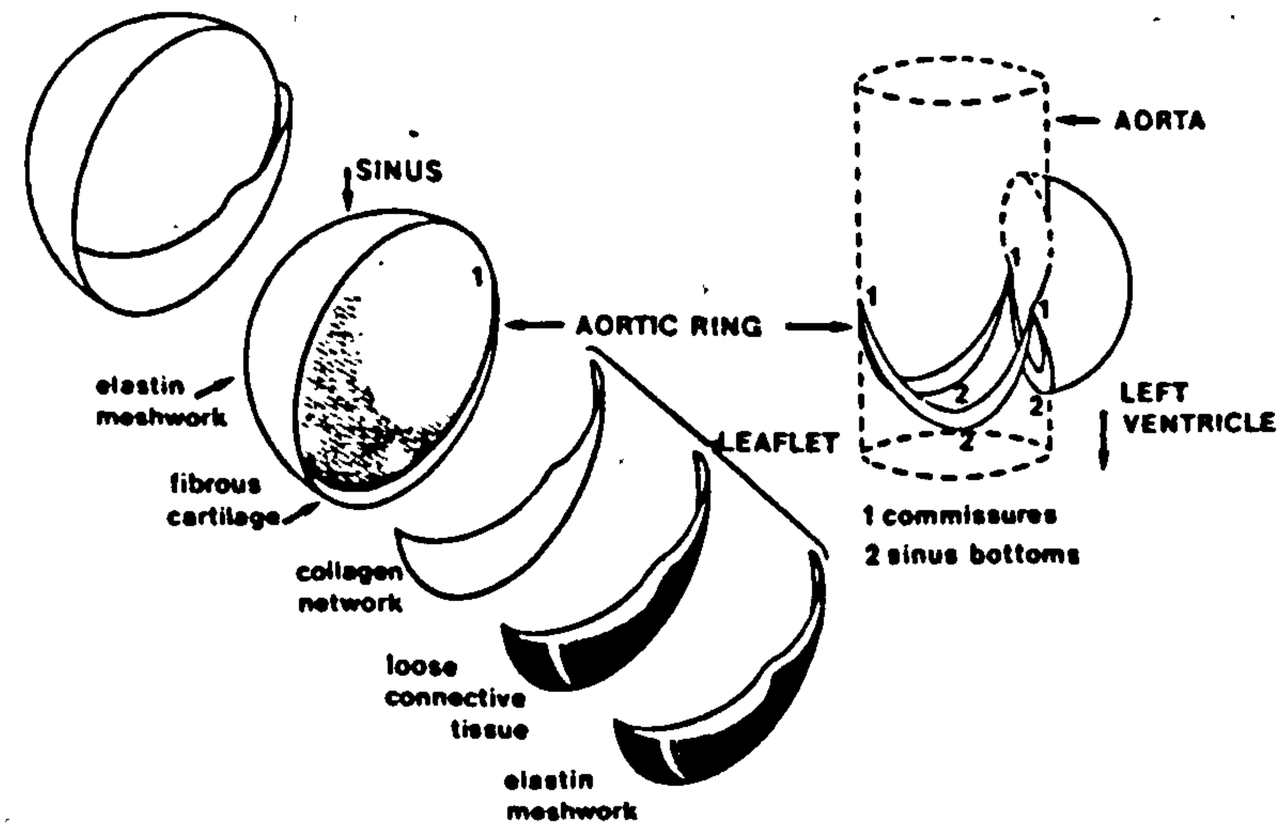

Clark, 1974); the thickness of the attachment arch increases from the commissures down to the sinus base (Sauren *et al*, 1980). The variety of reported shapes probably reflects the problems associated with handling soft tissue and the inherent biological variability. Of course, the aortic valve apparatus yields to back pressure and changes shape accordingly. Geometry changes have been followed *in vitro* by examining frozen aortic roots (Robel, 1972), silicone rubber casts (Swanson & Clark, 1974), and with displacement transducers attached to an intact aortic root in a pulse duplicator (Brewer *et al*, 1976). Similarly, movements have been followed *in vivo* using radiopaque markers (Thubrikar *et al*, 1981) or displacement transducers (Brewer *et al*, 1977) attached to canine aortic valves. With increasing back pressure, the aortic sinus region expands circumferentially and raises the leaflets upwards tilting them away from the ventricle, reducing the area of coaptation; the axial height of the valve is relatively unchanged. This rather surprising response is a result of sinus tissue being considerably more compliant than leaflet tissue and considerably more compliant in the circumferential rather than axial direction (Sauren *et al*, 1983).

Aortic valve histology has been studied with scanning electron (Clark & Finke, 1974; Lee *et al*, 1984) and light (Sauren et al, 1980) microscopy. Although there is disagreement on the fine details, each leaflet is generally accepted to consist of 3 major layers with a thin covering of endothelial cells on the external surfaces. The subendothelial ventricular layer, the *ventricularis*, is composed predominantly of elastin with some loosely organized collagen fibres. The *fibrosa*, the subendothelial aortic layer, consists of planes and bundles of collagen fibres which are predominantly oriented in the circumferential direction; in the relaxed state the fibrosa is folded up radially and individual collagen fibres are crimped. The *spongiosa* lies between

these 2 layers, it is a layer of loose connective tissue with a high mucopolysaccharide content. The spongiosa has negligible load-bearing capacity but may serve as a lubricant enabling relative motion of the fibrosa and ventricularis and/or a damping agent dissipating energy during valve closure.

The observed structure of aortic valve leaflets has been, to an extent, corroborated by mechanical testing of leaflet tissue. Uniaxial tests on circumferential and radial strips have revealed leaflet tissue to be anisotropic (Clark, 1973; Sauren *et al*, 1983; Lee *et al*, 1984; Mavrilas & Missirlis, 1991); as illustrated in figure 6.2, the tissue is considerably more compliant in the radial direction. The non-linear stress-strain relationship is due to crimped collagen fibres straightening out under tension, the straightened fibres being relatively stiff; this was demonstrated by Broom (1978) with simultaneous uniaxial testing and microscopic observation of the collagen arrangement. The structural layers of the aortic leaflet have also been investigated individually (Broom & Christie, 1982; Vesely & Noseworthy, 1992), showing that both the fibrosa and ventricularis are considerably stiffer circumferentially than radially. Vesely & Noseworthy (1992) found that the fibrosa became much less extensible radially when removed from the ventricularis. They concluded that the radial extensibility of the fibrosa *in situ* is due to its highly folded structure; the folds disappear when the fibrosa is stripped from the ventricularis which suggests that the fibrosa is under slight compression and ventricularis under tension in the relaxed leaflet. Results from uniaxial tests have been substantiated with biaxial (Mayne *et al*, 1989) and whole valve (Missirlis & Chong, 1978) mechanical testing. Note that much of the published work on aortic valve mechanical properties describes porcine aortic valve tissue; Mavrilas & Missirlis (1991) found that human tissue is rather less compliant.

Figure 6.2 Stress-strain characteristics for radial and circumferential strips of aortic valve leaflet tissue
(from Christie & Stephenson, 1990)

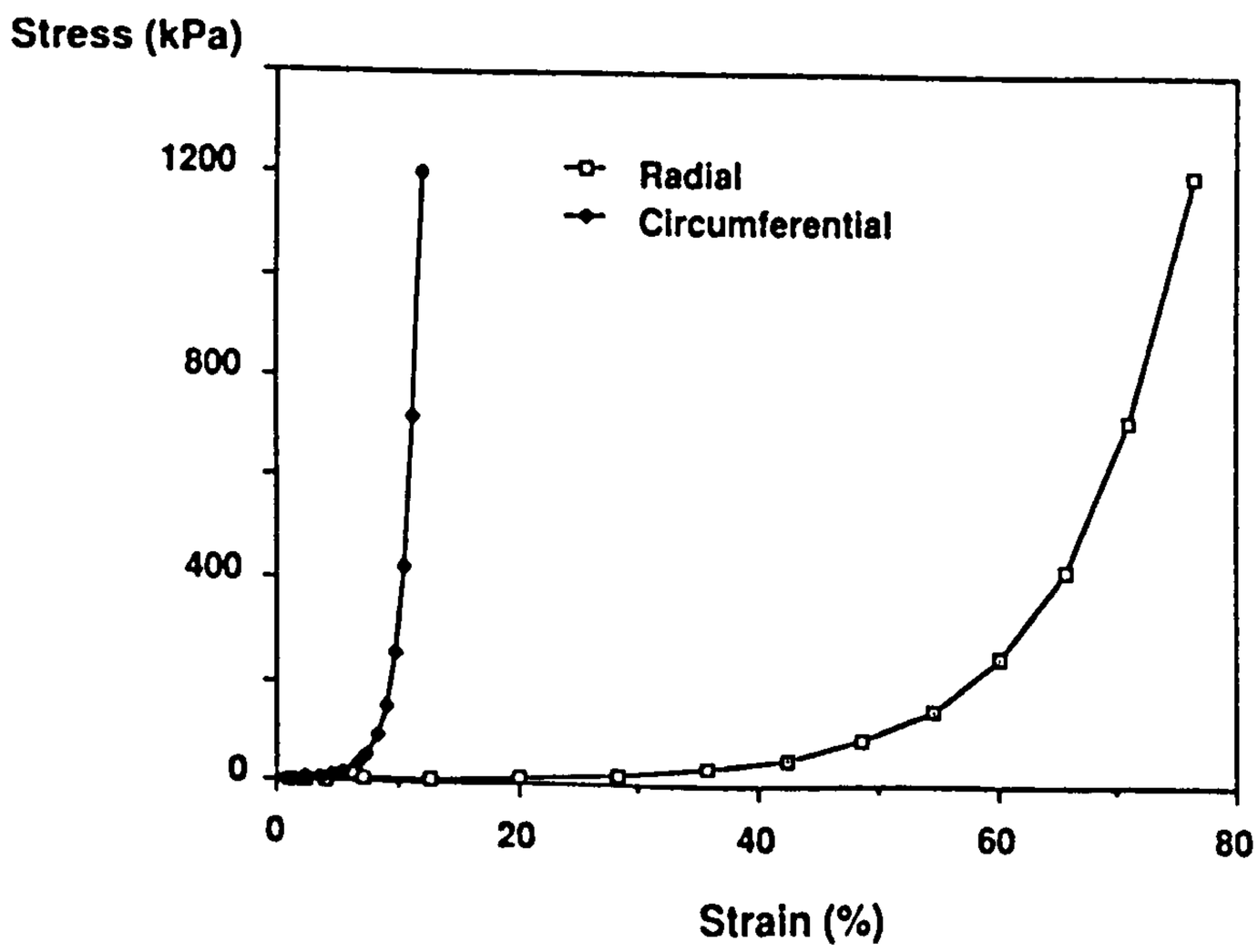

The mechanical properties of aortic valve tissue are time dependent, but this may not have a significant effect on valve function given the time scales involved. Stress relaxation (Clark, 1973; Sauren *et al*, 1983; Vesely & Noseworthy, 1992) and creep (Lee *et al*, 1984) measurements have been performed on strips of aortic valve tissue. In constant strain experiments, tensile stress fell quickly immediately after loading and then relaxed away more slowly. For example, Lee *et al* (1984) found that for an approximately physiological initial load, 10% of the original stress was lost within 10 seconds and the next 10% took over 2 minutes to dissipate. The reported orientational sensitivity for stress relaxation has been slight and variable, Lee *et al* (1984) finding that radial tissue samples relaxed at a slightly slower rate than circumferential, while Vesely & Noseworthy (1992) observed the opposite for fibrosa samples, and Sauren *et al* (1983) did not find any significant difference between the orthogonal directions. For constant load experiments, radial tissue strips crept considerably more than circumferential but the overall magnitudes were small: from the data of Lee *et al* (1984), for a typical diastolic period of 0.5 seconds the expected increase in leaflet dimension would be less than 0.1%. As well as explicit measurements of creep and stress relaxation, other time dependent phenomena have been reported: in order to generate repeatable results, uniaxial tests were generally preceded by a number of preconditioning cycles; hysteresis losses of 20-30% between loading and unloading have been observed (Lee *et al*, 1984). On the other hand, there have been contrary reports on the sensitivity of stress-strain responses to strain rate: some have observed only a very slight sensitivity to strain rate (Sauren *et al*, 1983; Lee *et al*, 1984) while others found that the stress-strain response varied markedly over a similar range of strain rates (Mavrilas & Missirlis, 1991). Interestingly, in a

biaxial study of leaflet tissue, Mayne *et al* (1989) found that hysteresis and preconditioning effects were negligible; they suggested that the viscoelastic behaviour observed in uniaxial tests was due to inelastic deformations associated with the unconstrained narrow strips. In a study of whole aortic valves, Missirlis & Chong (1978) found it necessary to precondition their valves but this may have been due to the valve mounting or alterations in the tissue brought about by the process of marking dots on the leaflet surfaces.

Vesely & Boughner (1989) reported on the bending behaviour of aortic leaflet tissue: radial tissue strips were more easily bent than circumferential strips, and circumferential strips were stiffer when bent with the fibrosa on the outside of the bend ('reverse' bending). By viewing collagen 'wavelengths' in bent strips with polarized light microscopy, they found that the neutral axis for reverse circumferential bending lay towards the outside of the bend, at a depth of 1/6 of the total tissue thickness from the outer surface; the implication being that the tissue is much less resistant to compression than stretching.

Notice that there are conceptual problems associated with the mechanical description of leaflet tissue. Firstly, defining stress as a force per unit tissue area is misleading in the case of nonhomogeneous leaflet tissue in which there are relatively stiff collagen bundles embedded in a soft matrix; the actual stress experienced by the load bearing collagen is greater than that given by the force per gross unit area. Secondly, thickness measurements are a problem due to the folded nature of the fibrosa; the measured thickness may not be the actual tissue thickness but a measure of fold depth.

In conclusion, the native aortic valve is a highly differentiated connective tissue structure. The valve function is reflected in its design and mechanical properties: the low pre-transition elastic modulus

combined with shearing spongiosa layer permit leaflets to open and close with minimal effort, whereas the high post-transition elastic modulus prevents large tissue extensions during diastole. Fibroblasts lay down collagen in response to the stress fields they experience, so the predominance of circumferentially oriented collagen may reflect the operational stresses within the valve leaflet and indicate a desirable design feature for a prosthetic tri-leaflet valve. Note, however, that integral in normal aortic valve function is the participation of the fibrocartilaginous attachment ring, aortic sinuses and surrounding tissue. A tri-leaflet prosthesis with flexible leaflets mounted on a rigid or semi-rigid stent, which attaches to the aortic root only by a sewing ring at its base, cannot mimic precisely this natural function. Also, it is unlikely that the leaflets of a prosthesis will match the complex mechanical properties of native valve leaflets. Therefore, the detailed design of the natural aortic valve is not necessarily the optimum design for a prosthetic replacement.

## 6.3 Tri-leaflet Prosthetic Valve Design

In general terms, the principal mechanical requirement for prosthetic valve design is to maximise valve durability whilst maintaining an acceptable haemodynamic function. The haemodynamic criteria are:

(1) To restrict fluid mechanical shear stresses to levels below that which causes blood damage and thrombus formation.

(2) Avoidance of areas of flow stagnation.

(3) Swift (but gentle) valve closure and a competent seal when closed.

(4) Minimal energy required for valve opening and closure and a minimal pressure drop across the open valve.

(5) Valve profile should be sufficiently low that haemodynamic (or other) functions of neighbouring cardiac structures are not compromised.

The mechanical durability of a prosthesis is related to the operational stresses experienced and as such may be amenable to mathematical analysis and optimization. The durability and haemodynamic design criteria are likely to conflict. For example, an increase in durability may be achieved by selectively reinforcing valve leaflets in the commissural region but this may result in an increased effort required to open and close the valve; a realizable optimal prosthesis is likely to be a compromise solution. As well as mechanical criteria, many other requirements related to prosthesis biocompatibility, surgical implantation, etc, need to be considered. Reul (1983) has compiled a list of 42 design criteria, but weighting such a list according to priority may be difficult.

### 6.3.1 Stress analyses

A detailed analysis of stresses experienced by a flexible leaflet prosthesis (or natural valve) throughout the cardiac cycle represents a formidable computational problem and has not been achieved as yet. For a complete analysis, the fluid and surrounding tissue would also have to be modelled. Nevertheless, advances have been made using simplified models. To date, most analyses have concentrated on hydrostatic loading of the closed valve. Leaflets are generally assumed to behave as thin membranes with bending effects negligible compared with

in-plane forces. However, recent results suggest that bending stress may be an important factor in determining valve durability.

Early analytical studies considered membrane stresses in closed valves, simplified in terms of leaflet geometries, material properties, and boundary conditions (Chong *et al*, 1973; Clark & Sutera, 1973; Rossow *et al*, 1978). In their membrane analysis, Missirlis & Armeniades (1976) introduced an elastic (constant) modulus which was larger in the circumferential than radial direction; for spherical and ellipsoid of revolution shaped leaflets, they found that the magnitude and distribution of the calculated stresses were acutely sensitive to the membrane geometry. A more detailed analysis was presented by Chong & Missirlis (1978): they combined measured local deformations under back pressure with nonlinear stress-strain relations (by means of piece-wise linearization) to calculate membrane stresses across porcine aortic valve leaflets. This analysis predicted higher radial than circumferential stresses and radial stresses which increased from the leaflet base towards the nodulus Aranti; however, these conclusions are at odds with most other analyses and unexpected given the valve structure. Membrane and bending stresses in open and closed valve configurations were estimated by Thubrikar *et al* (1980), but their highly simplified model, based upon Laplace's law, was far from realistic.

Finite element analysis provides a more sophisticated method for modelling leaflet stresses. Initial finite element studies were based upon linear (small deformation) theory, isotropic and linearly elastic materials of uniform thickness, simplified leaflet geometries, and neglected bending effects (Gould *et al*, 1973). Models have become progressively more realistic with the inclusion of geometry digitized from rubber moulds (Cataloglu *et al*, 1976), nonlinear (large deformation) theory (Hamid *et al*, 1985a), anisotropic and

nonlinearly elastic materials with a specified thickness distribution (Christie & Medland, 1982), and bending effects (Black *et al*, 1991). Some general trends emerge from the range of published analyses, despite being based on varying assumptions and materials. Under physiological back pressures, tensile stresses are predominantly greatest in the circumferential direction and tend to concentrate in the vicinity of the commissures and leaflet belly; small compressive stresses have been variably predicted at the centre of the leaflet free edge.

Finite element stress analyses have been particularly useful in demonstrating the relative importance of design and material parameters. Christie & Medland (1982) found that stiffening leaflets preferentially in the circumferential direction resulted in a reduction of stress concentration at the commissures and an increase in coaptation area. Extending this analysis, they modelled the porcine aortic leaflet as an isotropic nonlinearly elastic membrane (ventricularis) with circumferentially-oriented stiff embedded fibres (fibrosa); stresses in the ventricularis were less than 20% of those in the fibrosa and were greatest radially; under a back pressure of 120 mm Hg [15.8 kPa], the circumferential strains (12%) were such that the elastic modulus of the fibres was in the stiff, post-transition, phase of the stress-strain curve, whereas the radial strains (up to 60%) were such that the ventricularis was still in the pre-transition phase (fig 6.2, Christie & Stephenson, 1990a). Hamid *et al* (1986), and others (Rousseau *et al*, 1988; Chandran *et al*, 1991) have considered the influence of stent height upon leaflet stresses; they found that increasing the stent height, whilst maintaining a constant leaflet surface area, had a beneficial effect in reducing stress concentrations at the commissures. However, an increased stent height may have a detrimental effect on the valve haemodynamics and

result in interference with neighbouring structures. Christie & Stephenson (1990b) varied the angle between the stent post and the relaxed leaflet free edge from 90° to 60° in an isotropic model of a pericardial valve: as the angle was reduced, stress intensity at the commissures fell. Stent flexibility was considered by Chandran *et al* (1991) in their analysis of a linearly elastic polyurethane tri-leaflet prosthesis; replacing a rigid stent with a flexible one reduced tensile stress concentration (but increased shear stress) at the commissures and increased the area of coaptation. Upon selectively increasing the leaflet thickness at the commissures, Chandran *et al* computed a more uniform stress distribution, but this only applied when a rigid stent was used. Knierbein *et al* (1990) compared the strains induced in polyurethane valve leaflets of uniform and distributed thicknesses, under a back pressure of 300 mm Hg [39.5 kPa]; the constant thickness leaflet experienced smaller strains but only one distributed thickness was studied. Rousseau *et al* (1988) incorporated a viscoelastic frame and leaflets, along with a time varying pressure load, in their model of a Hancock porcine valve; however, the predicted viscoelastic behaviour (hysteresis) was very small.

The analysis of Rousseau *et al* (1988) is particularly interesting as there is an attempt to correlate model predictions with measured valve displacements. In the majority of stress analysis studies, although the areas of predicted highest stress do generally coincide with areas in which tears and perforations have been observed in explanted bioprostheses, there is no quantitative check made on the computed stresses. From their model, Rousseau *et al* calculated the radial commissure displacement and the axial displacement of the valve centre under physiological loading, and the actual displacements were measured in a pulse duplicator using an inductive

displacement transducer and Doppler ultrasound. There was qualitative agreement between predicted and measured displacements; the discrepancies reflect the approximate nature of the model (eg uniform leaflet thickness, coaptation area was not allowed to increase under loading).

Bending stresses, which are generally neglected, have been computed in finite element studies for both bioprosthetic (Hamid *et al*, 1985b; Huang *et al*, 1990; Black *et al*, 1991) and polyurethane (Ghista *et al*, 1978; Knierbein *et al*, 1990a) valves. Black *et al* and Knierbein *et al* predicted substantial bending stresses, particularly at the leaflet-frame attachment, for loaded closed valves. For their model of a bicuspid pericardial valve, Black *et al*, computed a stress 'hot spot' close to the commissures; this may be associated with their modelling of the coaptation area. Compressive stresses were generally not found, i.e. the neutral axis for bending lay outwith the leaflet. The results of bending studies suggest that analyses which consider in-plane stresses alone may be misleading.

The complex motion, and associated stresses, involved in opening and closing flexible leaflet valves have not been satisfactorily modelled as yet. Huang *et al* (1990) considered the transition from open to closed for radial and circumferential pericardial strips, allowing a rolling contact between the leaflet and frame. Although pressures required to initiate closure were very small, they found that substantial bending stresses were associated with closure, especially near the leaflet attachment where the bending radii of curvature were smallest and compressive stresses were calculated. Note that this 2-dimensional approach could not model stresses in the closed valve under physiological back pressures as the unsupported radial strips prolapsed. Knierbein *et al* (1990a) have attempted to model the 3-dimensional opening of a polyurethane valve of uniform leaflet thickness;

they assumed a linear pressure drop in the flow direction and constant pressure in the circumferential direction (radial pressure distribution was not stated). Their calculations revealed that the highest strains occurred in the leaflet belly and at the commissures, and were associated with bending. The authors expressed some reservations with their calculation, particularly concerning the assumed pressure distribution.

Recent interest in bending effects, both in the hydrostatically-loaded closed valve and associated with valve opening and closing, is particularly relevant given that collagenous tissue responds relatively poorly to cyclic compressive flexure (Broom, 1978) and compressive stresses induced by bending and buckling are believed to be contribute substantially to bioprosthetic valve failure (Vesely *et al*, 1988). Bending calculations are likely to depend critically upon the way in which the leaflet-frame boundary is modelled. Leaflets are usually assumed to be rigidly fixed to the frame. For example, Trowbridge & Crofts (1987) used an analytical model to study the large elastic deformation of a flat strip of pericardium subjected to a uniform transverse pressure of 100 mm Hg [13.2 kPa]. The strip ends were not free to move towards each other, in analogy with a circumferential strip in a bioprosthesis with a rigid frame. In the case where unrestricted rotation was permitted at the strip ends, maximum bending stress occurred at the strip mid-point and mid-plane tensile stress was greater than bending stress. However, when rotation at the strip attachment was completely restricted, maximum bending stress transferred to the point of attachment and a zone of compression was predicted for this area.

Note that in stress-related valve failure the fluid mechanical shear stresses may also contribute by damaging the leaflet surfaces while the valve is open (Einav *et al*, 1990).

### 6.3.2 Stress and calcification

The build up of rigid calcium deposits, both within and adhering to, flexing leaflets is a major cause of bioprosthesis dysfunction, particularly for porcine valves. Such mineralization occurs frequently in cardiovascular diseases and in association with implanted devices. The mechanism of calcification has not been fully elucidated. Several hypotheses are currently being investigated, any or all of which may be valid (Bernacca, 1991). For example, Schoen & Levy (1991) have proposed that intrinsic leaflet mineralization may develop due to high intracellular calcium concentrations within connective tissue cells from the bioprosthesis, with calcification subsequently involving the extracellular collagen. The raised intracellular calcium levels may result from aldehyde cross-linking or mechanical injury disrupting the cell membranes and interfering with the mechanisms for managing intracellular calcium concentrations. A similar mechanism could apply to the surface calcification, with the mediating cells originating from the host. Calcification in the context of synthetic leaflet valves will be discussed in the proceeding chapter.

Sites of calcium deposit generally coincide with areas of predicted high stress, for both explanted bioprostheses (Deck *et al*, 1982; Sabbah *et al*, 1986) and native aortic valves (Thubrikar *et al*, 1986). A similar calcium distribution has been demonstrated for pericardial valves in a dynamic *in vitro* study; furthermore, scoring the leaflet tissue before running the experiment was seen to promote calcification in the damaged area (Bernacca, 1991 & 1992b). How mechanical stress or strain interacts with the mineralization process is not clear at present. Perhaps there are mechanically-initiated calcification modes, or may be the associated structural disruption simply creates space

which enables initiating agents to come into contact more easily and allows for crystal growth. Once calcification has taken root, the surrounding area becomes increasingly stressed which encourages further material disruption and calcification (Sabbah *et al*, 1985).

Although there is an incomplete understanding of the complex biological interactions, it is probable that a reduction in leaflet stress levels will result in an enhanced *in vivo* valve performance.

## 6.4 Synthetic Valve Alternative

For bioprostheses, especially porcine xenografts, there are only a rather limited range of design options, mechanical and biochemical material properties, and manufacturing techniques available. These limitations may restrict the extent to which their relatively poor long-term performance can be improved. Further, the labour-intensive manufacturing/assembly methods used, combined with the inherent biological variability, result in bioprostheses which are expensive to produce and of variable quality. Note also that an additional cause of anxiety associated with the use of biologically derived materials is the potential for infection(s) being transmitted to patients; such concerns over bovine spongiform encephalopathy resulted in the recent withdrawal of the Glasgow pericardial valve from clinical use.

In contrast to bioprostheses, valves constructed with synthetic leaflets can, at least potentially, accommodate a much wider range of design options and material properties, and thus enable a degree of design optimization which would not be possible for bioprostheses. Also, synthetic valve manufacture may be amenable to automated mass-production techniques which could be advantageous in terms of quality control and ecomony.

A good example of design optimization as applied to a synthetic leaflet aortic valve is provided by Ghista & Reul (1983). They considered 4 design criteria: 1) minimally stressed leaflets, 2) a leaflet shape which enabled a smooth washout of the sinus region during diastole, 3) minimal pressure difference required to open the valve, and 4) adequate durability. The leaflet material was pre-selected (Avcothane: a proprietary composition of 90% polyurethane and 10% polydimethylsiloxane), leaving the leaflet shape and thickness as variable design parameters. The leaflet shape was characterised by 2 principal radii of curvature and their subtending angles. Design requirements 1) & 2) determined the leaflet shape, the stress criterion being developed from Laplace's law. A leaflet thickness, which represented an appropriate compromise between conflicting criteria 3) & 4), could then be defined. An expression for valve opening pressure was derived from an analogy with buckling of clamped spherical domes, and given by:

$$P_{opening} = C_1 \cdot E\ (h/R)^3 \ - \ C_2 \cdot E\ (h/R)^4 \qquad (6.1)$$

where E is the Young's modulus, h the leaflet thickness, R the leaflet radius of curvature, and $C_1$ & $C_2$ are constants. Note the relative sensitivity to leaflet geometry and thickness. The analysis of Ghista & Reul is rather simplified, and in particular, the analogy of valve opening with buckling spherical domes is questionable. However, a valve with good *in vitro* performance was developed as a result and it does illustrate the general point that synthetic valve design can be 'finely tuned' to match the operational requirements. A similar, though less comprehensive, design analysis was presented by Thubrikar & Nolan (1990). By considering the open and closed configurations of a tri-leaflet valve with cylindrical leaflet geometry, they sought to define geometrical design parameters which

eliminated leaflet folds and minimised leaflet flexion. However, the cylindrical leaflet geometry and the assumption that the entire leaflet surface aligns with the direction of flow in the fully open valve may not be widely applicable.

In order to fully exploit the design potential implied by the use of synthetic materials, sufficiently sophisticated manufacturing processes are needed. Complex leaflet geometries suggest the application of computer-aided design and manufacturing (CAD/CAM) techniques in order to produce appropriately shaped formers. Those synthetic materials which are suitable for use as valve leaflets can generally be shaped by a number of means. A particularly appealing method, appropriate to thermoplastic materials, is injection moulding. The merits and practicalities of injection moulding and other techniques, as applied to synthetic leaflet heart valves, are the subject of the succeeding chapters.

# Chapter 7. Polyurethane: A Candidate Material for Tri-Leaflet Prosthetic Heart Valves

## 7.1 Review of Synthetic Flexible Leaflet Valves

Since the earliest days of valve replacement surgery, plastics and other synthetic materials have been considered for the development of a tri-leaflet prosthesis. In the late 1950's and early 1960's, a variety of synthetic valves were developed and subsequently implanted in humans, as reviewed by Roe (1991). Leaflet materials used include silicone rubber reinforced with polyester, polytetrafluoroethylene (PTFE), or polypropylene; and polyurethane reinforced with polyester or PTFE. Generally, the clinical outcomes were poor with frequent thromboembolic complications and early valve failure; their use was abandoned when more reliable mechanical valves, such as the Starr-Edwards, became widely available. These early disappointing results may not reflect valve design or material deficiencies exclusively: patient selection, surgical procedure, and post-operative care may also have contributed. Indeed, Roe (1989) reported on a PTFE-reinforced silicone rubber prosthesis which was functionally sound after 6 years and 10 months human implantation, a second patient survived for 13 years with the same type of valve.

Despite over 30 years of research and development into heart valve replacements, the need for a durable and non-thrombogenic prosthesis persists and the search for a suitable synthetic leaflet valve continues. Furthermore, the potential application for such a synthetic leaflet valve has been extended with the development of ventricular assist devices, artificial hearts, skeletal

muscle ventricles, etc. Devices such as these may be used as a short-term bridge to heart transplantation, in which case long-term performance is less important and economy more so, thus favouring a synthetic valve.

Much of the recent effort in this field has been directed towards polyurethane tri-leaflet valves. Of the range of synthetic materials currently available, polyurethane is a promising candidate, being relatively durable, but flexible, and relatively biocompatible. However, by no means is polyurethane ideal, and further developments in polymer science are keenly awaited.

### 7.1.1 Polyurethane valves

A variety of polyurethane (PU) valves have been developed and evaluated in recent times, though none has reached the stage of human implantation.

Unfortunately, authors frequently publish little or no detailed information on their valve designs; this is particularly relevant given that leaflet stresses are highly sensitive to geometry (see Chapter 6). However, there are notable exceptions. Ghista & Reul (1983) chose an ellipsoid of revolution shaped leaflet: elliptical along the axis of flow and circular in the perpendicular plane. Notice that such a configuration may, depending on how the leaflets are mounted on the stent, result in a sizeable hole at the centre of the unloaded valve. Such a hole would require the leaflet material to stretch and/or the stent to bend inwards in order to prevent backflow. On the other hand, Wisman *et al* (1982) deliberately introduced a small central opening in order to improve their valve's opening characteristics. Despite using a cylindrical leaflet geometry which gave rise to a minimal coaptational area, the Wisman *et al* valve performed competently in a pulse duplicator. Spherical leaflet geometries, running into plane surfaces in the coaptation zone, have been widely adopted (Evans, 1987; Herold *et*

*al*, 1987; Knierbein *et al*, 1990b).

Unlike most others, Jansen *et al* (1991) moulded their valve in a partially open position. They used a conical former to stretch the frame while moulding the leaflets as flat as possible; the stent expansion enabled sufficient leaflet surface areas for good open and closed configurations. The resulting valve leaflets took up a cylindrical shape under back pressure (the closed leaflet geometry depends, to an extent, upon the shape of the stent) and opened by means of a 2-dimensional rolling motion without buckling. Comparing the associated *in vitro* energy losses of this valve with those of their earlier PU valve which was moulded in the closed position (Herold *et al*, 1987), the new valve shows considerably less energy loss when open but slightly more when closed. Similarly, Yu *et al* (1989) formed their artificial heart PU valve in the closed position but annealed in the open position.

Leaflet thickness distributions, qualitatively similar to that of the native aortic valve, have been incorporated into dip moulded valves (Herold *et al*, 1987; Knierbein *et al*, 1990b). This is rather difficult to accomplish in practice and requires sophisticated dipping and drying techniques. Dip moulded PU valves have been developed by other investigators, but the leaflet thickness distribution has not been explicitly referred to (Russell *et al*, 1980; Wisman *et al*, 1982; Ghista & Reul, 1983; Jansen *et al*, 1986 & 1991); presumably, these valves also had non-uniform thickness distributions as maintaining an even thickness across such curved leaflet surfaces would be problematic. Alternative methods of valve manufacture, such as vacuum forming (Jansen *et al*, 1986; Yu *et al*, 1989), are also likely to introduce non-uniform leaflet thicknesses as initially flat sheets of PU stretch to take up the leaflet shape. Evans (1987) constructed valves by mounting cast PU films onto frames, and then imposing a closed leaflet shape with a former

while immersing the valve in a hot part-solvent. Although the initial cast films were of uniform thickness, the moulding process may have stretched the leaflets and introduced a thickness distribution, depending on the way in which the leaflets were originally mounted on the stent.

Generally, tri-leaflet PU valves have hydrodynamic characteristics similar to those of bioprostheses, as discussed in Chapter 3. This is not surprising given their similarity of construction. PU valves can be constructed to function exceedingly efficiently, in terms of pressure gradient and energy required to open and close, simply by reducing the leaflet thickness. However, the enhancement in function may be accompanied by a decrease in durability (Ghista & Reul, 1983). Typical leaflet thicknesses used are in the range 100-200 $\mu$m. Published results for accelerated fatigue testing have generally been rather poor, with leaflet tears developing within a few tens of millions of cycles (Jansen *et al*, 1986; Evans, 1987; Herold *et al*, 1987; Yu *et al*, 1989), even with leaflets reinforced with nylon mesh (Tsutsui *et al*, 1985). Considerably better results have recently been reported by Jansen *et al* (1991), with several of their latest PU prototypes exceeding 400 million cycles; their blood-pump PU valves have also achieved similar fatigue lifetimes (Knierbein *et al*, 1990b). Earlier, Ghista & Reul (1983) reported fatigue lifetimes in excess of 560 million cycles, but they did not specify the leaflet thickness or state the number of valves involved.

PU valves have failed in animal trials owing to calcification and thrombus formation. The optimally-designed valve of Ghista & Reul (1983) was heavily calcified after 5 months implantation in the aortic position of a calf; mineral deposits appeared to be associated with microscopic defects on the leaflet surfaces (Hennig & Bücherl, 1984). More recent dip moulded valves have also accumulated thrombus and calcium

deposits in calves, although to a slightly lesser extent than in bioprostheses implanted as controls (Herold *et al*, 1987; Jansen *et al*, 1991). Vacuum formed PU valves similarly calcify (Hoffman *et al*, 1991). Hilbert *et al* (1987) distinguished 2 types of calcification in their PU valves explanted from sheep: gross calcification was identified with degenerated cells within thrombotic material and the fibrous sheathing; and microscopic plaque-like calcific lesions, with needle-like projections penetrating the leaflet surface, were also observed. The degree of calcification, under similar conditions, is highly variable and depends on the animal model used (Wisman *et al*, 1982).

It is not known whether the calcification occurring in PU valves is an intrinsic property of the polymer, or if it is mediated by external processes such as thrombus formation. Calcium deposits may be associated with surface defects and tend to accumulate in areas undergoing greatest dynamic flexure. Analogous correlations have been reported for PU blood pump diaphragms (Hennig & Bücherl, 1984; Harasaki *et al*, 1987). As in the case of bioprostheses, a PU valve design which reduces operational stresses will probably elicit an enhanced *in vivo* performance.

Finally, mention should be made of a novel PU blood pump valve, introduced by Imachi *et al* (1989). Their 'jellyfish' valve comprises of flat circular membrane of PU, attached at its centre to a base wheel; the base has 12 thin spokes which prevent prolapse of the valve membrane. Imachi *et al* have demonstrated that their valve can function efficiently *in vitro*. They did not, however, measure downstream flow velocities or shear stresses; such an investigation would be most useful, given the unique valve design. Artificial hearts utilizing this valve type were tested in goats for up to 112 days; a limited amount of thrombus congregated around the valves, but this was thought to be associated with the valve

mountings rather than the valves themselves.

### 7.1.2 Other synthetic valves

Though PU has received most recent attention, several alternative synthetic polymers have been considered as leaflet materials.

Valves with silicone rubber (Mohri *et al*, 1973; Chetta & Lloyd, 1980), or polyester reinforced silicone rubber (Gerring *et al*, 1974), leaflets have been developed. Such materials are relatively easy to process and facilitate single stage valve manufacture by compression or injection moulding (Black, 1973). Some of these valves have performed well in accelerated fatigue tests: for example, Mohri *et al* (1973) reported an average durability equivalent to 22 years of cycling. However, it should be borne in mind that these tests do not simulate biological processes nor do they necessarily represent a reliable measurement of the absolute durability which would be achieved under physiological loading in the absence of biological processes. Chetta & Lloyd (1980) reported that their silicone rubber valve work hardened and failed to open whilst undergoing an accelerated fatigue test. Generally, silicone rubber-based flexible leaflet valves have performed poorly as human implants, with leaflet tears appearing within a few months and frequent thrombotic complications (Fishbein *et al*, 1975). Recently developed silicone rubbers are claimed to be much stronger than the older types and are being used as tri-leaflet valve materials in prototype artificial hearts (Kolff & Yu, 1989). Also, polyolefin rubbers, which have promising mechanical and biological properties, have been used to compression mould tri-leaflet valves for intended use in blood pumps (Kiraly *et al*, 1982).

Flexible leaflet PTFE valves have been tested in dogs (Imamura & Kaye, 1977) and sheep (Nistal *et al*,

1990). Unfortunately, they have suffered a similar fate to PU valves, with calcification, thrombus and leaflet stiffening reported. Other leaflet materials investigated include polyester fabric with bonded heparin (Clark *et al*, 1974) or coated with hydrogel (Nardi *et al*, 1982).

## 7.2 Polyurethane

"Polyurethane" is a generic term representing a family of synthetic polymers. Those considered for use in flexible leaflet heart valves are the PU elastomers. They are composed of alternating blocks of hard and soft segments, and hence are termed block copolymers. PU elastomers typically exhibit a 2-phase microstructure with hard and soft segments segregating into domains; the microphase separation is believed to endow desirable mechanical and physical properties to the bulk polymer. A wide range of mechanical and physical properties can be realized within the range of molecular weight, molar ratios, and chemical constituents possible for each type of segment. Consequently, PU's have been considered, and in some cases used clinically, for various blood-contacting applications with differing mechanical requirements, including vascular prostheses, pacemaker lead insulation, cardiac-assist devices, catheters, as well as prosthetic heart valves (Lelah & Cooper, 1986).

### 7.2.1 Chemistry and structure

PU elastomers are generally produced by the addition of a polyglycol with a diisocyanate (fig 7.1); alternating segment units combine to form an $(AB)_n$ type block copolymer, with n = 10 to 20 typically. The polyglycol soft segment unit is frequently a polyether- or polyester-diol with molecular weight between 500 and

**Figure 7.1 Synthesis of polyurethanes**

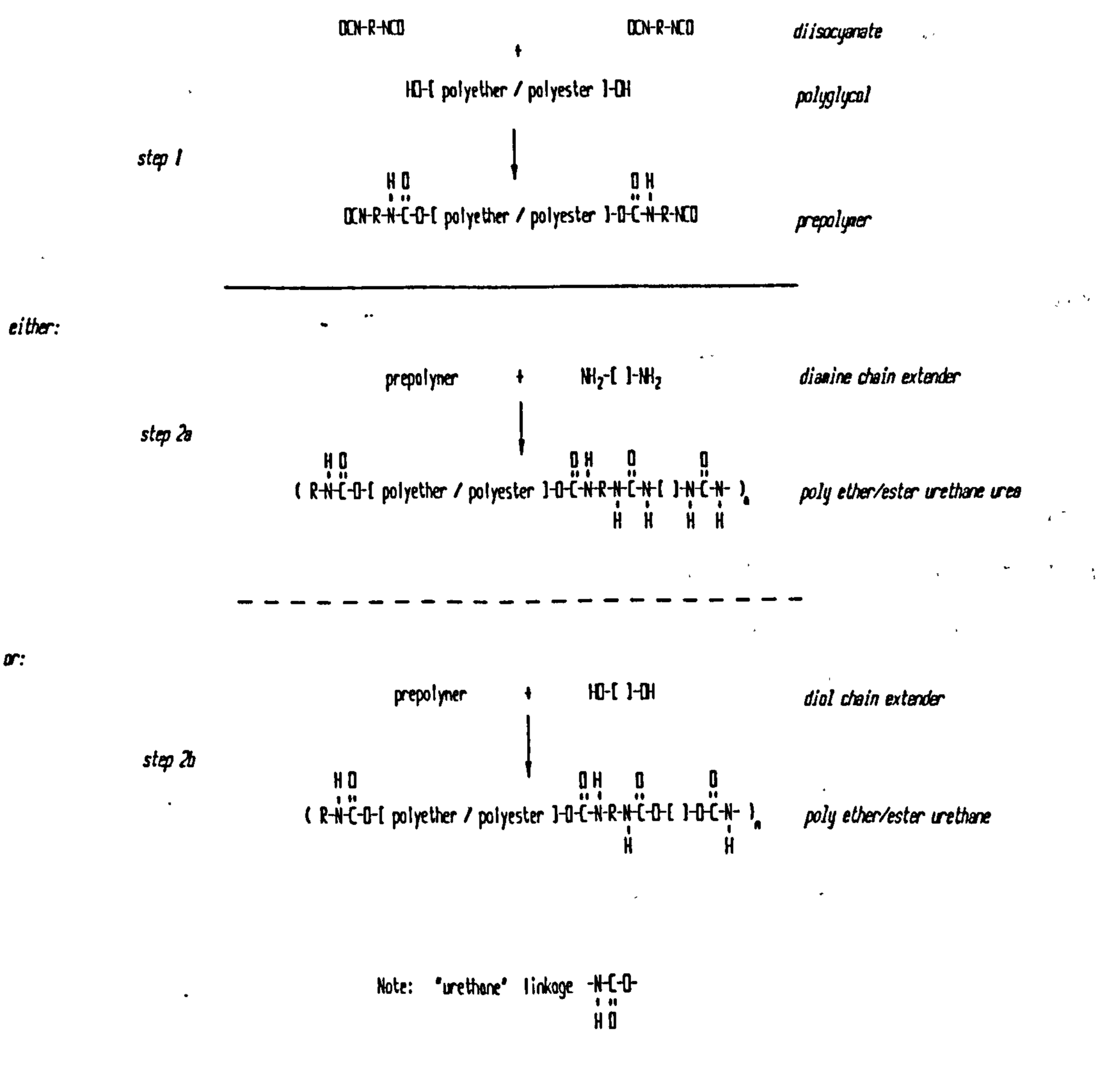


Note: "urethane" linkage -N-C-O-
H O

5000. The hard segment unit is usually a chain-extended aromatic diisocyanate of molecular weight 300 to 3000; low molecular weight diols or diamines are used as chain extenders. For the PU elastomers considered for use in flexible leaflet valves, the soft segments are in a rubbery state with glass transition temperatures well below room temperature, while the rigid hard segments may exist in a semicrystalline or glassy state. Incompatibility of the hard and soft segments results in a microphase separation with hard segments dispersed into domains 5 to 10 nanometres in size, within a matrix of soft segments. The detailed microphase structure has yet to be elucidated. The hard domains act as multifunctional cross linking sites and reinforcing fillers. The composition of rigid hard domains embedded in an elastomeric matrix results in a material which is flexible but tough.

The compositions of commercially available PU's used in the course of this study are given in table 7.1. Pellethane is much less soluble now than when it was first introduced in the early 1970's, suggesting that the bulk polymer has undergone significant structural changes (Gilding & Reed, 1987). A 'medical grade' polyester-based Estane is available, but the ester linkage is susceptible to hydrolytic degradation and polyether-based PU's are preferred for *in vivo* applications (Lelah & Cooper, 1986). Lycra, while not available as a 'medical grade' polymer, has the same basic composition as Biomer, and Biomer has been widely used in prototype cardiovascular prostheses. Unlike Biomer, Lycra has 3-5% polydimethylsiloxane blended with, and partially covalently linked to, the main polymer (McMillin, 1989). However, owing to the high concentration of urea groups in such diamine-extended PU's, these polymers degrade at temperatures close to their melting point and are not suitable for melt processing (Lelah & Cooper, 1986).

Table 7.1 Polyurethane compositions

| Polyurethane | Soft segment | Hard segement | Chain extender |
|---|---|---|---|
| Pellethane 2363 (Dow Chemical Co) | PTMG | MDI | Butanediol |
| Estane 58271 | Polyester-based | MDI | Butanediol |
| 58315 (BF Goodrich Ltd) | Polyether-based | | |
| Lycra (DuPont Co) | PTMG | MDI | Ethylene diamine |

Key:- PTMG = poly(tetramethylene ether glycol)
MDI = methylene bisphenyl diisocyanate

### 7.2.2 Mechanical properties

In the context of choosing a leaflet material for a prosthetic heart valve, an advantage of synthetic polymers over biological materials is that, by controlling their chemical composition, a wide range of mechanical properties can, in principle, be engineered. PU's demonstrate this well. For example, increasing the soft segment molecular weight results in a lower elastic modulus and tensile strength but greater ultimate elongation (Wouters *et al*, 1986; Hayashi, 1987).

PU's elastomers are generally tougher and more wear resistant than other polymers used in biomedical applications, such as silicone rubbers and PVC. However, compared with aortic valve tissue they are much less compliant, particularly at low strains. For example, compare the stress-strain characteristic for Avcothane (as used in the Ghista & Reul (1983) valve) reproduced in figure 7.2 with that for aortic valve tissue (fig 6.2). While PU becomes increasingly compliant at higher strains, aortic valve tissue behaves in the reverse manner. PU's do exhibit stress relaxation and creep in uniaxial tests, depending on their chemistry and structure (Wouters *et al*, 1986; Hayashi, 1987). Nevertheless, creep has not been reported as a problem in prototype PU valves, and a degree of relaxation may even be beneficial in reducing stresses in the closed valve.

Notice that even though elastomeric PU's may share the same basic chemical constituents, their mechanical and physical properties may be rather different owing to varying degrees of crosslinking or chain branching, the presence of additives such as stabilizers, processing aids, etc, and depending on the method of processing. There may also be a degree of batch-to-batch variability for a given PU.

Figure 7.2 Example stress-strain characteristic for polyurethane elastomer
(from Ghista & Reul, 1983)

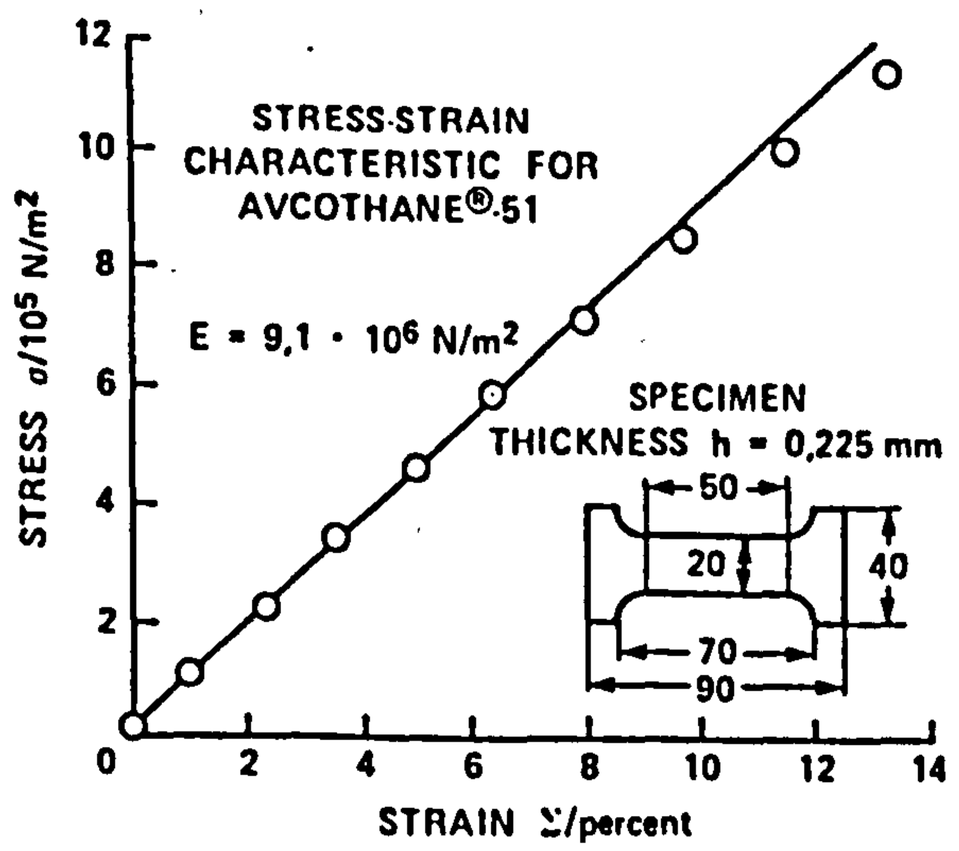

## 7.3 Manufacture of Polyurethane Valves

Prototype PU valves have been fabricated by several methods, as outlined in section 7.1.1. Dip moulding is probably the most common method. As well as forming the leaflet surfaces, dipping can also integrate the leaflets with a PU-coated frame. The principal drawback with this technique is the difficulty in controlling the leaflet thickness distribution. When the former is left to 'dry' after being dipped in a viscous PU solution, the PU coating flows across the curved mould surface under the influence of gravity and accumulates at the lowest points. The final leaflet thickness distribution is determined by a number of factors: the viscosity and evaporation rate of the particular PU solution; the ambient temperature and solvent concentration; the dipping and drying movement; and the former geometry. In an attempt to control the thickness distribution, Herold *et al* (1987) have developed a dipping and tumbling device which is used in a controlled environment within a glove box. The dipping and tumbling device has been designed to create a thickness distribution qualitatively similar to that of the native aortic valve, with the thinnest area in the leaflet belly. Despite these measures, they experienced problems producing PU valves with consistent thickness distributions.

Controlling the leaflet thickness distribution is generally a problem for manufacturing methods in which the leaflet material is softened, by heat or solvents, and then moulded by stretching over a former. This problem can be overcome by restraining both leaflet surfaces during moulding, i.e. using a male-female mould rather than a male or female only mould. Such a technique, suitable for thermoplastic PU's with the exception of the polyurethane ureas, is injection moulding.

This present study aims to investigate the

feasibility of injection moulding PU valves. As compared to other manufacturing methods, injection moulding presents several advantages:

(1) The most intricate of valve designs may be realized in a controlled manner, as molten PU may be squeezed into the most convoluted of cavities.

(2) Leaflet thickness distributions may be accurately controlled. Thus, thickness distributions similar to that of the native aortic valve could be incorporated. Also, an effect similar to the circumferential reinforcement of the native aortic valve could be achieved by introducing circumferential ribbing (Wouters *et al*, 1986). The optimum thickness distribution for a PU valve has yet to be defined.

(3) Complete valves could be manufactured in a single stage operation, with integral leaflets and frames. Valves could be made entirely from PU, or if PU frames were not sufficiently rigid, frames could be reinforced with inserts which become encapsulated during the moulding process. Similarly, sewing rings could be incorporated as inserts.

(4) A high degree of consistency is associated with injection moulded parts, particularly when the process is fully automated.

(5) With an automated injection moulding process, inexpensive PU valves could be mass-produced. A typical cycle time for a valve-sized PU moulding might be less than 30 seconds. In this

country the cost of prosthetic valves is of secondary importance. However, in overseas countries in which financial resources are scarce and rheumatic fever considerably more prevalent, economic considerations are of major importance. Inexpensive valves are also required for cardiac-assist devices intended for short-term use.

(6) Injection moulding does not involve the use of those highly toxic solvents which are necessary to dissolve PU.

Furthermore, injection moulding is a general technique applicable to a wide range of thermoplastic materials. If an injection moulding process could be successfully applied to the manufacture of PU valves, then the same process, or a similar one, may also be used to produce valves from other thermoplastics. This is an important consideration given that calcification of PU valves may prove to be unavoidable, and that materials more biocompatible and more durable than PU may be developed in the future. Additionally, the shaped cavity of an injection moulding tool could easily be converted for use as a dip moulding tool. Thus, if it turned out that a PU valve could not be practicably injection moulded, within the limits of existing technology, then the machining effort required to create the injection moulding tool could be exploited to produce dip moulded valves.

Potential drawbacks associated with injection moulding are:

(1) The high injection pressures required to fill thin leaflet sections, and the associated molecular contortions, might give rise to some degree of 'frozen-in' stress in the mouldings.

Such 'frozen-in' stresses may compromise the material's mechanical properties. Also, they may be relieved when the valve is worked, resulting in geometrical distortion. PU mouldings can be dry-heat annealed, however, to minimize such effects.

(2) A small degree of shrinkage is associated with injection moulding and annealing: typically < 1%, depending on the part and tool design and the processing conditions.

(3) The construction of an injection moulding tool may involve a considerable amount of rather intricate machining. This may be particularly so for a tri-leaflet valve tool with complex leaflet geometries. However, with the introduction of CAD/CAM techniques, involved machining operations have become much less of a problem.

There is a further concern associated with melt processing PU's with hard segments based on methylene bisphenyl diisocyanate (MDI). Upon melt processing, particularly in the presence of moisture, MDI may thermally decompose to the carcinogenic methylene dianiline (MDA). However, data on the potential carcinogenesis of PU's implanted in rats are in many cases contradictory, and there is no evidence of a carcinogenic response to extruded PU's in humans. MDA formation may be avoided by using PU's with aliphatic-based hard segments; such PU's are also more resistant to ultraviolet light but they may be less water and heat stable than their aromatic analogues (Lelah & Cooper, 1986; Gogolewski, 1989). Note that if MDA is produced as a result of melt processing, it may be possible to remove it by solvent extraction.

In melt processes such as injection moulding and extrusion, flowing polymer molecules tend to orientate themselves in the direction of travel. Consequently, the resultant mouldings may have a preponderance of molecules orientated in one particular direction and exhibit a degree of anisotropy. By judicious tool design, it may be possible to introduce such anisotropy into an injection moulded valve in a manner which enhances the valve's function and durability. Given the structure of the native aortic valve and the predictions of finite element stress modelling, it would probably be beneficial to preferentially orientate the polymer molecules circumferentially in the valve leaflets, depending on the leaflet geometry and thickness distribution. However, designing the injection moulding tool to orientate the polymer molecules in a given direction may conflict with the requirement of producing a moulding with minimal 'frozen-in' stress and warpage, and/or may not be practical. Notice that, in general, the molecular architecture, and most pertinently the molecular arrangement at the surface, may be different for an injection moulded PU valve than for a dip moulded valve made from the same PU. Therefore, an injection moulded valve may well provoke a biological response which is rather different to that elicited by the analogous dip moulded valve.

## 7.4 Summary

In response to the need for a durable and non-thrombogenic prosthesis, several PU prototype valves have been developed but all have performed rather poorly in subsequent animal trials. An improved *in vivo* performance may result from the use of a chemically-modified PU or an alternative synthetic material, combined with an optimal low-stress valve design. The modifications necessary to eliminate PU calcification have yet to be developed and a

better suited material does not appear to be presently available. Similarly, an optimal valve design has yet to be defined. In light of this situation, a study has been undertaken to consider the feasibility of producing PU valves by injection moulding. Such a manufacturing technique is capable of realizing the full design potential associated with the use of a synthetic material and is generally applicable to a range of thermoplastics; there are further advantages in terms of simplicity of manufacture, quality control, and economy.

# Chapter 8. Towards an Injection Moulded Polyurethane Valve (I)

## 8.1 Introduction

Injection moulding is a well established manufacturing process, commonly employed in the mass-production of PU devices. The case for applying this technique to the fabrication of tri-leaflet PU valves was presented in the previous chapter. Initial attempts at moulding PU valves, using simple moulding tools and machines, are described in this chapter. An integrated CAD/CAM system, based upon commercially available software, was developed in order to construct injection moulding tools. These early moulding trials demonstrated the necessity for a more sophisticated approach. The work described in this chapter was carried out entirely within the Universities of Strathclyde and Glasgow.

## 8.2 Overview of Injection Moulding

In general terms, injection moulding is a process whereby thermoplastic material is melted and forced into a cool, closed mould. The pressurized melt adopts the shape of the mould cavity and cools; once the plastic has solidified the moulded part can be ejected.

Injection moulding machines come in a range of designs and capacities, and allow varying degrees of control over the moulding conditions. The simplest of moulding machines are manually-powered and, essentially, function as large heated syringes. More sophisticated, and more powerful, machines employ hydraulically-powered injection and ejection mechanisms. Depending on the particular machine, operating conditions such as melt and mould temperature, injection pressure or melt flow, and injection time, can be controlled. These processing

conditions can greatly influence the quality of the mouldings produced.

The pressure applied by a moulding machine during a typical moulding cycle is shown in figure 8.1. The cycle is divided into 3 stages: *filling*, *packing*, and *cooling*. Initially the injection pressure rises as the mould fills, and once the mould is apparently full a packing pressure is maintained. During this holding period more molten plastic is packed into the mould. Under the considerable pressures involved, the molten plastic is significantly compressible: typically 10% more material can be squeezed into the mould under a pressure of 100 MPa. Since the polymer density increases slightly as the melt solidifies, the packing phase helps to maintain a constant volume of plastic within the mould and prevent shrinkage. Once the *gate*, which is simply a restriction in the flow path between the machine nozzle and the mould cavity, freezes solid the moulding cannot be packed any further and molten plastic is prevented from flowing backwards out of the mould; the moulding is then left to solidify before being ejected. During this cooling period and the subsequent ejection stage, the moulding machine is usually charged with the next shot of plastic in preparation for the next cycle.

Filling a relatively cool mould with hot molten plastic involves an interesting interaction of fluid dynamic and heat transfer processes. When a melt first enters a mould, the skin of plastic immediately in contact with the cool walls freezes rapidly while the central core remains molten (fig 8.2). As more material is injected, molten plastic flows into this central region displacing the material already there forwards and outwards. The outward flowing plastic forms the next section of frozen skin while the forward flowing material continues the molten core. Further material entering the mould passes along these molten channels lined with frozen layers of plastic. As hot plastic flows into the

Figure 8.1 Typical cavity pressure profile throughout moulding cycle

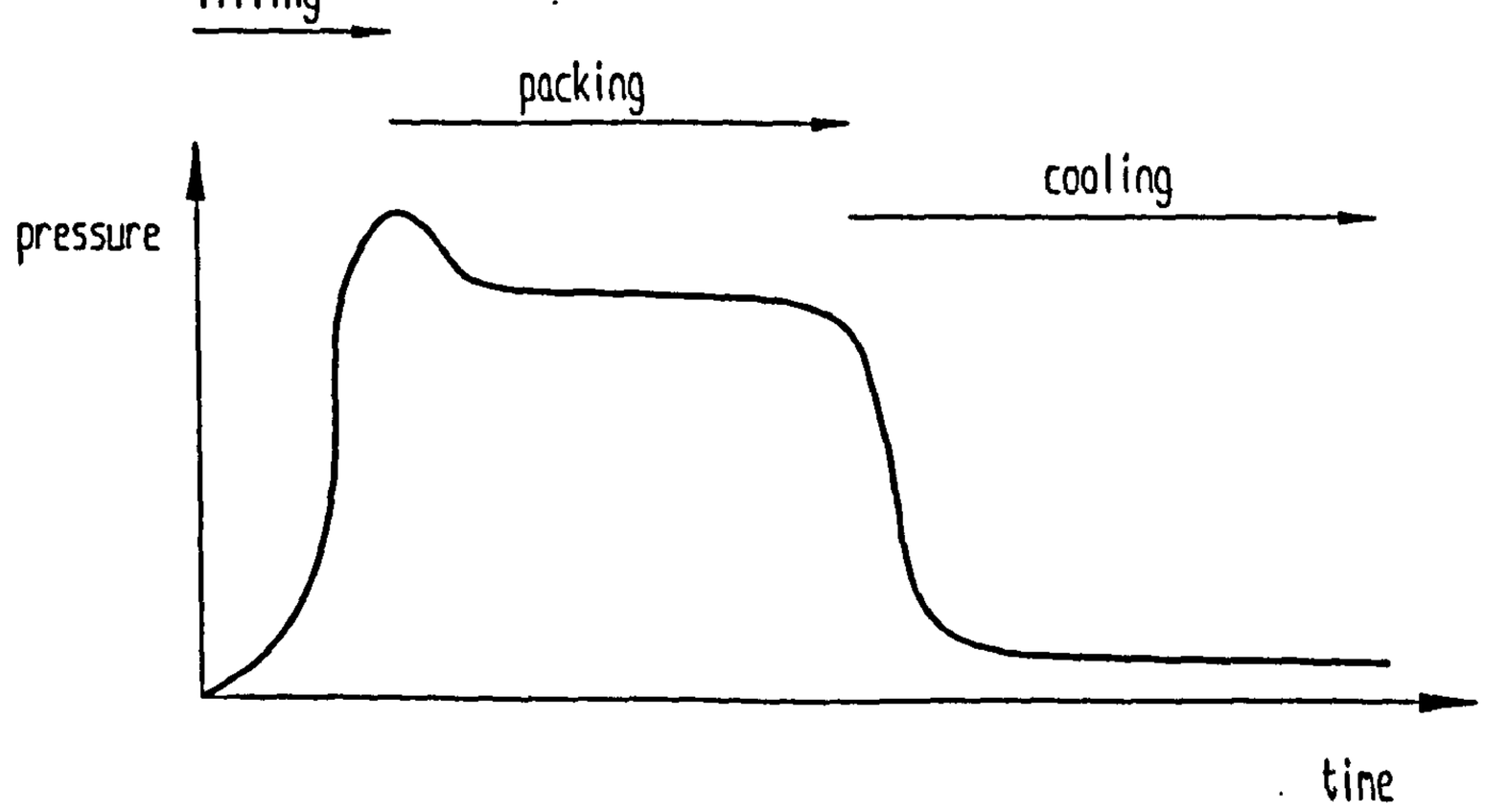

Figure 8.2 Schematic melt flow through mould cavity

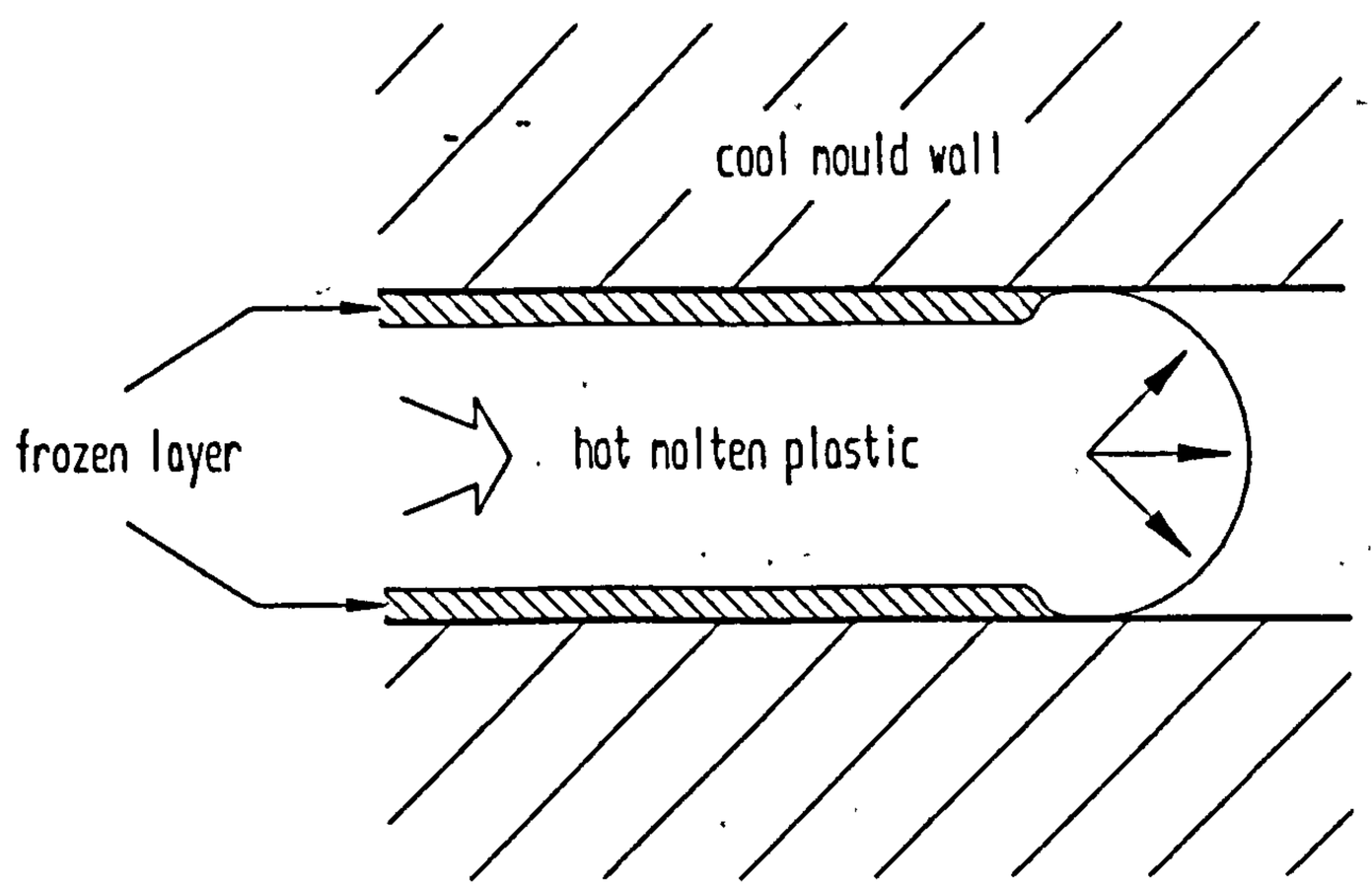

mould it looses heat through the frozen layer to the cool mould walls, but some frictional heat is also being generated. Initially the frozen layer is very thin and heat is rapidly lost to the walls. Consequently, the frozen layer thickens as more plastic freezes and thus less heat is lost by conduction. After a time an equilibrium frozen layer thickness is attained. The equilibrium can be shifted by, for example, increasing the injection rate. This would increase both the heat flow input and the frictional heating effect and result in a thinner frozen layer. A similar effect could be achieved by raising the melt or mould temperature.

There is a tendency to amplify slight instabilities that may be inherent in the filling process. For example, if one localised part of the melt was slightly cooler than the surrounding molten plastic, then melt flow would be decreased locally. Less hot plastic would flow into the locally cool region and less frictional heat would be generated, thus the frozen layer would thicken and may eventually span the entire flow channel, freezing off the entire area. Correspondingly, a localised area of slightly hotter plastic would encourage greater flow into this area and reduce the frozen layer thickness. Further, note that the frozen layer is produced by the melt flow front inflating, and as such it is subject to only a relatively low shear stress. Thus, the surface of the unstressed moulding might be expected to show little evidence of a preferred molecular orientation. On the other hand, those layers of plastic which were just inside the frozen layer during the filling phase might be expected to show a much higher degree of preferred molecular orientation. These layers experience the greatest shear rates as the melt flows into the mould. Also, these molten layers are closest to the walls and will freeze immediately the flow stops, thereby entrapping molecular orientations induced by the high shear stresses. Plastic layers nearer the centre of the

flowing core experience lower shear stresses and take a longer time to solidify after the flow has halted, thus what molecular alignment there is has more time to relax away.

As was mentioned earlier, the moulding conditions can greatly influence the integrity of the moulded part. For example, dropping the melt temperature while maintaining a constant filling and packing pressure may result in a decrease in part weight (fig 8.3). Melt viscosities are, generally, highly sensitive to temperature, so reducing the temperature results in a greater pressure drop over the runner system (which is the flow path connecting the machine nozzle to the mould cavity). Thus, there is less pressure available to pack the cavity and the resultant moulding shows sink marks. Raising the melt temperature gives rise to an increased cavity pressure and a better packed part, but increasing the melt temperature too much may increase the volumetric shrinkage associated with cooling to such an extent that the advantage of having a slightly higher packing pressure is outweighed, and again may result in a reduced part weight. Also, increasing the melt temperature may increase thermal degradation. Equivalent effects can result from increasing the mould temperature. Similarly, holding the melt and mould temperatures constant and varying the injection rate reveals an optimum injection rate (fig 8.4). For short fill times high shear rates and therefore high pressures are required. However, long fill times also require higher pressures: the slower moving melt looses more heat by conduction and generates less frictional heat, thus the melt viscosity increases and greater force is required to fill the cavity. Note that the quality of the moulded part is also dependent upon the mould tool design.

Shrinkage of the moulded part, or warpage caused by differential shrinkage, can be a problem in injection moulding. There are several potential causes of warpage.

Figure 8.3 Schematic effect of melt temperature upon moulded part weight

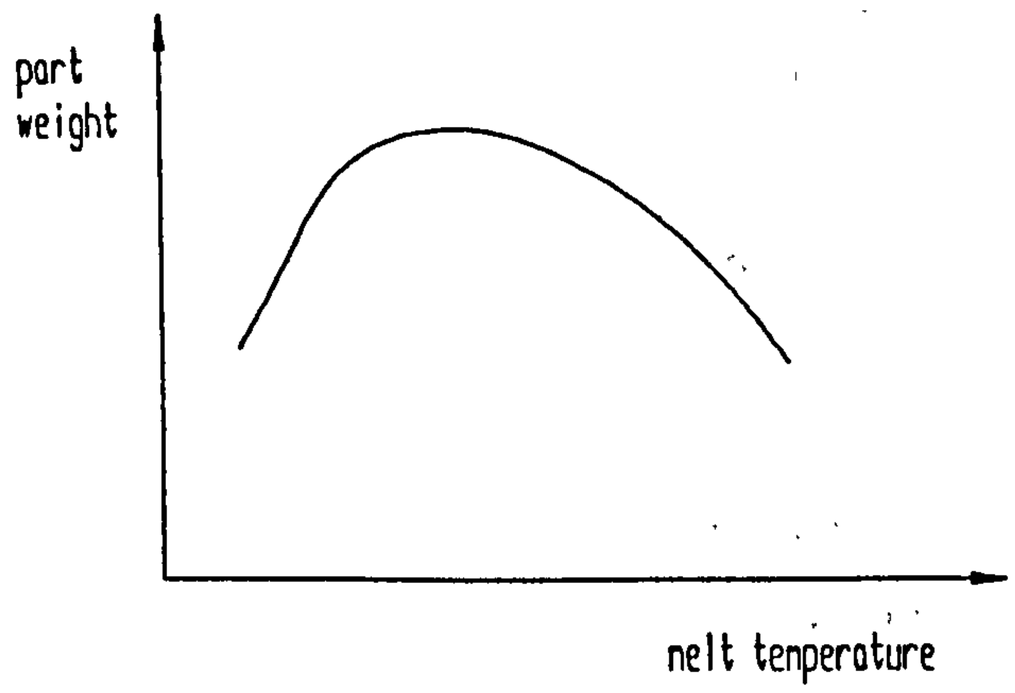


Figure 8.4 Schematic effect of injection rate upon pressure required to fill

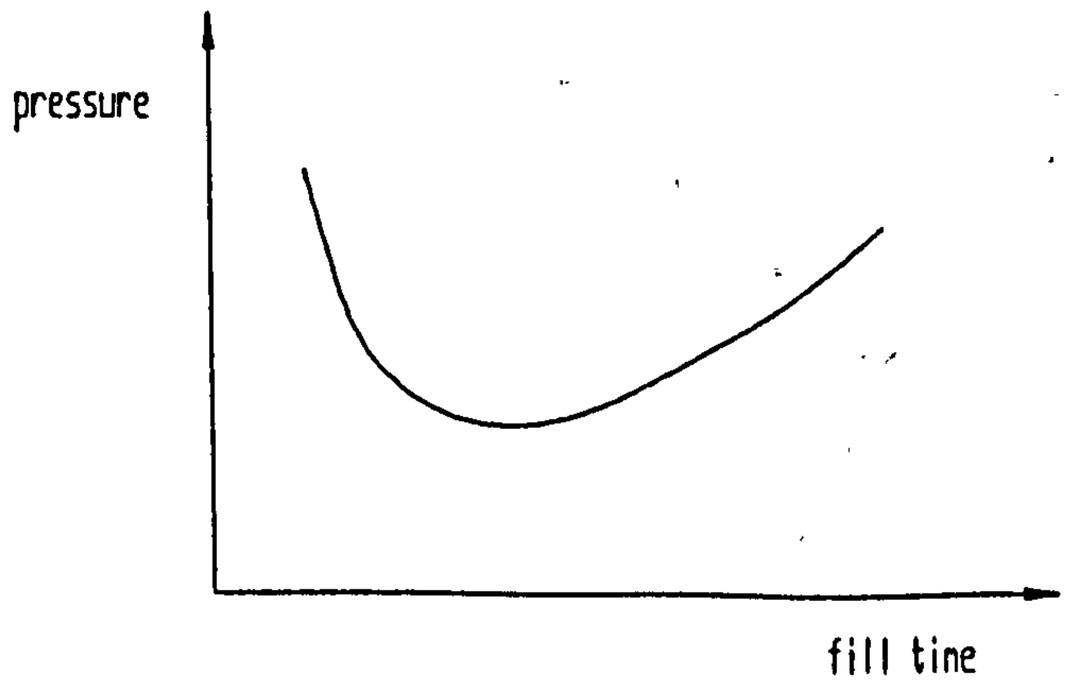

For example, warpage may arise if one area of a moulding is packed to a greater extent than another. Generally, areas in which there is a degree of preferred molecular orientation shrink more upon cooling than areas of random molecular orientation, therefore differential degrees of molecular orientation may result in warpage. Similarly for crystalline thermoplastics, areas of the moulding which cool at a slower rate than others may result in differential degrees of crystallinity and thus differential shrinkage. Warpage can also occur even though each area of the moulding shrinks the same amount, if different areas cool at different times.

## 8.3 Computer-assisted Design and Manufacturing System

The optimal design configuration for a tri-leaflet PU valve, with design parameters such as leaflet geometry and thickness distribution, is unknown. Plausible-looking leaflet shapes have rather complex geometries, particularly in the region where the leaflet belly runs into the coaptation zone. In order to construct injection moulding tools suitable for PU valves, an integrated CAD/CAM system, based upon commercially available software, has been developed. The system is generally applicable to any leaflet geometry which can be described in terms of conic sections or cubic splines, and is capable of realising the most complex of mould geometries. Additionally, since male and female mould surfaces can be described independently, mould cavities with the most complex of leaflet thickness distributions can also be achieved. The intricate machining operations which can be accomplished with this CAD/CAM approach would be difficult, if not practically impossible, to achieve by conventional methods. The unavailability of such computerised technology may have discouraged investigators from attempting to injection mould PU valves in the past.

The CAD/CAM software runs on a DOS-based IBM PC. The design and drafting procedure utilises CADKEY 3.0 (Cadkey Inc.). This program provides 2 methods for generating valve designs. Firstly, CADKEY has a solid-modelling facility. This allows representations of solid objects to be created by the addition or subtraction of intersecting, pre-defined, solid primitives. Solids are described in terms of a surface mesh of triangular or square elements. For example, a surface-mesh representation of a tri-leaflet valve with a spherical leaflet geometry may be generated by subtracting 3 spheres from an intersecting cylinder (fig 8.5). CADKEY is supplied with a library of solid primitives, such as spheres, cubes, cylinders etc, and new solid primitives can be user-created from wire-frame constructions of straight lines, arcs, cubic splines etc. However, the process of subtracting solid primitives proved to be rather slow and unreliable, particularly when more complex leaflet geometries were involved. A better method of creating valve representations is to describe the desired surface in terms of families of coordinate points lying on the valve surface. CADKEY can then be used to interpolate between the defined node points using cubic splines, and the surface is thus described (fig 8.6). By incorporating a large number of coordinate points, a very smooth representation of the curved leaflet geometry can be achieved; much smoother, in fact, than the meshed representation which is produced by the solid-modelling facility. The initial coordinate points which define the valve surface could be input manually, but this would be very slow and tedious. The preferred alternative, and the method adopted here, is to write a short program to generate the coordinate points and store them in an ASCII file, as CADKEY is capable of reading coordinate data files in this format. A listing of an example program, written in Turbo Pascal 5.0, is reproduced in Appendix 2. The program simply calculates points of intersection

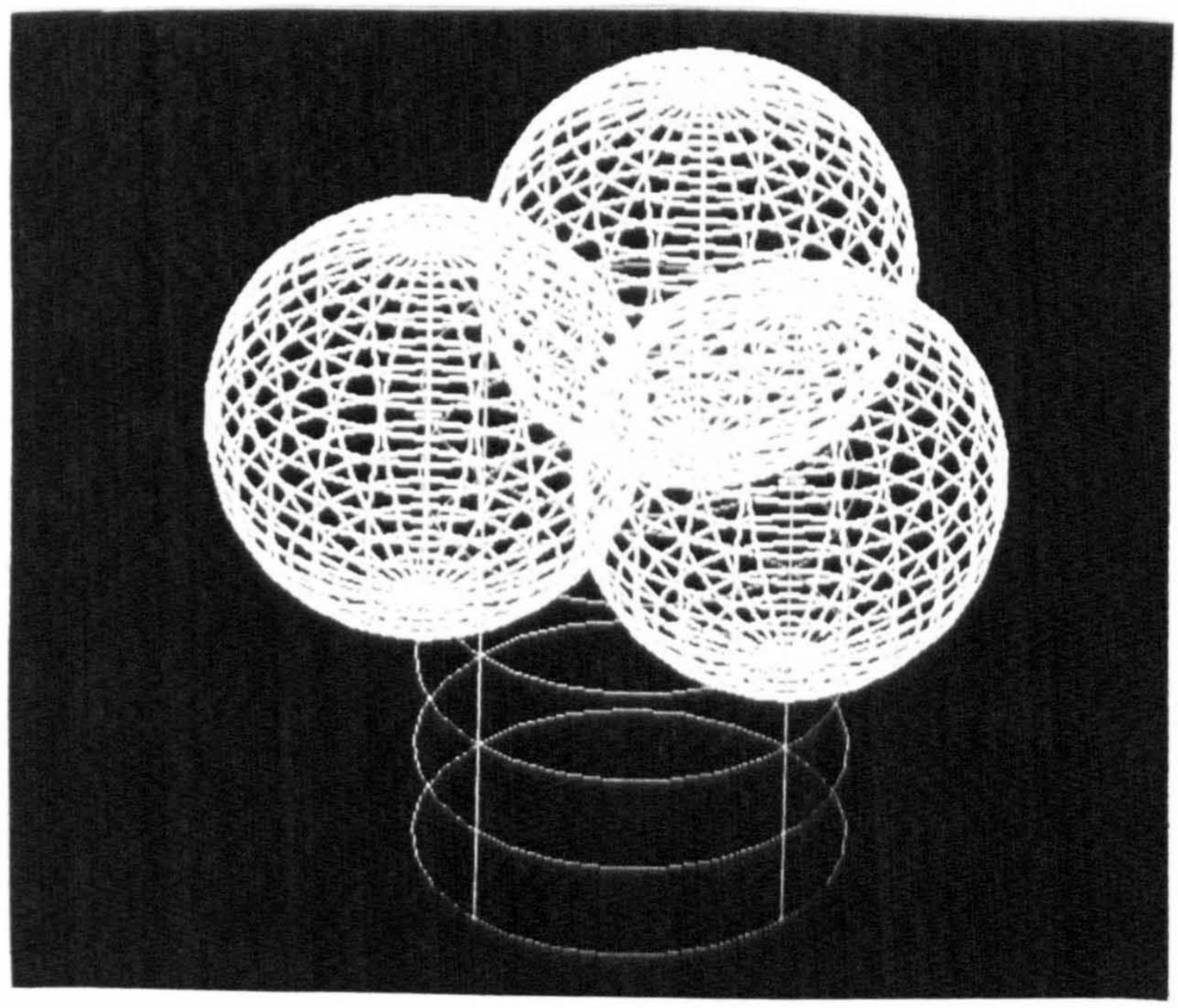

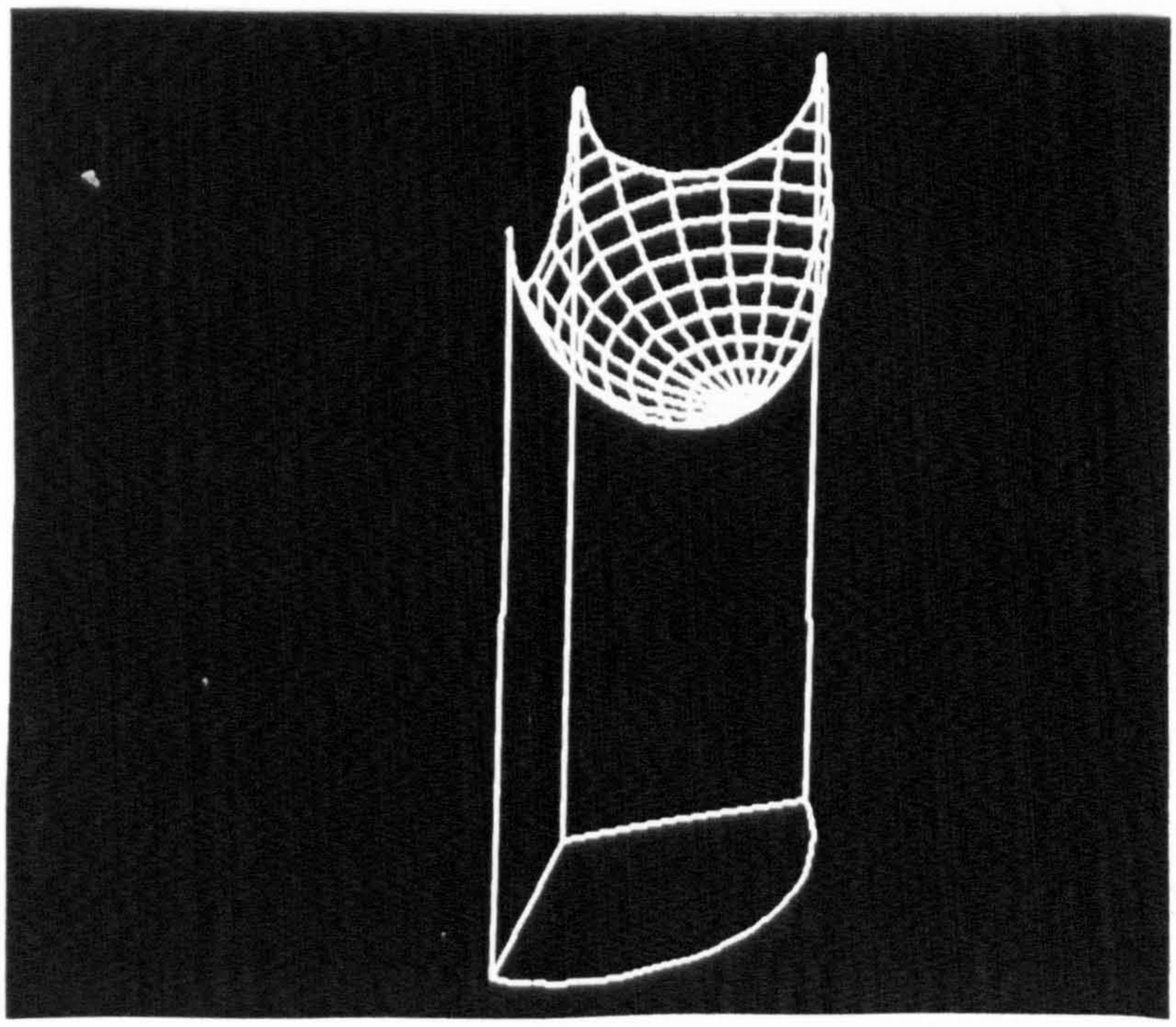

Figure 8.5 CADKEY solid modelling facility

(Creating a spherical leaflet representation by subtracting 3 spheres from a cylinder)

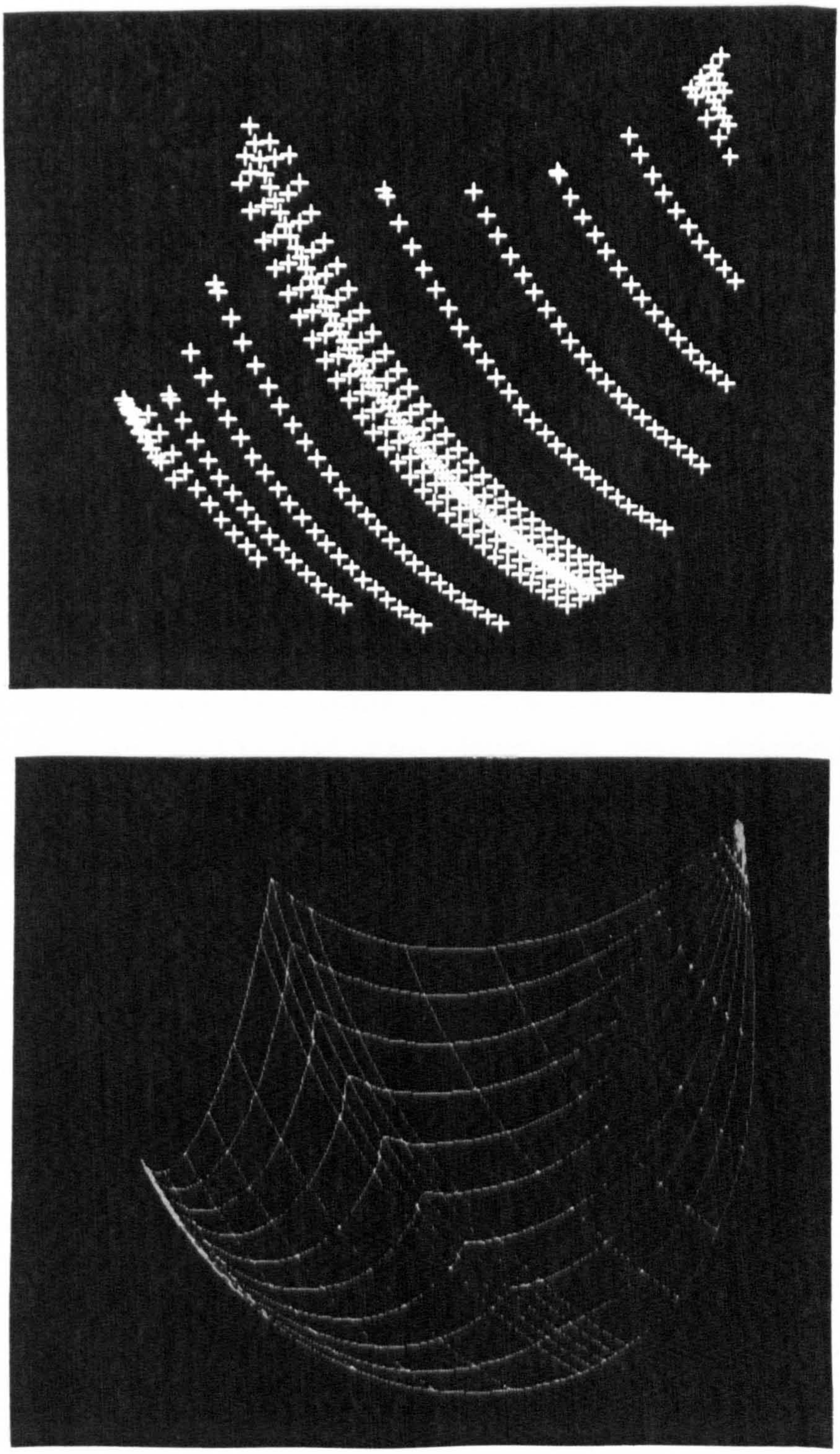

Figure 8.6 Representation of spherical leaflet generated by interpolating (3D cubic spline) between defined coordinate points

between a 1/3 segment of a cylinder and the desired leaflet shape, which in the example given is an ellipsoid of revolution. Greater concentrations of points are calculated in areas of greater curvature. Only one leaflet need be described for a valve with three identical leaflets; the other 2 leaflets can easily be generated by a *copy-rotate* operation within CADKEY. (Strictly, only half a leaflet need be given but it is more convenient to work with complete leaflets.)

Once the basic leaflet geometry has been defined, by either of the above methods, the surfaces can, if required, be blended into the coaptation area or frame region. This is most conveniently done by the addition of surfaces described in terms of cubic splines. The valve surface representation in terms of cubic splines interpolating between defined coordinate points has the advantage that any of the node points can be displaced in x, y, z space at will and the surface re-interpolated. Thus, the most convoluted of leaflet shapes can be accommodated.

As well as creating and modifying surface representations of valves, CADKEY enables such representations to be viewed from any perspective and outputs the valve design data in a convenient format for input to the CAM procedure.

The CAM procedure involves a second software package, MASTERCAM 3D 3.0 (CNC Software, Inc.), which generates code for a numerically-controlled milling machine (or lathe). Using the valve geometry information defined in the CAD procedure, MASTERCAM calculates an appropriate toolpath. That is, MASTERCAM computes the path which the tip of a cutting tool should follow in order that the defined valve surface be carved out (fig 8.7). The toolpath incorporates 3-dimensional compensation for the shape and size of a specified cutting tool; toolpath increment size and direction can be set by the MASTERCAM user. Milling machine operating

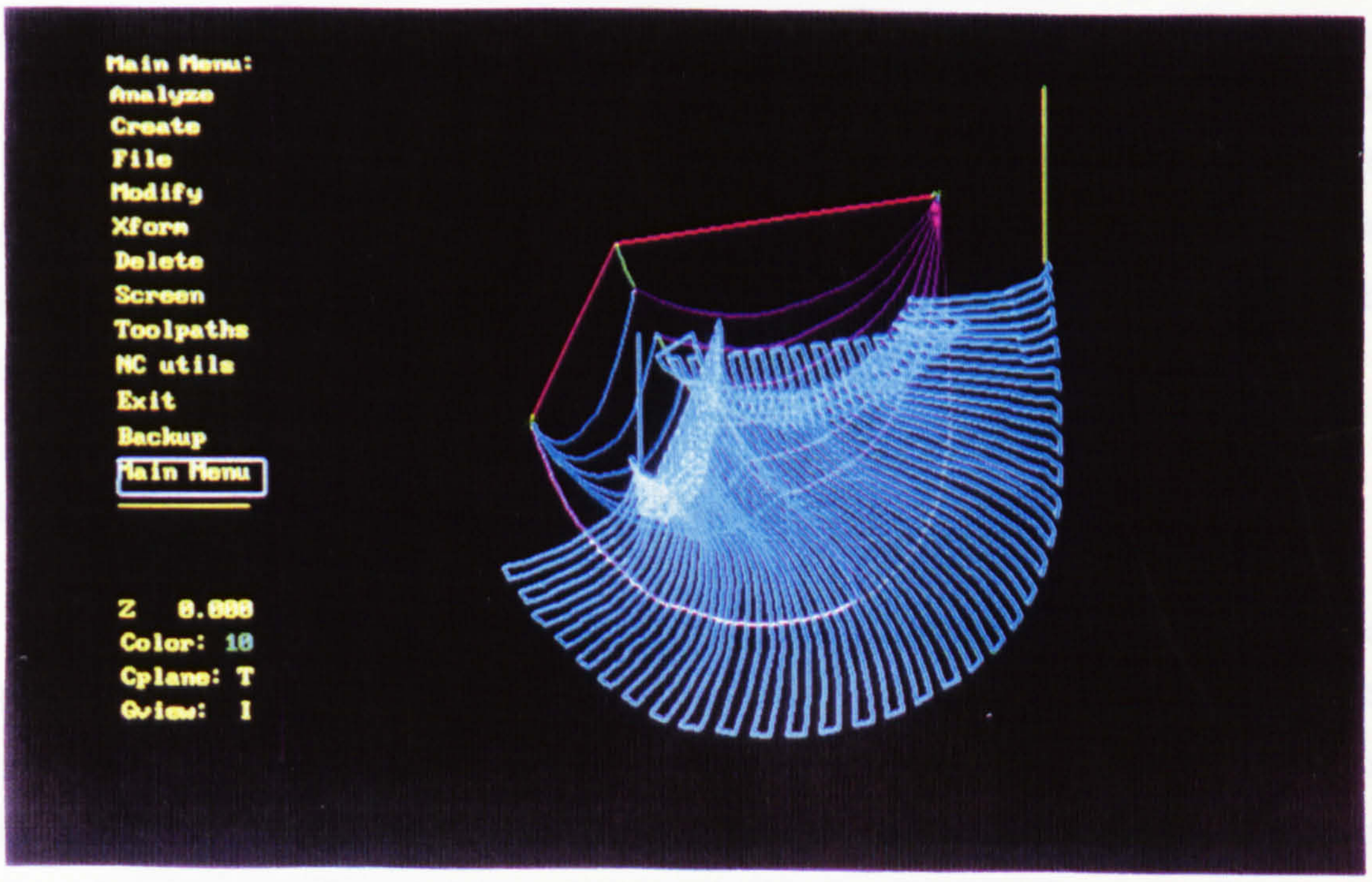


Figure 8.7 Toolpath computed using MASTERCAM

(This particular toolpath has been calculated for a leaflet geometry which is spherical in the belly region and blended at the free edge and at the leaflet-frame junction. The toolpath, shown in pale blue, fans out in a radial direction from the centre of the leaflet free edge.)

conditions, such as spindle speed and feed rate, may also be programmed but these can generally be overridden using controls on the machine.

The computed toolpath data is specific to a given milling machine control unit. The milling machine used here was a Deckel FP4NC with Dialog 4 control (fig 8.8). The machine's cutting tool may be advanced by means of 3-dimensional linear interpolation and circular interpolation in the 3 principal planes of the machine coordinate system.

Curved surfaces, such as valve leaflet surfaces, can be machined using 3D linear interpolation. A smoother representation of such convoluted surfaces may be achieved by increasing the number of points along the toolpath and using a smaller cutting tool. Valve mould diameters can be cut using circular interpolation. An example of the numerically-coded toolpath data used by the Deckel is shown in Appendix 3.

## 8.4 Initial Injection Moulding Trials

As a first step towards producing an injection moulded PU valve, the CAD/CAM system was used to construct some simple moulding tools. The tools were designed to be used with equally basic moulding machines. Emphasis was placed on simplicity of tool manufacture. Consequently, the valve designs incorporated were not thought to be optimal but the tools could be machined in a straightforward manner. The intention was to investigate the limits of what could be achieved with this simple approach.

### 8.4.1 Prototype tool (I)

The first injection moulding tool to be constructed is shown in figure 8.9. Owing to the inaccessibility of the coaptation region, the female side of the mould was

Figure 8.8 Deckel FP4NC milling machine

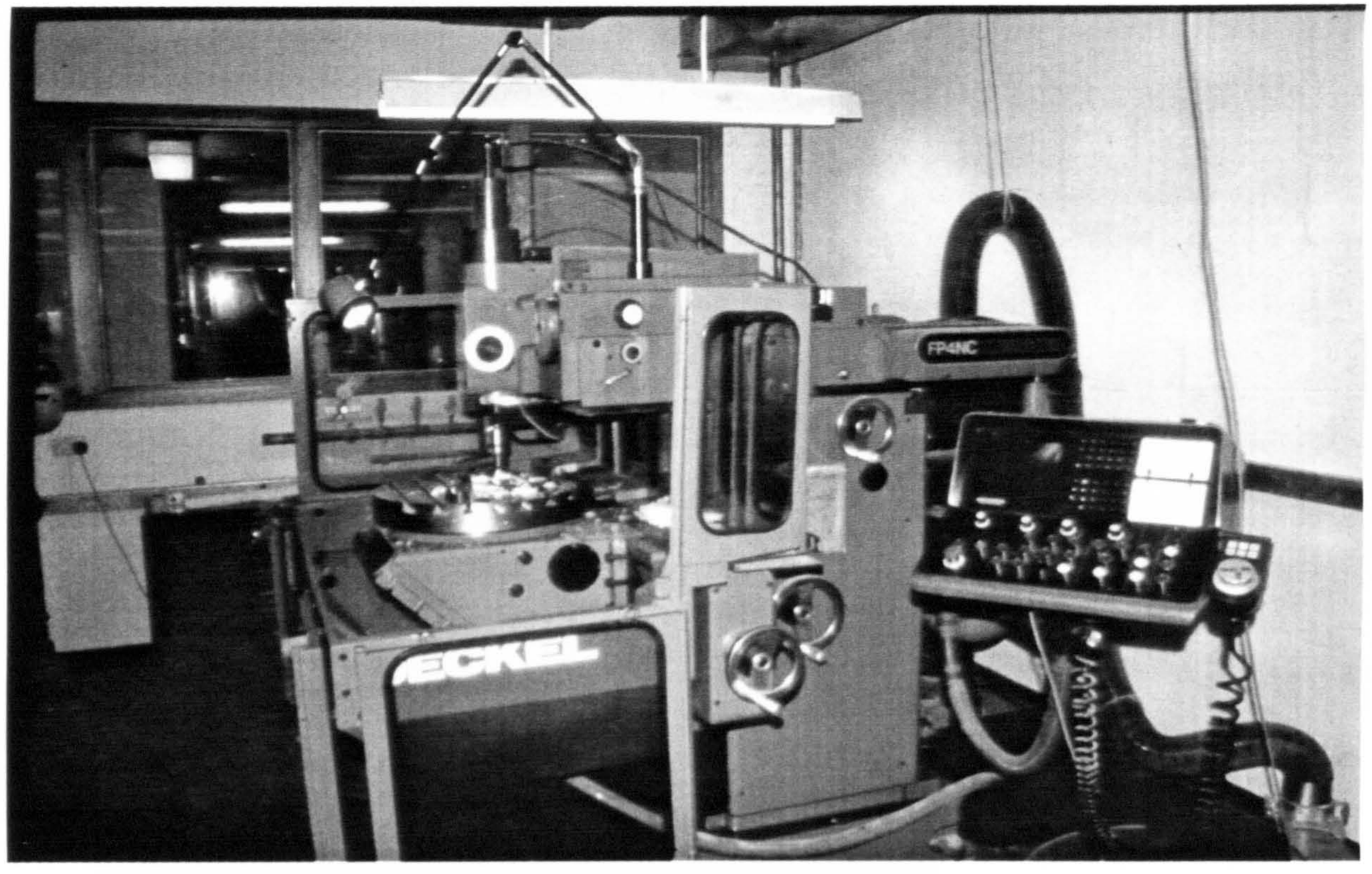

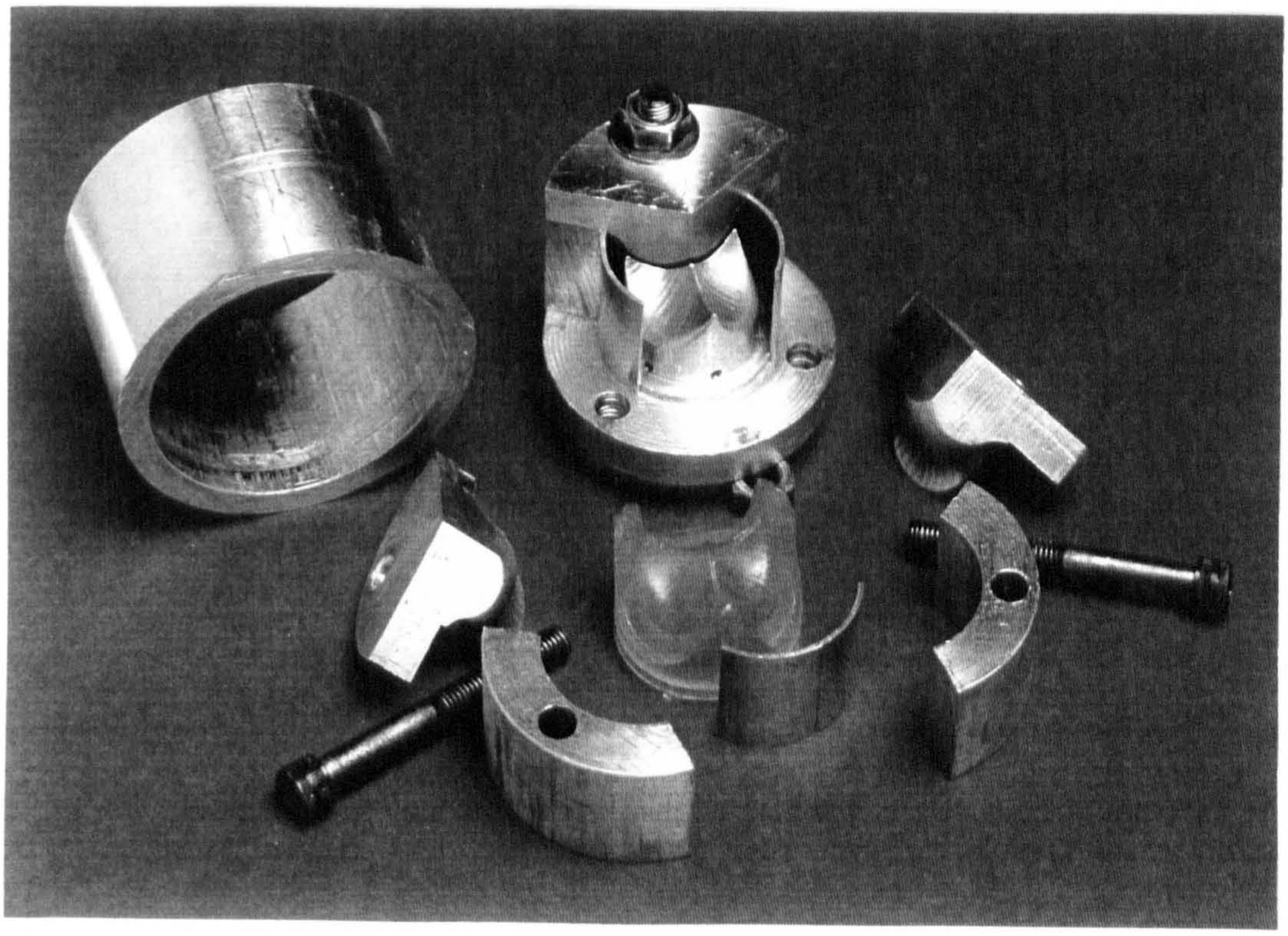

Figure 8.9 Prototype moulding tool I

made in 3 segments. Male and female mould components are held apart by a collar; 3 holes, bored axially through the collar and flanges on the male and female parts, provide for rotational alignment. The spacing between the male and female parts, and thus the leaflet thickness of the mouldings, could be varied by placing shims between the collar and flanges or by machining the collar ends. However, since the leaflet surfaces are curved, axial displacement of the male and female components distorts the leaflet thickness distribution. The tool was designed to give a uniform leaflet thickness with the male-female surface separation set at 200 $\mu$m. The mould cavity could be gated either circumferentially through the base of the frame or axially through the leaflet free edges. The tool was made from aluminium.

The valve design was based on a spherical leaflet geometry and a blended leaflet-frame junction. The undulating leaflet free edge, which arises from the spherical leaflet shape, enabled the male mould component to be machined with a reasonably large cutting tool (in this case a 8 mm diameter ball-nosed cutter). A flatter free edge would probably result in a more efficient valve, but a smaller cutting tool would then be required to access the 120° angle at the centre of the free edge on the male component. Blending the leaflets gradually into the frame region was thought to assist both with the moulding process and the valve function. As with the coaptation region, a sufficiently large blending radius was incorporated in order that a reasonably large cutting tool could be used to produce the female mould parts.

The tool was used with a simple, plunger-type moulding machine. As illustrated in figure 8.10, the machine consists of a heated barrel with a valved-nozzle at one end and a feed hopper at the other. The PU granules to be moulded are fed into the barrel and a manually-driven piston forces molten plastic out through the nozzle and into the mould tool. The lever arm, which

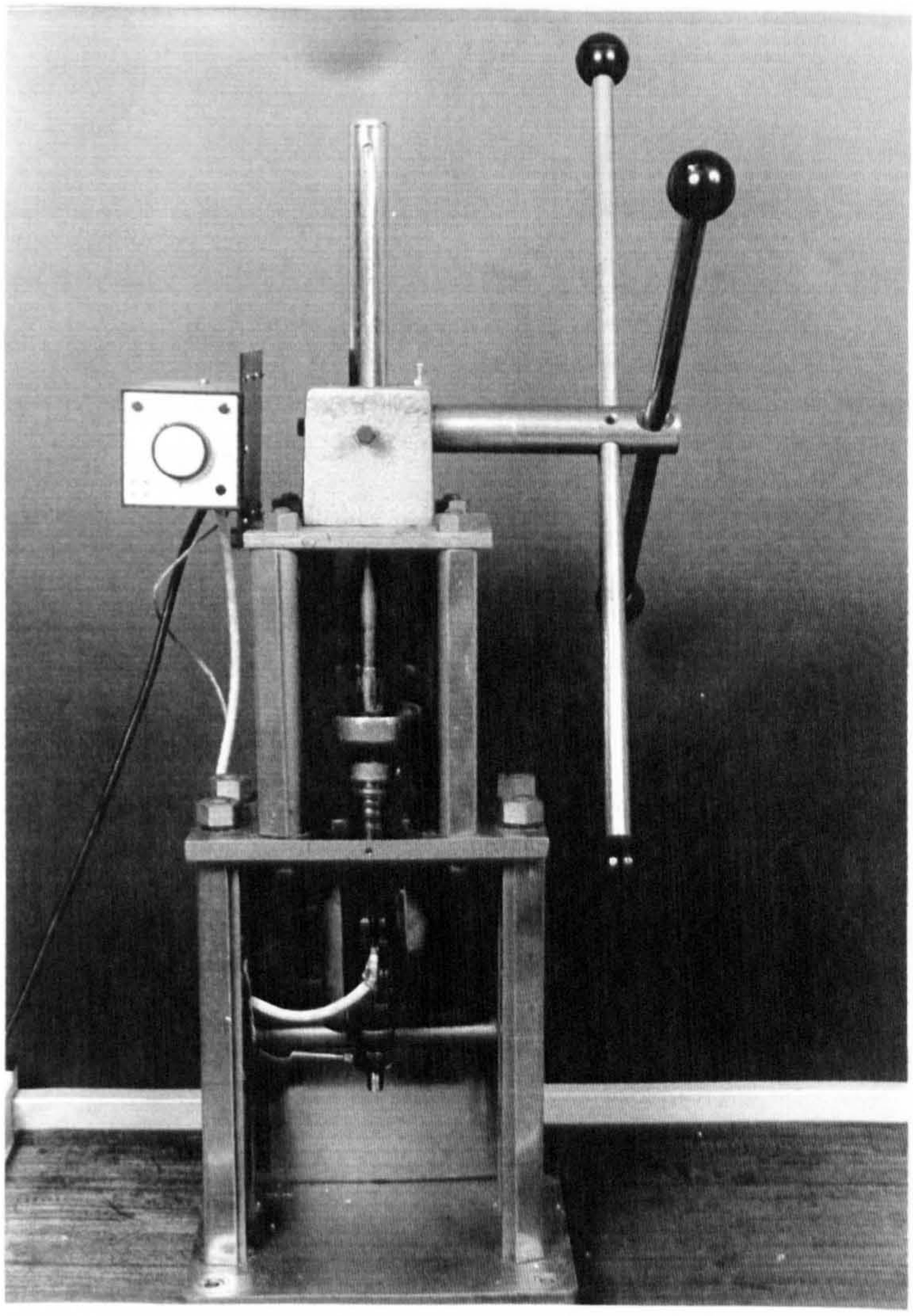

Figure 8.10 Manually-powered plunger-type injection moulding machine

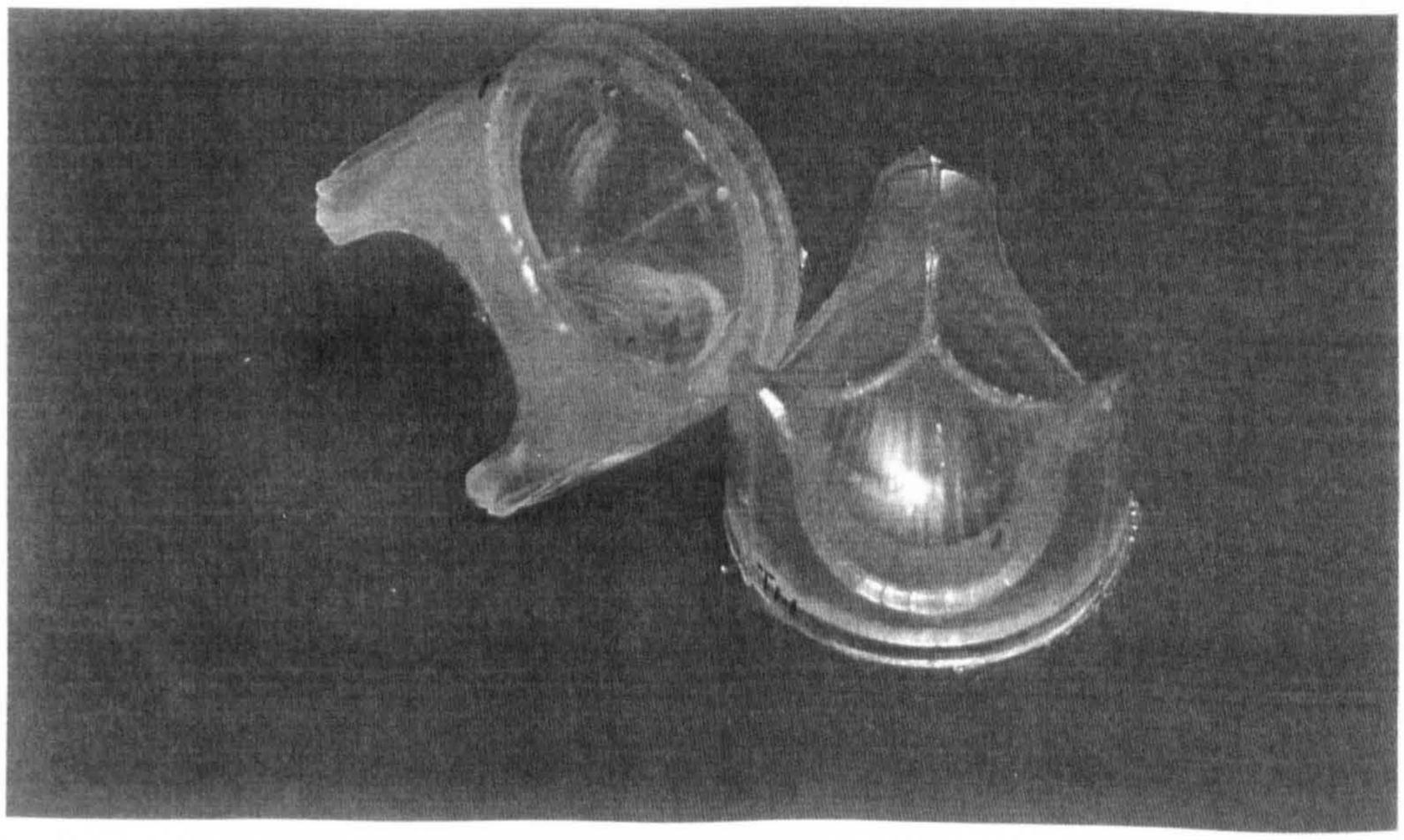

Figure 8.11 Mouldings from prototype tool I

drives the piston downwards using a rack-and-pinion mechanism, provides a mechanical advantage of approximately 20; a maximum force of approximately 900 N could be exerted on the lever arm. Thus, neglecting losses, a maximum piston force of 18000 N could be developed, which, combined with a barrel diameter of 1.9 cm, gives a maximum injection/holding pressure of approximately 16 MPa (or 2300 psi).

At best, mouldings of reasonable quality could be produced when the leaflet cavity thickness was greater than approximately 800-900 $\mu$m (fig 8.11). However, for a PU valve with an acceptable hydrodynamic performance, a leaflet thickness of less than 200 $\mu$m is required.

The best mouldings were achieved with a barrel temperature of 175°C and with the mould tool pre-heated in an oven at 80°C. The actual temperatures of the melt as it entered the tool, and the tool itself, at the time of filling were not measured. The melt entering the tool would likely have been closer to 200°C due to frictional heating in the nozzle: raising the barrel temperature above 175°C resulted in rather yellowed, charred-looking mouldings, and the manufacturers estimate that their PU's degrade above 210-220°C. The tool cools immediately after being removed from the oven, and especially so when in contact with the cold steel of the moulding machine. However, the tool also gains heat from the hot molten plastic which fills the mould cavity and through its contact with the hot nozzle: throughout the moulding process the tool was always hot to touch. With these optimal temperature settings, and with others, there was a general lack of consistency in the mouldings produced. The inconsistencies reflect the rather poor degree of temperature and pressure control associated with the simple moulding machine.

Frequently there were inhomogeneities visible in the mouldings; these may have been either fragments of partially melted PU or fragments of thermally-degraded

PU. The inhomogeneities indicate inadequate mixing of the melt. The plunger-type moulding machine does not allow the melt to be mixed in the barrel, and what mixing there is occurs as the melt is forced out through the nozzle.

When the male and female mould surfaces were brought closer together, such that the leaflet cavity was less than 800-900 $\mu$m thick, it was found that the cavity could not be filled. Holes appeared on the leaflet areas of the mouldings and the frame areas became more discoloured and warped. The maximum injection pressure could not be applied to the PU filling the leaflet cavity. When attempting to mould thinner leaflets at the maximum developable pressure one of several 'failure modes' occurred: the mould tool sprang a leak at the junction of the collar and flanges, or burst completely; molten PU escaped between the mould tool and the nozzle; or molten PU, rather than passing out through the moulding machine nozzle, squeezed backwards through the annular clearance between the barrel and the plunger. Through repeated use, the tool became more prone to leakage as the aluminium deformed slightly and contiguous surfaces became more uneven.

Changing the gating position from the base of the frame to the leaflet free edges made little difference to the appearance of the mouldings produced. The exception being when the cavity would not fill, in which case better moulded frames were achieved by gating through the frame, as might be anticipated.

In conclusion, the simple tool-machine combination could be used to mould passable valve frames, albeit inconsistently. Sufficiently thin leaflets could not be moulded: the injection pressures generated by the machine and containable within the tool were not great enough to overcome the resistance presented by a leaflet cavity less than 800-900 $\mu$m thick.

### 8.4.2 Prototype tool (II)

A second, more robust, moulding tool was built from stainless steel (fig 8.12). The tool construction was similar to that of the first tool, with 3 female mould segments and a collar separating the male and female components. As before, rotational alignment is provided by a pin passing axially through the collar and flanges, the leaflet cavity thickness could be varied by machining the collar, and a male-female separation of 200 $\mu$m would result in a uniform leaflet thickness. The tool was gated through an axial aperture which was bored through the centre of the female side and emerged in the middle of the leaflet cavity free edges. A simple valve design, based on a cylindrical leaflet geometry, was incorporated. The minimal coaptation area provided by this design would probably result in a rather regurgitant valve. However, machining considerations took priority, especially so given the hardness of stainless steel.

Moulding trials were carried out on a hydraulically-powered, screw-type machine: a Peco 15MR (fig 8.13). Figure 8.14 shows the schematic workings of the machine. Plastic granules enter the heated barrel through a feed hopper, and are carried along the flights of a rotating Archimedean screw to the nozzle end. The screw is free to reciprocate, and as softened plastic accumulates the screw is pushed back against a pressure pad. Once sufficient plastic to fill the mould has accumulated, the screw stops rotating. The mould is filled by applying hydraulic pressure to the screw through the pressure pad: the screw is pushed forwards and molten plastic is displaced out through the nozzle and into the mould. As compared with the manually-powered machine used with the first prototype tool, this screw-type machine is superior in that greater injection pressures can be generated (up to 96 MPa or 14000 psi), a metered volume of molten plastic is injected at a time, the melt is more

Figure 8.12  Prototype moulding tool II

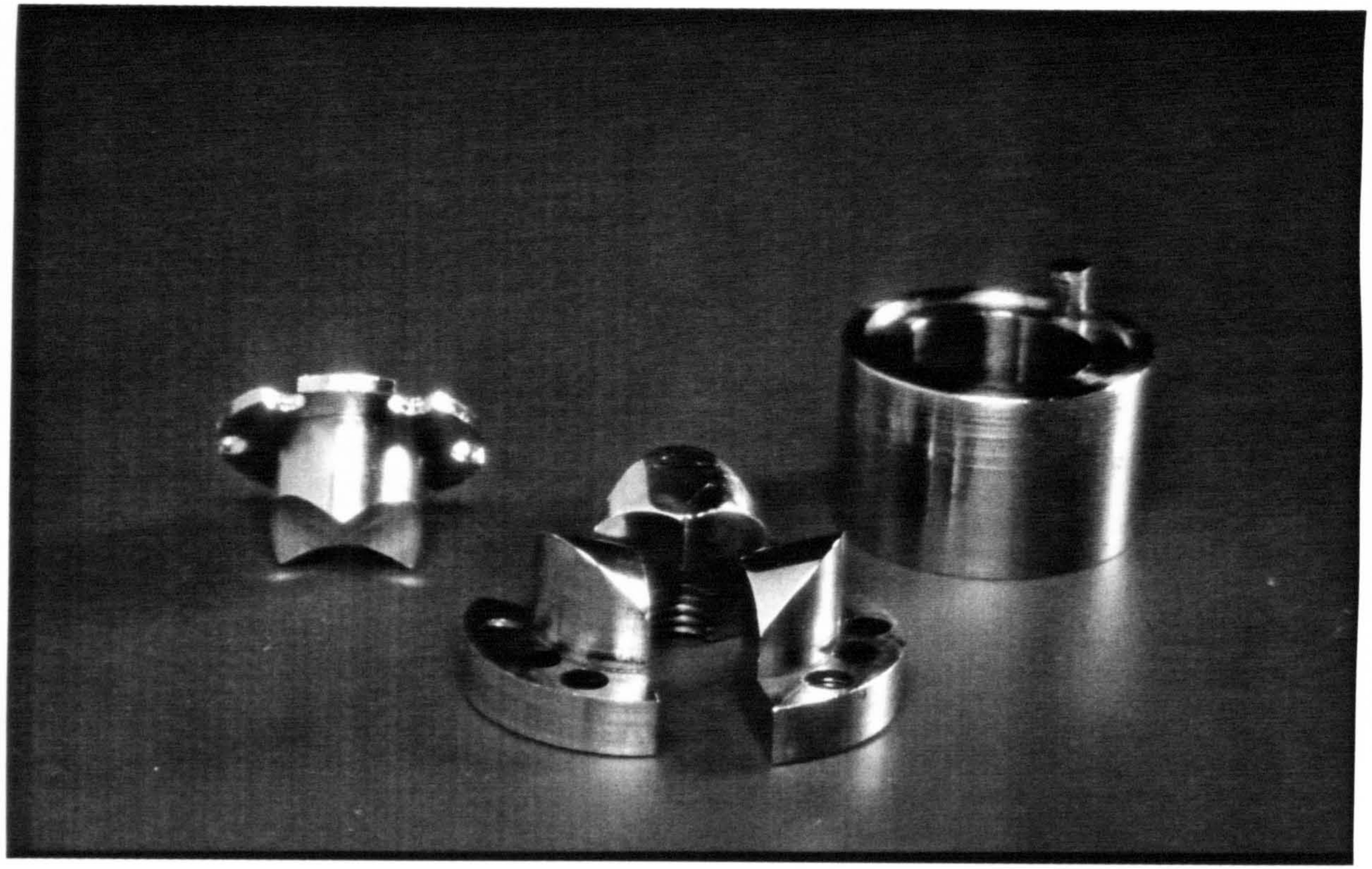

Figure 8.13  Peco 15MR screw-type injection moulding machine

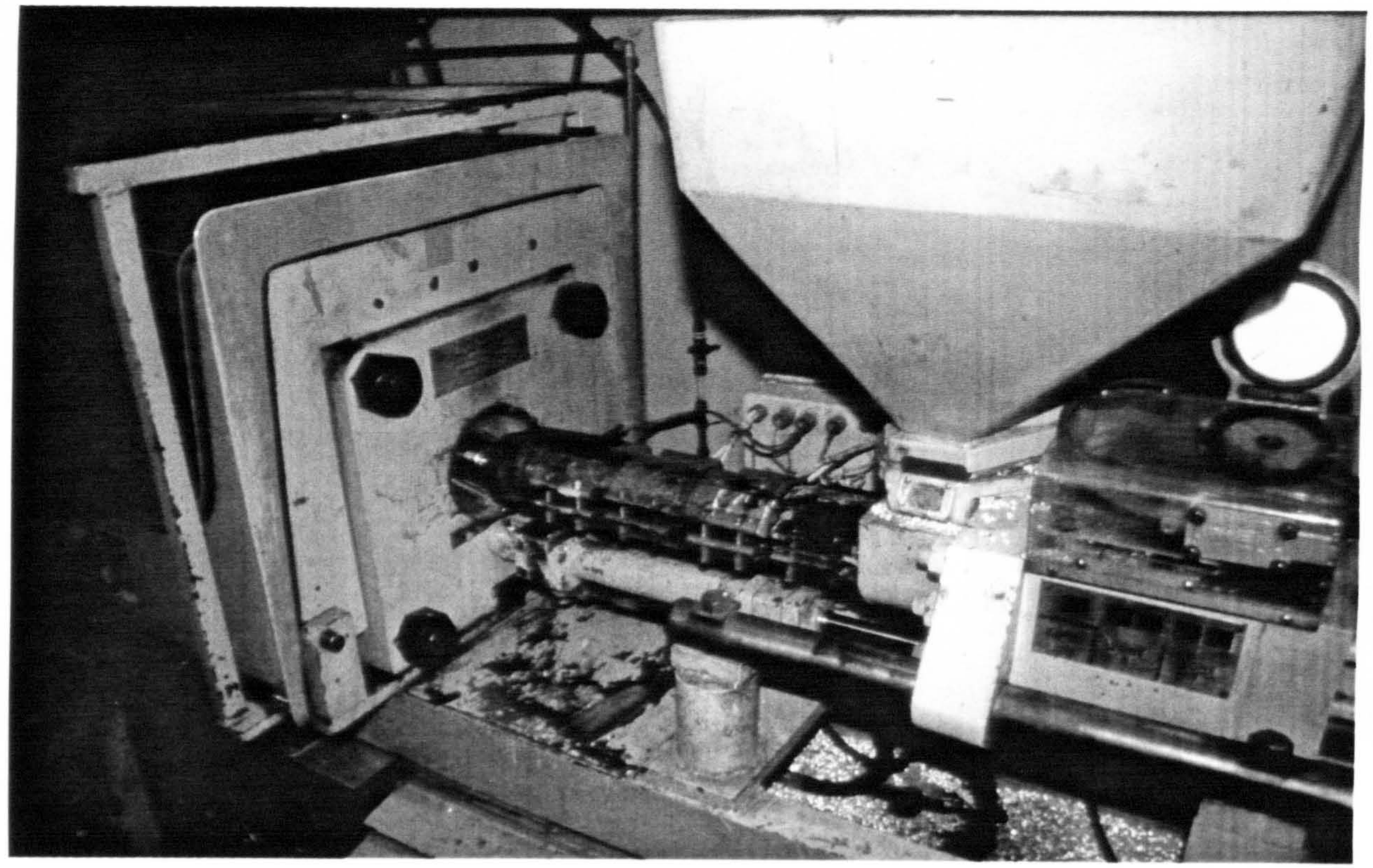

Figure 8.14 Schematic screw-type injection moulding machine

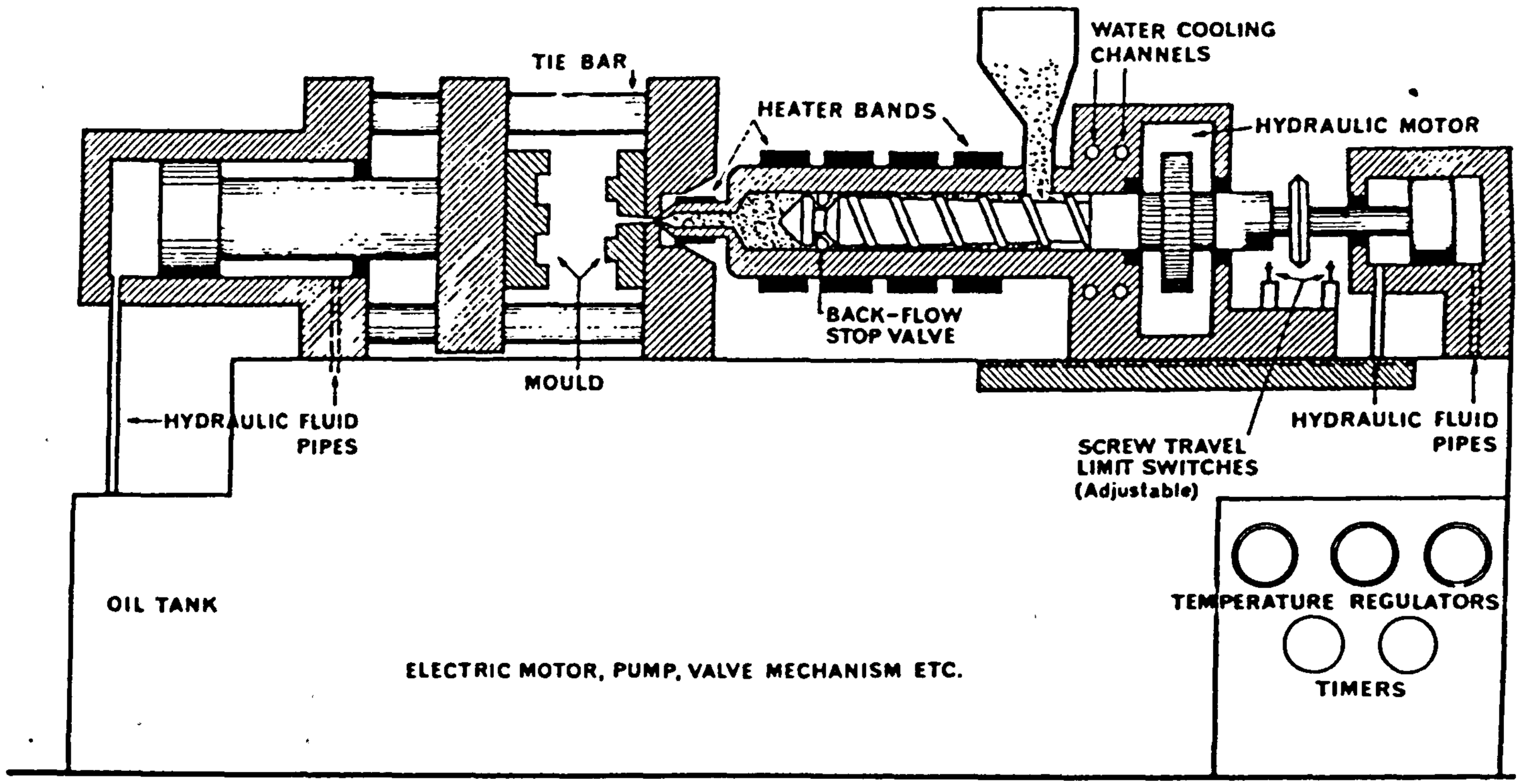

thoroughly mixed, and there is a greater degree of pressure and temperature control.

Ordinarily, the mould is housed within a pair of interlocking steel platens, one of which is fixed and the other can slide along 4 tie bars in order to open and close the mould. A mechanism for ejecting the moulded part is commonly incorporated into the moving half of the mould tool. However, in view of the machining effort which would be required to mount the mould shown in figure 8.12 within such pair of platens and given the preliminary nature of the moulding trials, the moulding machine was not used in its conventional mode. Instead, the moulding tool was fixed between the nozzle end and the fixed platen (fig 8.13). Thus, the rigidity and capacity for temperature control associated with the platen housing were forfeit.

Good quality mouldings could be produced fairly consistently with leaflet thicknesses down to 500-600 $\mu$m. The mouldings were clear and generally free from inhomogeneities. These were achieved with the barrel heater bands set to 180-190°C; raising the barrel temperature resulted in degradation. The tool was always hot to touch due to its contact with the hot nozzle.

Upon reducing the male-female separation below 500-600 $\mu$m, however, the leaflet cavity would not fill and holes appeared in the mouldings (fig 8.15). As with the manually-powered machine, the maximum developable injection pressure could not be applied to the PU traversing the leaflet cavity. Rather than filling the thin leaflet cavity, molten PU frequently escaped between the collar and the flanges on the male and female mould components. In normal operation mode the mould cavity is sandwiched between a pair of large steel platens. A substantial hydraulic force is applied to the moving platen in order to clamp the platens together and prevent the melt escaping. In the case of the machine used here, the maximum clamping force is 30 tons. The clamping force

Figure 8.15 Mouldings from prototype tool II

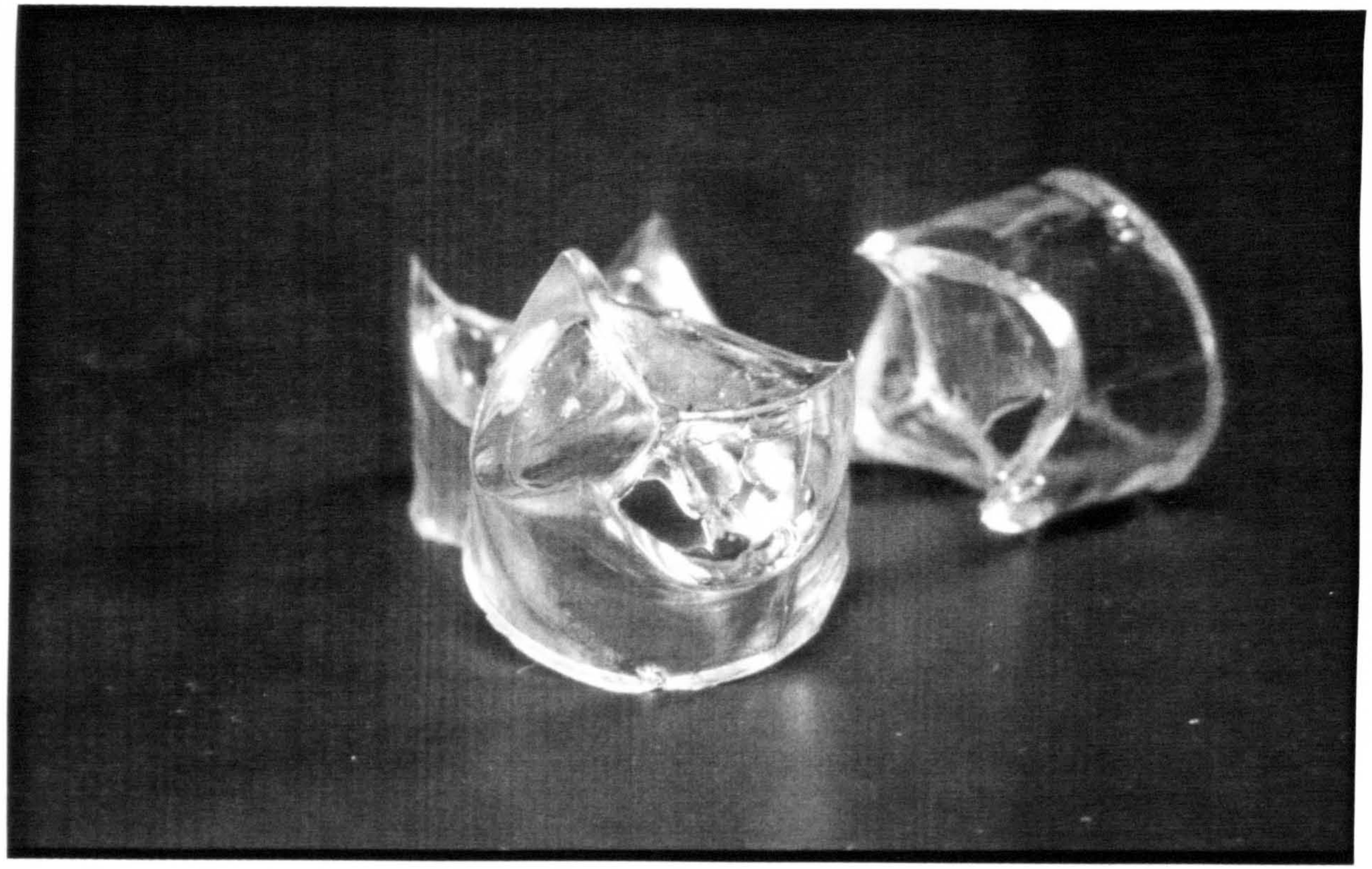

required depends upon the injection/holding pressure and the projected area of the moulding. However, here the force acting to clamp the mould together is that which holds the nozzle in contact with the fixed platen. That is, the barrel sits on a hydraulically-manoeuvred carriage which can slide the nozzle into contact with the fixed platen and holds it in place with sufficient force to prevent leakage between the nozzle and the platen. This nozzle holding force is relatively modest.

The principal finding from this investigation is the same as before: insufficient pressure could be generated across the leaflet cavity to mould valves with acceptably thin leaflets. The use of a screw-type machine gave rise to much better quality mouldings and the higher injection pressures resulted in thinner moulded leaflets.

### 8.4.3 General observations and discussion

The PU's used for these initial moulding trials were usually Estanes, although Pellethanes were used occasionally (see table 7.1). There were no visible differences between the mouldings produced using polyester- and polyether-based Estanes, but the Pellethane mouldings had a slightly more glossy surface. All the PU's were processed under the same conditions. The PU's were of extrusion or injection moulding grade which means that they contain a small amount of a silicone-based lubricant to assist melt processing. The melt appearance and quality of mouldings were rather sensitive to the moisture content of the PU granules. Best results were obtained using granules which had been baked for several hours in an oven at 90°C with circulating dried air.

In the course of these trials, PU thermal degradation was a frequent problem. The thinnest leaflet sections were moulded with barrel temperatures just below those which would result in degradation; with slightly

lower barrel temperatures, say 10°C less, the melt was considerably more viscous and only much thicker leaflet cavities could be filled. Interestingly, thermal degradation appeared to be dependent upon the melt residency time within the heated barrel. Even at relatively cool barrel temperatures, say 15°C below optimum, the emanating melt would appear degraded if it had remained in the barrel for 10 minutes or more.

A second common problem involved releasing the moulded parts from the mould cavity. The mouldings tended to stick, at times tenaciously, to the mould surface. Parts released with least resistance when the cavity surfaces were highly polished and liberally coated with a dry-film silicone lubricant.

A leaflet cavity 100-200 $\mu$m thick presents a large resistance to the melt attempting to fill it. The viscous resistance effect is compounded by the fact that such a cavity has an extremely large surface area to volume ratio. Consequently, there may be considerable conductive heat loss and a concomitant increase in viscosity. Of course, the likewise relatively large frictional heating effects may compensate to some degree. However, it is possible to extrude extremely thin sections of these PU's. When moulding on the hydraulically-powered machine, small quantities of PU would frequently escape from the moulding tool by squeezing through extremely narrow gaps between steel parts which were supposed to have been clamped together. Such *flashings* of PU were sometimes less than 100 $\mu$m thick, albeit they were produced in an uncontrolled manner and they were smaller in area than one valve leaflet.

These preliminary moulding trials have demonstrated that in order to injection mould a PU valve with sufficiently thin leaflets a more sophisticated approach is necessary. Extending this work, a moulding tool is required which combines an ability to withstand substantial injection/holding pressures with a

satisfactory means of temperature control: ie, referring to figure 8.14, a tool in which the mould cavity is enclosed within a large pair of interlocking steel platens.

# Chapter 9. Towards an Injection Moulded Polyurethane Valve (II)

## 9.1 Introduction

Preliminary attempts at injection moulding a PU valve, as described in the preceding chapter, prompted the construction of a 'second-generation' moulding tool. The new tool is of the standard type used with screw-type injection moulding machines, with the mould cavity housed within a large pair of interlocking steel platens. This format enables substantial filling/packing pressures to be applied and facilitates mould temperature control. The tool was built under the patronage of IBM (UK) Ltd, using facilities at their Greenock plant. Moulding trials have been undertaken in collaboration with the Polymer Technology Group at Napier University, Edinburgh, using their moulding machine. To date, mouldings have been produced with leaflet thicknesses down to 500 $\mu$m; attempts to mould thinner leaflets are ongoing.

The machining effort which was required to create the IBM moulding tool has been exploited to produce PU valves with injection moulded frames and dip moulded leaflets. These prototypes provide a means for assessing the efficiency of the valve design. Dip moulded PU valves have been made which perform satisfactorily in the pulse duplicator, and accelerated fatigue studies are in progress.

## 9.2 The IBM Moulding Tool

### 9.2.1 Tool overview

The tool comprises 2 mating halves: the female side being that which moulds the valve outflow surface, and the male that which moulds the inflow surface. The female half remains fixed in place on the moulding machine while

the male half slides along 4 tie bars (figs 9.1 & 9.2). Male-female location is provided by means of 4 symmetrically-placed pillars on the moving side and corresponding bore holes on the fixed side. The fixed half of the tool includes 4 symmetrically-placed knock back pins with neoprene rubber pads; these are standard devices intended to assist in opening the tool after the cooling phase. Also incorporated, within both tool halves, are heating (or cooling) channels, bored through the steel housing.

The tool is gated axially, through the centre of the female side, such that plastic enters the valve cavity at the centre of the leaflet free edges. A heated runner system keeps molten PU hot as it passes from the machine nozzle to the valve cavity.

The moving side of the tool incorporates a stripper-plate ejection mechanism. The thought behind the ejection mechanism is as follows. During the cooling phase, the moulded part freezes onto the shaped pin which moulds the valve inflow surface, such that when the tool opens the valve moulding clings to the moving side and the frozen PU breaks off from the molten PU at the end of the hot runner system. Once the tool has opened, the plate through which the male pin passes is then pushed forwards, while the pin itself is held fast, and the moulding is thereby eased off the male former.

Each half of the tool is actually an assembly of 3 large plates; the surfaces which mould the valve are relatively small inserts and can be replaced without changing the housing plates. Thus, by using a range of inserts, the tool housing could be used to mould valves of different sizes or designs.

### 9.2.2 Valve design

Access to sophisticated machining facilities enabled a plausible-looking valve design to be incorporated. The

Figure 9.1 IBM injection moulding tool

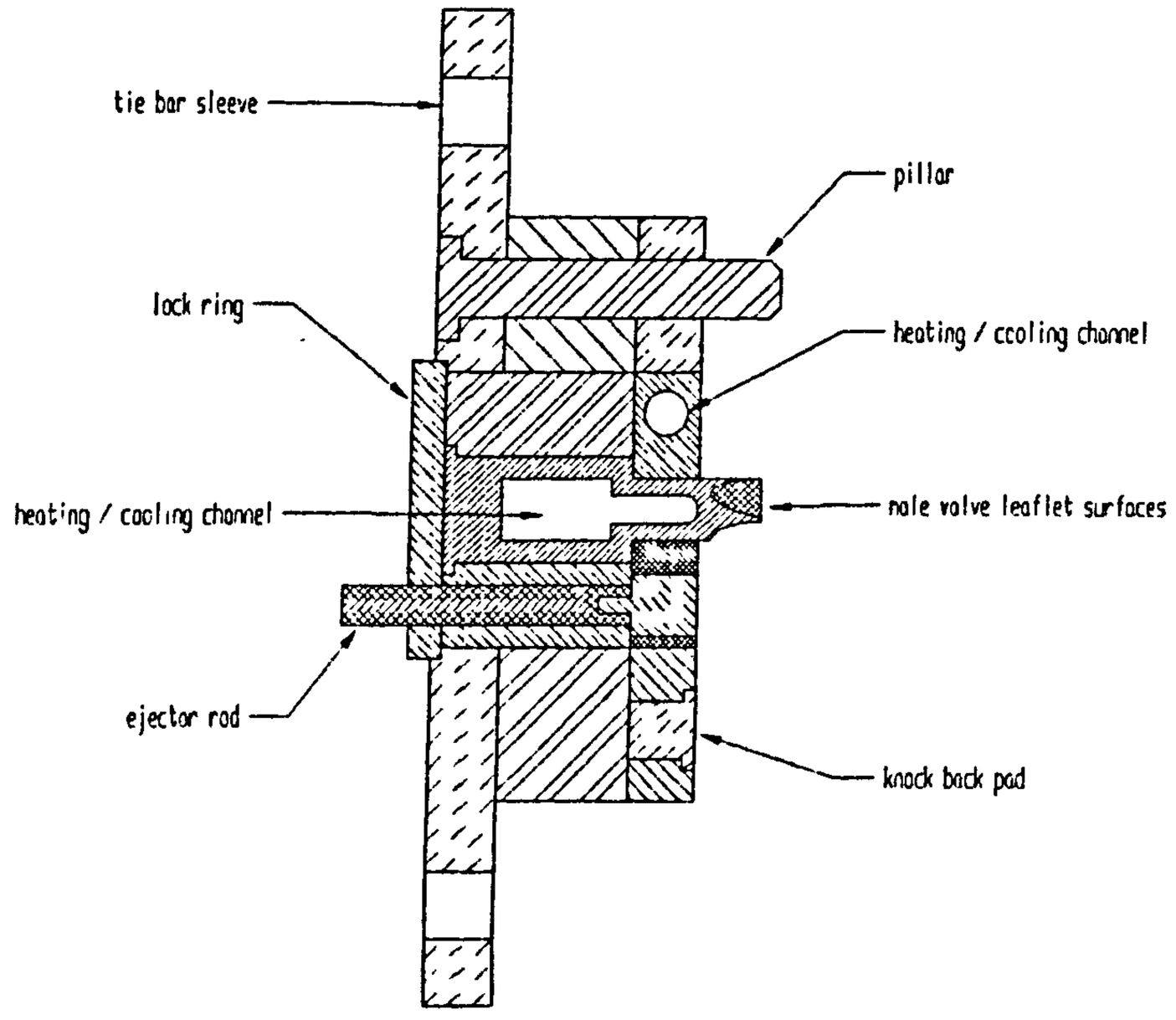


moving side

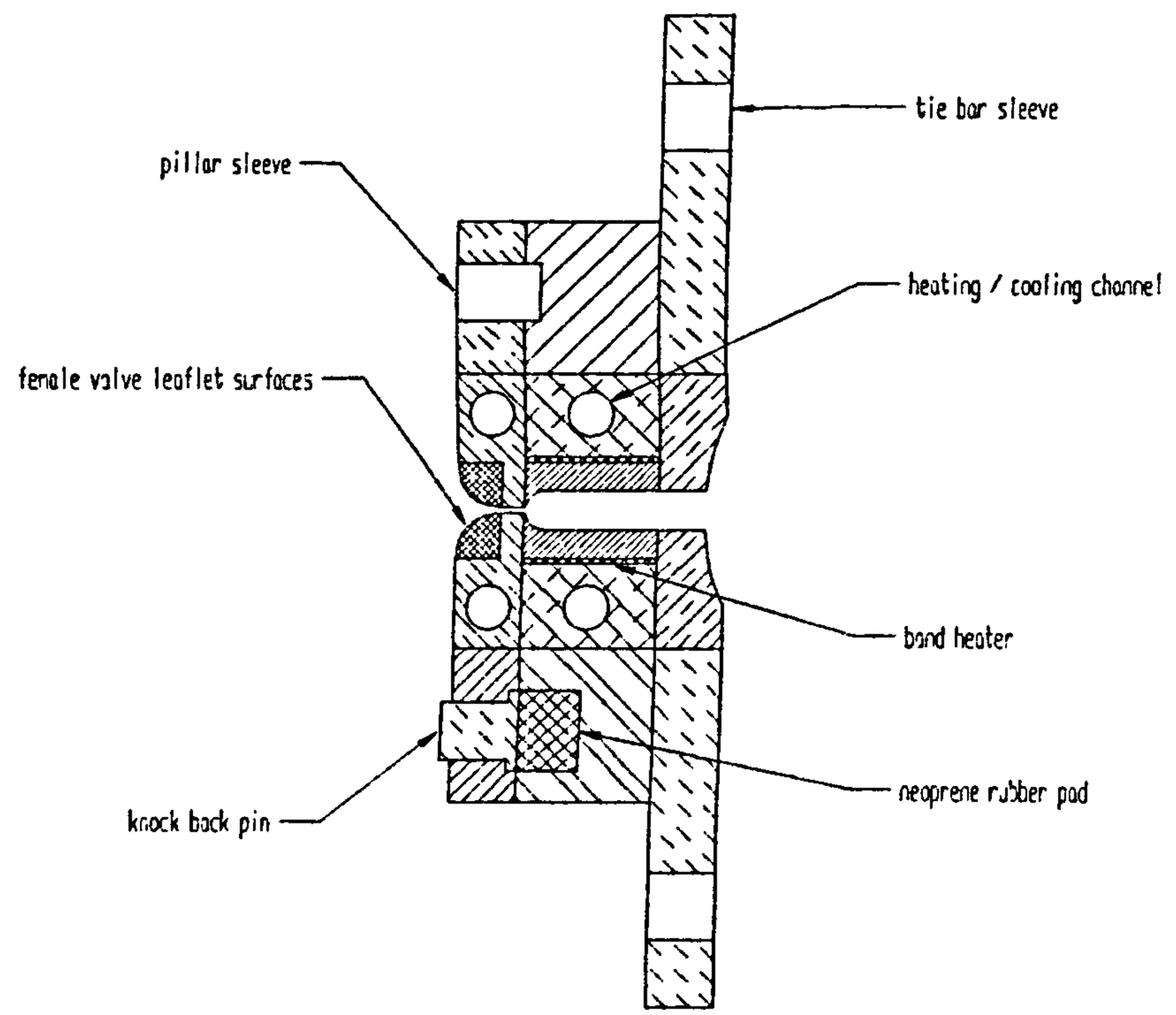


fixed side

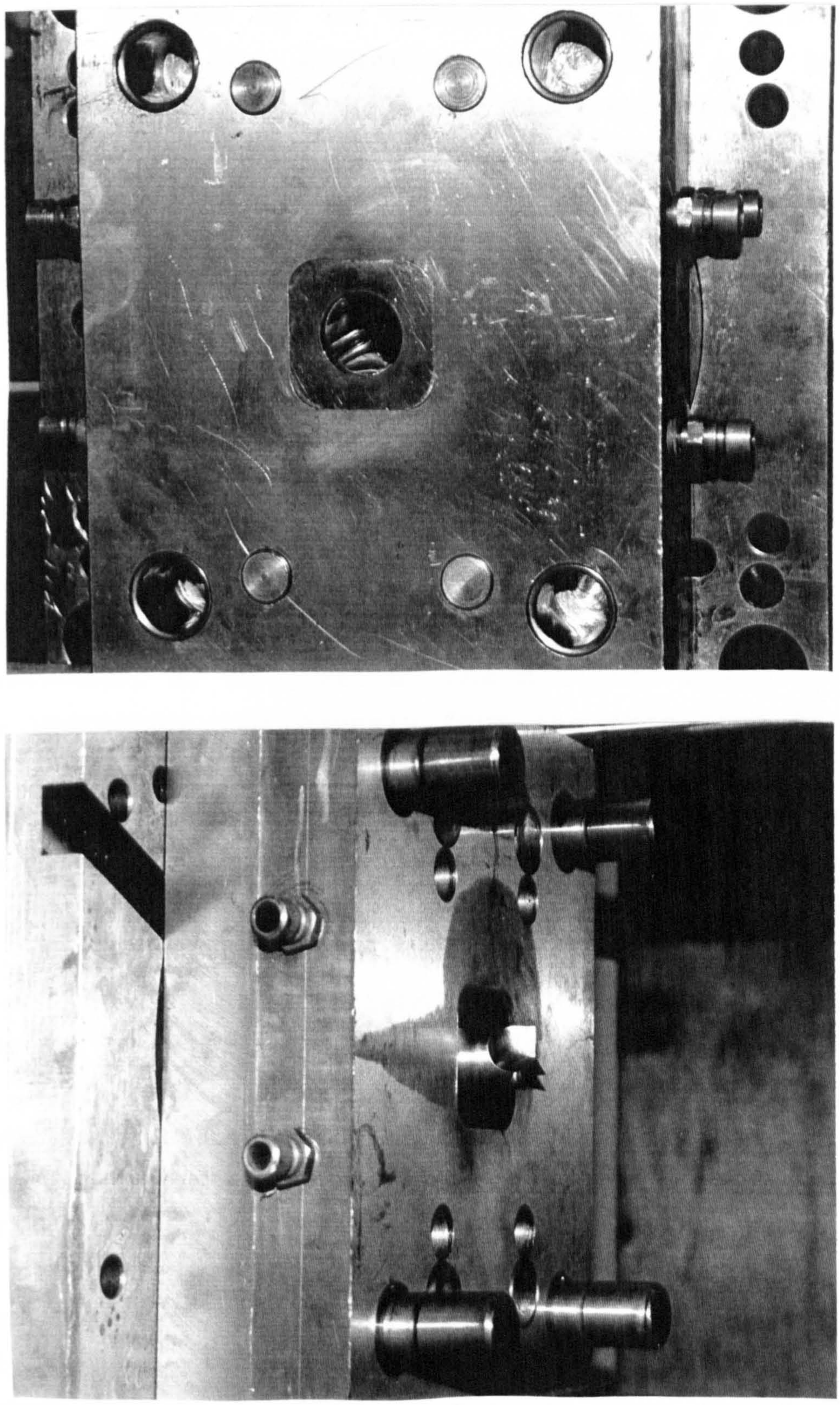

Figure 9.2 IBM injection moulding tool: fixed side (upper) and moving side (lower)

leaflet shape chosen was similar to that used in the Glasgow pericardial bioprosthesis. The closed leaflet geometry is defined by an ellipse along the mid-line (that is, along the direction of flow), and by a continuous series of hyperbolae in the orthogonal plane, as illustrated in figure 9.3. Formally, the geometry is given by:

$$[(x-E_o)/MajAx]^2 + [z/MinAx]^2 = 1 \qquad (9.1a)$$

$$[(x-H_o)/a]^2 - [y/b]^2 = 1 \qquad (9.1b)$$

with

$$a = E_o - ( MajAx \cdot [1 - (z/MinAx)^2 ]^{\frac{1}{2}} ) - H_o \qquad (9.1c)$$

$$b = a \cdot \tan 60° \qquad (9.1d)$$

using the coordinate system of figure 9.3, with z = 0 in the plane of the free edge. The major axis length of the hyperbolae, *a*, is given by the mid-line ellipse, and as such increases continuously from the free edge to the leaflet base. While the major axis length increases, the eccentricity of the hyperbolae remains fixed, giving a constant enclosed asymptote angle of 120°. The designated values for the geometry parameters are given in table 9.1; a uniform leaflet thickness of 150 $\mu$m has been specified. A valve outer diameter of 28.4 mm, and inner diameter of 22.4 mm, were selected; the outer diameter chosen is mid-range for prosthetic valves, and a frame thickness of 3 mm is typical for bioprostheses.

The 3 hyperbolae which define the leaflet free edges were offset ($H_o$) from the valve axis (z axis). The offset had to be sufficiently small so that the 3 leaflets could come together and seal the closed valve efficiently with minimal leaflet and frame stretching. On the other hand, the offset had to be large enough so that the 3 steel 'fins' on the male former, which shape the coaptation region, were rigid enough not to deform during the moulding process. The offset selected was such that 3

Figure 9.3 Ellipto-hyperbolic IBM valve leaflet geometry

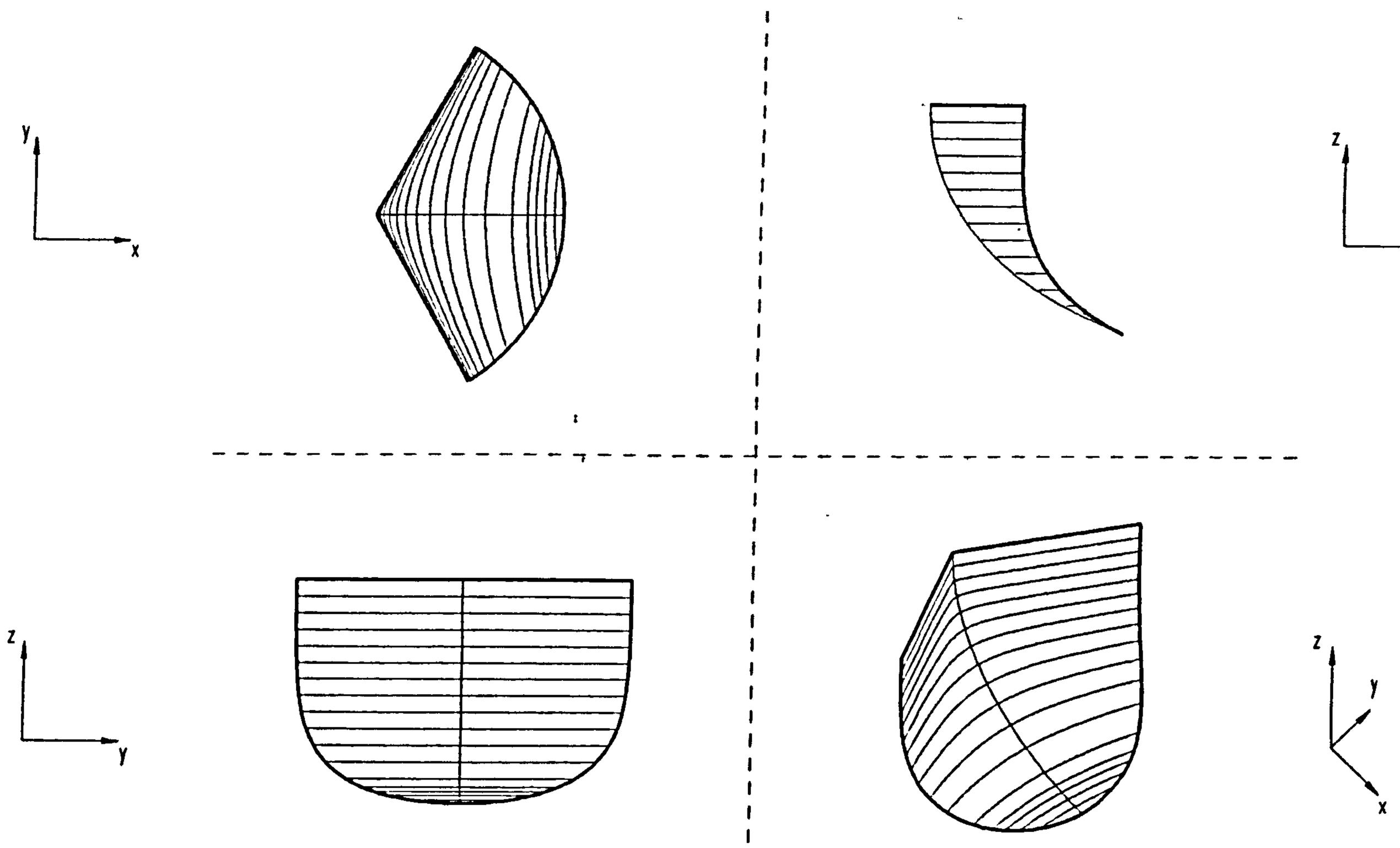

Table 9.1 Ellipto-hyperbolic leaflet geometry parameters

| | Male (inflow) surface | Female (outflow) surface |
|---|---|---|
| $E_o$ | 22.332 | 22.332 |
| MajAx | 22.032 | 22.032 - 0.150 |
| MinAx | 15.574 | 15.574 - 0.150 |
| $H_o$ | 0.230 | 0.230 + 0.150/cos30° |

in mm's, for a leaflet thickness of 0.150 mm.

'fins' were approximately 0.4 mm thick; this was taken as a reasonable compromise.

The elected valve design erred on the side of incorporating an overly generous coaptation area, as excess leaflet material could always be cut away from the free edge post-moulding. The leaflet free edge was chosen to lie in a single plane perpendicular to the frame post, as is the case for the Glasgow pericardial valve. However, the angle between the free edge and the frame post could be reduced from 90° by manually carving the mouldings; Christie & Stephenson (1990b) have suggested that such an angled free edge may be beneficial in reducing stress concentrations in the commissure region. The effects of design modifications such as these could be assessed in the pulse duplicator and accelerated fatigue tester.

The valve design incorporated in the IBM moulding tool, although believed to be reasonable as a prototype, is probably not ideal. As before, machining considerations took priority. In the present design, there is an abrupt change in wall thickness from the leaflets to the frame. Leaflets which blend gradually into the frame region would likely reduce stress concentrations along the leaflet-frame junction in the functioning valve, and may also promote the flow of molten PU during the moulding process . Further, leaflets which rise slightly above the frame posts would likely allow the closed valve to seal more efficiently; this feature is included in the Glasgow pericardial prosthesis, and could perhaps be introduced into the PU valve manufacture as a post-moulding process. The original valve design for the IBM moulding tool, prior to modifications to accommodate subsequent machining requirements, is illustrated in figure 9.4.

Notice that the leaflet geometry incorporated in the Glasgow pericardial valve, upon which this PU valve design is approximately based, has not been defined

Figure 9.4 Isometric view of original valve design for IBM moulding tool

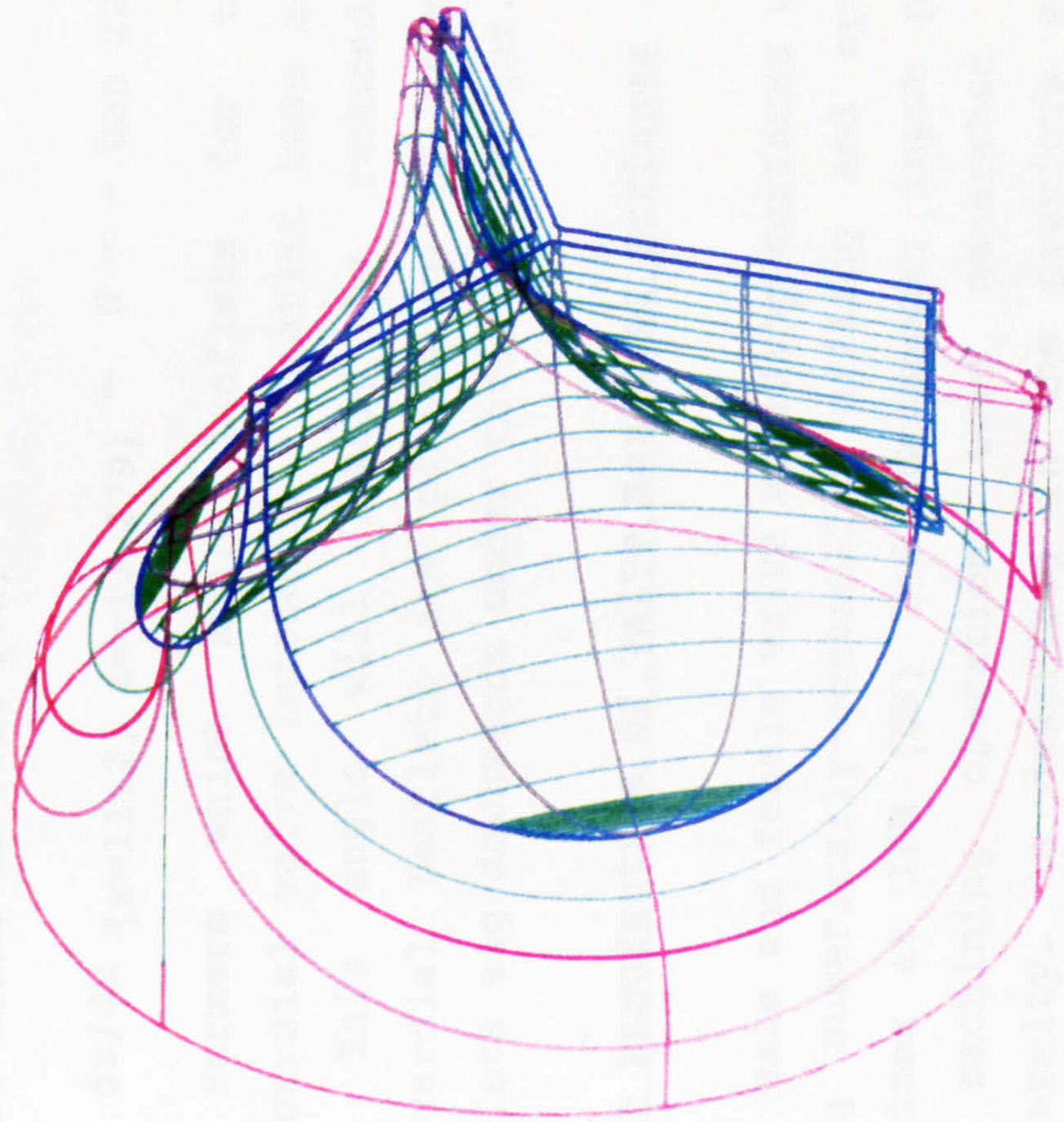

mathematically. The pericardial leaflets are individually moulded on formers which have a specified shape (specified by the intersection of a ball-nosed cutting tool with a cylindrical workpiece). However, once the leaflets are removed from the formers and mounted onto a frame, the pliable leaflets adopt a new undefined shape, with the support of their neighbouring leaflets and under the influence of gravity. Note that differentiating equation (9.1a), with respect to x, gives:

$$dz/dx = (MinAx/MajAx)^2 \cdot (E_o - x) \cdot 1/z \qquad (9.2)$$

so that the gradient of the leaflet mid-line ellipse at the frame is (fig 9.5):

$$dz/dx_{(x=11.2,\ z=-13.279)} = \beta = -\tan 22.6° \qquad (9.3)$$

Formers which mould leaflets for the Glasgow pericardial valve introduce a leaflet base angle, ß, of 25°. This angle will likely be reduced once the pericardial leaflets are pinned on to frames, as the leaflets sag downwards under their own weight.

### 9.2.3 Manufacture of valve moulding surfaces

Male and female valve moulding surfaces were created using numerically-controlled milling and spark erosion machines at IBM (UK) Ltd, Greenock; input programs for the machining operations were generated within the university. As described in the previous section, the valve design specified a rather small radius of curvature at the centre of the leaflet free edges, in order to ensure an efficient seal for the closed valve (that is, the free edge is defined by a hyperbola with a very small major axis length). This rather tight corner prevented the male mould component from being created directly on a milling machine: to do so would have required exceedingly small cutting tools and several tool changes, which would

Figure 9.5 Gradient of mid-line ellipse at leaflet-frame junction

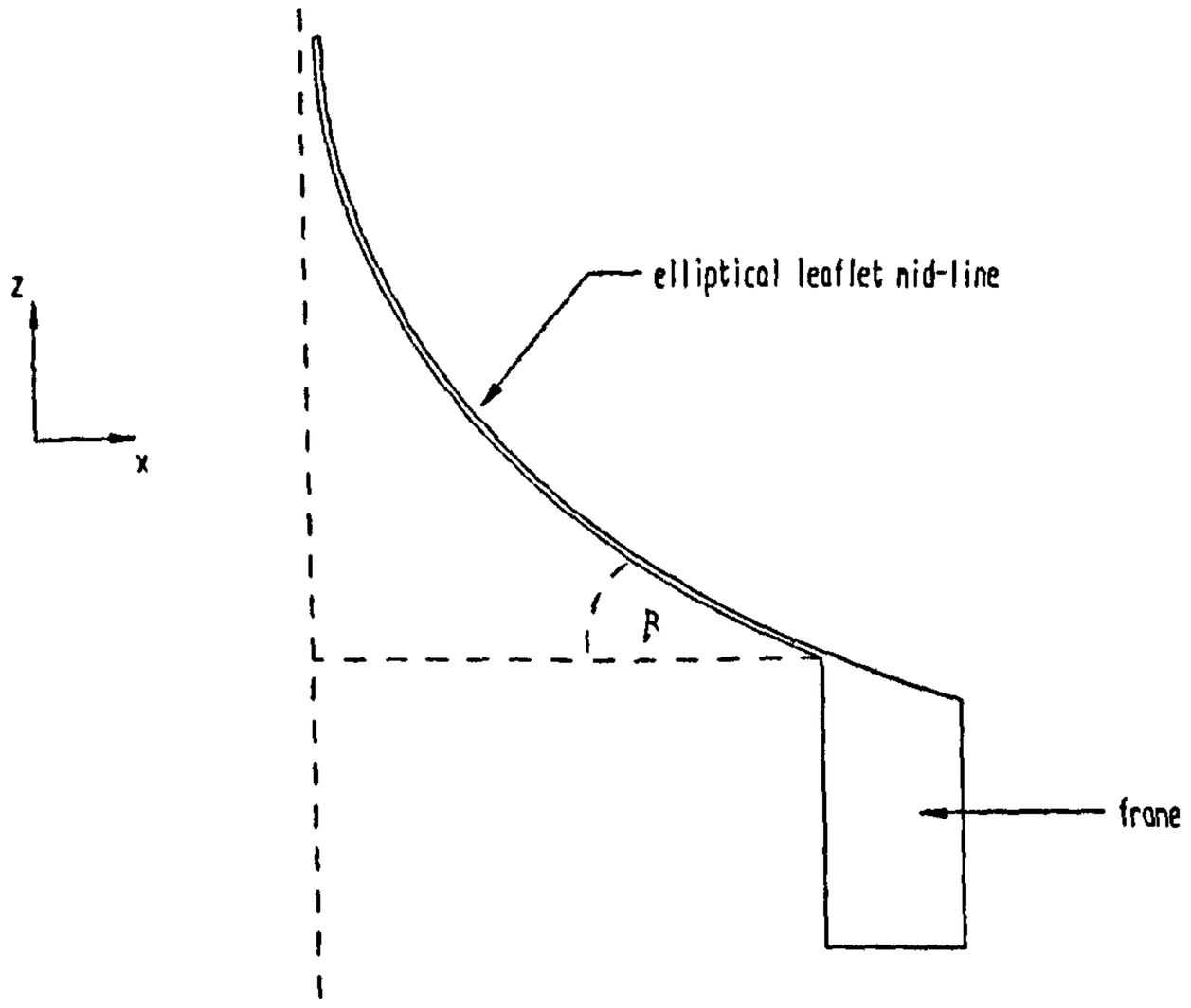

not have been practicable. Instead, the male component was machined by a process of spark erosion; the electrodes, for which the radii of curvature are reversed, were produced on a milling machine. The inaccessibility of the coaptation region required the female mould component to be made in 3 segments; the segments were created directly on a milling machine.

The toolpath data required to carve out the male electrodes and female mould segments were generated directly by writing short programs in Turbo Pascal 5.0, bypassing the CAM procedure outlined in the previous chapter. The MASTERCAM software package, which was used to compute toolpath data for the earlier moulding tools, was rather unreliable, inflexible, and slow, and particularly so when more complex leaflet geometries were involved. Generating the toolpath data *de novo* provides a means for greater control and allows, for example, the toolpath increment size to be reduced preferentially in areas of greater curvature.

Toolpath data input to the milling machine comprises a stream of coordinates points; the tip of the cutting tool moves from one point to the next (by 2 or 3D linear interpolation), thus carving out the desired part. The toolpath coordinate points are offset from the desired surface by the shape and size of the cutting tool to be used. That the leaflet geometry is defined in terms of conic sections (eqns 9.1) provides a convenient means for calculating the required toolpath offset. When using a 10 mm diameter ball-nosed cutting tool, for example, the appropriate toolpath offset surface for one of the female mould segments is given by adding 10 mm to the ellipse major and minor axes, subtracting 5/cos 30° mm from the hyperbolae offset, and displacing the entire surface by -5 mm in the z direction (fig 9.6):

$$MajAx' = MajAx + 5 \qquad (9.4a)$$

$$MinAx' = MinAx + 5 \qquad (9.4b)$$

Figure 9.6 Toolpath offset for ball-nosed cutter

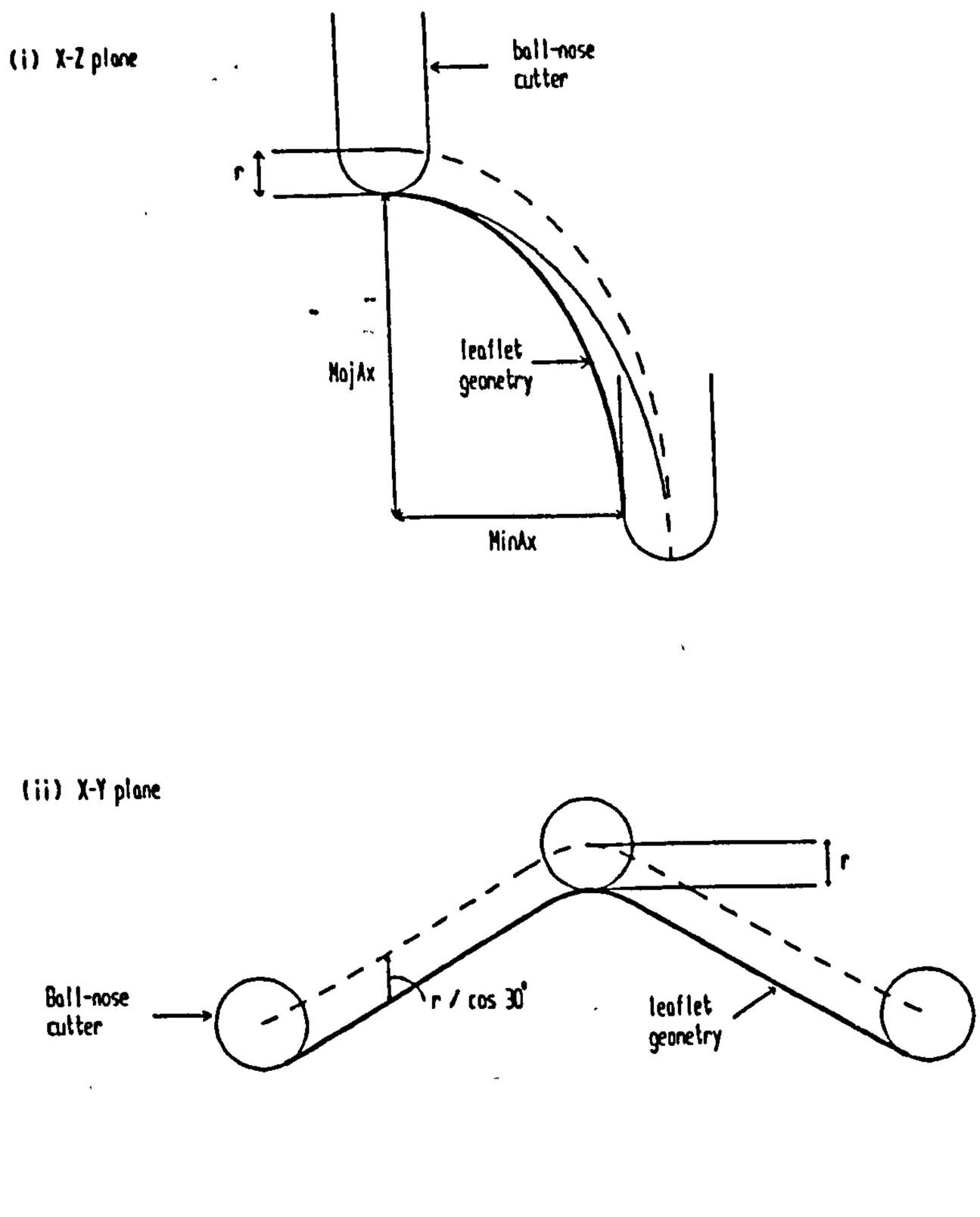

$$H_o' = H_o - 5/\cos 30° \quad (9.4c)$$

$$z' = z - 5 \quad (9.4d)$$

There is, however, a slight problem with this procedure in that the addition of an offset of 10 mm to both the major and minor axes does not preserve the eccentricity of the ellipse: the new ellipse has a slightly different shape from the original. The correct offset can be found by differentiating the original ellipse at each point, then projecting 5 mm along the normals to each point (in fact, the correct offset profile is not an ellipse at all). The error introduced is greatest for points midway between the major and minor axis apices of the ellipse. For example, consider the point on the female leaflet surface for which angle θ in figure 9.7 equals 45°. Substituting into equations (9.2 & 9.1a) gives the coordinate points as:

$$dz/dx_{(x=4.447,\ z=-8.886)} = \theta = -\tan 45° \quad (9.5)$$

and the normal at this point is given by:

$$z + 8.886 = x - 4.447 \quad (9.6)$$

The point of intersection with the toolpath ellipse can thus be found by substituting equation (9.6) and solving:

$$(z+13.333-Eo/MajA')^2 + (z/MinA')^2 = 1 \quad (9.7)$$

which gives x = 0.952, z = -12.381. The straight-line distance between this point on the offset ellipse and the corresponding point on the original ellipse (eqn 9.5) is 4.943 mm, and therefore the female mould segments will be slightly undersized in the leaflet belly region. This discrepancy between the ellipse offset and the correct 5 mm offset, although small (1%), is of the same order as the leaflet cavity thickness. However, the same type of error also occurs on the male mould surfaces, and

Figure 9.7 Correction to toolpath offset for elliptical leaflet geometry

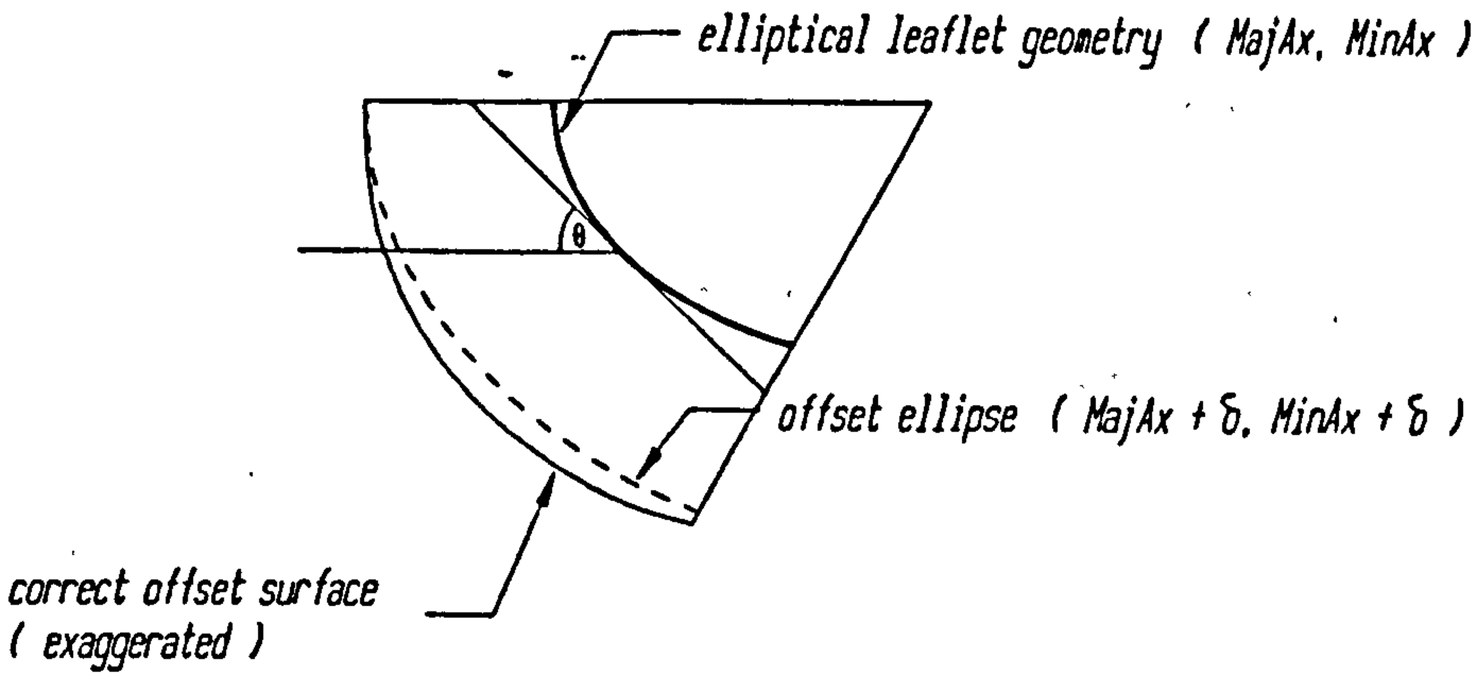

the two opposing errors tend to cancel each other out (the male electrodes are cut slightly undersized but this results in the finished male mould surface being slightly oversized, due to the reversal of curvature in the spark erosion process). To appreciate the error on the leaflet cavity, consider that point on the female offset ellipse (eqns 9.4a & b) for which angle θ in figure 9.7 equals 45°. In an analogous manner to that demonstrated before, the point is found to be x = 0.927, z = -12.356, and the normal at that point intersects the corresponding male offset ellipse (MajAx' = 27.032, MinAx' = 20.574) at x = 0.952, z = -12.461, which results in a male-female separation of 0.148 mm. Therefore, the leaflet cavity is approximately 2 μm (1%) thinner in the belly region than originally specified in table 9.1. This discrepancy could be eliminated by writing a program which differentiates the specified surface and projects along normals. However, given the small error incurred, it was felt that the method of offsetting the major and minor axes was acceptable.

An example of a program used to generate part of the female mould surface is listed in Appendix 4. A greater concentration of points, and consequently a smaller toolpath increment, is computed near the apices of the hyperbolae where there are smaller radii of curvature. The cutting direction is along the hyperbolae (2D linear interpolation), and thus the female leaflet shape could, in principle, be carved out on a 2-axis numerically-controlled milling machine (although, in fact, a 3-axis machine was used). Note that the program only generates the toolpath for the planes between z = -3.25 and -5.5. This is because the milling machine controller has a limited data memory buffer (32 kilobytes) and, in order to be input in manageable blocks, the entire toolpath data had to be broken down. The toolpath was split into 10 segments, each incorporating a stream of approximately 1000 coordinate points. That is, one entire leaflet area

was defined by slightly more than 10000 points (approximately 5000 points per $cm^2$, although the points were not uniformly distributed).

As mentioned earlier, the male leaflet moulding surfaces were made by a process of spark erosion, with the electrodes machined on a milling machine. Spark erosion, or electrical discharge machining (EDM), is a thermal process which utilises spark discharges to erode electrically conductive materials. A sculptured electrode defines the area over which erosion will occur, and thus determines the shape of the resulting cavity in the workpiece. A pulsed DC power supply maintains a potential difference between the electrode and workpiece, and a dielectric fluid is flooded between the two.

The sequence of events occurring during one pulse of an EDM cycle, which typically lasts for a period of micro- to milliseconds, is described by Benedict (1987). Briefly, when a DC pulse is delivered, an intense electric field is created at the point where surface irregularities provide the narrowest gap. Microscopic contaminants migrate to this region and form a high-conductivity bridge across the gap. The temperature of the bridge increases to a point where the bridge material and surrounding dielectric fluid vaporize and ionize, resulting in the formation of a spark channel. The heat of the spark channel is sufficient to vaporize a small amount of material from both the electrode and workpiece, and the resulting gaseous products expand outwards from the spark channel. Upon termination of the electrical pulse, the vapour bubble collapses violently, leaving a small crater on both the electrode and workpiece surface. By appropriately selecting the electrode material, dielectric fluid, and operating parameters, the wear on the electrode wear can be limited to only a small fraction of that experienced by the workpiece.

One particularly appealing aspect of EDM is the potential for controlling surface finish. By operating at

a low current, high frequency mode, a very smooth surface can be achieved (i.e. minimise the amount of energy available for material removal per pulse). Conversely, increasing the current and/or decreasing the frequency gives rise to a textured surface finish. This feature may be of interest when considering blood-contacting devices, as there may well be a preference for either a smooth or textured surface when wishing to inhibit or encourage host tissue ingrowth.

Inherent to the EDM process, the electrodes produce an overcut in the workpiece as a result of the finite size of the spark gap. The size of the spark gap must therefore be considered when machining the electrodes. The overcut is uniform across the electrode surface and, consequently, can be accounted for in the same way as an offset for a ball-nosed cutting tool (eqns 9.4). Thus, the program used to compute the appropriate toolpath code for cutting the electrodes, had the same format as that used for the female mould segments, but with the inclusion of a spark gap offset, SG:

$$MajA' = MajA + 5 - SG \quad (9.8a)$$

$$MinA' = MinA + 5 - SG \quad (9.8b)$$

$$H_o' = H_o - (5/\cos 30°) + (SG/\cos 30°) \quad (9.8c)$$

$$z' = z - 5 \quad (9.8d)$$

The electrode material used was a copper-tungsten alloy. This material is relatively easy to cut but also has a relatively high wear resistance in EDM. Two sets of electrodes were machined. For producing *roughing* electrodes a spark gap of 320 $\mu$m was allotted. These were used to erode the bulk of the workpiece material. The roughing electrodes left a relatively coarse surface finish on the workpiece, and there was considerable wear on the electrodes themselves. The final smooth surface was achieved using *finishing* electrodes with a spark gap of 160 $\mu$m. A fresh finishing electrode was used for each

leaflet area.

### 9.2.4 Injection moulding trials

Moulding trials with the IBM tool have been conducted in collaboration with the Polymer Technology Group at Napier University, Edinburgh. The moulding machine used, a Battenfeld 350 CD with Unilog 4000 control, is the modernised equivalent of the hydraulically-powered Peco 15MR described in the previous chapter (fig 8.14). The machine has a computerised control system (incorporating displacement and velocity transducers rather than limit switches) and is capable of injecting molten plastic at a profiled flow rate (fig 9.8).

The first attempts at moulding were carried out with the male and female mould components set slightly apart, to ensure that the cavity would fill. The moulding machine was programmed to fill the cavity at a constant speed until a pressure of 100 MPa was reached, at which point this constant packing pressure would be maintained (i.e. at the end of the filling stage the machine switched from being a constant flow generator to being a constant pressure generator). A cycle time of 45 seconds was selected. There are 4 independently-controllable temperature zones along the barrel of the moulding machine; these were set to 198, 200, 190, & 165 °C respectively, from the nozzle end. The PU's used were Estanes.

A typical moulding is shown in figure 9.9. The cavity does not fill through the leaflets first and then the frame. Instead, from the gate, molten PU flows along 3 arms running above and along the leaflet free edges, down the posts into the frame region, and then into the leaflet areas last. A few small specks of black, burnt PU can be seen in the mouldings; this was subsequently found


Figure 9.8 Battenfeld 350 screw-type injection moulding machine

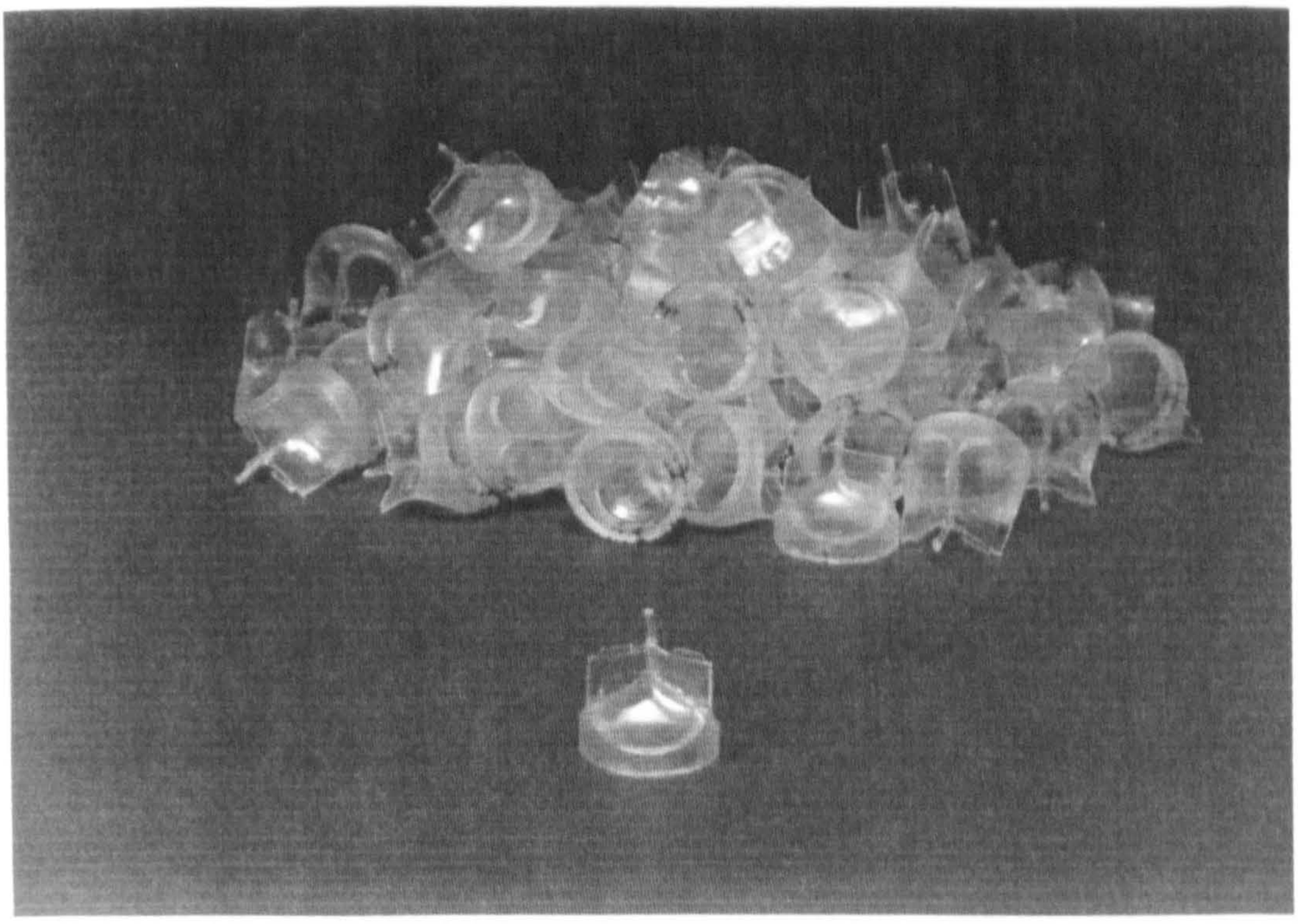

Figure 9.9  Mouldings from IBM tool

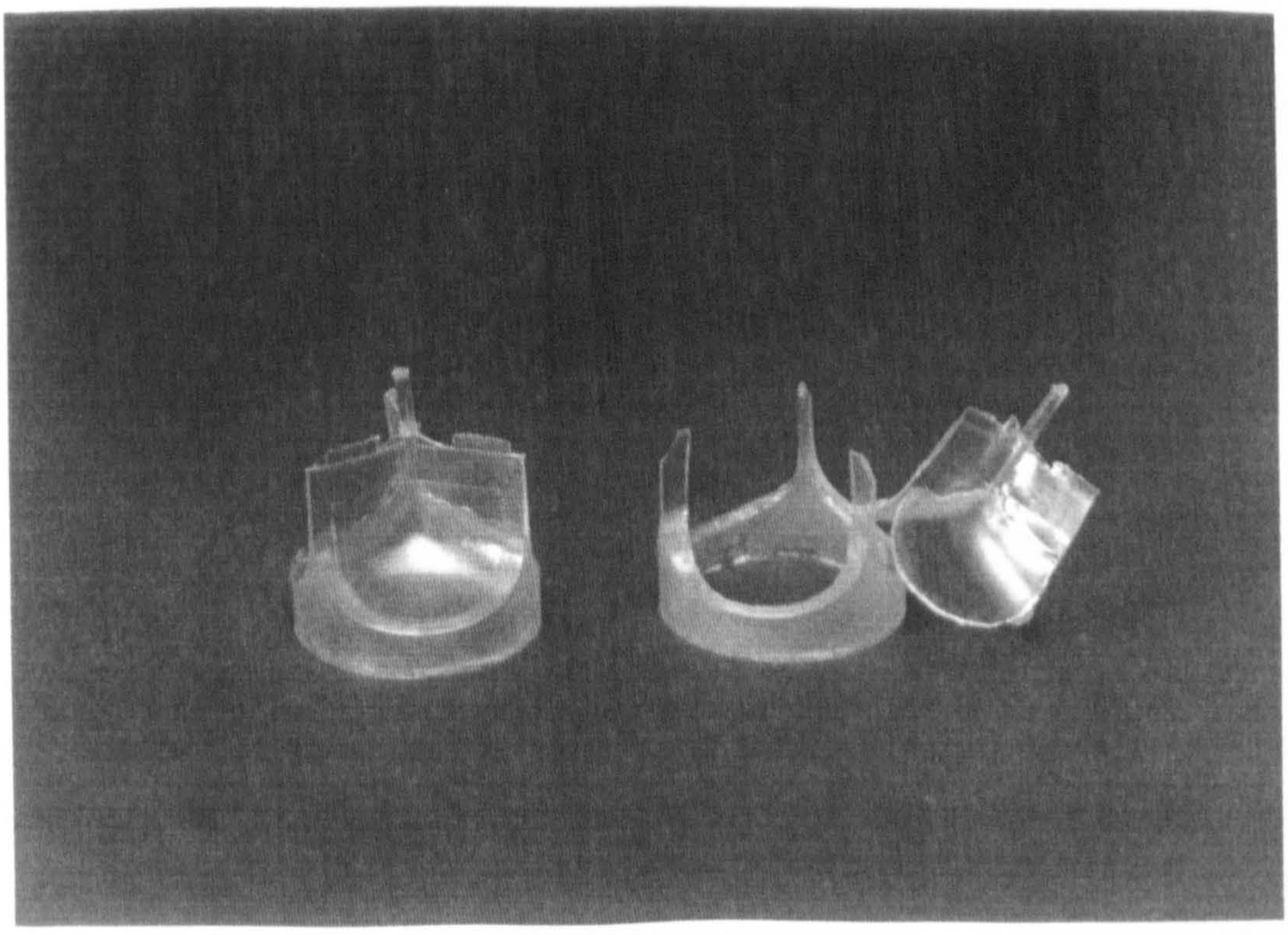

Figure 9.10  Leaflets cut away to produce frames

to be the result of a partial blockage in the hot runner system. Otherwise, the mouldings appeared to be of good quality. As with earlier moulding trials described in the previous chapter, liberal quantities of dry-film silicone lubricant were required as a mould release agent.

At present, valves with leaflet thicknesses down to 400-500 $\mu$m have been moulded, and attempts to mould thinner leaflets, by sliding the male and female moulding surfaces closer together, are ongoing.

### 9.2.5 Summary

An elaborate moulding tool, incorporating a plausible valve design, an ejection mechanism, channels for temperature control, and capable of withstanding substantial injection/holding pressures, has been built. Sophisticated CAD/CAM techniques were employed to machine the valve moulding surfaces. The tool construction is such that the parts which mould the valve surfaces are replaceable inserts, and the tool is of a standard format which can be used with a range of moulding machines. Using a computerised moulding machine, valves have thus far been moulded with leaflet thicknesses in the region of 500 $\mu$m.

## 9.3 Dip Moulded Valves

The sculptured male and female formers incorporated within the IBM injection moulding tool can also be used to fabricate PU valves by alternative means. One such method, which has been widely used to manufacture PU valves (see Chapter 7), is dip moulding. Once the former has been made, the dip moulding process is relatively easy to set up and, unlike injection moulding, very thin sections of PU can be readily produced. However, there are formidable difficulties associated with this technique, in terms of controlling leaflet thickness

distributions and achieving reproducibility. Although dip moulding may not be ideal, it does offer a relatively convenient means for creating a functioning PU valve.

### 9.3.1 Valve manufacture

The mouldings produced by the IBM tool (fig 9.9) and the male mould former (fig 9.2) provided the starting point for the fabrication of these dip moulded valves. Leaflets were cut away from the PU mouldings to produce frames (fig 9.10), and the frames were then mounted onto a dipping former (fig 9.11). The former was not actually the same one as used in the moulding tool, but a copy. The frame-former assembly was then carefully dipped into a solution of PU, taken out, and allowed to 'dry'. As the solvent evaporates, a thin film of PU is left behind to form the leaflets and encapsulate the frame. An example of the finished article is shown in figure 9.12.

A variety of dipping configurations were tried out in an attempt to find the method which resulted in the most uniform leaflet thickness distributions and gave most consistent results. As was discussed in Chapter 7, the flow of PU solution across the sculptured surface of the dipping former and the final leaflet thickness distribution are influenced by a number of factors, namely:

1) viscosity and evaporation rate of the particular PU solution

2) ambient temperature and solvent concentration

3) manipulation during dipping and drying

4) geometry of former

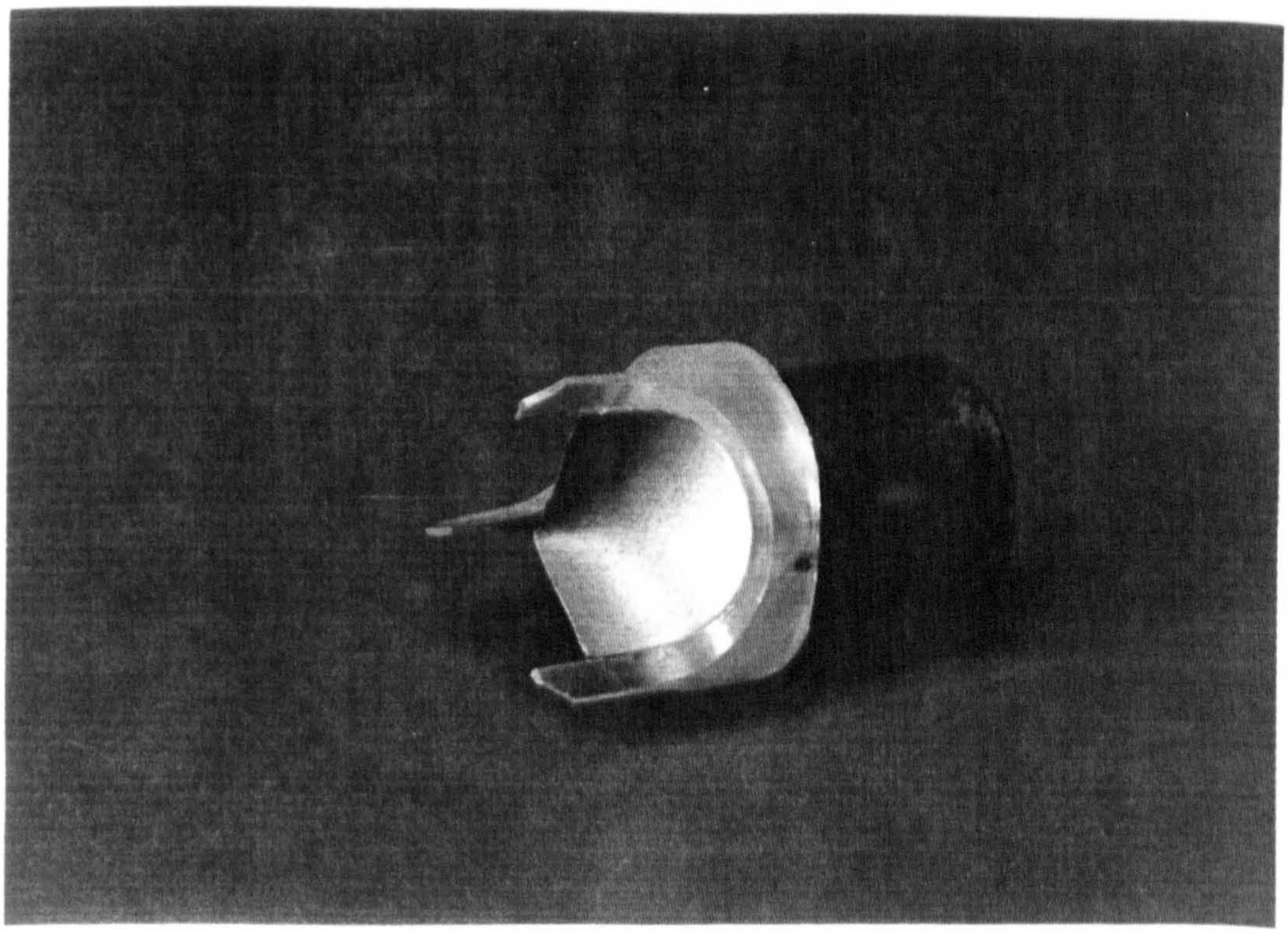

Figure 9.11 Frame mounted on dipping former

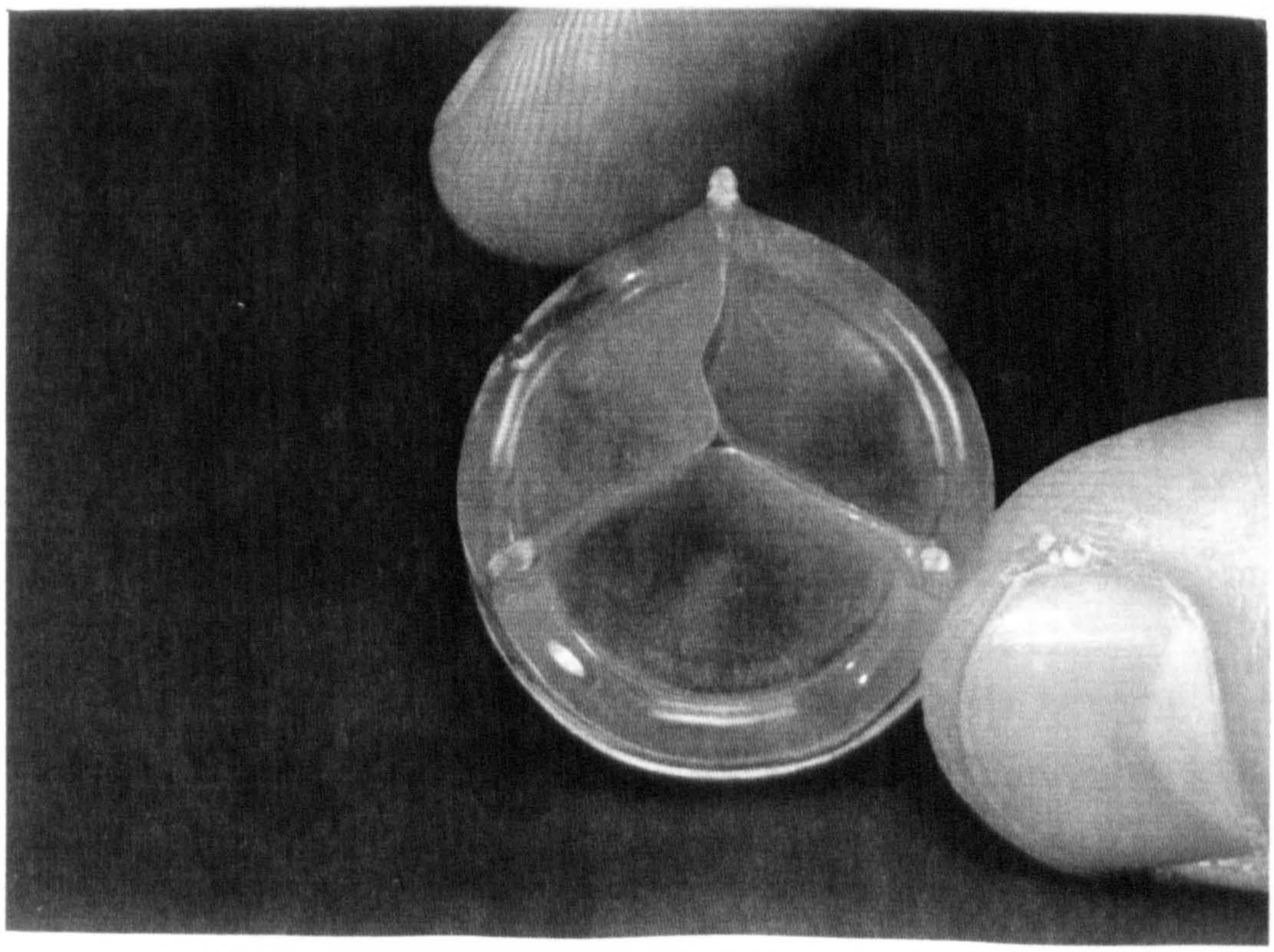

Figure 9.12 Dip moulded valve

Best results were obtained from a single dip into a concentrated PU solution, for example, a 60% solution (by weight) of Estane 58271 in DMAc (dimethyl acetamide). Multiple dipping into a more dilute solution gave rise to more pronounced thickness gradients, and also resulted in the PU frames gradually dissolving and flowing into the leaflet region. There are only a very limited number of solvents available which will dissolve PU elastomers; all are highly polar and toxic. The solvents used were DMAc and DMF (dimethyl formamide). Estane and Lycra solutions were selected for dipping; Pellethane was reluctant to dissolve and produced rather inhomogeneous solutions.

Dipping of the frame-former assembly was performed inside a fume cupboard, at room temperature. Pre-heating the former prior to dipping made no discernible difference to the leaflet thickness distributions produced, but the frames appeared to fit more snugly around the heated formers. Drying was carried out in a sealed oven at 65°C; dried air was continuously flushed through the oven, and the exhaust air-DMAc/DMF vapour mixture was bubbled through a water trap to remove the solvent.

A reasonably consistent means of dipping was achieved simply by inserting the frame-former assembly into a flask containing PU solution, inverting the flask and waiting for the solution to completely encapsulate the frame-former assembly, and then re-inverting the flask. Conveniently, the neck internal diameter of the flask was just fractionally greater the valve frame outer diameter, and this prevented PU solution escaping when the flask was turned upside down. After dipping, the frame-former assembly was held in place at the flask neck until PU solution had stopped flowing continuously off it (typically, 30 seconds); it was then promptly put in the oven. A converted mixing/tumbling device provided the means for slowly rotating the frame-former assembly as it dried (fig 9.13); the electrical drive unit sat outside

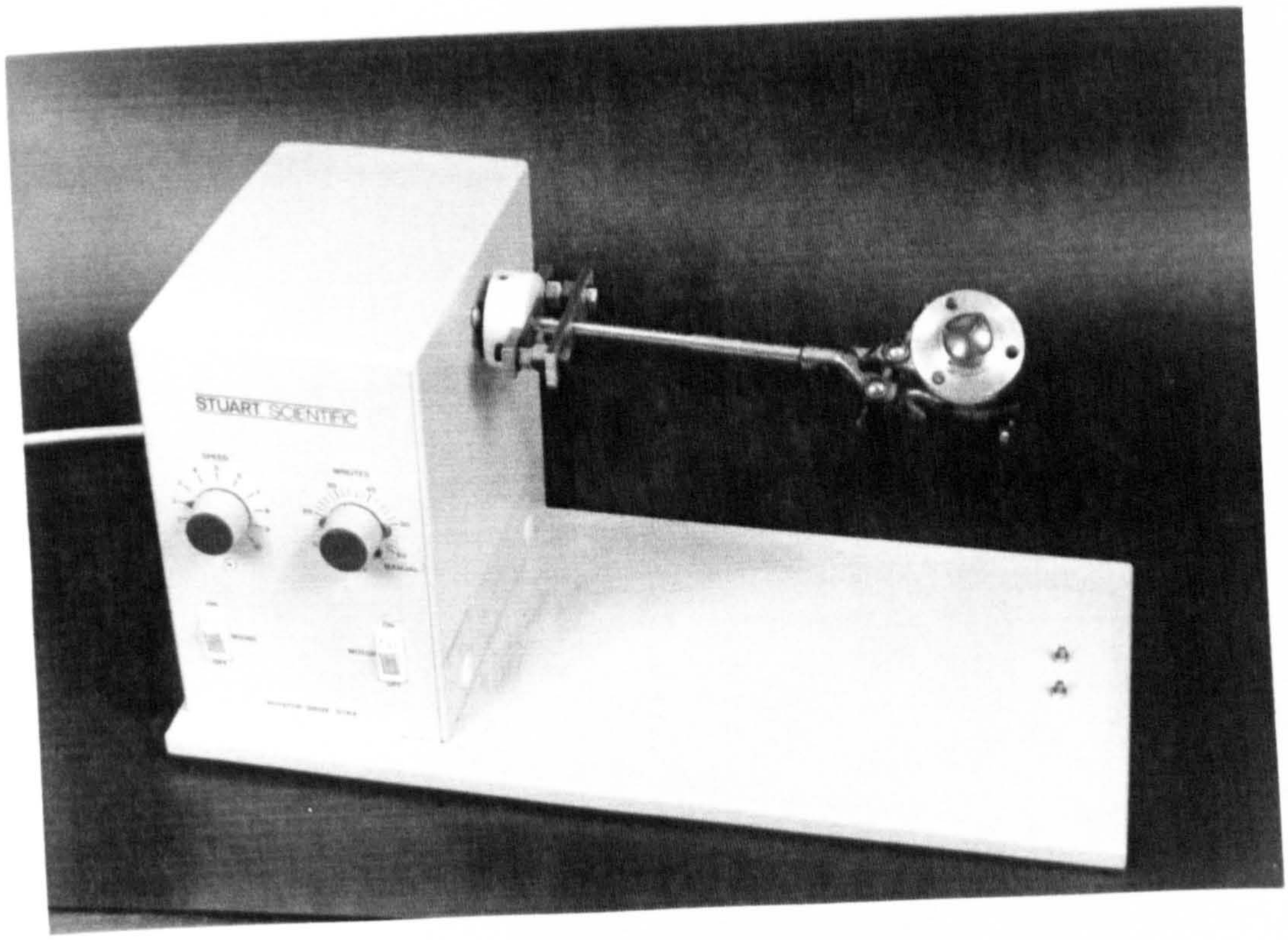


Figure 9.13 Device for rotating dipping former

the oven, and the frame-former assembly was connected to a rotating axle which passed through a hole in the side of the oven. Unfortunately, rotating the former in this manner resulted in the PU solution flowing predominantly to the leaflet-frame junction, and the valves produced in this way were rather reluctant to open. After some experimenting, the most uniform leaflet thickness distributions, and those which resulted in valves which opened most easily, were obtained by simply suspending the frame-former assembly upside down in the oven during drying. Predictably, the valves made in this way had a thick ridge of PU along the leaflet free edges. However, this thick band could easily be cut away post-moulding without compromising the closed valve's ability to seal competently. The dipped frame-former assembly was dried upside down for 24 hours; the valve was then removed from the former, rinsed thoroughly in water, and dried again for a further 24 hours.

Consistency of leaflet thickness was difficult to achieve, both between leaflets on the same valve and between valves. For example, leaflet thickness maps for 2 of the better dip moulded valves are shown in table 9.2. There are several possible factors contributing to the inconsistencies. Firstly, the frame-former assembly was manually dipped, and consequently there is clearly a limit to how repeatable this process can be. In particular, it was especially difficult to transfer the freshly dipped frame-former assembly from the flask to the oven, and the mount the former in the oven, in the same way each time. Also, this stage immediately post-dipping is likely to be the most critical as the PU solution is then least viscous. Variable leaflet thicknesses may also arise from inhomogeneities in the PU solution. The solutions were mixed thoroughly before dipping. However, mixing tends entrap air into the solutions and so they were left to stand for a period immediately before dipping. The standing period, which

Table 9.2 Leaflet thicknesses (μm) for valves PU1 & PU2

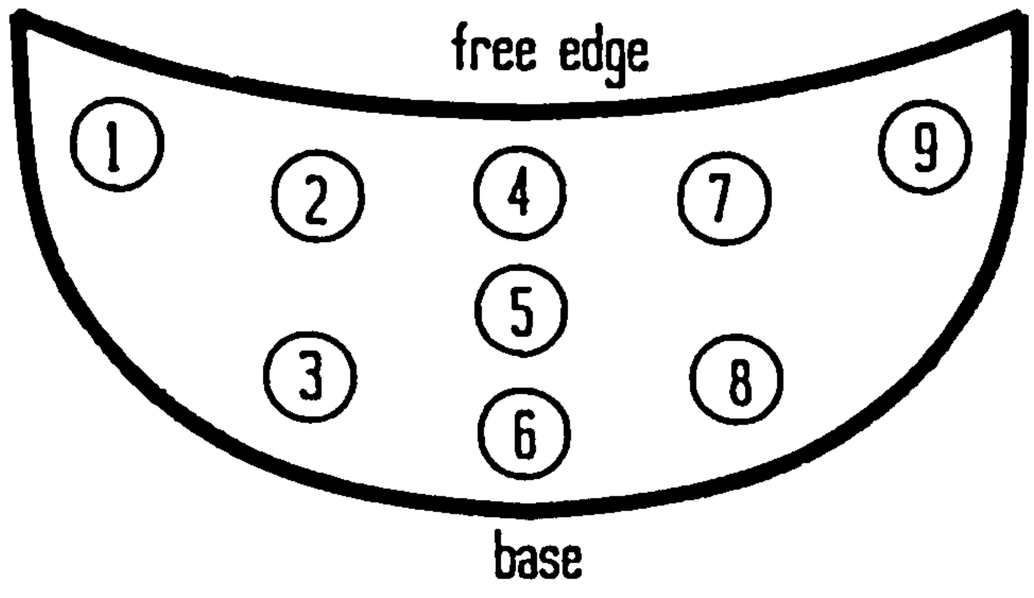


| valve | PU1 | | | PU2 | | |
|---|---|---|---|---|---|---|
| leaflet number | 1 | 2 | 3 | 1 | 2 | 3 |
| position | | | | | | |
| 1 | 87 | 63 | 56 | 134 | 183 | 182 |
| 2 | 51 | 55 | 56 | 92 | 94 | 99 |
| 3 | 45 | 44 | 48 | 100 | 107 | 93 |
| 4 | 52 | 51 | 54 | 89 | 92 | 92 |
| 5 | 52 | 50 | 53 | 100 | 100 | 102 |
| 6 | 47 | 45 | 49 | 88 | 89 | 85 |
| 7 | 55 | 52 | 52 | 98 | 94 | 85 |
| 8 | 45 | 81 | 43 | 112 | 80 | 109 |
| 9 | 45 | 86 | 114 | 154 | 136 | 163 |

mean leaflet thickness: PU1 = 56.7 μm (SD = 16.1)
PU2 = 109.3 μm (SD = 28.8)

can be hours for the highly concentrated solutions, may allow time for inhomogeneities to regroup. Other potential sources of variability include thermal gradients inside the oven, inherent variability in the frames which were manually finished, etc.

A second problem, which occurred apparently at random, was the presence of small air bubbles in the dip moulded leaflets. Frequently they would occur at the frame-leaflet junction. Prior to dipping, the injection moulded frames were trimmed by hand using a small pair of scissors. Care was required not to cut away too much frame material as this may result in a small cavity arising between the frame and dipping former. Such cavities may well provide a lodging place for air bubbles.

The 2 principal problems of variable leaflet thickness distributions and the occurrence of air bubbles afflicted the majority of valves made. For example, for 10 successive dip moulded valves, each made in the same way given the limits of the method outlined above, perhaps only 2 or 3 would be both free from air bubbles and have leaflet thickness distributions as uniform as those given in table 9.2.

Finally, notice that dipping the frame-former assembly into a PU solution results in the frame surface being partially dissolved. This gives rise to a very strong bond between the leaflets and frame and the 2 become apparently continuous: the finished valves have a very smooth, fluid-like appearance. Also, to a small degree, the frames appear to have flowed into the leaflet areas during the moulding process. The resulting gradual tapering from the frames to the leaflets is probably a most desirable feature which may reduce stress concentrations along the frame-leaflet junction in the operating valve.

## 9.3.2 Hydrodynamic testing

Dip moulded PU valves have been tested hydrodynamically in the GRI pulse duplicator, under the standard testing conditions specified in chapter 4 (equivalent cardiac output range of 3.6 to 9.6 litres per minute). Results are presented here for the 2 valves described in table 9.2, one with slightly thicker leaflets than the other. For comparison, a range of other types of prosthetic valve, of comparable sizes, were also tested. These valves were of near clinical quality. The types and dimensions of the valves tested are listed in table 9.3. All valves were tested in the mitral position.

The valvular EOA's, computed from flow and pressure drop recordings measured across the range of pulsatile flow rates, are displayed in figure 9.14. Based upon 15 repeated measurements made over a period of 5 consecutive days using a tilting disc valve, the standard deviation on the calculated EOA's is ± 0.15 $cm^2$. The dip moulded PU valves present no more of a resistance to forward flow than do the other valve types. Indeed, the PU valve with thinner leaflets, PU1, together with the Glasgow pericardial valve, have the highest EOA's across the test range. Across the test range, PU1 has an EOA consistently larger than PU2 by approximately 4 standard deviations. For all valve types, there is a general increase in EOA with flow rate. As discussed in chapter 3, this may be the result of viscous dissipation, and, in the case of the tri-leaflet valves, be due to valves opening to a fuller orifice area at higher flow rates. The calculated EOA's are all considerably less than the actual orifice areas based on the valve internal diameters, which for the PU valves equals 3.80 $cm^2$. Note that the EOA for the porcine valve shows a more dramatic increase with flow rate than do the other valve types. This reflects the more erratic opening and closing behaviour of the porcine valve; at lower flow rates one leaflet was not fully

Table 9.3  27 mm valves tested in pulse duplicator

| | internal diameter (mm's) | external diameter* (mm's) |
|---|---|---|
| Glasgow Pericardial (Bioflo) | 21.8 | 27.5 |
| Hancock Porcine | 20.5 | 27.5 |
| Omniscience (tilting disc) | 21.2 | 27.5 |
| PU dip moulded | 22.0 | 28.2 |

* excluding sewing ring

Figure 9.14 Effective orifice area versus RMS flow

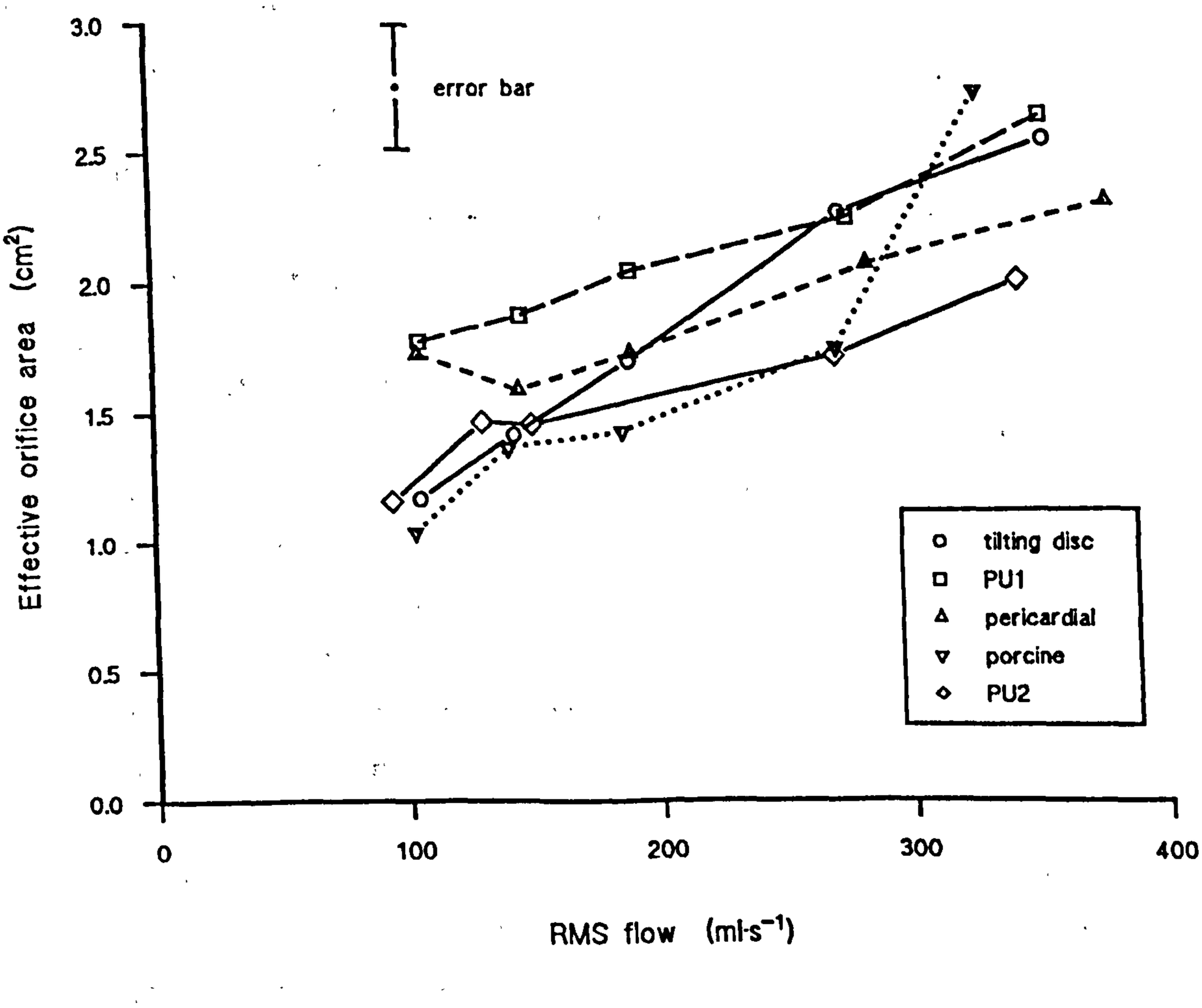

opening, but as the flow rate increased a threshold was reached beyond which the valve did fully open.

Performances of the valves whilst closing and closed are compared in figure 9.15, which charts the measured regurgitant and leakage volumes across the range of test flow rates. Again, based upon 15 repeated measurements with a tilting disc valve, the standard deviation on the sum of these measured volumes is ± 0.5 ml. The PU valves regurgitate and leak no more, and in the case of PU1 slightly less, than other valve types. This may be attributed to the very small major axis length and offset ($H_o$) for the hyperbolae describing the leaflet free edges (table 9.1), and to the fact that the leaflets are attached to the inside of the frame. For the Glasgow pericardial valve the leaflets are pinned onto the outside of the (inner) frame, and consequently there is a slight problem sealing the valve at the tops of the frame posts; a suture attaches neighbouring leaflets together at the commissures and helps to seal the closed valve. On the other hand, however, the valve construction with leaflets fastened to the outside of the frame, rather than the inside, enables the leaflets to open up more easily to a wider orifice. Note that the figures quoted in figure 9.18 for the pericardial valve are slightly atypical, usually valves of this type exhibit less reverse flow. The negative flow volumes become less as the flow rate increases, for all valve types. This simply reflects the shorter periods of time available for reverse flow at higher rates.

Describing the hydrodynamic efficiency of the valves in terms of energy loss provides a means for comparing performance during periods of both forward and reverse flow, as shown in figure 9.16. The energy loss calculations, across the range of test flow rates, confirm that the PU valves are as efficient as the other valve types during forward flow and slightly more efficient during reverse flow, and also that the PU valve

Figure 9.15 Reverse flow volumes

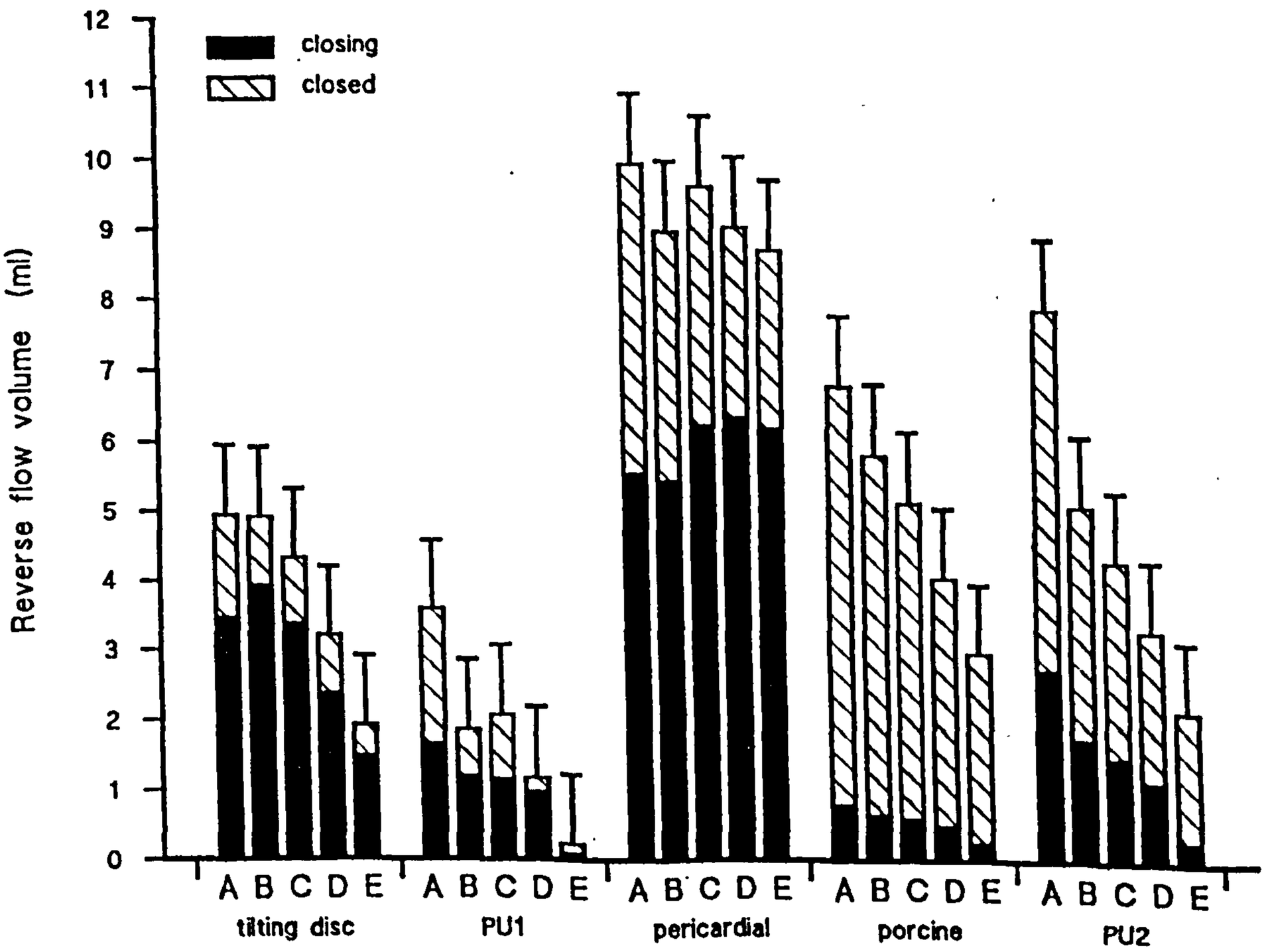

Figure 9.16 Energy losses for forward and reverse flow

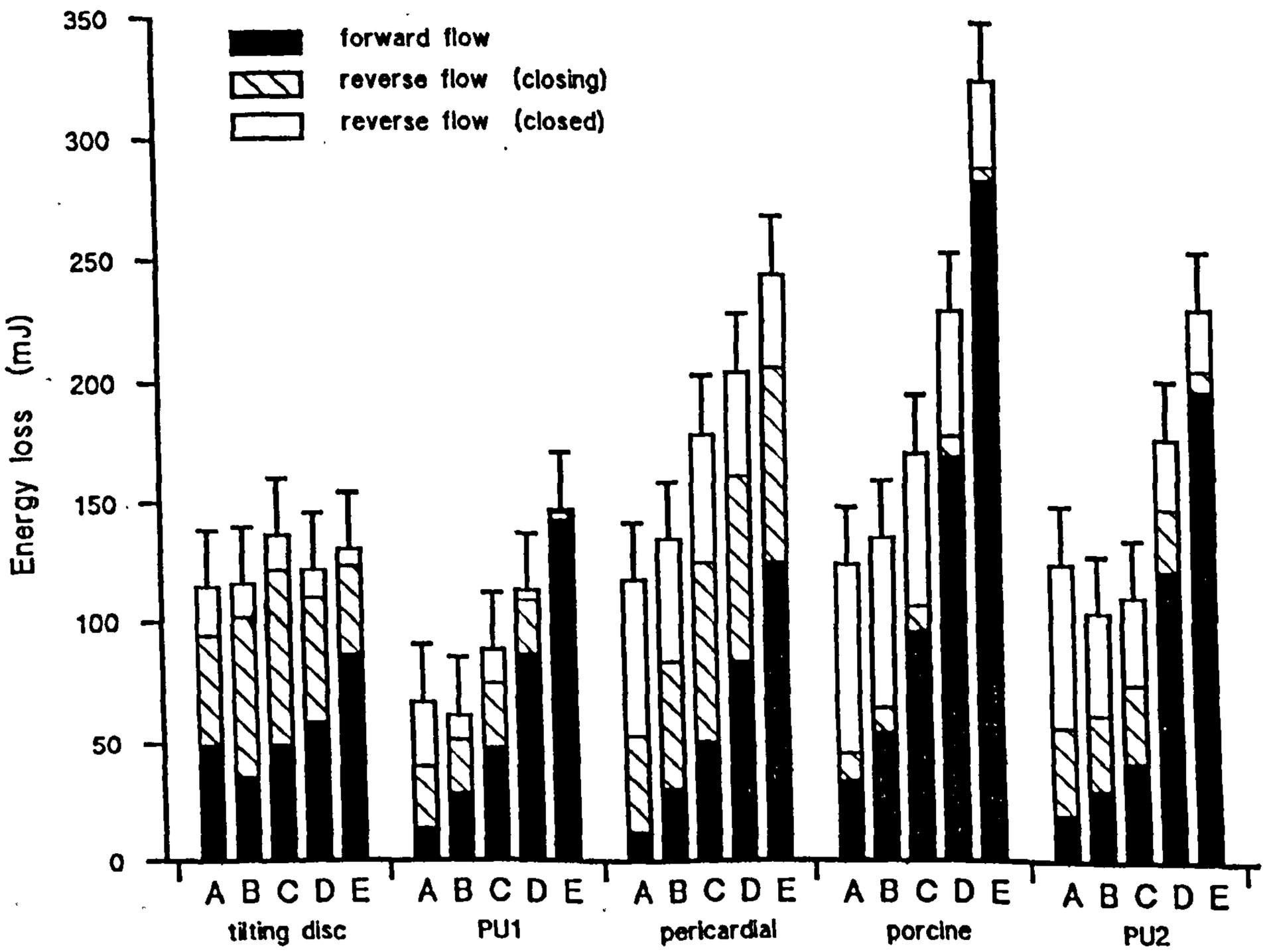

with the thinner leaflets has the better overall performance.

Visualisation of the PU valve leaflet movements, using video and synchronised flash photography, provides further useful information. Photographs of PU2 as it opens and closes are displayed in figure 9.17. Notice that in the first frame of figure 9.17b the valve PU2 is already partially closed: that is, the valve opens more quickly than it closes. Also, note that when the valve is open to its maximum extent (frame 6, fig 9.17a), the open orifice area defined by the leaflet free edges is considerably less than the area encircled by the mounting frame. Attaching the leaflets to the outer surface of the frame rather than the inner aspect would probably result in a greater open orifice area (although this may be accompanied by a slight increase in leakage flow).

Both of the dip moulded valves, PU1 and PU2, have had approximately 2-3 mm of their leaflet free edges trimmed away, and they have been trimmed in such a way that the free edges are no longer perpendicular to the frame posts but at an angle of approximately 75° (i.e. the mid-point of the free edge becomes lower than the top of the frame). Prior to cutting away the excess material, both valves experienced some degree of leaflet flutter when the valves were fully open. Trimming the free edges greatly reduced the degree of fluttering, and both PU1 and PU2 are as stable in the open position as the bioprostheses, if not more so. Comparing the hydrodynamic performances before and after cutting, the valves were slightly less stenotic and leaked slightly more after the free edge had been trimmed. The increased leakage was greater for PU2; in retrospect, perhaps too much leaflet material was removed from this valve.

Figure 9.17a Valve PU2 opening in pulse duplicator

(mitral position, test conditions A,
10 millisecond frame interval)

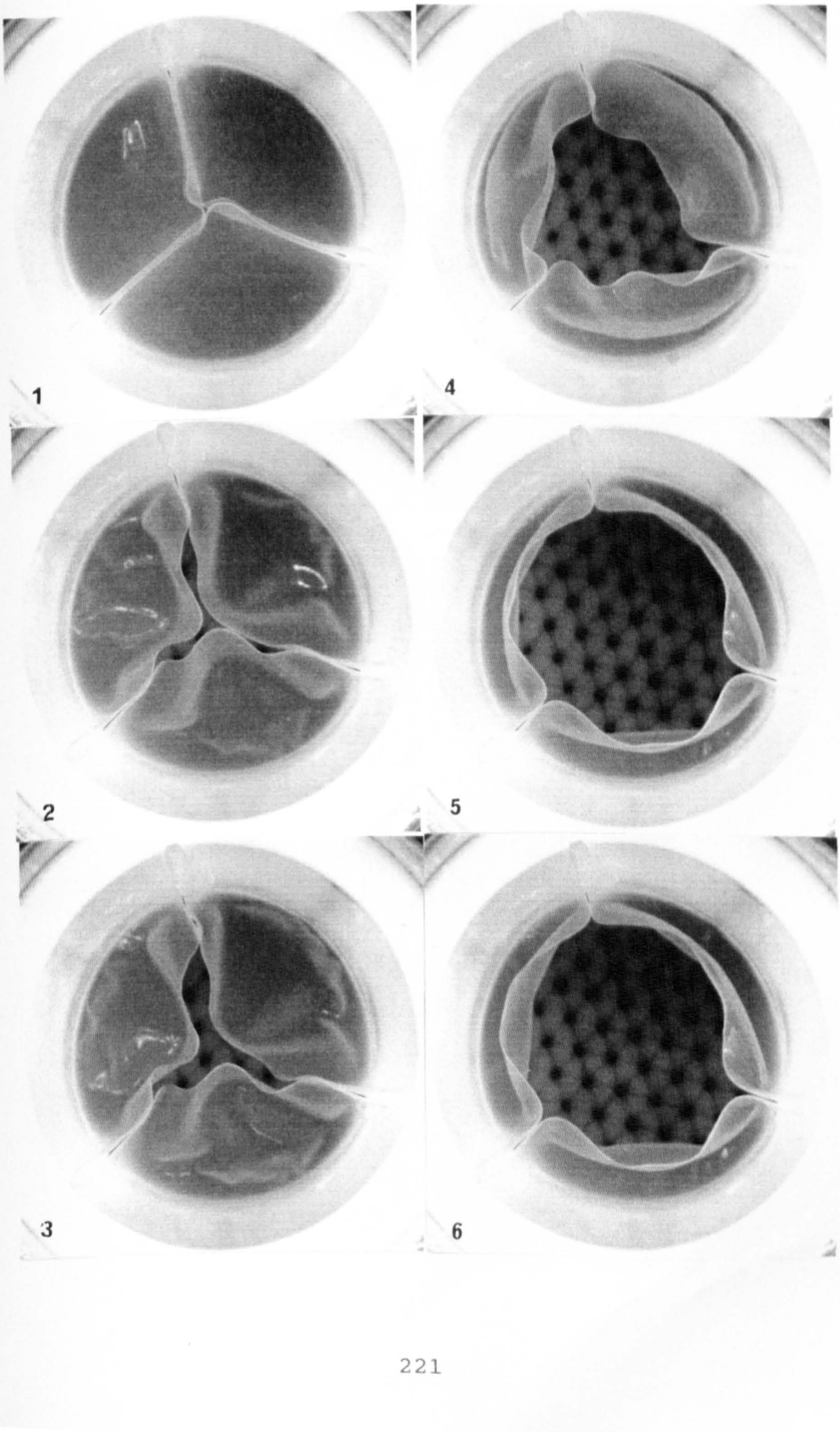

Figure 9.17b Valve PU2 closing in pulse duplicator

(mitral position, test conditions A,
10 millisecond frame interval)

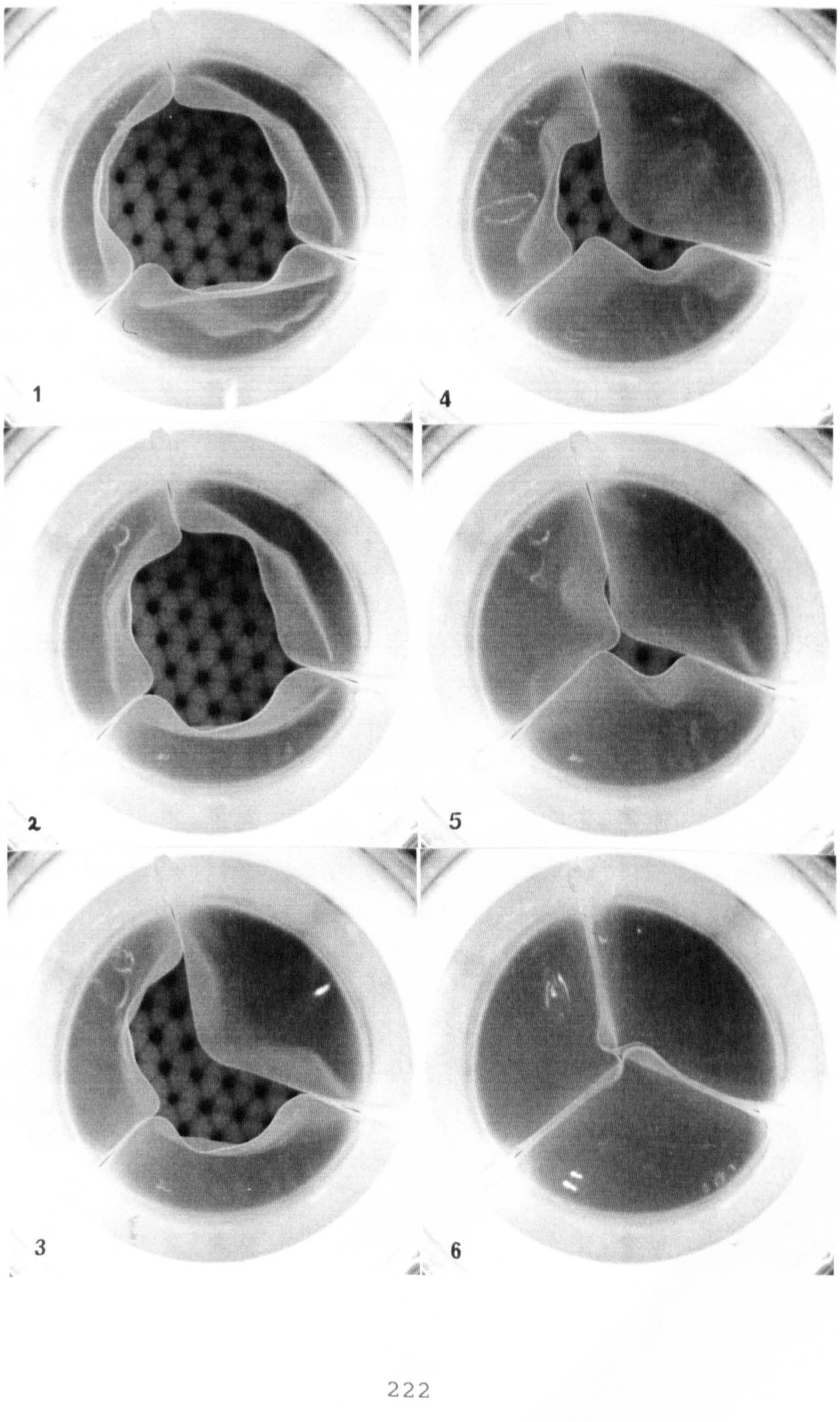

### 9.3.3 Accelerated fatigue testing

A Rowan Ash accelerated fatigue tester has been used to study the durability of dip moulded PU valves with a range of leaflet heights, thicknesses, and thickness distributions. The valves were cycled at 12 Hz, and with a peak back pressure of 110 - 130 mm Hg [14.5 - 17.1 kPa] on the closed valves (see figs 5.5 to 5.9). The amplitude of oscillation was set to approximately 4 mm, which corresponds to a mean flow rate of around 11 litres per minute through the open valve. The valves being tested were viewed approximately daily using a stroboscope, and once a week the test was stopped to allow a closer inspection of the valves and to check the pressure drops developed across each valve.

Synchronised flash photography has been used to study the leaflet movements. Figure 9.18 shows the valve PU2 opening and closing in the fatigue tester; a second valve, PU3, with a greater amount of coaptation area is shown in figure 9.19. As can be seen by comparing figures 9.17 & 9.18, the PU valves do open and close rather differently at 12 Hz in the fatigue tester from the way they do at 1.0 Hz in the pulse duplicator.

Of the 6 valves originally under test, 4 appear to be unscathed at the present, having completed over 80 million cycles (2 years equivalent use), 2 failed after 65 million cycles and were replaced, and the 2 replacement valves are both intact after 15 million cycles. Of the 2 damaged valves, one failed due to a leaflet tear, running from the commissures along the leaflet-frame junction, and the other developed a hole in a leaflet belly, as shown in figure 9.20. In both cases, the PU leaflets were less than 50 $\mu$m thick in the damaged region.

Figure 9.18a Valve PU2 opening in fatigue tester

(12 Hz cycling frequency,
2 millisecond frame interval)

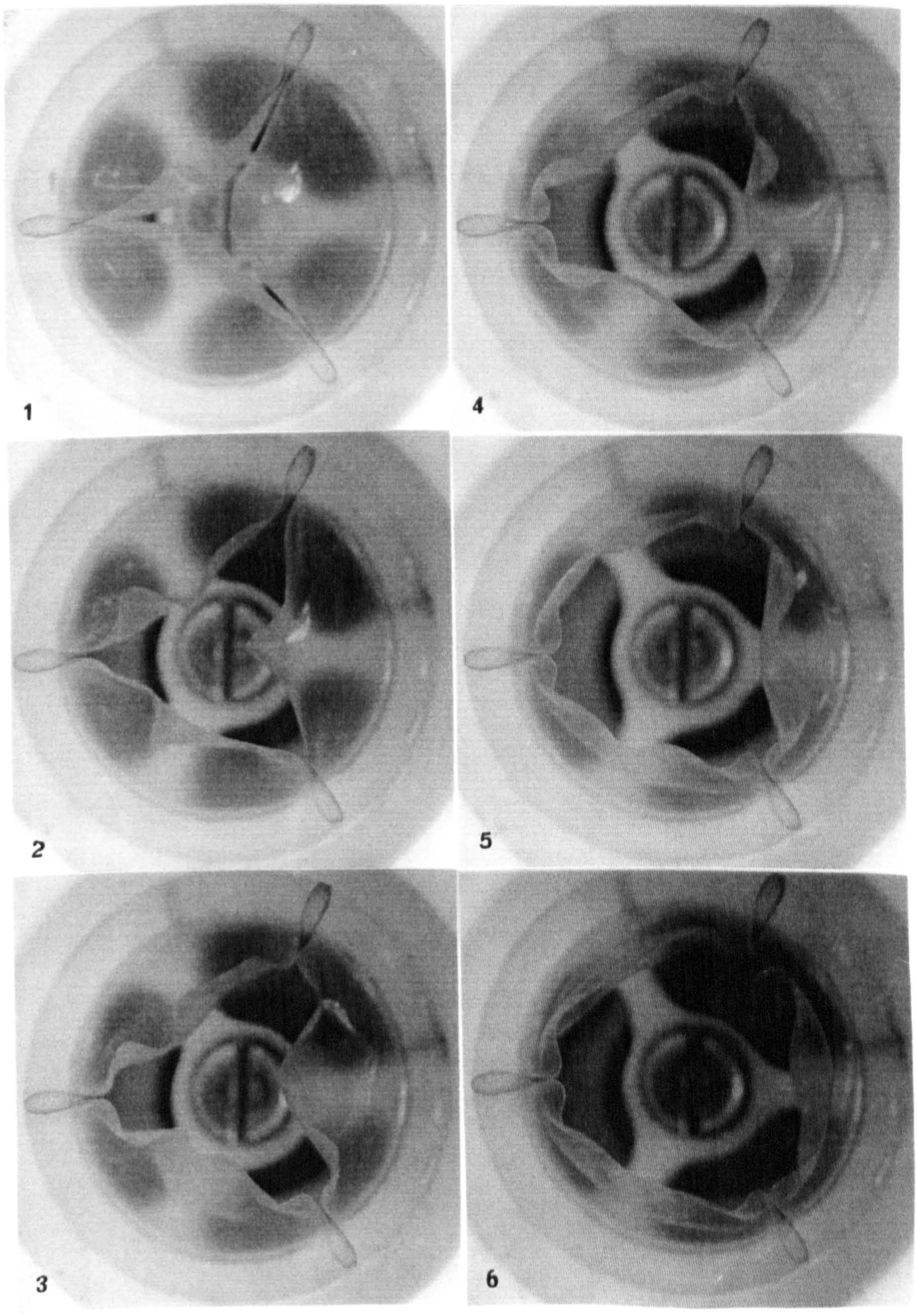

Figure 9.18b Valve PU2 closing in fatigue tester

(12 Hz cycling frequency,
2 millisecond frame interval)

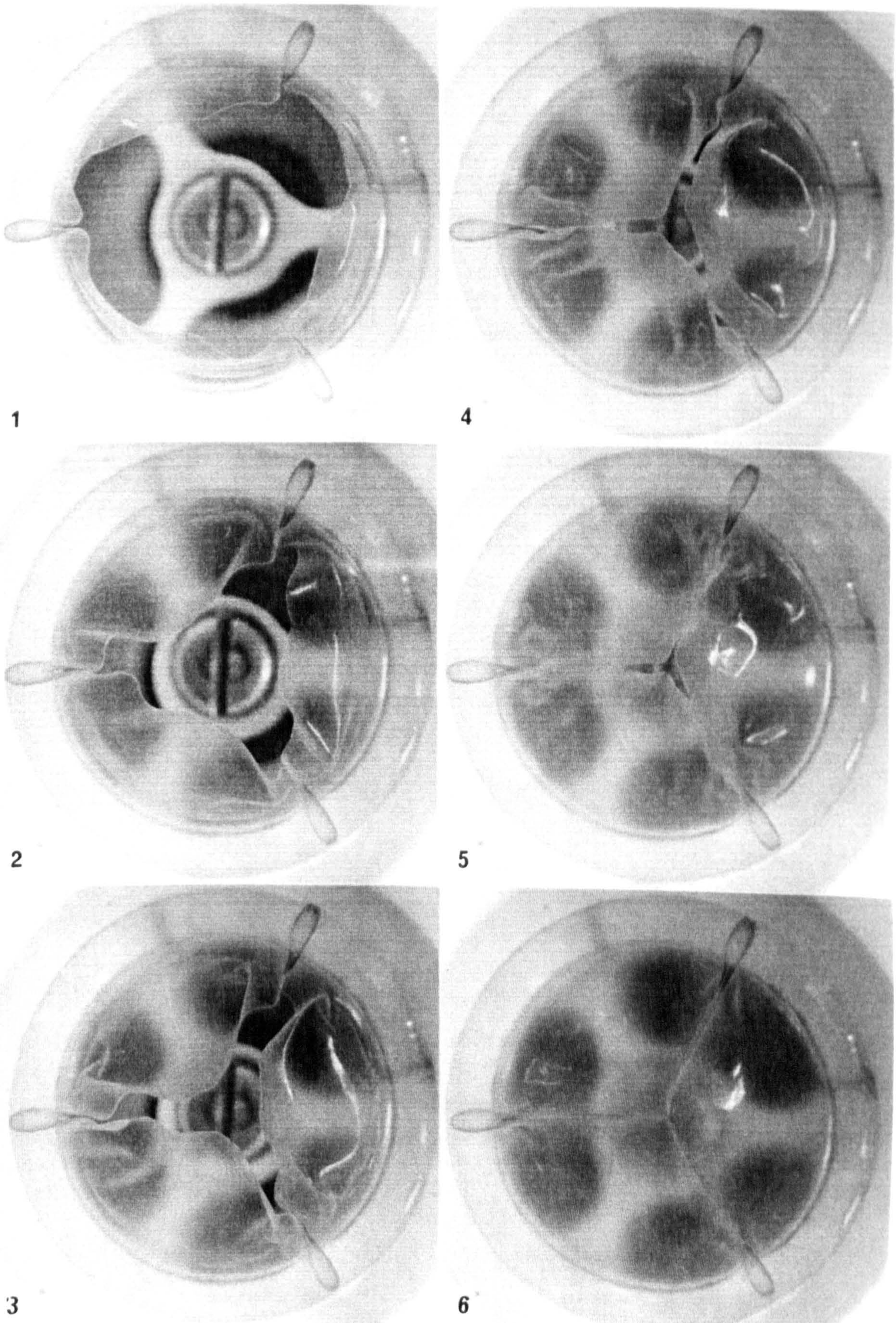

Figure 9.19a  Valve PU3 opening in fatigue tester

(12 Hz cycling frequency,
2 millisecond frame interval)

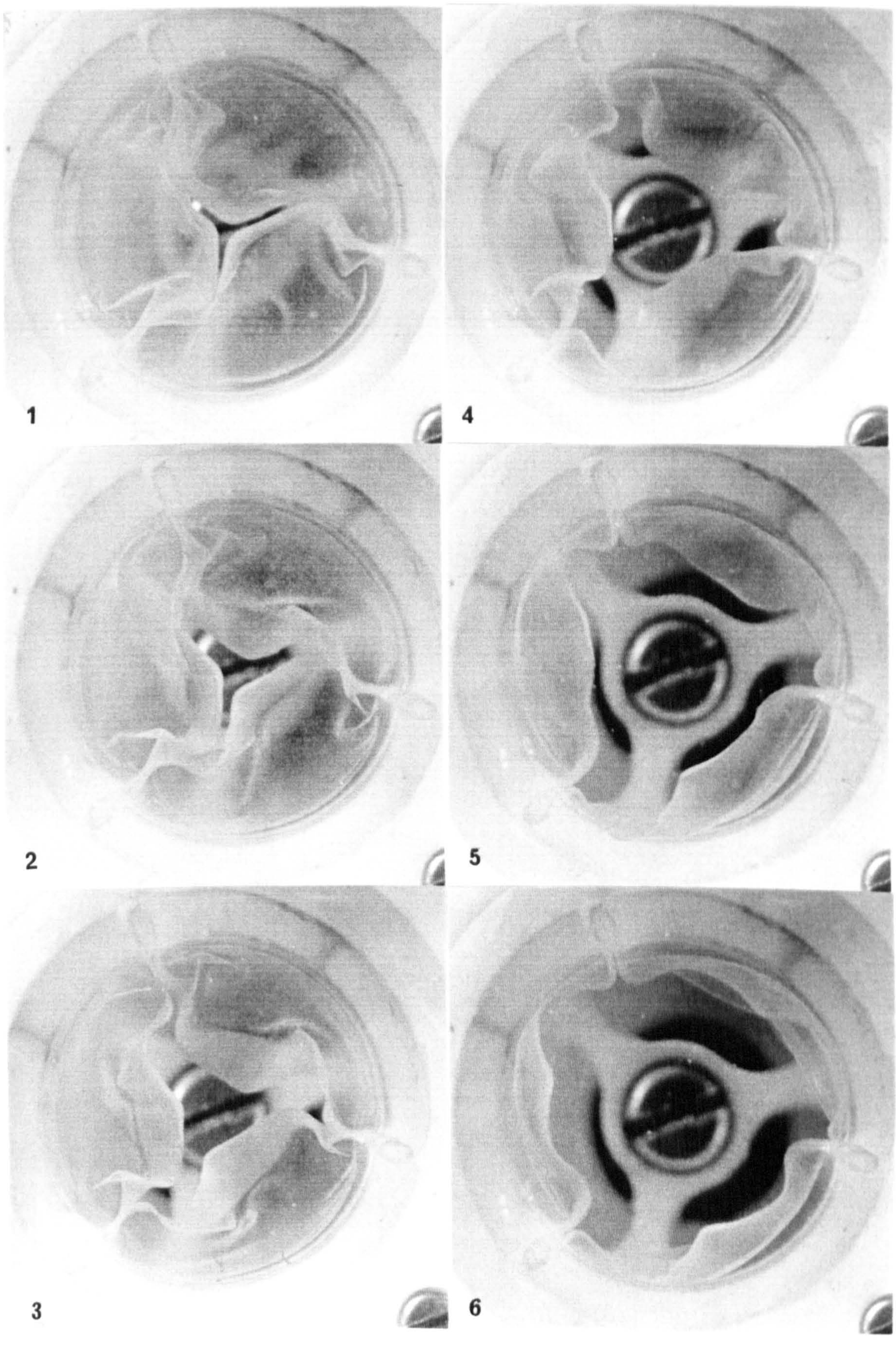

Figure 9.19b  Valve PU3 closing in fatigue tester

(12 Hz cycling frequency,
2 millisecond frame interval)

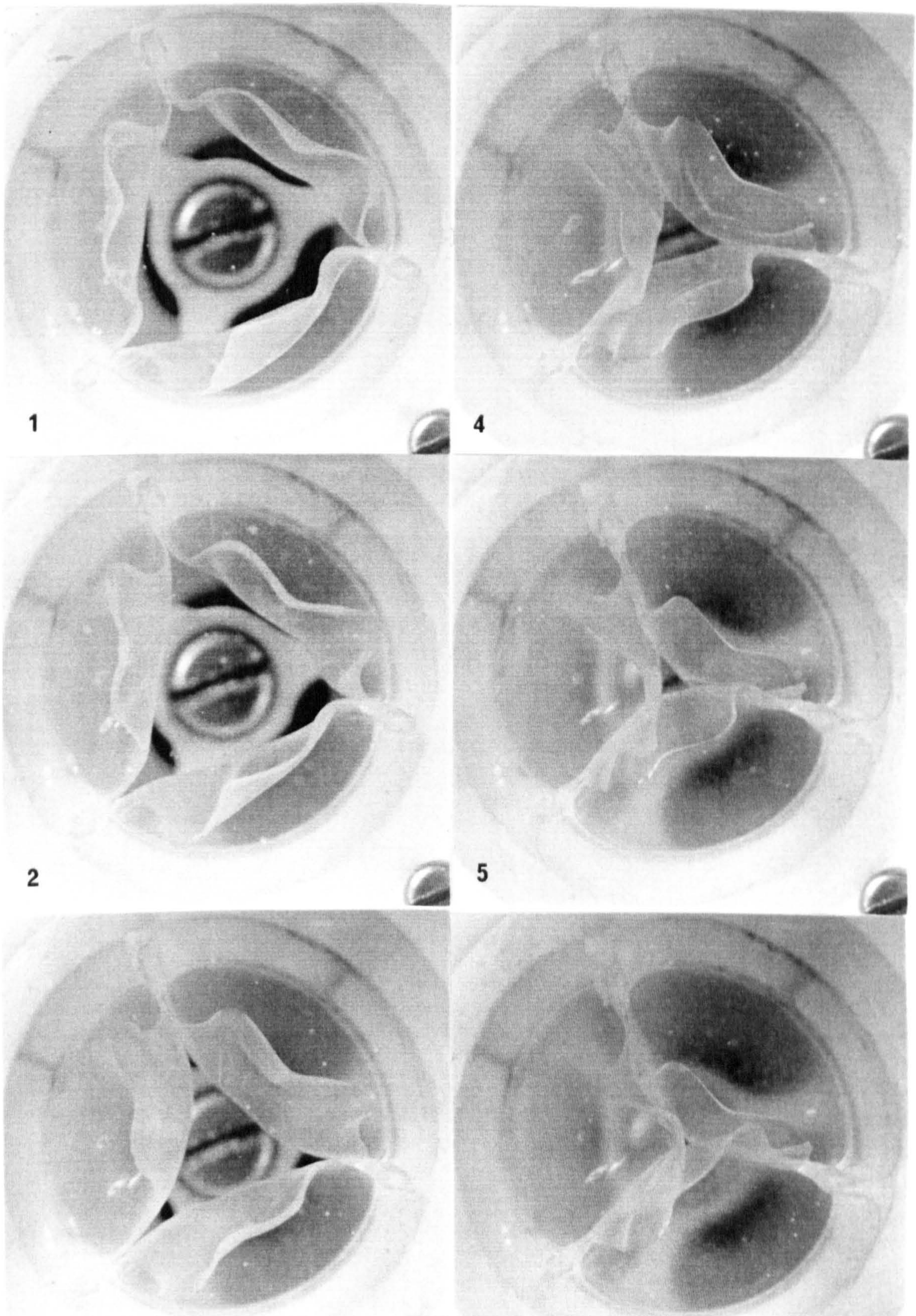

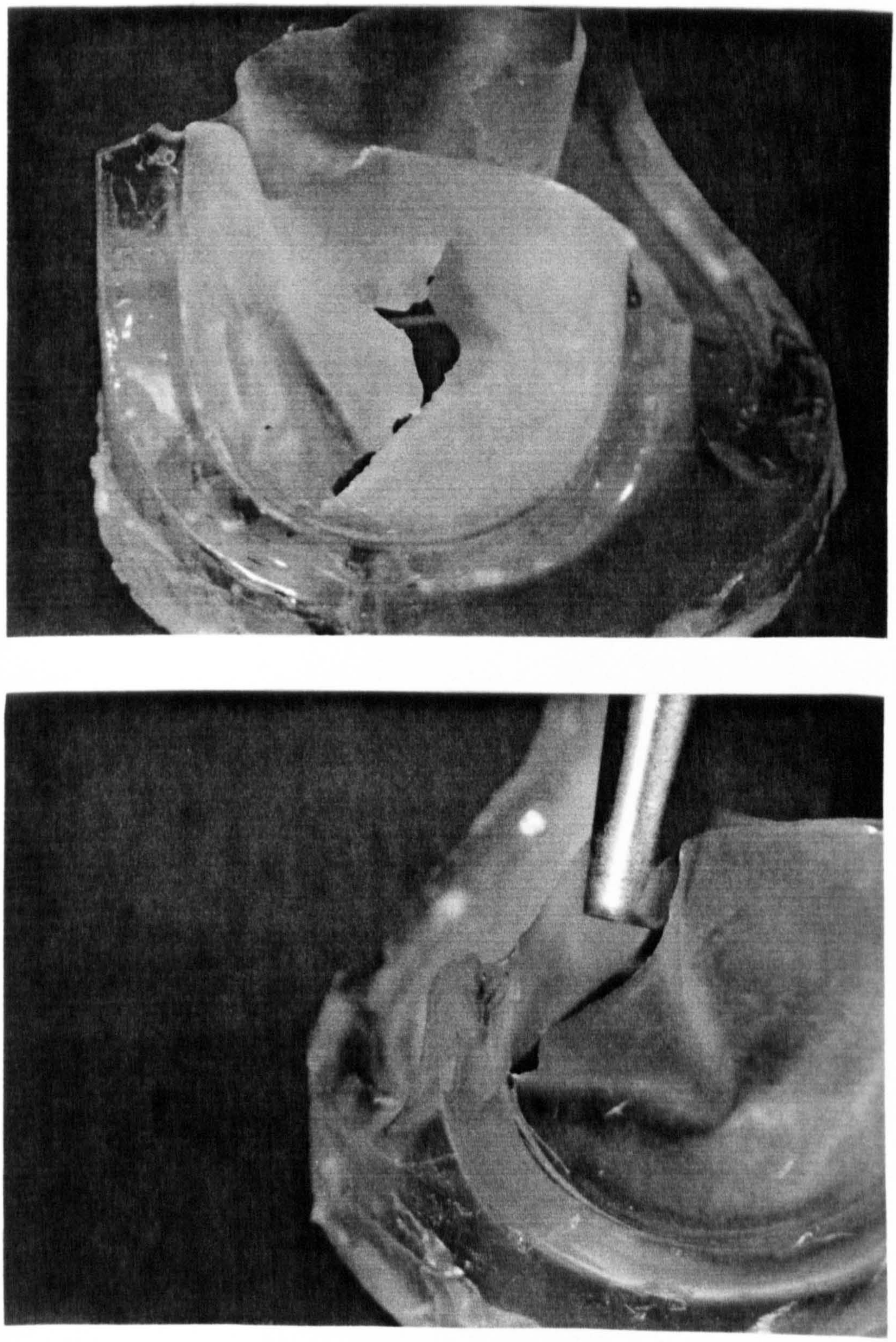

Figure 9.20 Two failed dip moulded valves from accelerated fatigue tester (after 65 x $10^6$ cycles)

### 9.3.4 Discussion

The considerable machining effort which was required to create the IBM moulding tool has been exploited to produce PU valves with dip moulded leaflets and injection moulded frames. Dip moulding is clearly not as attractive as injection moulding, with particular drawbacks in terms of control and reproducibility. However, functioning dip moulded PU valves can be fabricated with relative ease. The reliability of the dip moulding process, as used here, could perhaps be improved by mechanizing the dipping stage, and by using a custom-designed cutting tool rather than a pair of scissors to trim the frames away from valve mouldings (or, alternatively, injection moulding the fames directly).

Dip moulding provides a means for assessing the valve design in terms of hydrodynamic function and durability, albeit for valves with nonuniform leaflet thicknesses. The hydrodynamic tests demonstrate that the PU valves perform at least as well as other types of prosthetic valve. A concern with the original valve design was that the PU frame might not have been sufficiently strong to support the closed leaflets under back pressure, and it may have been necessary to incorporate a reinforcing insert into the moulded frame. In the event, however, the frames do support the leaflets adequately and none of the leaflets (of any of the dip moulded valves tested) have been observed to prolapse under back pressure. The frames do bend inwards under back pressure, to a greater extent than for either the pericardial or porcine valves. This is probably a desirable feature, relieving some stress from the leaflets, provided, of course, that it does not lead to the frames creeping and sustaining some permanent deformation.

The hydrodynamic data in isolation are a little ambiguous, since a PU valve can be made which functions

exceedingly well in the pulse duplicator simply by incorporating very thin leaflets. For example, in figure 9.14, the PU valve with thinner, more flexible leaflets (PU1), has a considerably greater EOA. However, the leaflet thickness should be such that the valve is sufficiently durable, but unfortunately the necessary information will not be available until the accelerated fatigue tests have been completed. It is likely that a PU leaflet thickness in the range 100 - 150 $\mu$m will be required (i.e. closer to PU2 rather than PU1) in order to achieve a durability comparable to that of bioprosthetic valves. In accelerated fatigue tests, 4 dip moulded valves have successfully completed over 80 million cycles, and 2 valves, which had thinner leaflets than the others, failed after 65 million cycles. For comparison, in a study of 27 and 29 mm Glasgow pericardial valves, carried out in the same fatigue tester, Fisher & Wheatley (1987) found that 8 out of 9 valves survived intact after completing more than 400 million cycles. Whether the PU valves can match the durability of the pericardial valves remains to be shown. Notice, however, that for valves to be incorporated into blood pump devices intended for short-term use, the 80 million cycles survival (2 years equivalent) achieved so far by the dip moulded valves may well be more than adequate.

The difference that the extra coaptational area makes to valve durability remains to be seen, as the valves in figures 9.18 & 9.19 have both survived unscathed after the same number of cycles. This point is of particular interest given that the finite element stress analyses of Christie & Stephenson (1990b) suggests that having an angled leaflet free edge in the manner of PU2 (fig 9.18), rather than a flat free edge as in the valve shown in figure 9.19, may result in reduced stress concentrations at the commissures, while others have claimed that increasing the overall leaflet height may also help to reduce stresses at the commissures (Hamid *et*

*al*; 1986; Rousseau *et al*, 1988; Chandran *et al*, 1991). However, even after the accelerated fatigue tests have been completed and assuming one valve fails before the other, it may be difficult to make a definitive statement on the effect the additional leaflet material has on valve durability as the leaflet thickness distribution is slightly different for each. This same problem also applies when investigating the consequences of design modifications on hydrodynamic performance: each dip moulded valve has a slightly (or considerably) different leaflet thickness distribution. To resolve this problem, the dependency of valve function and durability upon leaflet thickness distribution needs to be quantified by testing a large number of valves, and/or a more reliable means of dip moulding needs to be found.

In conclusion, dip moulded PU valves have been produced which function well and can survive at least 2 years equivalent cycling. The means of valve manufacture is not ideal but there is scope for improvement. The dip moulded valves provide a means for assessing the valve design and design modifications, and they may even be useful as valves in their own right. Indeed, these valves are presently being used in a concurrent study into PU valve calcification (Fisher *et al*, 1992).

# Chapter 10. Mathematical Modelling of the Injection Moulding Process

## 10.1 Introduction

The intimately related fluid mechanical and heat transfer processes associated with injection moulding are amenable to numerical analysis. Recent interest in this field has been fuelled by the increasing use of injection moulding in industry, combined with the ever increasing availability of computing resources. As a result, more and more complex parts are being successfully moulded with the minimum of moulding experimentation or tool modifications. At present, there are several software packages commercially available which model various aspects of the injection moulding process, with varying degrees of sophistication. One such package has been used to investigate the filling stage of the moulding cycle with the IBM moulding tool.

The theory behind mathematical models of injection moulding is considered in section 10.2. One of the principal difficulties encountered in solving the appropriate momentum and heat transfer equations lies in the shear rate and temperature dependency of the polymer melt viscosity, which couples the 2 sets of equations together. Section 10.3 describes the method which was used to measure the viscosity of molten PU as a function of temperature and shear rate. The remainder of this chapter is concerned with details of the actual model used and the presentation and discussion of results obtained. The prediction of this study is that it should indeed be possible to mould a PU valve with sufficiently thin leaflets, within the range of available processing conditions (injection pressure 100 MPa, mould temperature of 90°C, melt temperature of 200°C, and a profiled injection rate), albeit with a gating arrangement rather different to that incorporated in the IBM moulding tool.

The work described in this chapter was carried out using the facilities of the Polymer Technology Group at Napier University, Edinburgh.

## 10.2 Theoretical Considerations

Analytically, the injection moulding process represents a highly complex system: unsteady, non-isothermal flows of compressible, viscoelastic polymer melts through complex flow channels. However, valuable insights into the process may be gained by applying appropriate approximations and idealizations.

After Tadmor & Gogos (1979) and Kamal & Ryan (1989), the 3 transport equations, which are the continuous analogues of the conservation laws for mass, momentum, and energy, form the basis for any analysis. Conservation of mass is expressed in the continuity equation:

$$\partial\rho/\partial t + \mathbf{v}\cdot(\rho\mathbf{v}) = D\rho/Dt + \rho(\mathbf{v}\cdot\mathbf{v}) = 0 \qquad (10.1)$$

where $\rho$ is the density, $\mathbf{v}$ the velocity vector, and $D/Dt$ represents the *substantial* derivative defined by:

$$D/Dt = \partial/\partial t + \mathbf{v}\cdot\mathbf{v} \qquad (10.2)$$

The continuity equation simply states that the rate of mass accumulation within a specified volume is given by the net flux of mass transferred into the volume.

The stress tensor $T$ may be conveniently divided into 2 parts:

$$T = -P\delta + \tau \qquad (10.3)$$

where P is a scalar representing an isotropic normal stress (pressure), $\delta$ the unit tensor, and $\tau$ the *deviatoric* stress tensor. Then, in the absence of body forces such as gravity, the equation of motion becomes:

$$\rho Dv/Dt = -\nabla P + \nabla\cdot\tau \qquad (10.4a)$$

or

$$\rho(\partial v_i/\partial t + v_j \partial v_i/\partial x_j) = -\partial P/\partial x_i + \partial \tau_{ij}/\partial x_j \quad (10.4b)$$

in the summation notation. That is, the rate of change of momentum of a fluid volume, by conduction and convection, equals the sum of the forces acting upon it.

For a fluid with internal energy U per unit mass, conservation of energy leads to:

$$\rho DU/Dt = -(\nabla \cdot \mathbf{q}) - P(\nabla \cdot \mathbf{v}) - (\tau : \nabla \mathbf{v}) \quad (10.5)$$

where $\mathbf{q}$ is the heat flux vector. In words, the rate of gain of internal energy per unit volume ($\rho DU/Dt$) is equal to the rate of internal energy input by conduction per unit volume ($-\nabla \cdot \mathbf{q}$) plus the reversible rate of internal energy increase per unit volume by compression ($-P(\nabla \cdot \mathbf{v})$) plus the irreversible rate of internal energy increase per unit volume by viscous dissipation ($-\tau : \nabla \mathbf{v}$). The irreversible degradation of mechanical to thermal energy represented by:

$$\begin{aligned} \tau : \nabla \mathbf{v} = {} & \tau_{xx}\partial v_x/\partial x + \tau_{yy}\partial v_y/\partial y + \tau_{zz}\partial v_z/\partial z + \\ & \tau_{xy}(\partial v_x/\partial y + \partial v_y/\partial x) + \tau_{yz}(\partial v_y/\partial z + \partial v_z/\partial y) + \\ & \tau_{zx}(\partial u_z/\partial x + \partial v_x/\partial z) \end{aligned} \quad (10.6)$$

which along with the temperature dependency of the melt viscosity, couples the equations of motion and heat transfer together and necessitates their simultaneous solution.

Notice that the energy equation can be expressed more conveniently in terms of temperature T and specific heat at constant volume $C_v$:

$$\rho C_v DT/Dt = -(\nabla \cdot \mathbf{q}) - T(\partial P/\partial T)_\epsilon (\nabla \cdot \mathbf{v}) - (\tau : \nabla \mathbf{v}) \quad (10.7)$$

where $\epsilon$ is the specific volume ($1/\rho$).

Since the equation of motion is a vector equation, the transport equations (10.1, 10.4 & 10.7) constitute 5

equations in terms of 15 unknown functions ($\rho$,v,P,$\tau$,T,q). Clearly, additional *constitutive* equations are needed in order to determine the variables of interest. These may include an equation of state relating the density, pressure and temperature, a rheological constitutive equation relating the stress tensor to the material deformation or rate of deformation, and a thermal constitutive equation relating the heat flux vector to the temperature gradient.

An understanding of the polymer P-$\epsilon$-T behaviour is particularly important when analysing moulding operations in which compressibility and shrinkage effects are significant. A modified Van der Waal's equation has been extensively used as an empirical P-$\epsilon$-T relation for polymer melts:

$$(P + a)(\epsilon - b) = RT/M \qquad (10.8)$$

where R is the universal gas constant, and a, b & M are arbitrary constants. Theoretical equations of state, based on statistical mechanics, have also been developed.

Although a great many rheological constitutive equations have been proposed for polymer melts, only a few have been used in mathematical models of the moulding process. As yet, there is no usable constitutive equation which describes quantitatively all the associated flow phenomena. Consequently, constitutive equations tend to be selected on the basis that they may predict only those aspects of the flow behaviour which are of main interest. Under the assumption of purely viscous behaviour, a frequently used generic relation is that of the *generalized Newtonian fluid* (GNF):

$$\tau = \eta(II_S)\mathbf{s} \qquad (10.9)$$

where the viscosity $\eta(II_S)$ is some function of the $2^{nd}$ scalar invariant of the rate of strain tensor s:

$$\varepsilon_{ij} = (\partial v_i/\partial x_j + \partial v_j/\partial x_i) \qquad (10.10)$$

A variety of relations have been proposed for the function $\cap(II_S)$ to account for the observed non-Newtonian behaviour. A popular GNF model is that of the power law fluid for which:

$$\cap(II_S) = m\,[(\tfrac{1}{2}II_S)^{\frac{1}{2}}]^{n-1} \qquad (10.11)$$

giving

$$\tau = m\,[(\tfrac{1}{2}II_S)^{\frac{1}{2}}]^{n-1}\,\varepsilon \qquad (10.12)$$

where the consistency index m and power law index n are independent of the rate of strain. In the case of simple shear flows:

$$\varepsilon = S\begin{bmatrix} 0 & 1 & 0 \\ 1 & 0 & 0 \\ 0 & 0 & 0 \end{bmatrix} \qquad (10.13)$$

and:

$$II_S = \varepsilon:\varepsilon = \varepsilon_{ij}\varepsilon_{ij} = 2S^2 \qquad (10.14)$$

where S is the shear rate ($= |\varepsilon_{21}| = \partial v_y/\partial x$). The power law relation then simplifies to:

$$\tau = m(S^{n-1})\varepsilon \qquad (10.15)$$

with

$$\cap = mS^{n-1} \qquad (10.16)$$

The consistency index is generally taken to be exponentially dependent upon the temperature and hydrostatic pressure:

$$m = m_o \exp[a(T_o-T)] \exp[b(P-P_o)] \qquad (10.17)$$

with a & b constants.

The principal limitation of the power law model is

that it overestimates the viscosity at low shear rates: polymer melts exhibit near Newtonian behaviour as S approaches zero (i.e. the power law index should correspondingly tend to unity). However, the algebraic simplicity of the model, combined with its predictive capabilities, have resulted in the power law fluid being one of the most widely used representations.

Fourier's law of heat conduction is generally taken to be an appropriate thermal constitutive equation:

$$\mathbf{q} = -k\,\nabla T \qquad (10.18)$$

The thermal conductivity k of polymer melts is only a weak function of temperature and molecular weight, and varies little from polymer to polymer.

In addition to the transport and constitutive equations, a number of simplifying assumptions are made. For example, a thin film approximation (lubrication approximation) is often introduced. In this case, inertial forces are taken to be negligible as compared with viscous shear forces, any motion of the melt normal to the plane of the film is neglected (i.e. only 2 non-zero velocity components), and convective rather than conductive heat flow dominates in the direction of the non-zero velocity components.

## 10.3 Polymer Melt Rheology

The rheological behaviour of polymer melts in simple flow situations can be characterised by measurable material functions, such as viscosity, which can then be used to relate the stress to the rate of deformation for more general computational purposes. Such material functions also provide a means for classifying and comparing melts.

The mathematical model, which was used to simulate the injection moulding of a PU valve, required viscosity

data as input. The melt viscosity was needed over the range of shear rates and temperatures encountered in the moulding process. Viscosity data was not available from the PU manufacturer and was measured using a capillary viscometer at Napier University. This section comprises a description of the viscometry technique and the presentation of measured data.

### 10.3.1 Capillary flow viscometry

Capillary flow viscometry is based upon steady, laminar flow down the axis of long tube, as shown schematically in figure 10.1. Flow is assumed to be angularly symmetrical ($v_\theta=0$, $\partial/\partial\theta=0$), with no radially directed flow ($v_r=0$), and with the axial velocity component independent of axial position ($\partial v_z/\partial z=0$). Following the derivation of Tadmor & Gogos (1979), the equations of motion, in cylindrical coordinates, then take the form:

$$\partial P/\partial r = 0 \qquad (10.19a)$$

$$\partial P/\partial \theta = 0 \qquad (10.19b)$$

$$\partial P/\partial z = 1/r[\partial/\partial r(r\tau_{rz})] \qquad (10.19c)$$

The left-hand side of equation (10.19c) is a function of z only, whereas the right-hand side is a function of r only. Thus:

$$P = A_1 z + A_2 \qquad (10.20)$$

with $A_1$ and $A_2$ constants. Taking the boundary conditions $P = P_o$ at $z = 0$ and $P = P_L$ at $z = L$, gives $A_1 = (P_L-P_o)/L$; substituting into equation (10.19c) and integrating yields:

$$\tau_{rz} = \tfrac{1}{2}r(P_o - P_L)/L + C/r \qquad (10.21)$$

Figure 10.1 Capillary flow

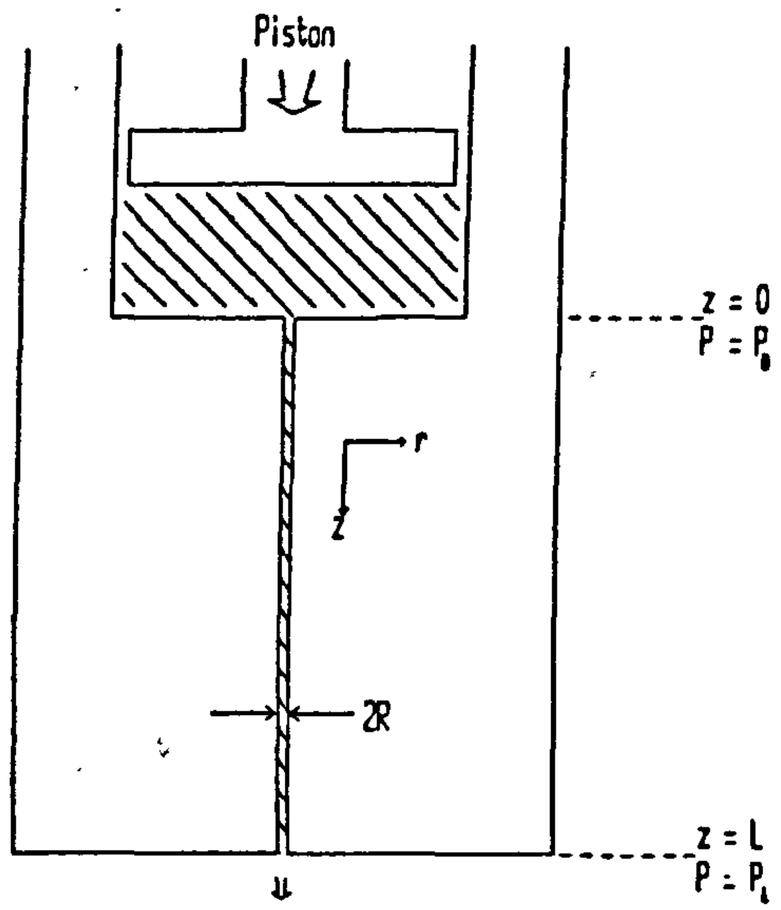


Figure 10.2 Schematic capillary viscometer

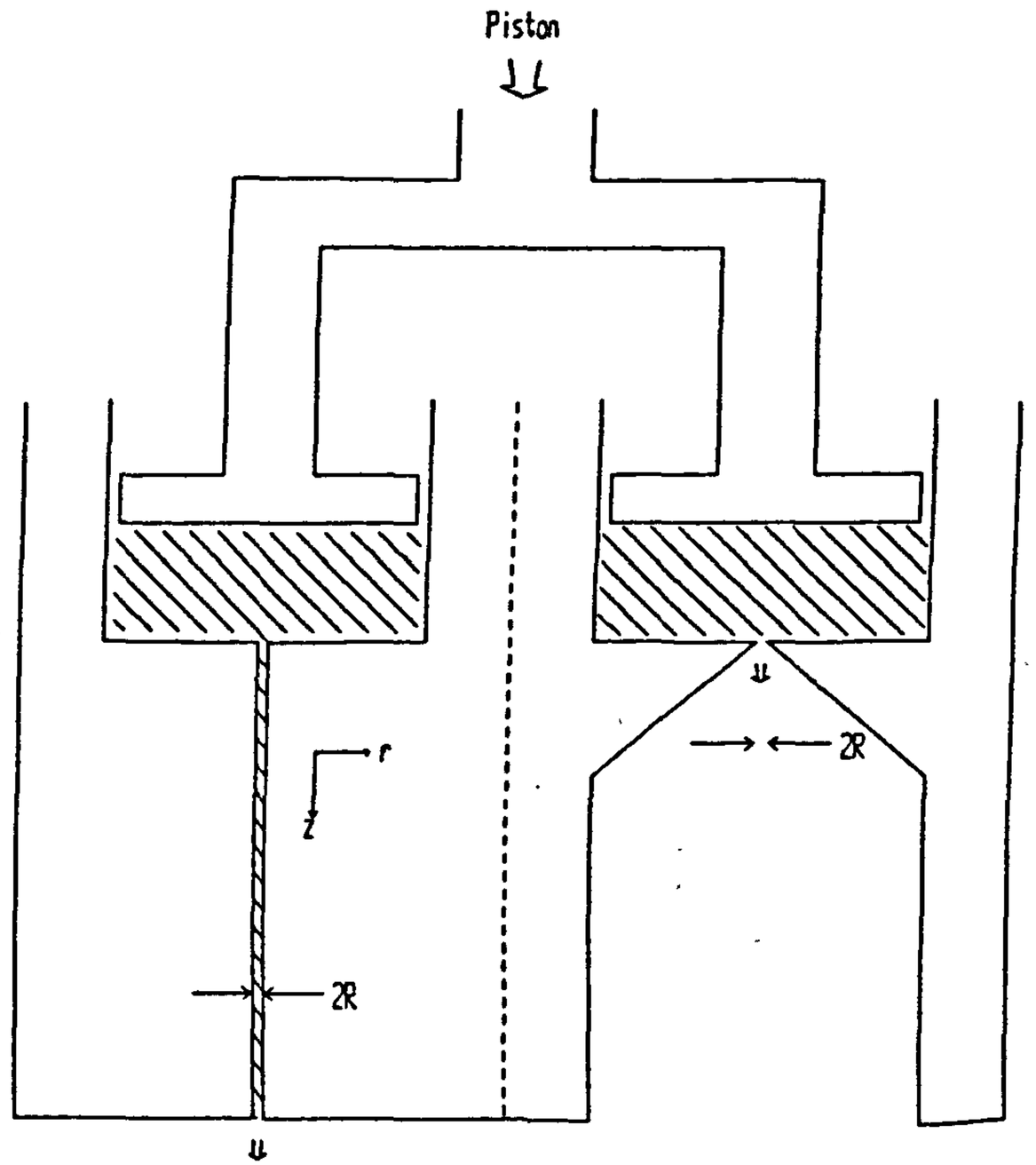

where the integration constant C must be zero to prevent an infinity at r = 0. Thus, the shear stress at the wall (r = R) can be experimentally evaluated by measuring L, R and $P_o$-$P_L$:

$$\tau_w = \tfrac{1}{2}R(P_o - P_L)/L \qquad (10.22)$$

Consider now the volumetric flow rate Q which may be expressed as:

$$Q = \int_0^R 2\pi r v_z(r)\, dr \qquad (10.23)$$

Integrating by parts, and assuming no slip at the wall ($v_z(R) = 0$):

$$Q = -\pi \int_0^R r^2 (dv_z/dr)\, dr \qquad (10.24)$$

From equations (10.21 & 10.22), $r = \tau_{rz}R/\tau_w$ which can be used to change the integration variable:

$$Q = -\pi R^3/\tau_w{}^3 \int_0^{\tau_w} (dv_z/dr)\tau^2_{rz}\, d\tau_{rz} \qquad (10.25)$$

Differentiating with respect to $\tau_w$ using Leibnitz's rule gives:

$$\tau^2_w/\pi R^3\ [\tau_w(dQ/d\tau_w) + 3Q] = -(dv_z/dr)_{r=R}\tau^2_w \qquad (10.26)$$

where $-(dv_z/dr)_{r=R}$ is the shear rate at the wall $S_w$. Finally, with equation (10.22), equation (10.26) may be re-written in terms of $P_o$-$P_L$ as:

$$S_w = 1/\pi R^3\ [3Q + (P_o\text{-}P_L)\ dQ/d(P_o\text{-}P_L)] \qquad (10.27)$$

Thus, equation (10.27), known as the *Rabinowitsch equation*, can be used to infer the shear rate at the wall from measured values of Q and $P_o$-$P_L$.

Therefore, from equations (10.22 & 10.27), the coefficient of viscosity, which is defined as the ratio of shear stress to shear rate for simple shear flow, and the exponent and consistency index for a power law fluid (eqn 10.15), can be experimentally evaluated.

In practice, the pressure drop $P_o$-$P_L$ is usually measured with a transducer in the wall of the reservoir above the capillary tube, with the bottom of the capillary tube open to atmospheric pressure (fig 10.1). However, the assumptions made in deriving equations (10.22 & 10.27) are not valid near the ends of the capillary tube. Selecting a capillary tube with a large length to diameter ratio helps to minimize end effects. The pressure drop due to entrance effects can be measured directly by using a second, exceedingly short, die in parallel with the first, such that the melt flows through the 2 dies at the same rate (fig 10.2). The entrance pressure drop measured across the short die can then be subtracted from that measured across the long capillary tube to give the true, fully developed flow, pressure drop $P_o$-$P_L$ (*Bagley* correction).

A second difficulty arises from viscous heating, particularly at high shear rates. A well thermostated, small diameter capillary tube helps to alleviate this problem. Viscosity measurements at high shear rates are also limited by the phenomenon of *melt fracture*: there is a critical shear stress (of the order $10^5$ $Nm^{-2}$) above which the emerging extrudate exhibits irregular distortion and slip-stick flow may occur (Tadmor & Gogos, 1979).

## 10.3.2 Measurement of polyurethane viscosity

The viscosity of molten PU was measured with a Rosand Capillary Rheometer (RH7-2C). The machine is of the type shown schematically in figure 10.2, incorporating 2 capillary dies with the very short die

used to measure the entrance pressure drop. Both dies are of 1 mm diameter and the long die length is 16 mm; the die entry angle is 180° for both. The rheometer is interfaced to a personal computer which both controls the piston movements and monitors the transducer signals. From the measured pressures and piston speeds, the computer software calculates shear stresses, shear rates and viscosities, applying equations (10.22 & 10.27) and the Bagley correction, and plots appropriate graphs.

The operational procedure was to hold the temperature of the capillary dies constant while the piston speed was stepped either up or down. Immediately after the piston speed had been changed, a short period of time elapsed before steady state conditions were again established and measurements could be made. Once a constant pressure signal was received, a maximum of 50 pressure points were sampled before going onto the next piston speed setting. The piston speed running schedule used for measuring the PU viscosity was programmed to be: 200, 100, 50, 20, 10, 5, 10, 20, 50, 100, 200 mm per minute. Measurements were made sequentially at each of these speeds in a single run (i.e. while the reservoir above the capillaries went from full to empty). This procedure was carried out at 4 capillary temperatures: 170, 180, 190 and 200°C. The PU used was Estane 58315.

The calculated shear stresses and viscosities are plotted on log-log graphs against shear rate in figures 10.3 & 10.4 respectively. Note the near power law behaviour and the slight tendency of the viscosity graphs to flatten out at low shear rates.

Irreversible effects associated with the melt processing, or a sensitivity to flow-history, may be revealed by comparing the data measured as the piston speed was stepped down with that measured as the piston speed was stepped up. Figure 10.5 shows the pressure traces recorded throughout the 200°C run. The slight differences in the 2 halves of the graphs may perhaps be

Figure 10.3 Shear stress versus shear rate for Estane 58315

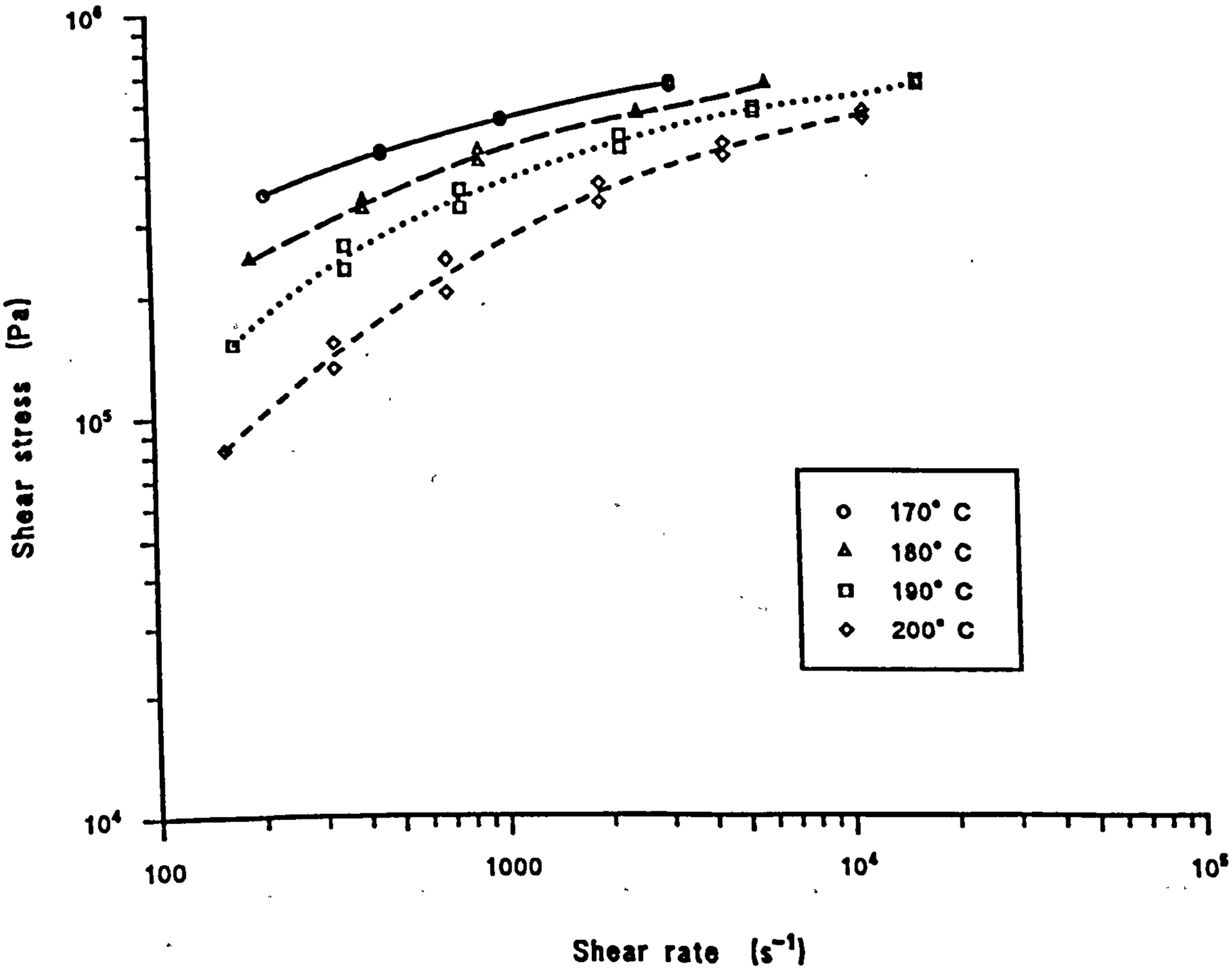

Figure 10.4 Viscosity versus shear rate for Estane 58315

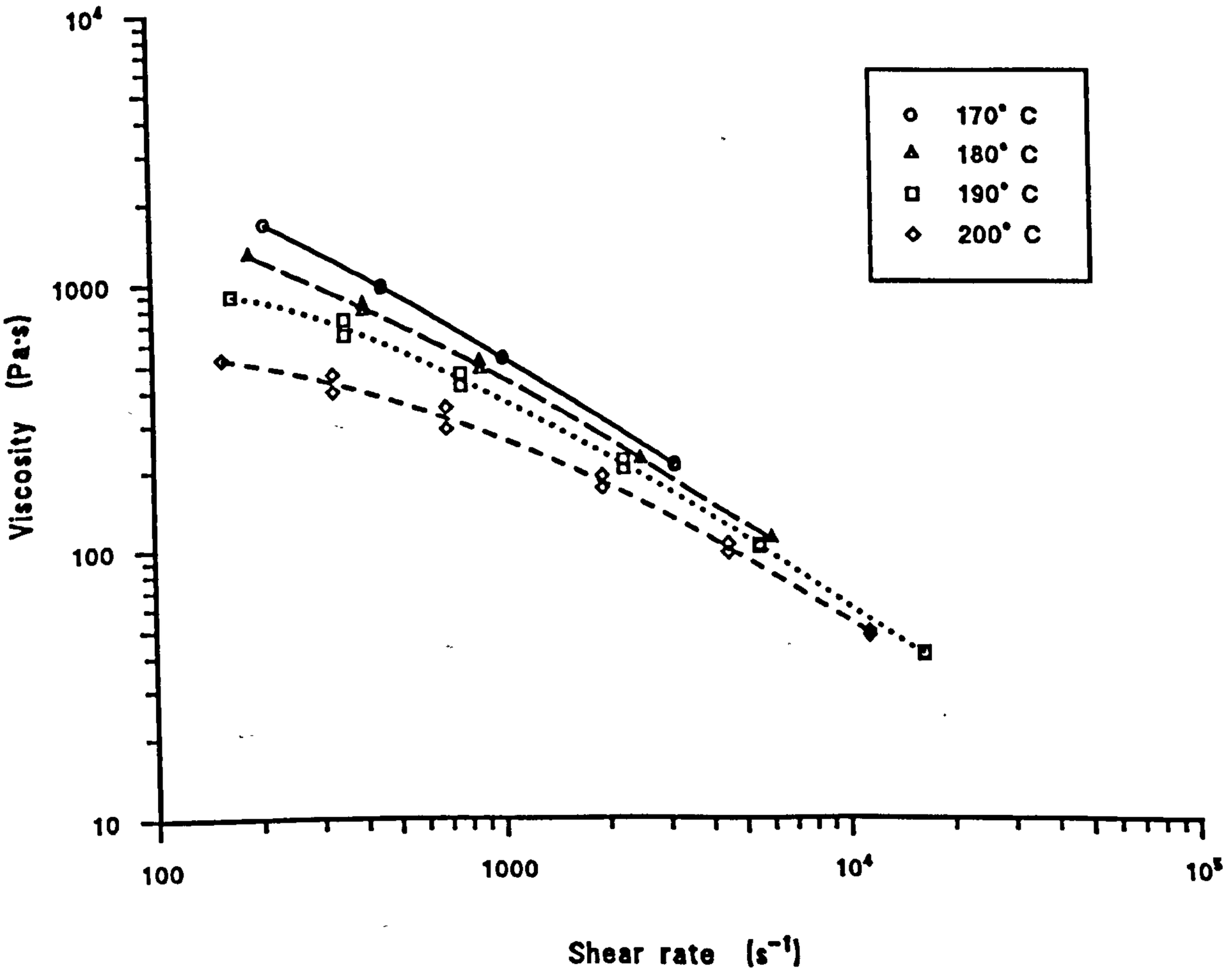

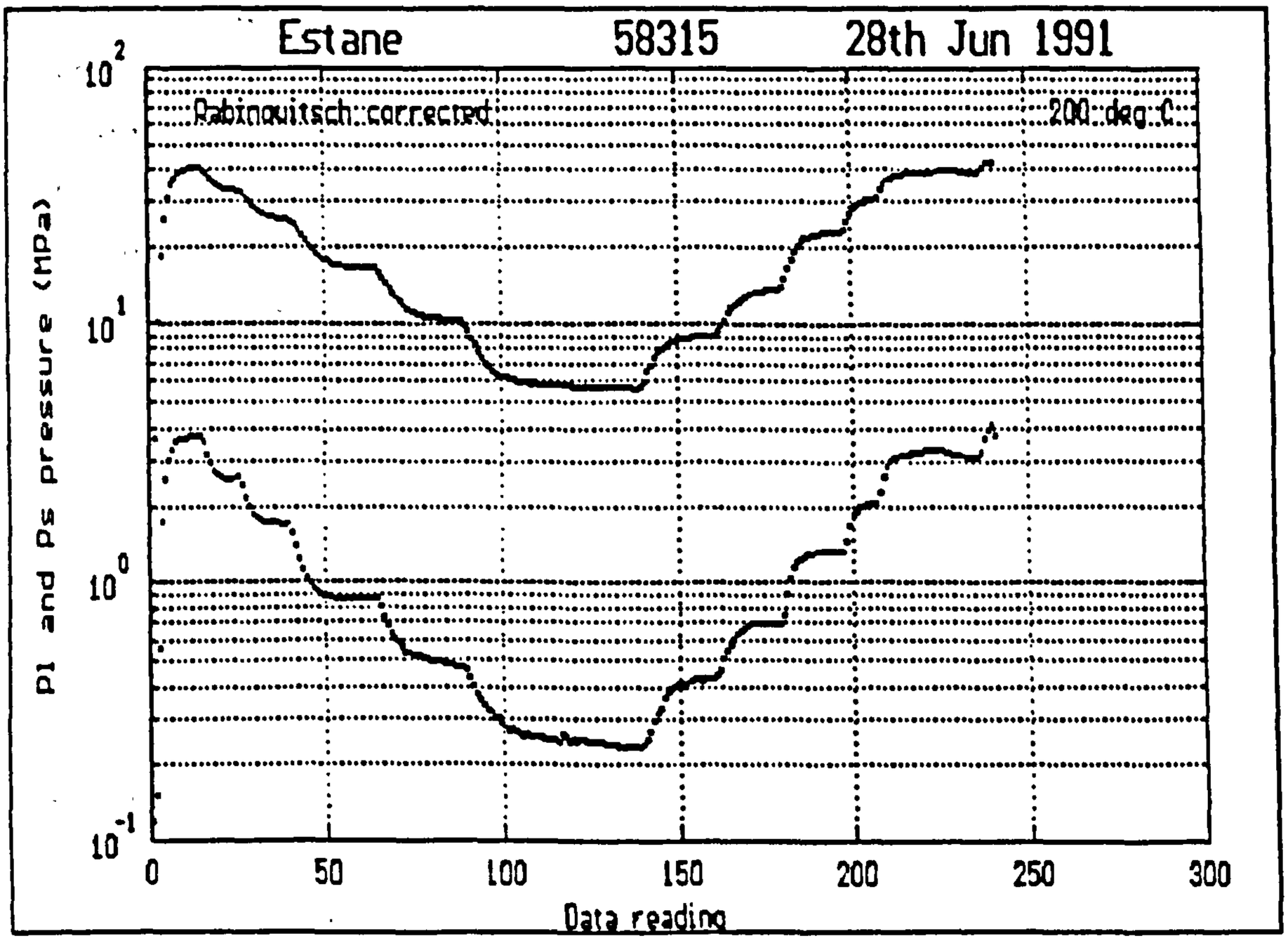


**Figure 10.5 Pressure traces from capillary rheometer**

(The lower trace, $P_S$, is a tracing of the pressure above the very short die, while the upper trace, $P_L$, is a tracing of the pressure above the long capillary die).

related to thermal degradation, shear-induced molecular re-arrangements, or diffusion of lubricants in the melt. The viscosities measured as the piston speed was stepped down were preferred for the mathematical model, as the associated flow and thermal histories were probably closer to those experienced in the injection moulding process. However, as figures 10.3 & 10.4 demonstrate, the differences were generally very small.

## 10.4 The Mathematical Model: MOLDFLOW

A commercially-available software package, MOLDFLOW (Moldflow (Europe) Ltd), has been used to simulate the filling stage of the moulding cycle with the IBM moulding tool. The aim was to explore the possibilities of moulding a PU valve: could a valve with 0.15 mm leaflets actually be moulded at all with the IBM tool, if so what were the optimum moulding conditions, and if not could the tool be modified in such a way to allow the part to be moulded?

### 10.4.1 Overview

'MOLDFLOW' is actually a suite of computer programs which model various aspects of the moulding process; the particular program used here to investigate the filling operation is called MFLP 1.5.6. In general terms, the program is required to solve the coupled equations of motion and energy conservation described in section 10.2, given the moulding tool geometry and the material properties of the PU and mould, and for a specified set of initial operating conditions. The solutions are computed using a combination of finite element and finite difference methods. The program has been developed iteratively: initial predictions were compared with experimental observations and the model subsequently modified to give a better prediction, and so on.

Consequently, the modelling may be described as semi-empirical rather than strictly theoretical, with the justification for this approach being that MOLDFLOW has been found to give quantitatively accurate predictions over a wide range of injection moulding applications. The solutions computed by the modeller can be checked by a variety of means (Tadmor & Gogos, 1979): using transparent moulds combined with flow visualization or flow birefringence measurements (banding observed in polarized light related to stress field); using moulds incorporating thermocouples and pressure transducers; filling patterns can readily be investigated by injecting a series of short shots (i.e. injecting only enough material to partially fill the cavity).

### 10.4.2 Model geometry

The valve geometry adopted was approximately that incorporated in the IBM moulding tool (see eqn (9.1) & table 9.1). In order to minimize computation times, and because of the valve symmetry, only 1/6 of the valve was considered: half a leaflet and the corresponding portion of frame. As will be discussed in section 10.5, 2 valve geometries were used. The first (HV1), which is illustrated in figure 10.6, is described by 27 planar surfaces, which are in turn defined by 44 points digitized from the CAD representation of the valve. A thickness of 0.15 mm was attributed to each of the 16 leaflet plates, while the 11 frame plates were specified as being 3.0 mm thick. For the second valve geometry (HV2), a region of intermediate thickness (0.5 mm) was introduced at the leaflet-frame junction, as shown in figure 10.7. This blending region was not incorporated into the actual moulding tool, but it was thought that such a zone may encourage melt flow into the leaflet areas (and also assist valve function and durability). A

Consequently, the modelling may be described as semi-empirical rather than strictly theoretical, with the justification for this approach being that MOLDFLOW has been found to give quantitatively accurate predictions over a wide range of injection moulding applications. The solutions computed by the modeller can be checked by a variety of means (Tadmor & Gogos, 1979): using transparent moulds combined with flow visualization or flow birefringence measurements (banding observed in polarized light related to stress field); using moulds incorporating thermocouples and pressure transducers; filling patterns can readily be investigated by injecting a series of short shots (i.e. injecting only enough material to partially fill the cavity).

### 10.4.2 Model geometry

The valve geometry adopted was approximately that incorporated in the IBM moulding tool (see eqn (9.1) & table 9.1). In order to minimize computation times, and because of the valve symmetry, only 1/6 of the valve was considered: half a leaflet and the corresponding portion of frame. As will be discussed in section 10.5, 2 valve geometries were used. The first (HV1), which is illustrated in figure 10.6, is described by 27 planar surfaces, which are in turn defined by 44 points digitized from the CAD representation of the valve. A thickness of 0.15 mm was attributed to each of the 16 leaflet plates, while the 11 frame plates were specified as being 3.0 mm thick. For the second valve geometry (HV2), a region of intermediate thickness (0.5 mm) was introduced at the leaflet-frame junction, as shown in figure 10.7. This blending region was not incorporated into the actual moulding tool, but it was thought that such a zone may encourage melt flow into the leaflet areas (and also assist valve function and durability). A

Figure 10.6 MFLP model geometry HV1

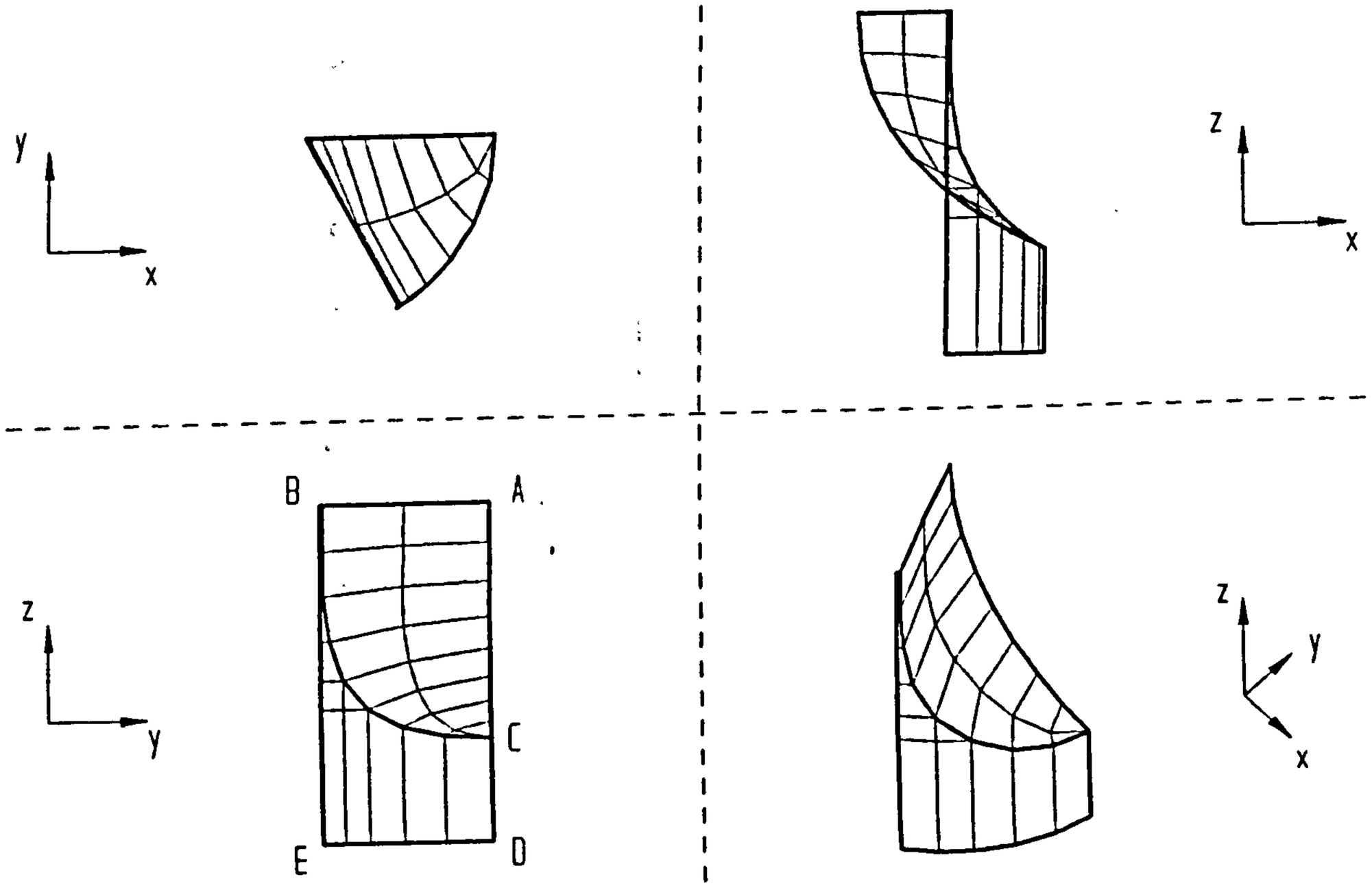

Figure 10.7  MFLP model geometry HV2

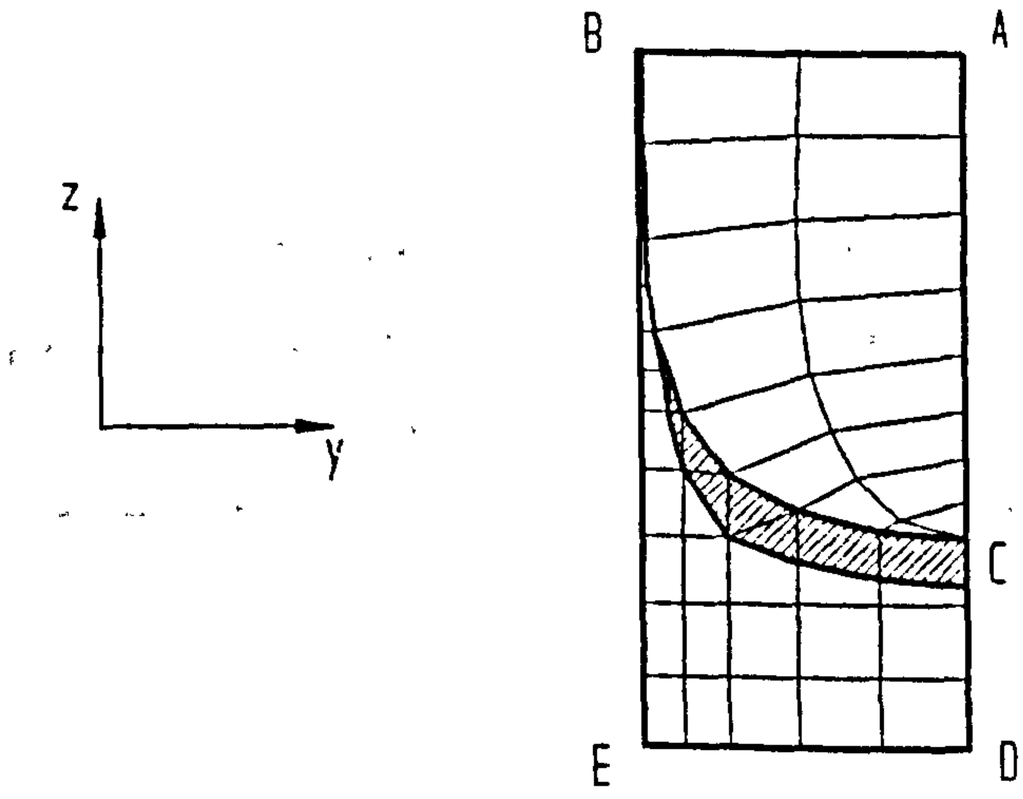

variety of gating configurations were investigated with each valve geometry.

The valve geometries, HV1 and HV2, were meshed before running MFLP. Generally, a mesh of approximately 1000 triangular elements (550 nodes) was selected. Solutions to the equations of motion and energy were computed at each mesh node by the finite element method. Also, at each node point, solutions were calculated at 25 discrete depths (normal to the mesh plane) by the finite difference method. As figure 10.8 shows, 20 lamination layers of uniform thickness were set between the flow mid-plane and the steel mould wall, and a further 5 layers, each 48 times thicker than those in the cavity, were set in the mould wall. Thus, in the leaflet region where the mould cavity is 0.15 mm thick, the bottom of the $25^{th}$ lamination lies at a depth of 0.9 mm into the steel, whereas for the frame region (3.0 mm thick) it lies 18.0 mm from the cavity wall. When running MFLP, a single mould temperature $T_o$ is specified and the entire mould is assumed to be at this temperature prior to the melt being injected. Once the hot melt starts to flow into the cavity, heat is conducted into the walls and the mould temperature rises. However, MFLP assumes that throughout the complete filling process the temperature at the bottom of the $25^{th}$ lamination remains constant at $T_o$ (i.e. beyond the $25^{th}$ layer there is an infinite heat source).

### 10.4.3 Input

In addition to a description of the mould geometry, the material properties of the PU and steel mould, and the injection moulding operating conditions, have to be specified.

The measurement of PU viscosity for a range of temperatures and shear rates was described in the previous section (fig 10.4). MFLP models the PU melt as a

Figure 10.8 MFLP solutions calculated at 25 discrete depths

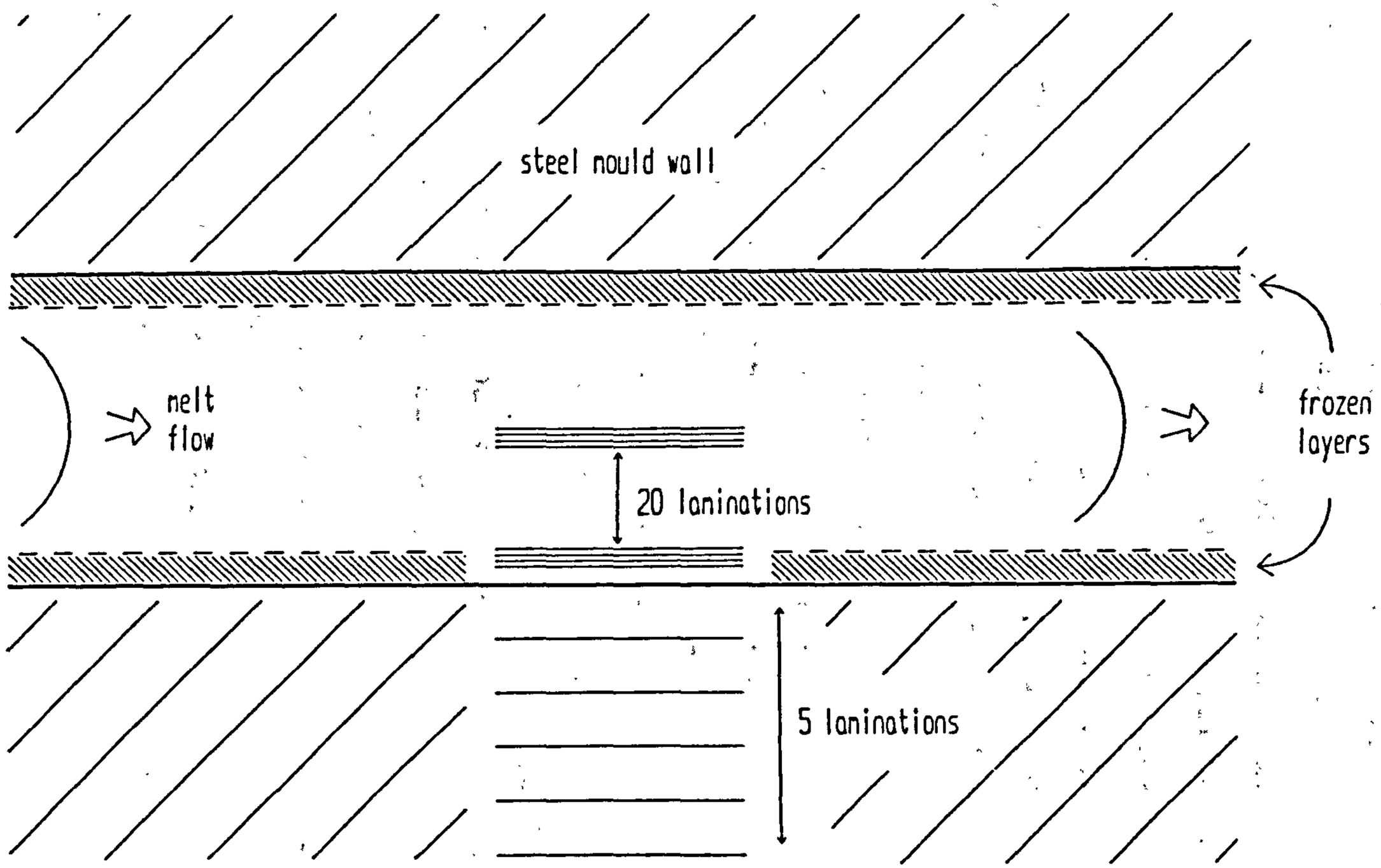

power law fluid, using one of 2 relations for the viscosity function. Either a so-called 1st order relation:

$$\cap = a\ S^b \exp[cT] \qquad (10.28)$$

or a more general 2nd order relation:

$$\log_e(\cap) = A_1 + A_2\log_e(S) + A_3T + A_4[\log_e(S)]^2 + A_5T\log_e(S) + A_6T^2 \qquad (10.29)$$

where a, b, c and $A_{1->6}$ are constants.

A curve fitting program within MOLDFLOW, called VISDAT 1.3, was used to apply both of these functions to the measured viscosity data, and the constants were evaluated for the best fits. The results are displayed in tables 10.1 and 10.2 for the 1st and 2nd order relations respectively. Comparing the measured viscosities with those calculated using either equation (10.28) or (10.29), the 2nd order relation clearly provides a more representative description of the true rheological properties. Consequently, the 2nd order relation, with the constants listed in table 10.2, was selected for the MFLP runs described in the following results section. (In fact, it was discovered that using the 1st order relation gave rise to very similar MOLDFLOW predictions, with reduced computation times.)

The physical properties of the PU and steel mould, as used in MFLP, are listed in table 10.3. The thermal conductivity of PU was not available from the manufacturer: the value quoted in table 10.3 is actually a mid-range value for polymer melts. As was mentioned earlier, thermal conductivities vary little from polymer to polymer. A volume compressibility of 10% at 100 MPa was assumed for molten PU; again this information was not available from the manufacturer and 10% is a typical value. The value quoted for melt density (952 $kg \cdot m^{-3}$) is actually 15% less than the manufacturer's quoted value

Table 10.1 1st order viscosity relation graph fit

| Point number | Temp (°C) | Shear Rate ($s^{-1}$) | Measured $\eta$ (Pa.s) | Calculated $\eta$ (Pa.s) | % error |
|---|---|---|---|---|---|
| 1 | 170 | 3215.0 | 204.9 | 232.5 | 11.9 |
| 2 | 170 | 1035.0 | 530.2 | 520.7 | -1.8 |
| 3 | 170 | 463.6 | 979.5 | 922.0 | -6.2 |
| 4 | 170 | 213.2 | 1655.0 | 1602.2 | -3.3 |
| 5 | 180 | 6070.0 | 109.3 | 119.0 | 8.1 |
| 6 | 180 | 2569.0 | 219.2 | 219.3 | 0.0 |
| 7 | 180 | 886.9 | 507.9 | 467.3 | -9.1 |
| 8 | 180 | 409.4 | 829.8 | 810.0 | -2.4 |
| 9 | 180 | 192.3 | 1275.0 | 1386.6 | 8.0 |
| 10 | 190 | 16525.0 | 41.1 | 46.9 | 12.4 |
| 11 | 190 | 5603.0 | 104.0 | 101.3 | -2.7 |
| 12 | 190 | 2287.0 | 216.7 | 191.6 | -13.1 |
| 13 | 190 | 780.8 | 462.4 | 411.5 | -12.4 |
| 14 | 190 | 360.8 | 732.5 | 712.6 | -2.8 |
| 15 | 200 | 11556.0 | 49.4 | 48.7 | -1.6 |
| 16 | 200 | 4553.0 | 104.2 | 94.4 | -10.4 |
| 17 | 200 | 1980.0 | 188.5 | 170.7 | -10.4 |
| 18 | 200 | 705.1 | 346.9 | 355.8 | 2.5 |
| 19 | 200 | 332.0 | 460.8 | 608.0 | 24.2 |

mean |%error| = 7.5%

Coefficients for $\eta = aS^b \exp[cT]$ :

$a = 2.95472 \times 10^6$ ($Pa.s^{b+1}$)
$b = -7.11431 \times 10^{-1}$
$c = -2.17937 \times 10^{-2}$ ($°C^{-1}$)

Table 10.2 2nd order viscosity relation graph fit

| Point number | Temp (°C) | Shear Rate ($s^{-1}$) | Measured ∩ (Pa.s) | Calculated ∩ (Pa.s) | % error |
|---|---|---|---|---|---|
| 1 | 170 | 3215.0 | 204.9 | 201.3 | -1.8 |
| 2 | 170 | 1035.0 | 530.2 | 534.0 | 0.7 |
| 3 | 170 | 463.6 | 979.5 | 973.3 | -0.6 |
| 4 | 170 | 213.2 | 1655.0 | 1618.8 | -2.2 |
| 5 | 180 | 6070.0 | 109.3 | 108.4 | -0.9 |
| 6 | 180 | 2569.0 | 219.2 | 229.9 | 4.6 |
| 7 | 180 | 886.9 | 507.9 | 517.0 | 1.4 |
| 8 | 180 | 409.4 | 829.8 | 857.6 | 3.2 |
| 9 | 180 | 192.3 | 1275.0 | 1314.4 | 3.0 |
| 10 | 190 | 16525.0 | 41.1 | 40.1 | -2.4 |
| 11 | 190 | 5603.0 | 104.0 | 106.4 | 2.3 |
| 12 | 190 | 2287.0 | 216.7 | 215.4 | -0.6 |
| 13 | 190 | 780.8 | 462.4 | 443.2 | -4.3 |
| 14 | 190 | 360.8 | 732.5 | 684.7 | -7.0 |
| 15 | 200 | 11556.0 | 49.4 | 50.1 | 1.3 |
| 16 | 200 | 4553.0 | 104.2 | 104.9 | 0.7 |
| 17 | 200 | 1980.0 | 188.5 | 186.3 | -1.2 |
| 18 | 200 | 705.1 | 346.9 | 339.3 | -2.2 |
| 19 | 200 | 332.0 | 460.8 | 485.6 | 5.1 |

mean |% error| = 2.4 %

Coefficients for:

$$\log_e(\cap) = A_1 + A_2\log_e(S) + A_3T + A_4[\log_e(S)]^2 + A_5T\log_e(S) + A_6T^2$$

$A_1 = 8.3633$
$A_2 = -1.2814$
$A_3 = 7.05171 \times 10^{-2}$
$A_4 = -5.85324 \times 10^{-2}$
$A_5 = 7.64522 \times 10^{-3}$
$A_6 = -3.93664 \times 10^{-4}$

Table 10.3 Physical Properties of Melt and Mould

| | Polyurethane Melt | Steel Mould |
|---|---|---|
| Thermal Conductivity k ($Js^{-1}m^{-1}°C^{-1}$) | 0.14 | 25.0 |
| Specific Heat $C_p$ ($JKg^{-1}°C^{-1}$) | 2200 | 460 |
| Density p ($Kgm^{-3}$) | 952 | 7750 |

Melt freeze-off temperature: 100°C

Melt compressibility: 10% at 100 MPa

for PU at room temperature: a 15% drop in density is typically associated with the polymer transition from solid to pressurized melt. The melt freeze-off temperature was estimated to be 100°C. The model is not sensitively dependent upon this value, since at lower temperatures the extrapolated viscosities are so high that very little flow can occur. Note that PU elastomers do not exhibit a well defined melting point, rather they soften gradually upon heating (Bernacca, 1991).

A melt and mould initial temperature had to be specified (i.e. the temperature of the PU in the barrel and the temperature of the mould prior to injection). The mould temperature at the bottom of the $25^{th}$ lamination is held constant throughout the filling simulation, but elsewhere the processes of conduction, convection and viscous heat generation determine the temperature gradients which evolve as the melt flows into the mould. All of the MFLP results described in the following section were acquired with an initial mould temperature of 90°C and a barrel melt temperature of 200°C.

The final input parameter to be specified relates to how quickly the cavity is to be filled. Either a constant volumetric flow rate is selected, or the flow curve can be profiled by specifying up to 10 discrete flow rates. (The Battenfeld 350 moulding machine, described in the previous chapter, can operate with such a profiled flow curve). Along with the shape of the flow curve, a fill time is specified. However, there is a pressure cap which limits how fast the melt can flow. As shorter fill times are requested, so greater pressures are required to drive the flow (see fig 8.4). Once a maximum pressure has been reached then the flow rate is reduced to maintain a constant pressure. Therefore, if a very short fill time is requested, the actual fill time may be considerably longer due to pressure capping. The pressure cap is set at 500 MPa. In the course of this study various flow curves and fill times were used.

### 10.4.4 Output

Given the boundary conditions, the material properties, and the initial conditions, MFLP computes numerical solutions to the coupled equations of motion and energy. That is, throughout the filling process, the shear rate, shear stress, temperature, pressure, and viscosity are calculated as discrete functions of time and position, with the positions being at each node and for 25 discrete depths per node. Another MOLDFLOW program, called MFVIEW, is used to create appropriate graphic displays of the results which may then be viewed directly or printed out.

Running MOLDFLOW on a 80386-based IBM PC, typical computation times were 6 to 12 hours with several megabytes of results data generated per run, depending on how many intermediate results files were requested and the specified mesh size.

## 10.5 MOLDFLOW Predictions

The starting point for the MOLDFLOW study was the valve geometry HV1, gated at the centre of the free edge (fig 10.6, point A). The immediate aim was to see if the part could be moulded at all with this configuration. Initial trial runs revealed that the principal difficulty lay in getting the PU to flow across the thin leaflet area without freezing off. In the leaflet region, where the surface area to volume ratio is very large, the conduction of heat to the steel walls appeared to far outweigh the viscous heating effect. It became apparent that the best chance of getting the PU to successfully cross the leaflet area lay in specifying as high a temperature as possible for the mould and melt, and setting as large a flow rate as possible. From past experience it was felt that 200°C was the highest barrel

melt temperature that could be safely used without encountering problems with thermal degradation. 90°C was selected as the highest initial mould temperature, bearing in mind that the melt freeze-off temperature was set at 100°C. With these temperature settings, the optimum fill time was sought.

Running MFLP with the mould and melt at 90 and 200°C respectively, and with a requested fill time of 0.3 seconds at a uniform flow rate, resulted in the prediction of a short shot (called run MF1). That is, the PU in the mould cavity has frozen solid with the cavity only partially filled. Figure 10.9 is a time map showing the progressive flow of PU into the mould cavity. The shaded area represents that portion of the cavity which had filled by the time the PU froze. The time taken for the cavity to partially fill was 0.17 seconds. Specifying a longer fill time than 0.3 seconds resulted in even less of the cavity being filled: the melt crosses the leaflet area more slowly, allowing more time for heat conduction to the walls. However, this effect became less marked at higher flow rates and requesting a shorter fill time than 0.3 seconds made little difference to the extent the cavity filled. Furthermore, a 0.3 second fill time is sufficiently small that the pressure cap is reached early on the filling process, so specifying a shorter fill time does not greatly alter the calculated flow.

Referring to figure 10.9, as the melt first enters the cavity it spreads out in an even, radial manner across the leaflet surface. However, when the flow front reaches the frame section at the commissure, the melt encounters a region in which there is much less resistance to flow and so PU preferentially floods down into the frame section while flow in the leaflet area is halted. This process continues until the flow front in the frame eventually freezes (mainly due the heat lost in the leaflet area which had to be crossed before reaching the frame section). Notice that had the flow in the frame

Figure 10.9 Melt distribution in time - MF1

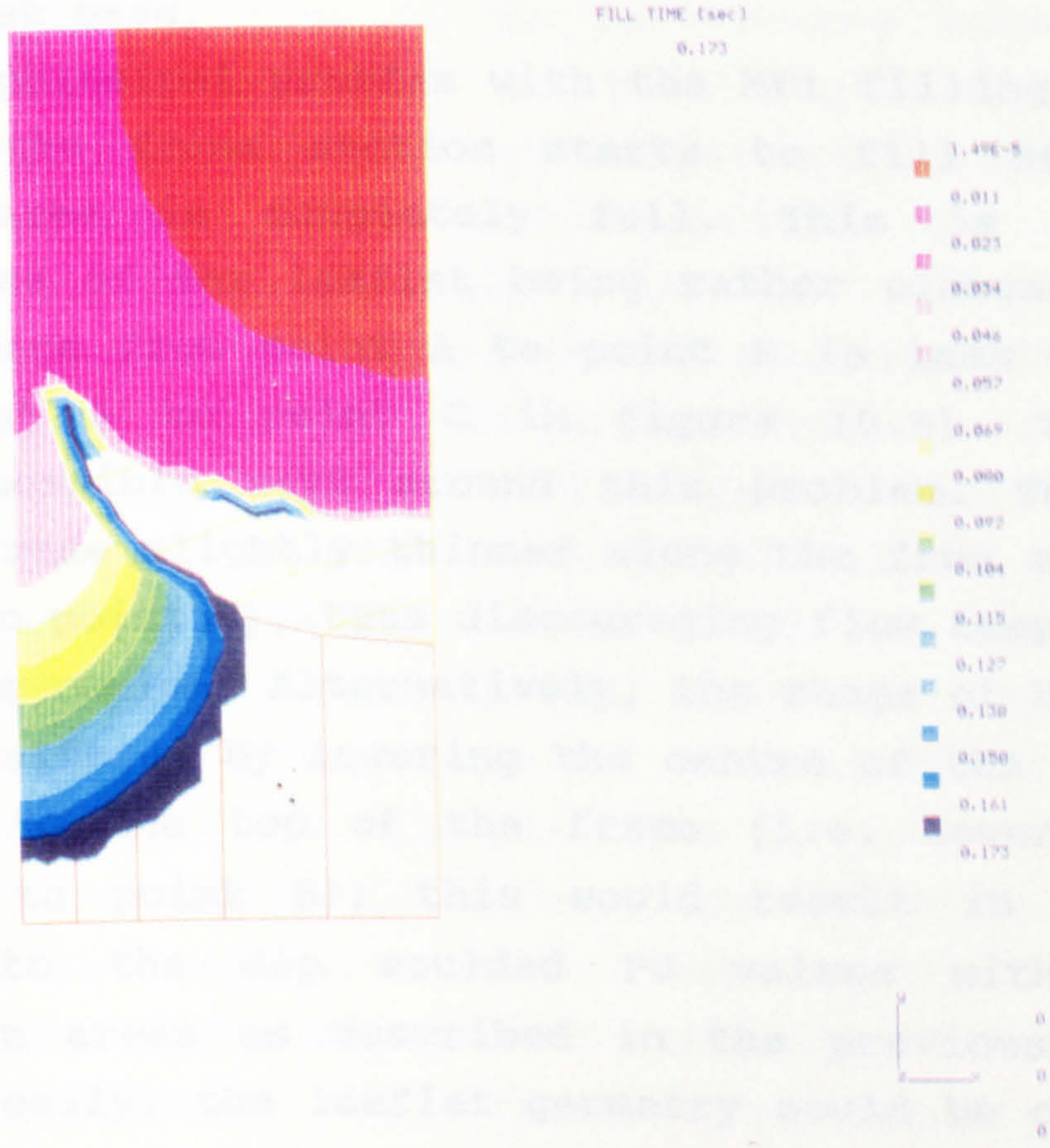


Figure 10.10 Melt distribution in time - MF2

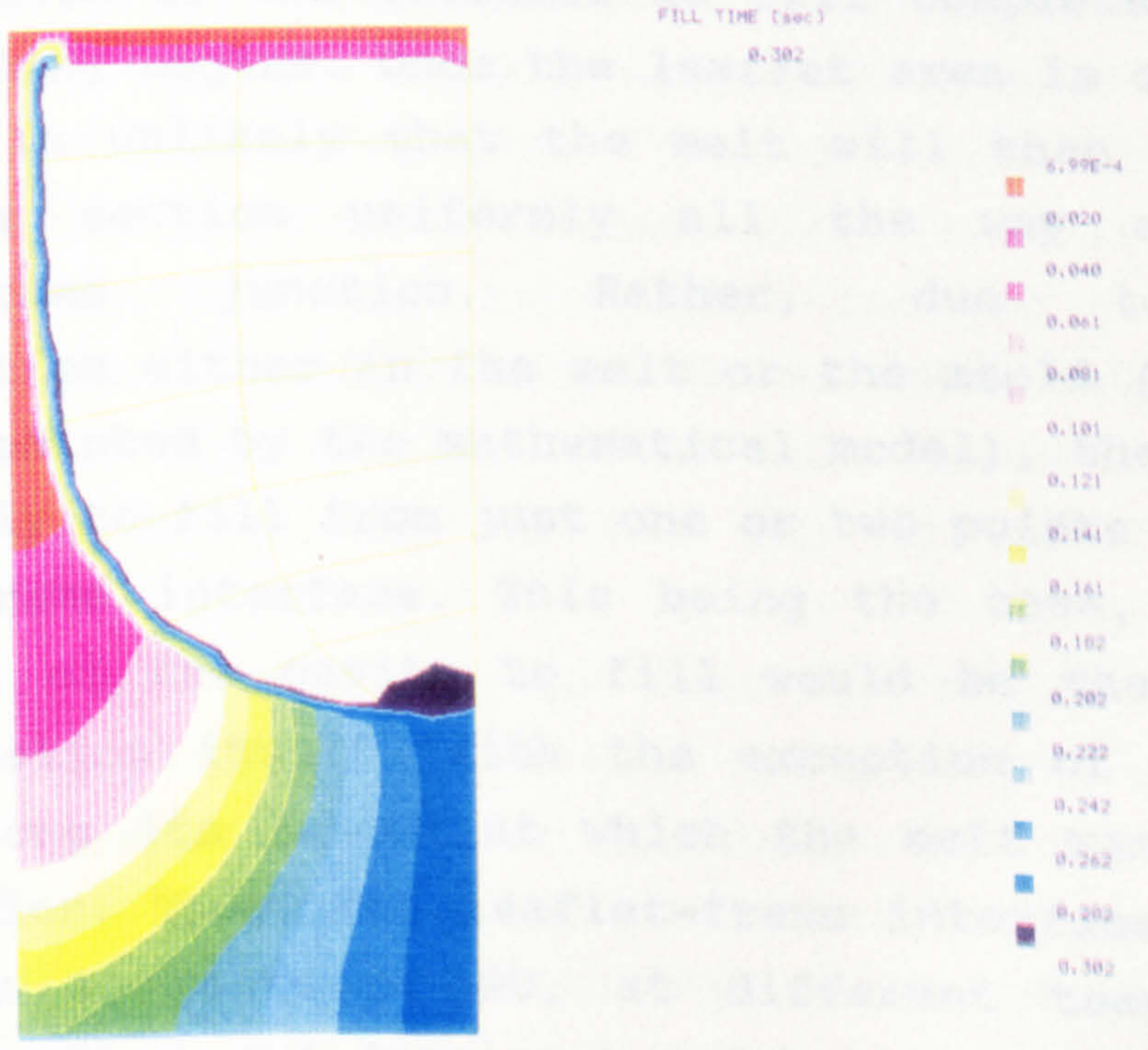

section not frozen off but continued to fill the entire frame and start to fill the leaflet from the bottom upwards, then an undesirable gas trap would be formed in the leaflet base.

The principal problem with the MF1 filling sequence is that the frame section starts to fill before the leaflet area is completely full. This is simply a consequence of the leaflet being rather elongated (i.e. the distance from point A to point B is less than that from point A to point C in figure 10.6). There are several possible ways around this problem. The cavity could be made slightly thinner along the free edge (from point A to point B), thus discouraging flow away from the commissure region. Alternatively, the shape of the cavity could be altered by lowering the centre of the free edge relative to the top of the frame (i.e. lower point A relative to point B); this would result in mouldings similar to the dip moulded PU valves with trimmed coaptation areas as described in the previous chapter. More radically, the leaflet geometry could be changed to a more spherical shape. However, there may well be problems even if the leaflets do fill completely before frame filling begins. Once the leaflet area is completely full, it is unlikely that the melt will then flow into the frame section uniformly all the way along the leaflet-frame junction. Rather, due to local instabilities either in the melt or the mould (which may not be predicted by the mathematical model), the frame is more likely to fill from just one or two points along the leaflet-frame interface. This being the case, then the last part of the cavity to fill would be the leaflet-frame junction itself, with the exception of those few points along its length at which the melt was crossing the junction. Thus, the leaflet-frame interface would be formed by 2 fronts of PU, at different temperatures, coming together and forming a weld line, and perhaps a gas trap. Discontinuities in the polymer structure may be

associated with such weld lines and they may result in areas of local weakness. This is of particular concern given that bending stresses are concentrated along the leaflet-frame junction in the functioning valve, and if the structural integrity of this region were to be compromised then valve failure would rapidly follow.

The gating arrangement selected for run MF1 (centrally gated at point A) is only partially representative of the gating system incorporated into the IBM moulding tool. In the actual tool, the melt is conveyed along a heated runner and enters the tool cavity at the centre of the free edges (point A), but there is a small recess between the free edge of the male pin and the corresponding section on the fixed half of the tool. Molten PU can run along these 3 recesses, above and along the free edges of the male pin (from point A to point B), and thus the cavity is effectively gated all the way along the free edges. However, running MFLP with valve geometry HV1, gated all the way along the free edge (from point A to point B), and under the same conditions as run MF1 (90°C mould, 200°C melt, 0.3 second fill time at uniform flow rate), likewise results in a predicted short shot (called run MF2). The progressive flow of PU, up to the point at which the flow front freezes, is shown in figure 10.10. As with MF1, the frame section fills in preference to the high resistance leaflet areas. Note that the filled leaflet area is so small that a very similar flow distribution would have resulted had the cavity been gated only at the top of the frame post (point B).

It is apparent from the runs MF1 and MF2 that any attempt at moulding a valve with the cavity gated through the thin leaflet area is unlikely to be completely successful. Therefore, alternative gating configurations were considered. The difficulty with introducing the gate(s) into the frame section can be appreciated by studying figure 10.10, as run MF2 was carried out with

the cavity effectively gated through the frame at point B. PU floods down the frame post into the base of the frame with relative ease, in a uniform manner. The plastic which flows to the leaflet-frame border does not cross over into the leaflet area but is halted and cools. Once the frame section has filled and the cavity pressure builds up, PU is forced into the leaflet area at the point where flow resistance is least. As the frame has been filling, the plastic at leaflet-frame junction has been cooling, with the result that in the filled frame there is a temperature gradient running along the length of the leaflet-frame border (i.e. coolest at point B and hottest at point C). Therefore, PU is driven into the leaflet area from the base of the leaflet-frame junction (point C), where the melt is hottest (and so least viscous, and the frozen layer is thinnest). The flow front only manages to penetrate a short distance into the leaflet area before freezing off. The general point to be noted from MF2 is that, when the cavity is gated through the frame, the melt enters the leaflet area from the last point on the leaflet-frame junction to be filled. If the melt enters the leaflet from only one point, then as the leaflet fills there is likely to be a weld line formed along the leaflet-frame interface as PU at 2 different temperatures come together. It is therefore more desirable to have the leaflet filling, not from one point, but uniformly along the entire length of the leaflet-frame margin.

In order to confirm that the leaflet area would indeed fill satisfactorily if the melt was fed in uniformly along the leaflet-frame junction, MFLP was run using only the leaflet area from geometry HV1 (called run MF3). The unaccompanied leaflet was gated along the length of the frame margin (from point B to point C) and a fill time of 0.02 seconds at a constant flow rate was specified. The fill time was selected to give the same volumetric flow rate as in runs MF1 and MF2 (leaflet

volume = 7.5% valve volume). The operating temperatures specified were the same as before. MFLP predicted that the leaflet would indeed fill in a uniform manner. The predicted distribution in time of PU is shown in figure 10.11.

The challenge then was to find a gating arrangement, through the frame, which would result in the melt simultaneously reaching all points along the leaflet-frame junction. The valve geometry HV1 gated along the base of the frame (from point D to point E) was the first configuration to be considered. With the same operating conditions as for MF1 and MF2 (mould 90°C, melt 200°C, 0.3 second fill time at a constant flow rate), MFLP predicted a short shot (called run MF4). The progressive flow of PU into the cavity, up to the time of freezing off, is displayed in figure 10.12. The flow front reaches the base of the leaflet-frame junction before reaching the post section. Consequently, the leaflet area starts to fill near the commissures while flow at the leaflet base has frozen off.

Run MF4 demonstrated that gating valve geometry HV1 along the base of the frame does not result in the flow front arriving simultaneously at all points along the leaflet-frame interface, rather the flow front reaches the leaflet base first. As a means of retarding flow to the leaflet base, the valve geometry HV1 was modified by incorporating a region of intermediate thickness between the frame and leaflet. The intermediate region was tapered such that it was broadest at the leaflet base and ran out towards the frame post (fig 10.7). Running MFLP with this new valve geometry, HV2, with the same gating arrangement and operating conditions as MF4, resulted in a considerably greater proportion of the leaflet area being filled (called run MF5). The PU time distribution, up to the instant at which the flow front froze off, is shown in figure 10.13. Clearly, the introduction of the blending region between the leaflet and frame has been

Figure 10.11 Melt distribution in time - MF3

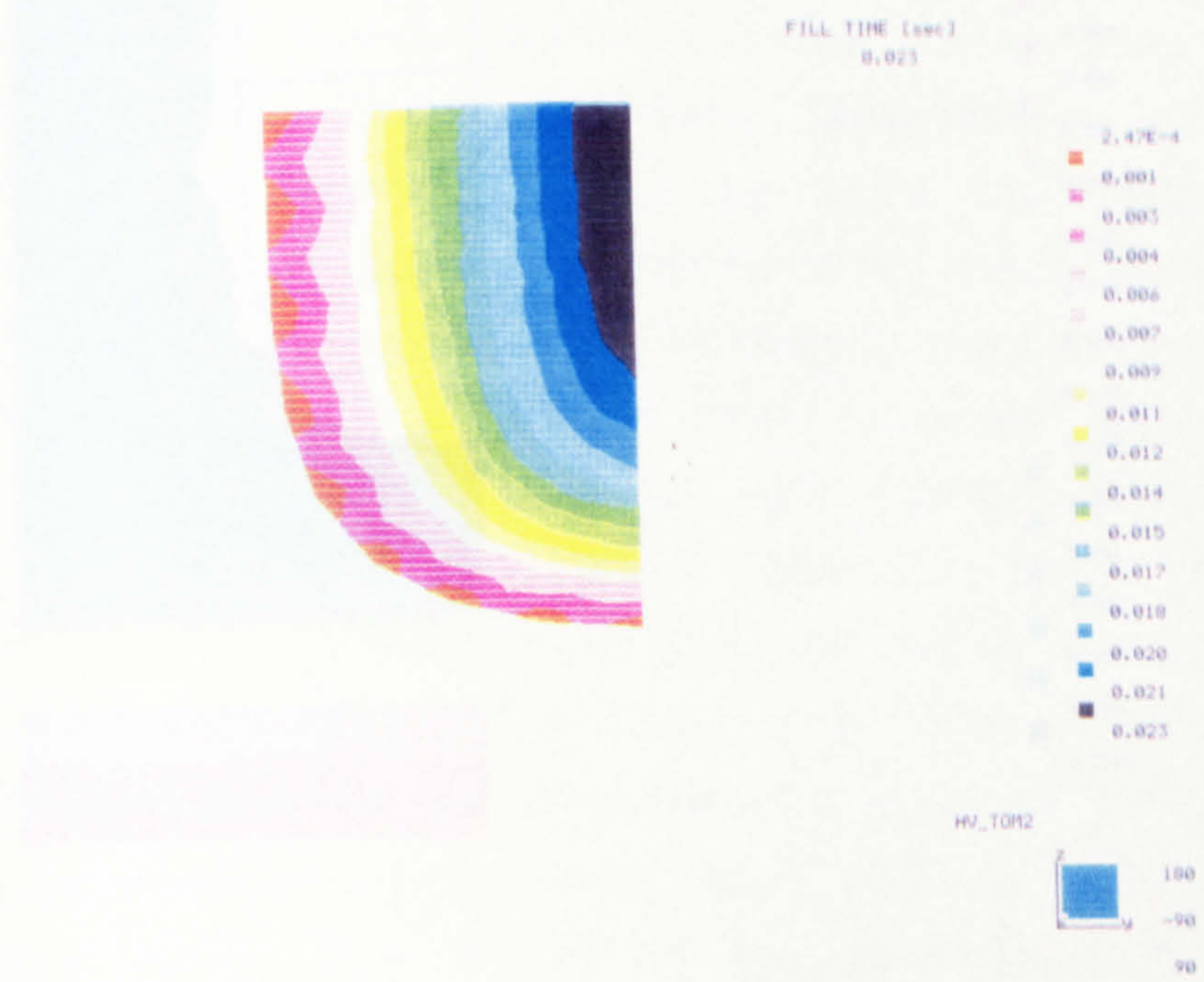


Figure 10.12 Melt distribution in time - MF4

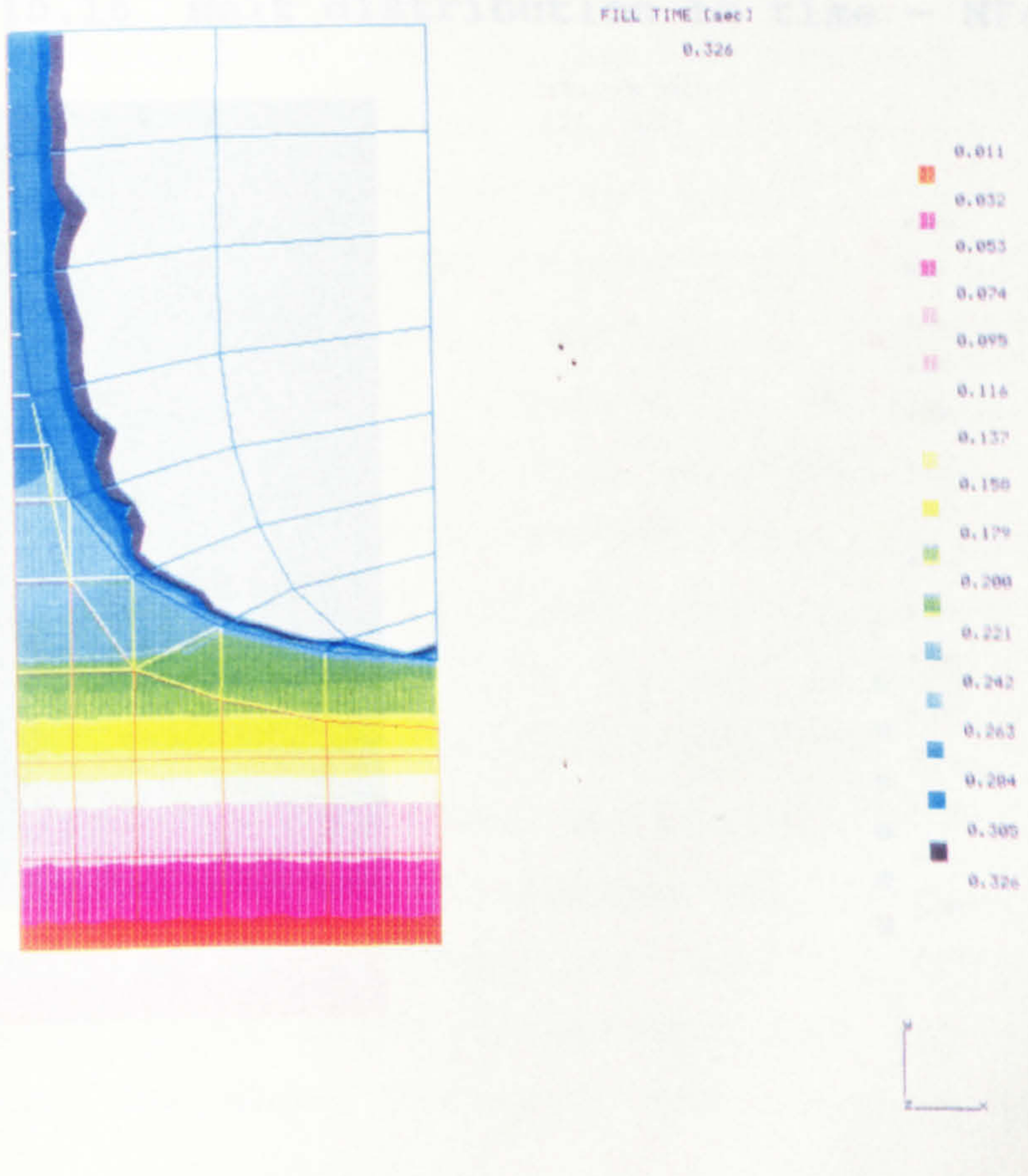

Figure 10.13 Melt distribution in time - MF5

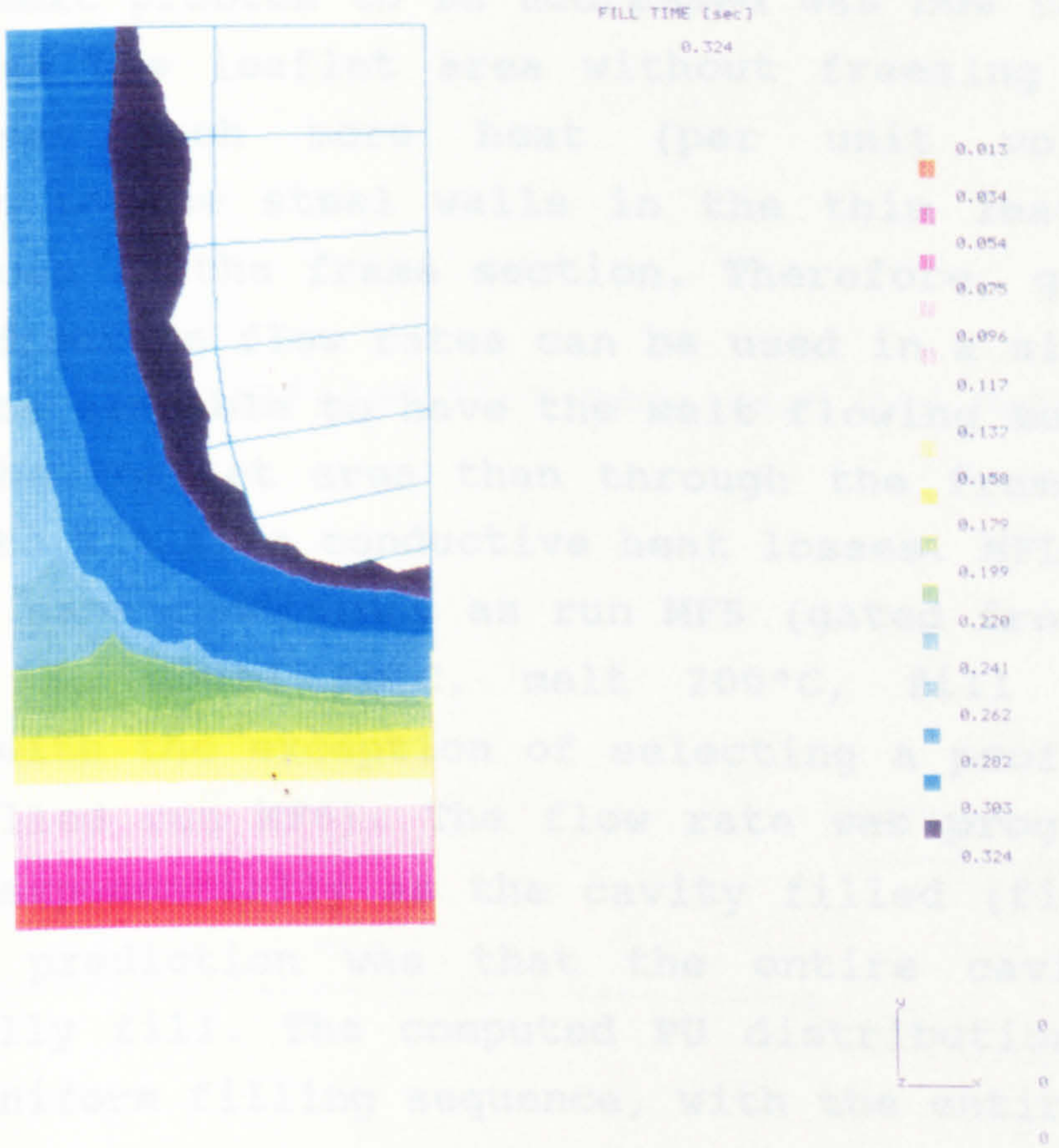


Figure 10.15 Melt distribution in time - MF6

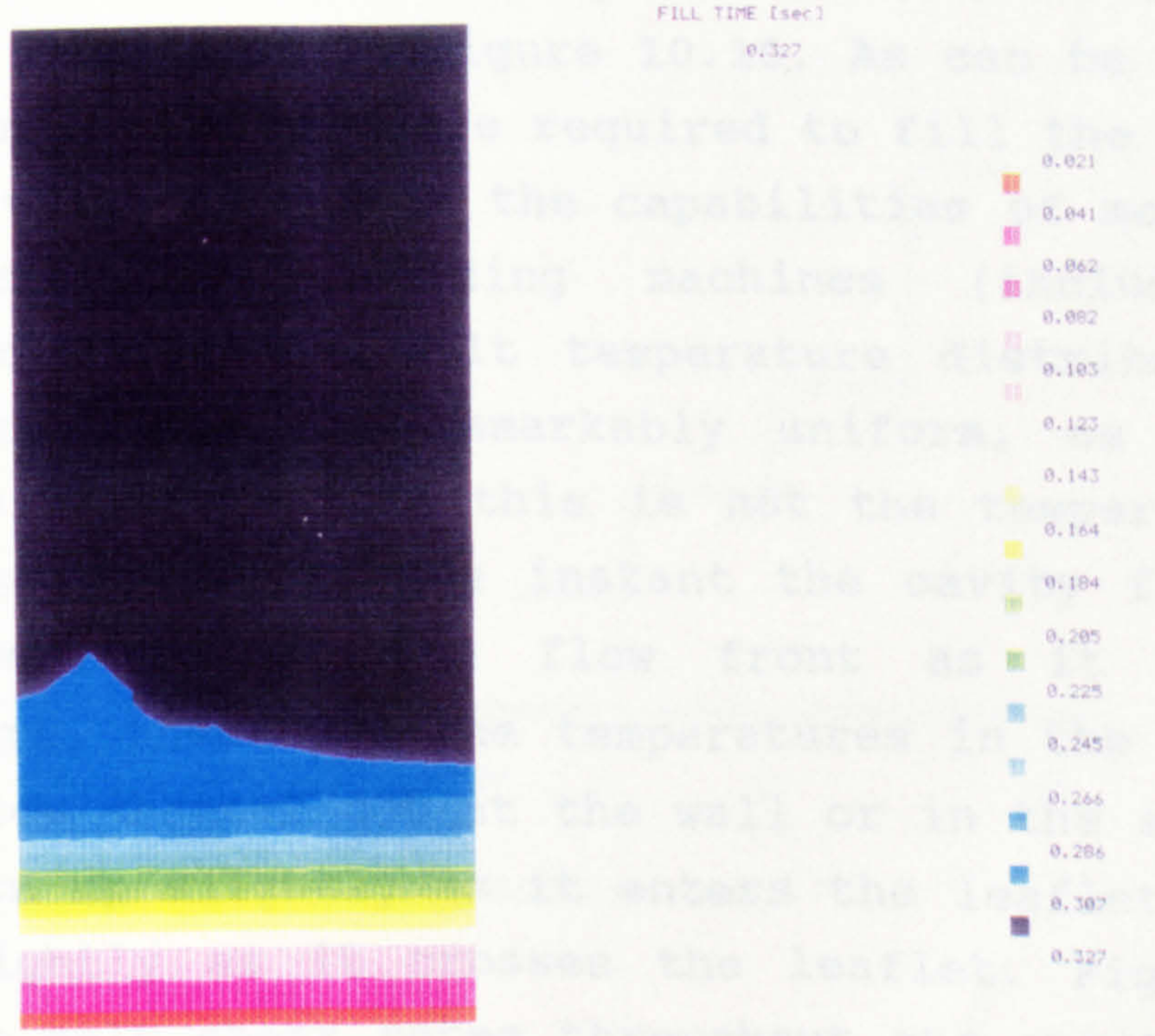

successful in bringing the flow front to the leaflet-frame border at much the same time at all points along its length.

The next problem to be addressed was how to get the melt across the leaflet area without freezing off. The melt looses much more heat (per unit volume) by conduction to the steel walls in the thin leaflet area than it does in the frame section. Therefore, given that up to 10 discrete flow rates can be used in a single run, it would be sensible to have the melt flowing much faster through the leaflet area than through the frame section in order to minimize conductive heat losses. MFLP was run under the same conditions as run MF5 (gated from point D to point E, mould 90°C, melt 200°C, fill time 0.3 seconds) with the exception of selecting a profiled flow curve (called run MF6). The flow rate was programmed to increase exponentially as the cavity filled (fig 10.14). The MFLP prediction was that the entire cavity would successfully fill. The computed PU distribution in time shows a uniform filling sequence, with the entire leaflet filling within 0.02 seconds (fig 10.15). The pressure distribution within the cavity, at the instant the cavity fills, is displayed in figure 10.16. As can be seen, the maximum injection pressure required to fill the cavity is 107 MPa, which is within the capabilities of most medium sized screw-type moulding machines (including the Battenfeld 350). The melt temperature distribution, as the cavity fills, is remarkably uniform, as shown in figure 10.17. Note that this is not the temperature map within the cavity at the instant the cavity fills, but the temperature of the flow front as it advances. Furthermore, these are the temperatures in the mid-plane of the flow channel not at the wall or in the steel. The melt heats up slightly as it enters the leaflet area but cools slightly as it crosses the leaflet. Figure 10.18 shows the melt shear rates throughout the cavity. Again, these are not the shear rates at the instant the cavity

Figure 10.14 Profiled flow rate used for MFLP run MF6

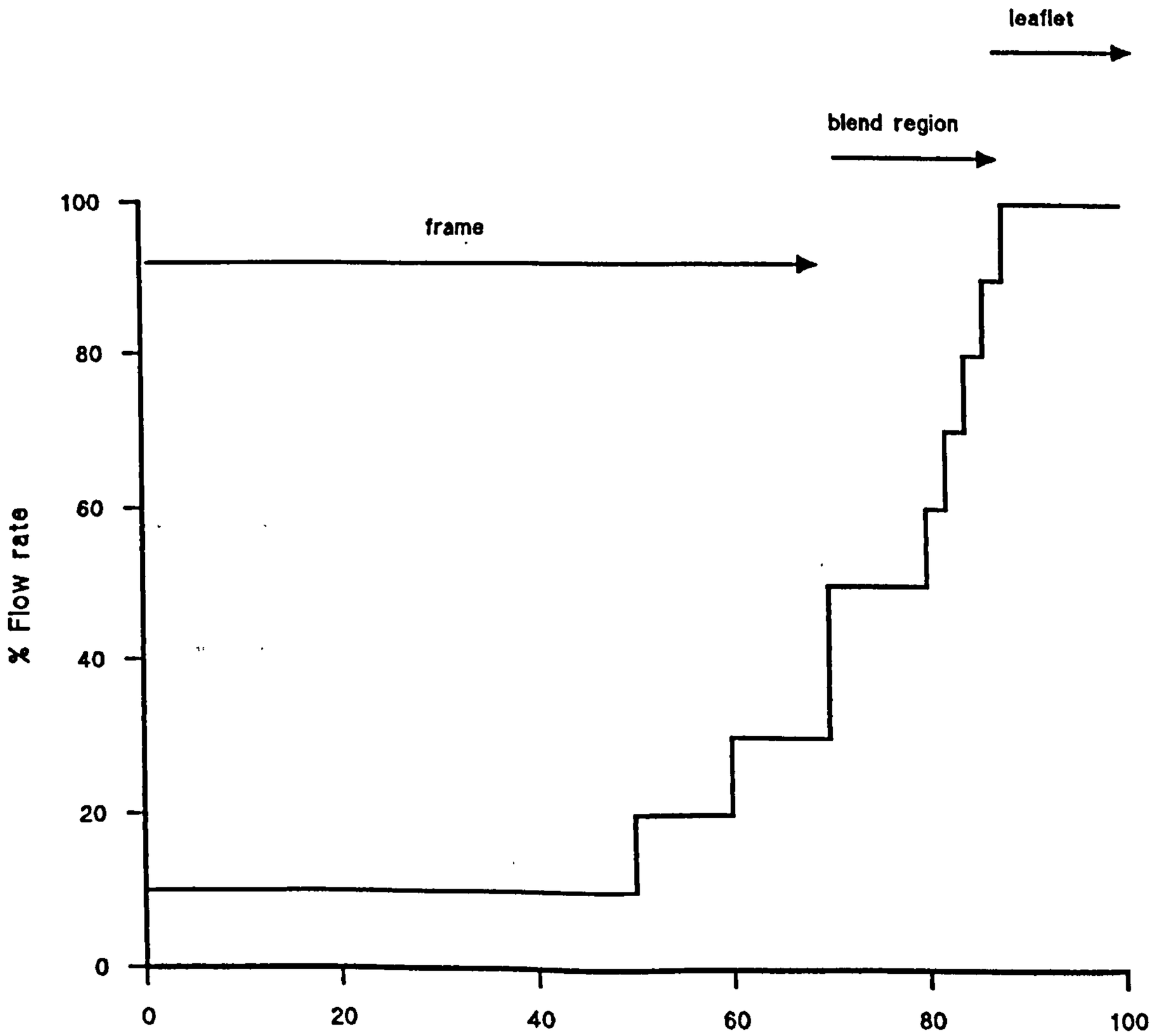

Figure 10.16 Pressure at instant of fill - MF6


Figure 10.17 Temperature of flow front - MF6

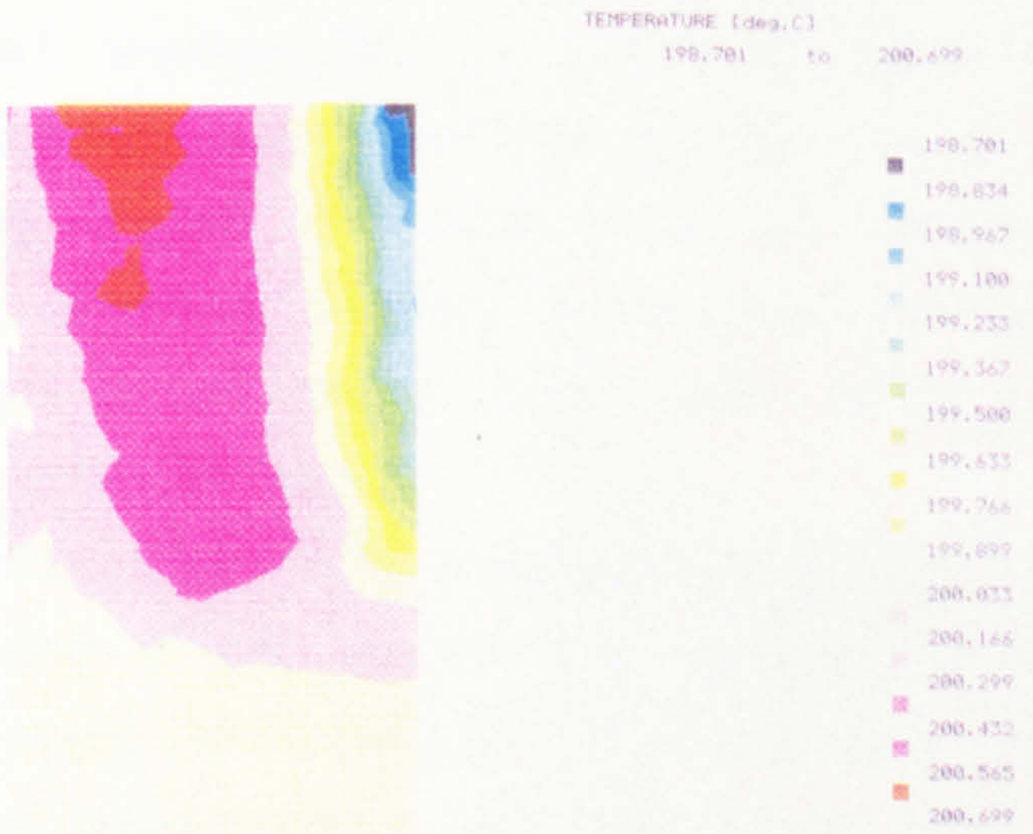

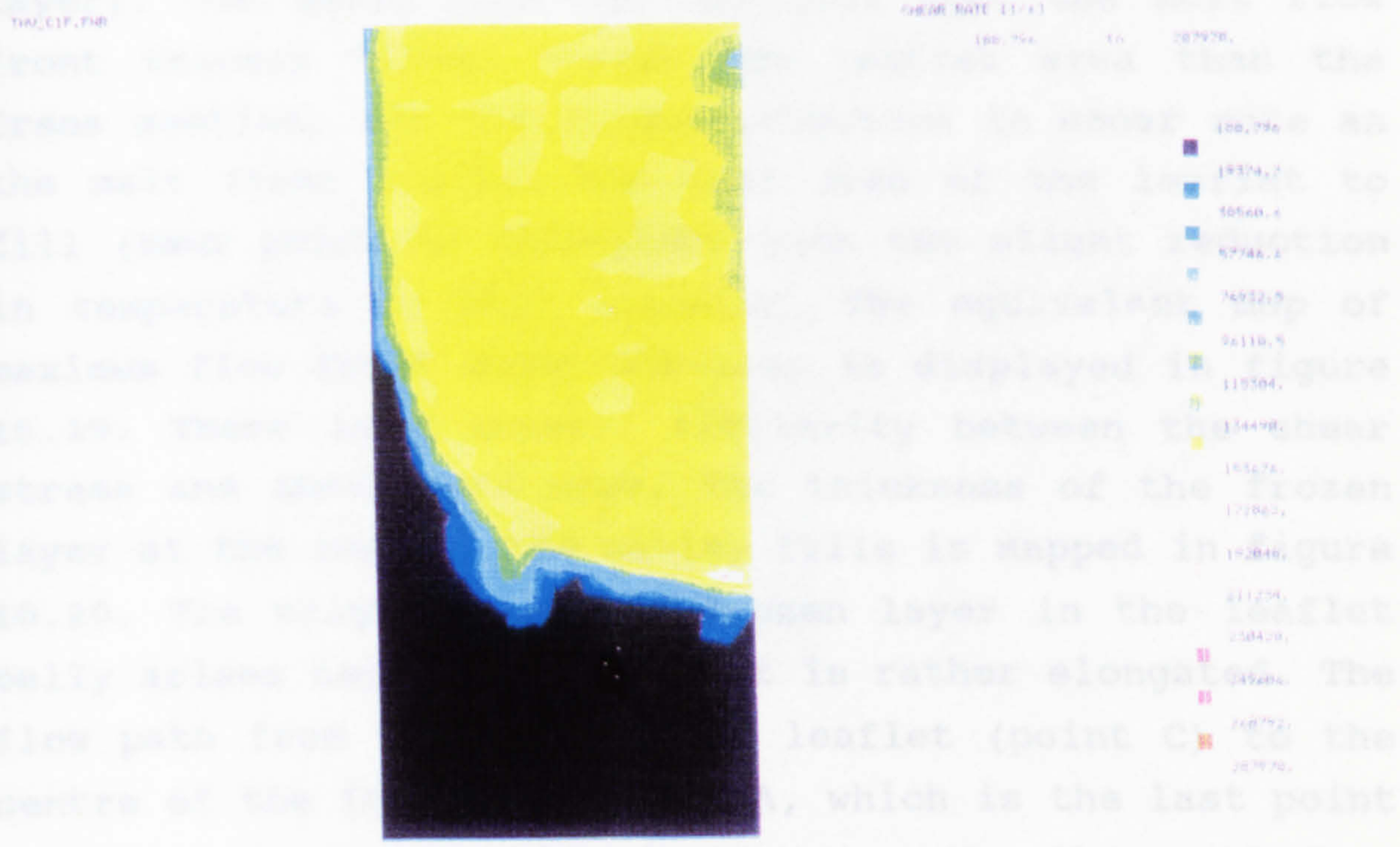


Figure 10.18 Maximum shear rate distribution - MF6

fills, but those of the advancing flow front. Also, of the shear rates calculated for each of the melt layers at each node, these are the maximum shear rates (which generally are those from layers close to the frozen layer). The shear rate map confirms that the melt flow front travels faster across the leaflet area than the frame section, and the slight reduction in shear rate as the melt front reaches the last area of the leaflet to fill (near point A) correlates with the slight reduction in temperature in this vicinity. The equivalent map of maximum flow front shear stresses is displayed in figure 10.19. There is a general similarity between the shear stress and shear rate maps. The thickness of the frozen layer at the instant the cavity fills is mapped in figure 10.20. The slightly thicker frozen layer in the leaflet belly arises because the leaflet is rather elongated. The flow path from the base of the leaflet (point C) to the centre of the free edge (point A, which is the last point to fill), is considerably longer than the flow path from the top of the frame post (point B) to the centre of the free edge. Thus, when the cavity is almost full, the preferred route for the melt trying to reach the last area to fill (at point A) is along the leaflet free edge rather than up through the leaflet base. Therefore, less 'fresh' molten PU is flowing into the leaflet base and the frozen layer builds up slightly. The slightly thicker frozen layer in the leaflet belly correlates with a small, rather faint, localised maximum which can be seen on the shear rate map, and to a lesser extent on the shear stress map.

Finally, one concern with run MF6 was that perhaps a gas trap might be formed somewhere along the leaflet mid-line when the entire leaflet was filled. The flow front coming across the leaflet area from the frame post could perhaps meet the symmetrically opposite flow front while the flow front in the leaflet belly was retarded by the increased frozen layer thickness, and thus a gas trap

Figure 10.19 Maximum shear stress distribution - MF6

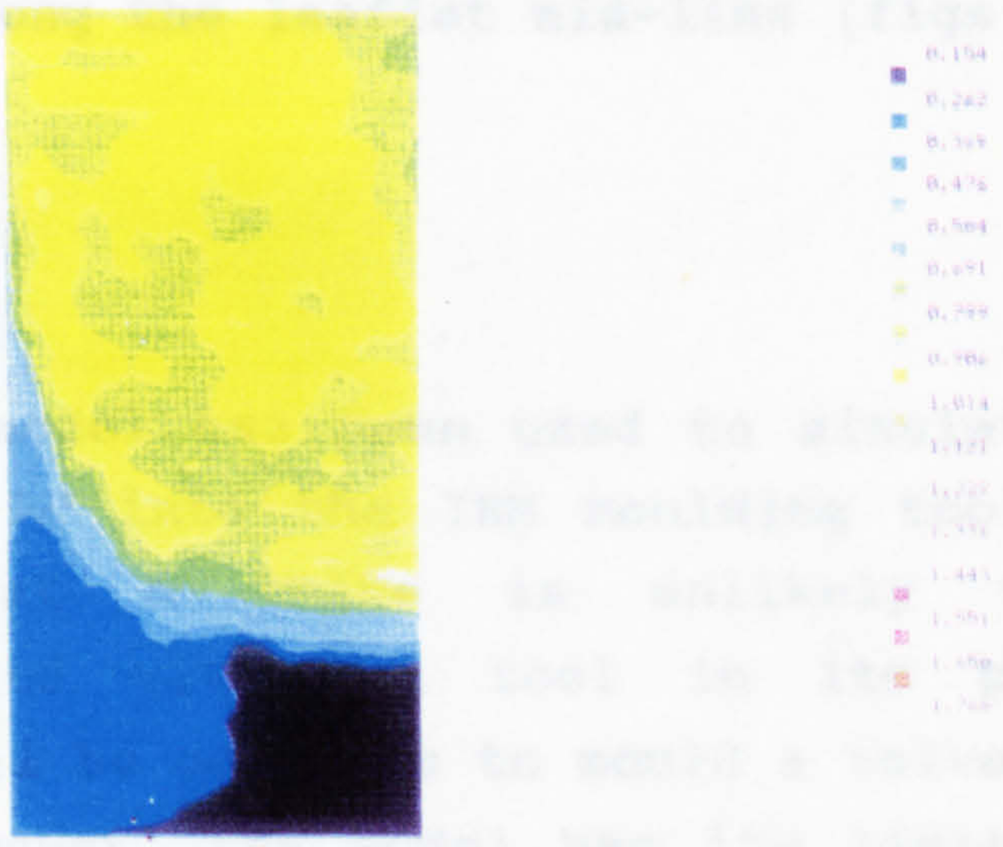

Figure 10.20 Frozen layer thickness at instant of fill - MF6

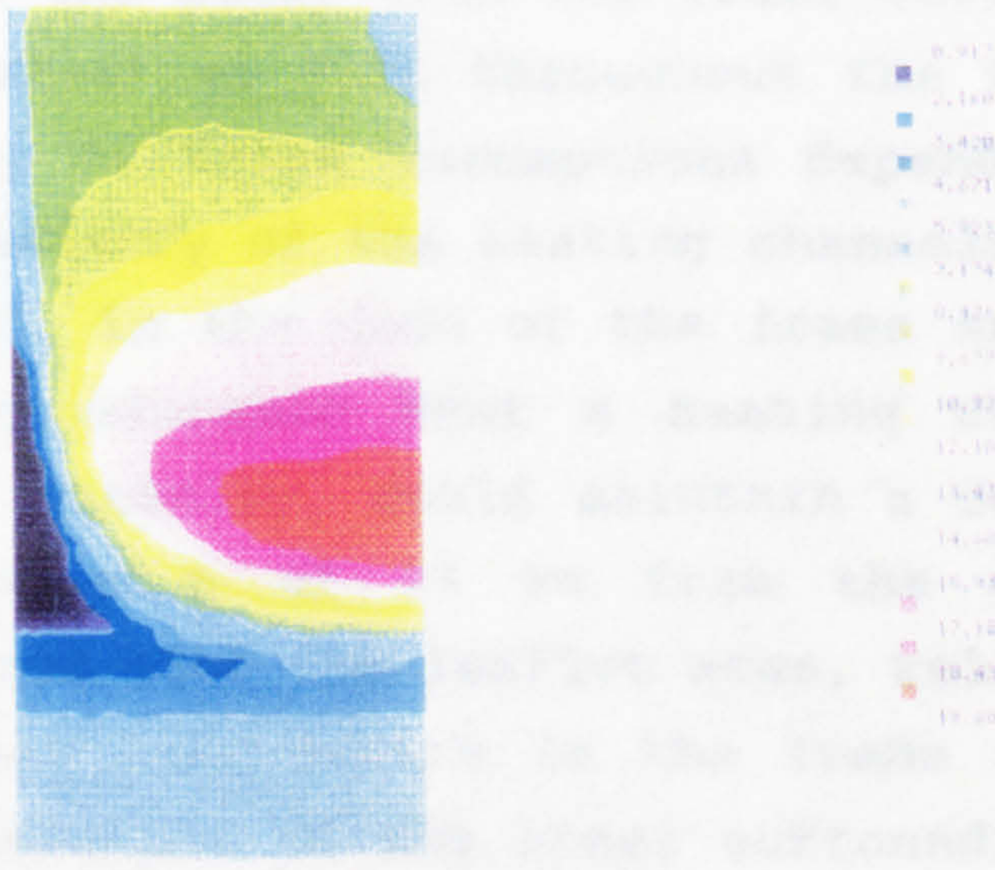

could form. In order to investigate, run MF6 was repeated but with the valve geometry HV2 reflected in the leaflet mid-plane to create the entire leaflet and corresponding section of frame (i.e. 1/3 of a valve, called run MF7). The MFLP calculations predict that there are no such problems occurring along the leaflet mid-line (figs 10.21 & 10.22).

## 10.6 Discussion

A mathematical model has been used to simulate the injection of molten PU into the IBM moulding tool. The results suggest that a valve is unlikely to be satisfactorily moulded with the tool in its present state, but it may well be possible to mould a valve given a modified tool. However, the model has its limitations and there are reasons to believe that the flow resistance across the leaflet area may have been overestimated.

The principal concerns with the MOLDFLOW model relate to the assumptions made about the temperature distribution in the steel mould. To recap, the temperatures 0.9 mm into the steel from the leaflet cavity and 18 mm into the steel from the frame cavity are taken to be held constant at 90°C throughout the filling process. The validity of these assumptions depends upon the location and efficiency of the heating channels which run through the mould. In the case of the frame section, it does not seem unreasonable that a heating channel, situated in the near vicinity, could maintain a constant temperature at a distance of 18 mm from the cavity. Besides which, compared with the leaflet area, relatively little conductive heat loss occurs in the frame section and the assumed temperature of the steel surrounding the frame section is probably of secondary importance. Of considerably more concern is the steel temperature surrounding the leaflet cavity. In order to maintain a temperature of 90°C, at a distance of only 0.9 mm from a

Figure 10.21 Melt distribution in time - MF7

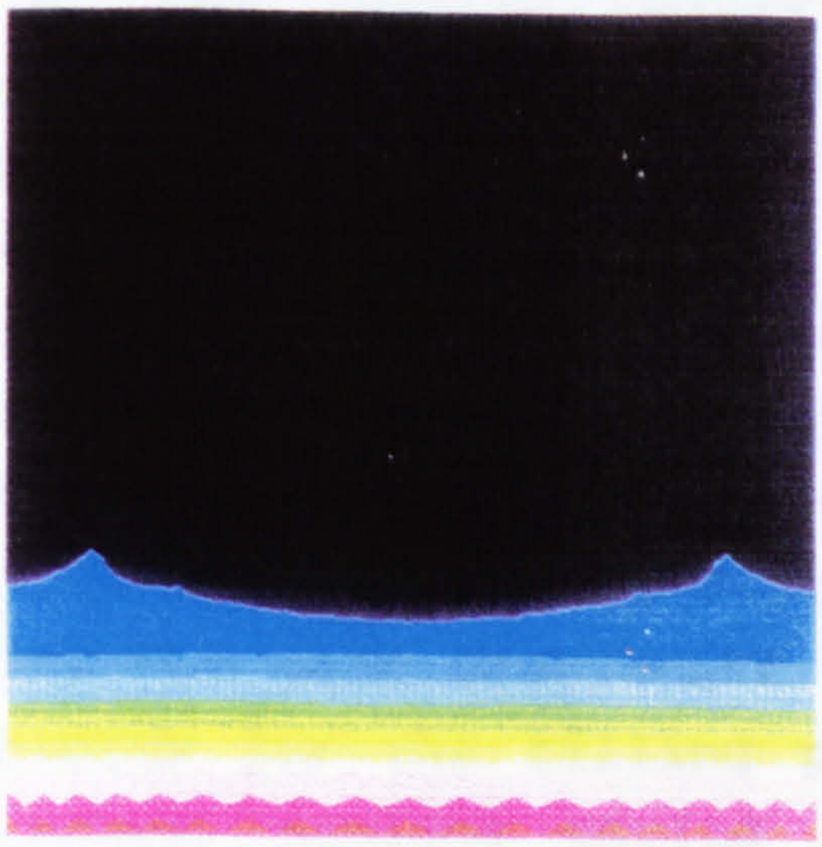

Figure 10.22 Pressure at instant of fill - MF7

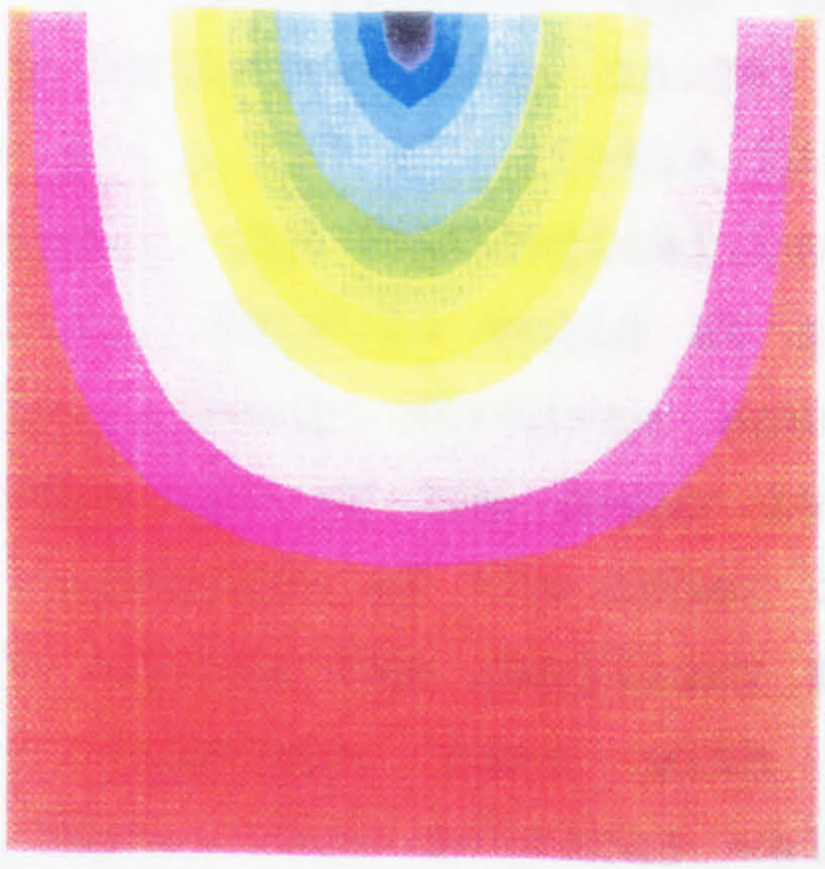

flow channel containing molten PU at 200°C, would seem to require an exceedingly efficient cooling system. (Although, bear in mind that the time scales are very short and the frozen layer does provide some insulation between the melt and steel). Furthermore, only 1/6 of the valve was modelled: the 3 thin fins on the male pin are only 0.4 mm thick at the free edges. Thus, for the upper portion of the leaflet cavity, the assumption of a constant temperature of 90°C at a distance of 0.9 mm from the cavity is invalid because the steel itself is only approximately 0.4 mm thick. As a result of the close proximity of the 3 leaflet cavities, particularly near the free edge, the steel temperature in this region would be greater than 90°C, and consequently there would be less resistance to flow. The fact that the steel fins may rise above the melt freeze-off temperature of 100°C is not a problem for the filling process, it simply means that a longer cooling period may be required before opening the tool and removing the moulded part.

A second source of concern is that on occasions the predicted shear rates rise well above the maximum rates which were used when measuring the PU viscosity. For example, in MF6 the computed shear rates across the leaflet area were in excess of $1.5 \times 10^5$ $s^{-1}$ (fig 10.18) whereas in calculating the constants $A_{1->6}$ for the viscosity relation (eqn 10.29) the maximum shear rate used was $1.6 \times 10^4$ $s^{-1}$ (table 10.2). Therefore, it is not known whether the rheological constitutive equation which was used for MFLP is valid at such high shear rates. In particular, shear stresses associated with these high shear rates are of the order $10^6$ $Nm^{-2}$ (fig 10.19) while at shear stresses of the order of $10^5$ $Nm^{-2}$ melt fracture generally occurs for capillary flow. Most published data on melt fracture deal with capillary dies, though encouragingly, the critical wall shear stress has been reported to be higher for slit dies than for capillaries using polystyrene melts. Also, the magnitude of the melt

fracture distortions can be decreased by die entrance streamlining (Tadmor & Gogos, 1979). Note that since the flow resistance in the leaflet cavity has been over estimated, then so the computed shear stresses are likewise artificially high.

The valve geometry HV1 is an apparently rather crude representation of the actual valve geometry incorporated into the IBM moulding tool. However, this is one of less important features of the mathematical model. It is, of course, crucially important to accurately represent the flow path lengths and their thicknesses, which HV1 does, but the cavity shape is of little consequence. (HV1 could reasonably be replaced with a carefully designed 2-dimensional representation.)

This study represents the initial steps towards a more comprehensive simulation, and there are a number of ways in which this work could be advanced. There is a pressing need to accurately model the heating channels running through the mould (i.e. size and location of channels, physical properties of coolant, coolant flow rate). Conveniently, a new sub-program of MOLDFLOW has recently become available which does allow the heating channels to be accounted for. Of course, if the temperature distribution in the mould is to be accurately modelled then the entire valve geometry, rather than 1/6, must be incorporated. Also, it would be useful to consider a wider range of geometrical configurations: gating at 1 or 2 points rather than all the way along the base of the frame; using a less exaggerated blending region between the leaflet and frame; and investigating the sensitivity of the flow distribution to the leaflet cavity thickness.

Finally, it should be mentioned that, in principle, flow analysis should precede tool design. Unfortunately, in this case the practicalities were such that the IBM tool was designed and built before MFLP became available to the project.

## 10.6 Summary

A mathematical model, which incorporates experimentally determined rheological data, has been used to simulate the injection of molten PU into the IBM moulding tool. Initial results suggest that a valve is unlikely to be satisfactorily moulded with the cavity gated centrally through the leaflet free edges. However, an alternative gating configuration has been identified which, when combined with a slightly modified valve geometry and appropriate processing conditions, may well result in an acceptably moulded valve. The tool modifications could practicably be applied to IBM tool, and the processing conditions are attainable on the Battenfeld 640 moulding machine. The model overestimates the melt flow resistance posed by the thin leaflet cavities, and further work is recommended.

# Chapter 11. Conclusions and Recommendations for Further Work

While existing mechanical and biological prostheses do offer enormous relief to patients suffering from valvular heart disease, the search for a more durable, less thrombogenic valve continues. To this end, existing hydrodynamic and durability testing facilities have been improved and some of the possibilities offered by tri-leaflet synthetic valves have been explored.

The GRI pulse duplicator has been enhanced by an improved data acquisition system. The new system allows valve function to be more efficiently and reliably assessed, and also provides a means for characterizing the pulse duplicator and its transducers. Additionally, the pump and valve photography were brought under direct computer control, thereby offering greater flexibility in testing valves. The accelerated fatigue testing facilities were similarly enhanced. In terms of instrumentation, the pulse duplicator could be considerably improved by introducing a means, such as laser Doppler anemometry, for quantitatively studying velocity flow fields. Although, bearing in mind that tri-leaflet, central-flow type valves generally create more uniform and less thrombogenic flow fields than do mechanical valves. Secondly, it would be worthwhile to run both hydrodynamic and accelerated fatigue tests at 37°C, particularly when testing PU or other types of synthetic leaflet valves.

One of the several attractions of synthetic leaflet valves is their potential for design optimization, in terms of leaflet geometry and thickness distribution as well as material properties. In order to fully exploit the geometrical potential, an integrated CAD/CAM system was developed for producing valve formers. The system is extremely flexible and can accommodate the most complex of valve designs. Furthermore, combining this system with

a forming technique, such as injection moulding, which involves restraining both the inflow and outflow leaflet surfaces, allows complete control over the leaflet thickness distribution.

Given that valves may be produced, at least in principle, to any geometrical specification, then future attention should be directed towards defining an optimum design configuration. To date, finite element stress analyses have gone some way towards describing the stress distributions in closed tri-leaflet valves under back pressure. However, a more complete description including the dynamic stresses incurred as the leaflets open and close is required. A complete stress analysis of the valve would, by necessity, also involve modelling the fluid. Therefore, valve design could be optimized in terms of both reducing leaflet stress concentrations and creating a more favourable flow field. Additionally, through stress analyses it may be possible to specify optimal mechanical properties for the valve leaflets, which may then, in principle, be realizable by varying the chemistry of the synthetic materials used. Such numerically-intensive calculations as would be required to perform these analyses are rapidly becoming more practicable, with advances in computer technology. Note that in the context of PU valves, there may also be the possibility for experimental stress analysis through analysing birefringence patterns in polarized light.

Injection moulding represents a highly attractive means of producing prosthetic valves, in terms of ability to realise complex designs, quality control, as well as economy. The practicalities of injection moulding PU valves were investigated with 3, increasingly substantial, moulding tools. It was discovered that the very thin leaflet sections, which were necessary in order to elicit an acceptable hydrodynamic performance, presented a very large resistance to melt flow. Attempts at moulding a PU valve with tolerably thin leaflets,

using a rather sophisticated moulding machine and robust moulding tool, are ongoing.

Initial investigations with a mathematical model of the injection moulding process suggest that it may indeed be possible to mould a PU valve with sufficiently thin leaflets. Although this may require a moulding tool which is gated rather differently from the tool currently being used. However, the model overestimates the melt flow resistance presented by the thin leaflet sections, and this work needs to be extended by using a model which more accurately represents the temperature distribution in the steel mould walls.

If the problem of moulding very thin leaflet sections proves to be insurmountable by conventional injection moulding methods, then there are more advanced techniques which could be applied. For example, injection-compression moulding: injecting the molten PU with the 2 tool halves set fractionally apart, and then clamping the tool shut immediately the cavity has filled, though such techniques require more elaborate tools and machines and may not be practicable.

PU valves with injection moulded frames and dip moulded leaflets have been developed. They have demonstrated an acceptable hydrodynamic performance and accelerated fatigue tests are in progress; at present 4 dip moulded valves have successfully completed over 80 million cycles, 2 others with thinner leaflets failed after 65 million cycles. Difficulty was experienced in controlling the leaflet thickness distribution and in producing valves with consistent leaflet thicknesses. Dipping techniques need to be developed which facilitate a greater degree of control over valve production.

Finally, the propensity for PU valves to calcify and the role of mechanical stress in this process require urgent study. The dip moulded PU valves are currently being used in a parallel investigation into the underlying mechanisms of PU calcification. Much of the

published work on PU biocompatibility and calcification relates to solvent cast PU, and further research is needed to elucidate the effects of melt processing upon the biocompatibility of PU.

## References


Aaslid R, Levang O, Fröysaker T, Skagseth E, Hall KV (1975), "In situ" evaluation of the aortic pivoting disc valve prosthesis. Scand J Thorac Cardiovasc Surg 9:81-84.

Aberg B, Henze A (1979), Comparison between the in vitro flow dynamics of the standard and the convexo-concave Björk-Shiley tilting disc valve prostheses. Scand J Thorac Cardiovasc Surg 13:177-189.

Akutsu T, Modi VJ, Brownlee RT (1980), Steady flow fluid dynamics of prosthetic heart valves with application to the prediction of orifice area and pulsatile pressure gradient. Proc ESAO 7:304-308.

Arabia FA, Talbot TL, Stewart SFC, Nast EP, Clark RE (1989), A computerized physiologic pulse duplicator for in-vitro hydrodynamic and ultrasonic studies of prosthetic heart valves. Biomed Instrum Technol 23:205-215.

Bellhouse BJ (1969), Velocity and pressure distributions in the aortic valve. J Fluid Mech 37:587-600.

Bellhouse BJ (1972a), Fluid mechanics of a model mitral valve and left ventricle. Cardiovascular Research 6:199-210.

Bellhouse BJ (1972b), The fluid mechanics of heart valves, in "Cardiovascular fluid dynamics", ed DH Bergel, Academic Press, London and New York, vol 1, pp261-285.

Bellhouse BJ, Bellhouse FH (1968), Mechanism of closure of the aortic valve. Nature 217:86-87.

Bellhouse BJ, Bellhouse FH (1969a), Fluid mechanics of model normal and stenosed aortic valves. Circ Res 25:693-704.

Bellhouse BJ, Bellhouse FH (1969b), Fluid mechanics of the mitral valve. Nature 224:615-616.

Bellhouse BJ, Talbot L (1969), The fluid mechanics of the aortic valve. J Fluid Mech 35:721-735.

Benedict GF (1987), Nontraditional manufacturing processes. Marcel Dekker, New York, pp207-229.

Bernacca GM (1991), Calcification in pericardial and polyurethane biomaterials used to fabricate prosthetic heart valve leaflets. PhD thesis, University of

Strathclyde.

Bernacca GM, Fisher AC, Mackay TG, Wheatley DJ (1992a), A dynamic in vitro method for studying bioprosthetic heart valve calcification. Journal of Materials Science: Materials in Medicine 3:293-298.

Bernacca GM, Fisher AC, Wilkinson R, Mackay TG, Wheatley DJ (1992b), Calcification and stress distribution in bovine pericardial heart valves. J Biomed Mat Res 26:959-966.

Black MM (1973), Development and testing of prosthetic heart valves: cardiovascular simulation and life support systems, in "Perspectives in Biomedical Engineering", ed RM Kenedi, MacMillan, London, pp21-28.

Black MM, Howard IC, Huang X, Patterson EA (1991), A three-dimensional analysis of a bioprosthetic heart valve. J Biomechanics 24:793-801.

Bloomfield P, Wheatley DJ, Prescott RJ, Miller HC (1991), Twelve-year comparison of a Björk-Shiley mechanical heart valve with porcine bioprostheses. N Engl J Med 324:573-579.

Brewer RJ, Deck JD, Capati B, SP Nolan (1976), The dynamic aortic root. Its role in aortic valve function. J Thorac Cardiovasc Surg 72:413-417.

Brewer RJ, Mentzer RM, Deck JD, Ritter RC, Trefil JS, Nolan SP (1977), An in vivo study of the dimensional changes of the aortic valve leaflets during the cardiac cycle. J Thorac Cardiovasc Surg 74:645-650.

Broom ND (1977), The stress/strain and fatigue behaviour of glutaraldehyde preserved heart-valve tissue. J Biomechanics 10:707-724.

Broom ND (1978), Fatigue-induced damage in glutaraldehyde-preserved heart valve tissue. J Thorac Cardiovasc Surg 76:202-211.

Broom ND, Christie GW (1982), The structure/function relationship of fresh and glutaraldehyde-fixed aortic valve leaflets, in "Cardiac bioprostheses", ed LH Cohn, V Gallucci, Yorke Medical Books, New York, pp476-491.

Broom ND, Thomson FJ (1979), Influence of fixation conditions on the performance of glutaraldehyde-treated porcine aortic valves: towards a more scientific basis. Thorax 34:166-176.

Bruss KH, Reul H, Van Gilse J, Knott E (1983), Pressure drop and velocity fields at four mechanical heart valve

prostheses: Björk-Shiley concave-convex, Hall-Kaster and St Jude Medical. Life Support Systems 1:3-22.

Burden RL, Faires JD (1985), Numerical Analysis, 3rd edition. Prindle, Weber & Schmidt, Boston, pp116-128.

Cannon SR, Richards KL, Crawford M (1985), Hydraulic estimation of stenotic orifice area: a correction of the Gorlin formula. Circulation 71:1170-1178.

Carabello BA (1987), Advances in the hemodynamic assessment of stenotic cardiac valves. J Am Coll Cardiol 10:912-919.

Carey RF, Herman BA (1989), The effects of a glycerin-based blood analog on the testing of bioprosthetic heart valves. J Biomechanics 22:1185-1192.

Cataloglu A, Clark RE, Gould PL (1977), Stress analysis of aortic valve leaflets with smoothed geometrical data. J Biomechanics 10:153-158.

Chambers JB, Cochrane T, Black MM, Jackson G (1989), The Gorlin formula validated against directly observed orifice area in porcine mitral bioprostheses. J Am Coll Cardiol 13:348-353.

Chandran KB, Cabell GN, Khalighi B, Chen C-J (1984), Pulsatile flow past aortic valve bioprostheses in a model human aorta. J Biomechanics 17:609-619.

Chandran KB, Fatemi R, Schoerster R (1986), Dependence of tissue valve leaflet motion on the viscosity of blood analogue fluid. Life Support Systems 4:289-303.

Chandran KB, Fatemi R, Schoephoerster R, Wurzel D, Hansen G, Pantalos G, Yu L-S, Kolff WJ (1989a), In vitro comparison of velocity profiles and turbulent shear distal to polyurethane trileaflet and pericardial prosthetic valves. Artificial Organs 13:148-154.

Chandran KB, Khalighi B, Chen C-J (1985a), Experimental study of physiological pulsatile flow past valve prostheses in a model of human aorta-I. Caged ball valves. J Biomechanics 18:763-772.

Chandran KB, Khalighi B, Chen C-J (1985b), Experimental study of physiological pulsatile flow past valve prostheses in a model of human aorta-II. Tilting disc valves and the effect of orientation. J Biomechanics 18:773-780.

Chandran KB, Khalighi B, Chen C-J, Falsetti HL, Yearwood TL, Hiratzka LF (1983), Effect of valve orientation on flow development past aortic valve prostheses in a model

human aorta. J Thorac Cardiovasc Surg 85:893-901.

Chandran KB, Kim S-H, Han G (1991), Stress distribution on the cusps of a polyurethane trileaflet heart valve prosthesis in the closed position. J Biomechanics 24:385-395.

Chandran KB, Schoephoerster R, Dellsperger KC (1989b), Effect of prosthetic mitral valve geometry and orientation on flow dynamics in a model human left ventricle. J Biomechanics 22:51-65.

Chetta GE, Lloyd JR (1980), The design, fabrication and evaluation of a trileaflet prosthetic heart valve. J Biomech Engng 102:34-41.

Chong KP, Wieting DW, Hwang NHC, Kennedy JH (1973), Stress analysis of normal human aortic leaflets during diastole. Biomat Med Dev Art Org 1:307-321.

Chong M, Missirlis YF (1978), Aortic valve mechanics part II: A stress analysis of the porcine aortic valve leaflets in diastole. Biomat Med Dev Art Org 6:225-244.

Christie GW, Medland IC (1982), A non-linear finite element stress analysis of bioprosthetic heart valves, in "Finite Elements in Biomechanics", eds RH Gallagher, BR Simon, PC Johnson, JF Cross, John Wiley & Sons, pp153-179.

Christie GW, Stephenson RA (1990a), Modelling the mechanical role of the fibrosa and the ventricularis in the porcine bioprosthesis,in "Surgery for heart valve disease", ed E Bodnar, ICR Publishers, London, pp815-827.

Christie GW, Stephenson RA (1990b), Stress-related failure modes of bovine pericardial heart valves, in "Surgery for heart valve disease", ed E Bodnar, ICR Publishers, London, pp265-276.

Clark C (1976a), The fluid mechanics of aortic stenosis I. Theory and steady flow experiments. J Biomechanics 9:521-528.

Clark C (1976b), The fluid mechanics of aortic stenosis II. Unsteady flow experiments. J Biomechanics 9:567-573.

Clark C (1978), Relation between pressure difference across the aortic valve and left ventricular outflow. Cardiovascular Research 12:276-287.

Clark C (1979), Energy losses in flow through stenosed valves. J Biomechanics 12:737-746.

Clark C (1980), The propagation of turbulence produced by

a stenosis. J Biomechanics 13:591-604.

Clark C (1985), A differential pressure transducer for the measurement of high-frequency fluctuations in liquids. J Phys E: Sci Instrum 18:297-302.

Clark C, Schultz DL (1973), Velocity distribution in aortic flow. Cardiovascular Research 7:601-613.

Clark RE (1973), Stress-strain characteristics of fresh and frozen human aortic and mitral leaflets and chordae tendineae. J Thorac Cardiovasc Surg 66:202-208.

Clark RE, Finke EH (1974), Scanning and light microscopy of human aortic leaflets in stressed and relaxed states. J Thorac Cardiovasc Surg 67:792-804.

Clark RE, Gould PL, Swanson WM, Kardos JL, Karara HM, Skelton J, Butterworth GAM (1974), Design and fabrication of prosthetic leaflet heart valves. Biomat Med Dev Art Org 2:379-385.

Clark RE, Sutera SP (1973), Methods of design of leaflet valvular prostheses. Stresses in the mitral valve leaflets in health and disease. J Thorac Cardiovasc Surg 65:890-896.

Clark RE, Swanson WM, Kardos JL, Hagen RW, Beauchamp RA (1978), Durability of prosthetic heart valves. Ann Thorac Surg 26:323-334.

Cochrane T, Kenyon CJ, Lawford PV, Black MM, Chambers JB, Sprigings DC (1991), Validation of the orifice formula for estimating effective heart valve opening area. Clin Phys Physiol Meas 12:21-37.

Collins JJ (1991), The evolution of artificial heart valves. N Engl J Med 324:624-626.

Cornhill JF (1977), An aortic-left ventricular pulse duplicator used in testing prosthetic aortic heart valves. J Thorac Cardiovasc Surg 73:550-558.

Deck JD, Thubrikar MJ, Nolan SP, Aouad J (1982), Role of mechanical stress in calcification of bioprostheses, in "Cardiac Bioprostheses", eds LH Cohen, V Galluci, Yorke Medical, New York, pp293-305.

Dellsperger KC, Wieting DW (1978), An in vitro fluid dynamic comparison of the new St Jude Medical prosthetic mitral valve with Starr-Edwards, Björk-Shiley, and Lillehei-Kaster prostheses, in "Advances in Bioengineering", eds RC Eberhart, AH Burnstein, ASME, New York, pp31-33.

Einav S, Stolero D, Avidor JM, Elad D, Talbot L (1990), Wall shear stress distribution along the cusp of a tri-leaflet prosthetic valve. J Biomed Eng 12:13-18.

Evans VM (1987), Development of a polyurethane tri-leaflet heart valve. MSc thesis, University of Strathclyde.

Farahifar D, Cassot, Bodard H (1985), Velocity profiles in the wake of two prosthetic heart valves using a new cardiovascular simulator. J Biomechanics 18:789-802,

Farthing S, Peronneau P (1979), Flow in the thoracic aorta. Cardiovascular Research 13:607-620.

Figliola RS, Mueller TJ (1981), On the hemolytic and thrombogenic potential of occluder prosthetic heart valves from in-vitro measurements. J Biomech Engng 103:83-90.

Fishbein MC, Roberts WC, Golden A, Hufnagel CA (1975), Cardiac pathology after aortic valve replacement using Hufnagel trileaflet prostheses: A study of 20 necropsy patients. Am Heart J 89:443-448.

Fisher AC, Bernacca GM, Mackay TG, Dimitri WR, Wilkinson R, Wheatley DJ (1992), Calcification modelling in artificial heart valves. Int J Artif Organs 15:284-288.

Fisher J (1986), Design development and evaluation of an improved pericardial bioprosthetic heart valve. PhD thesis, University of Glasgow.

Fisher J, Jack GR, Wheatley DJ (1986a), Design of a function test apparatus for prosthetic heart valves. Initial results in the mitral position. Clin Phys Physiol Meas 7:63-73.

Fisher J, Reece IJ, Wheatley DJ (1986b), In vitro evaluation of six mechanical and six bioprosthetic valves. Thorac Cardiovasc Surgeon 34:157-162.

Fisher J, Spyt TJ, Wheatley DJ (1989), Failure and hydrodynamic function testing of explanted pericardial and porcine bioprosthetic valves. Proc Inst Mech Eng: J Eng Med 203(H):65-70.

Fisher J, Wheatley DJ (1987), An improved pericardial bioprosthetic heart valve. Eur J Cardio-thorac Surg 1:71-79.

Fisher J, Wheatley DJ (1988), Hydrodynamic function of ten prosthetic heart valves in the aortic position. Clin Phys Physiol Meas 9:307-317.

Foreman JEK, Hutchison KJ (1970), Generation of sinusoidal fluid pressures of relatively high frequency. J Appl Physiol 29:511-516.

Gabbay S, Bortolotti U, Wasserman F, Factor S, Strom J, Frater RWM (1984), Fatigue-induced failure of the Ionescu-Shiley pericardial xenograft in the mitral position. J Thorac Cardiovasc Surg 87:836-844.

Gabbay S, Kadam P, Factor S, Cheung TK (1988), Do heart valve bioprostheses degenerate for metabolic or mechanical reasons ?, J Thorac Cardiovasc Surg 95:208-215.

Gabbay S, McQueen DM, Yellin EL, Becker RM, Frater RWM (1978), In vitro hydrodynamic comparison of mitral valve prostheses at high flow rates. J Thorac Cardiovasc Surg 76:771-785.

Gabbay S, McQueen DM, Yellin EL, Frater RWM (1979), In vitro hydrodynamic comparison of mitral valve bioprostheses. Circulation 60(Supp 1):62-70.

Gabbay S, Strom J, Yellin E, Frater RWM (1981), Comparison of rigid and flexible pulse duplicator chamber for testing heart valves. AAMI Proc 16:38.

Gabbay S, Yellin EL, Frishman WH, Frater RWM (1980), In vitro hydrodynamic comparison of St Jude, Björk-Shiley and Hall-Kaster valves. Trans Am Soc Artif Intern Organs 26:231-235.

Ganong WF (1981), Review of medical physiology, 10th edition. Lange Medical Publications, Los Altos, California.

Gentle CR (1977), A limit to hydraulic design of heart valve prostheses. Eng Med 6:17-21.

Gentle CR (1978), The role of simulation studies in cardiac valve prosthesis design. Eng Med 7:101-106.

Gerring EL, Bellhouse BJ, Bellhouse FH, Haworth WS (1974), Long term animal trials of the Oxford aortic/pulmonary valve prosthesis without anticoagulants. Trans Am Soc Artif Int Organs 20:703-707.

Ghista DN, Reul H (1983), Prosthetic aortic leaflet valve design: Peformance analysis of an Avcothane leaflet valve, in "Advances in cardiovascular physics", vol 5, part IV, Karger, Basel, pp31-42.

Ghista DN, Reul H, Ray G, Chandran KB (1978), Optimal design of aortic leaflet prosthesis. J Eng Mech Div, Proc Am Soc Civ Eng 104:97-117.

steady state flow model. J Biomechanics 20:353-364.

Hasenkam JM, Westphal D, Nygaard H, Reul H, Giersiepen M, Stodkilde-Jorgensen (1988a), In vitro stress measurements in the vicinity of six mechanical aortic valves using hot-film anemometry in steady flow. J Biomechanics 21:235-247.

Hasenkam JM, Giersiepen M, Reul H (1988b), Three-dimensional visualization of velocity fields downstream of six mechanical aortic valves in a pulsatile flow model. J Biomechanics 21:647-661.

Hasenkam JM, Nygaard H, Giersiepen M, Reul H, Stodkilde-Jorgensen H (1988c), Turbulent stress measurements downstream of six mechanical aortic valves in a pulsatile flow model. J Biomechanics 21:631-645.

Hasenkam JM, Pedersen EM, Ostergaard, JH, Nygaard H, Paulsen PK, Johannsen G, Schurizek BA (1988d), Velocity fields and turbulent stresses downstream of biological and mechanical aortic valve prostheses implanted in pigs. Cardiovascular Research 22:472-483.

Hayashi K (1987), Tensile and fatigue properties of segmented polyether polyurethanes, in "Polyurethanes in Biomedical Engineering II", eds H Planck, I Syré, M Dauner, G Egbers, Elsevier Science Publishers, Amsterdam, pp129-149.

Henderson Y, Johnson FE (1912), Two models of closure of the heart valves. Heart 4:69-82.

Hennig E, Bücherl ES (1984), Mineralization of circulatory devices made of polymers, in "Polyurethanes in Biomedical Engineering", eds H Planck, G Egbers, I Syré, Elsevier Science Publishers, Amsterdam, pp109-134.

Herold M, Lo HB, Reul H, Muckter H, Taguchi K, Giersiepen M, Birkle G, Hollweg G, Rau G, Messmer BJ (1987), The Helmholtz-Institute tri-leaflet polyurethane heart valve prosthesis: design, manufacturing, and first in vitro and in vivo results, in "Polyurethanes in Biomedical Engineering II", eds H Planck, I Syré, M Dauner, G Egbers, Elsevier Science Publishers, Amsterdam, pp231-256.

Hilbert SL, Ferrans VJ, Tomita Y, Eidbo EE, Jones M (1987), Evaluation of explanted polyurethane trileaflet cardiac valve prosthesis. J Thorac Cardiovasc Surg 419-429.

Hinze JO (1959), Turbulence. McGraw-Hill Book Company Inc, New York, pp13-20.

Hoffman D, Sisto D, Yu LS, Dahm M, Kolff WJ (1991), Evaluation of a stented polyurethane mitral valve prosthesis. Trans Am Soc Artif Intern Organs 37:M354-M355.

Huang X, Black MM, Howard IC, Patterson EA (1990), A two-dimensional finite element analysis of a bioprosthetic heart valve. J Biomechanics 23:753-762.

Hung TK (1983), Hydrodynamic analysis of the aortic valve mechanisms, in "Advances in cardiovascular physics", vol 5, part I, Karger, Basel, pp106-118.

Hwang NHC, Hussain AKMF, Hui PW, Stripling T (1977), Turbulent flow through a natural human mitral valve. J Biomechanics 10:59-67.

Idelsohn SR, Costa LE, Ponso R (1985), A comparative computational study of blood flow through prosthetic heart valves using the finite element method. J Biomechanics 18:97-115.

Imachi K, Mabuchi K, Chinzei T, Abe Y, Imanishi K, Yonezawa T, Maeda K, Suzukawa M, Kouno A, Ono T, Fujimasa I, Atsumi K (1989), In vitro and in vivo evaluation of a jellyfish valve for practical use. Trans Am Soc Artif Intern Organs 35:298-301.

Imamura E, Kaye MP (1977), Function of expanded-polytetrafluoroethylene laminated trileaflet valves in animals. Mayo Clin Proc 52:770-775.

Jansen J, Grevelink JMJ, Kim SW, Kolff WJ, Reul H (1986), New polyurethane trileaflet valves: performance and blood compatibility. Life Support Systems 4:130-132.

Jansen J, Willeke S, Reiners B, Harbott P, Reul H, Lo HB, Däbritz S, Rosenbaum C, Bitter A, Ziehe K, Rau G, Messmer BJ (1991), Advances in design principle and fluid dynamics of a flexible polymeric heart valve. Trans Am Soc Artif Intern Organs 37:M451-M453.

Jones M, McMillan ST, Eidbo EE, Woo Y-R, Yoganathan AP (1986), Evaluation of prosthetic heart valves by Doppler flow imaging. Echocardiography 3:513-525.

Kamal MR, Ryan ME (1989), Models of material behaviour, in "Fundamentals of Computer Modeling for Polymer Processing", ed CL Tucker, Hanser Publishers, New York, pp7-68.

Kawachi Y, Tokunaga K, Wantanabe Y, Nose Y, Nakamura M (1985), In vivo hemodynamics of prosthetic St Jude Medical and Ionescu-Shiley heart valves analyzed by computer. Ann Thorac Surg 39:456-461.

Kiraly R, Yozu R, Hillegass D, Harasaki H, Murabayashi S, Snow J, Nosé Y (1982), Hexsyn trileaflet valve: Application to temporary blood pumps. Artificial Organs 6:190-197.

Knierbein B, Mohr-Matuschek U, Rechlin M, Reul H, Rau G, Michaeli W (1990a), Evaluation of mechanical loading of a trileaflet polyurethane blood pump valve by finite element analysis. Int J Artif Organs 13:307-315.

Knierbein B, Reul H, Rau G (1990), Plastics technology aspects of the development and manufacture of blood pumps. Kunststoffe German Plastics 80:30-33.

Knott E, Reul H, Knoch M, Steinseifer U, Rau G (1988), In vitro comparison of aortic heart valve prostheses. Part 1: Mechanical valves. J Thorac Cardiovasc Surg 96:952-961.

Köhler J, Ehrentraut G, Störmer B (1981), Hemodynamics of four new prosthetic heart valves. Proc ESAO 8:361-368.

Kolff WJ, Yu LS (1989), The return of elastomer valves. Ann Thorac Surg 48:S98-S99.

Laniado S, Yellin E, Terdiman R, Meytes I, Stadler J (1976), Hemodynamic correlates of the normal aortic valve echogram. Circulation 54:729-737.

Lee CSF, Talbot L (1979), A fluid-mechanical study of the closure of heart valves. J Fluid Mech 91:41-63.

Lee JM, Courtman DW, Boughner DR (1984), The glutaraldehyde-stabilized porcine aortic valve xenograft I. Tensile viscoelastic properties of the fresh leaflet material. J Biomed Mat Res 18:61-77.

Leefe SE, Gentle CR (1987), Theoretical evaluation of energy loss methods in the analysis of prosthetic heart valves. J Biomed Eng 9:121-127.

Leefe SE, Tansley GD, Gentle CR (1986), Pulsatile flow testing of prosthetic heart valve conduits, in "Heart Valve Engineering", Mech Eng Publ Ltd, for IME, pp15-20.

Lewis JMO, Macleod N (1983), A blood analogue for the experimental study of flow-related thrombosis at prosthetic heart valves. Cardiovascular Research 17:466-475.

Lichtenstein O, Martínez-Val R, Méndez J, Castillo-Olivares JL (1986), Hydrogen bubble visualisation of the flow past aortic prosthetic valves. Life Support Systems 4:141-149.

MacDonald I, Fisher J, Evans AL, Wheatley DJ (1986), A microcomputer based data acquisition system for a prosthetic heart valve test apparatus. J Med Eng Technol 10:321-324.

McDonald DA (1974), Blood flow in arteries, 2nd edition. Edward Arnold, London.

McQueen DM, Peskin CS, Yellin EL (1982), Fluid dynamics of the mitral valve: physiological aspects of a mathematical model. Am J Physiol 242 (Heart Circ Physiol 11):H1095-H1110.

McMillin CR (1989), Current topics in biomedical rubbers and elastomers. IEEE Engineering in Medicine and Biology Magazine, June:30-36.

Malcolm JE, Taylor DEM (1989), Secondary intraventricular flow patterns and fluid mechanics of the mitral valve, in "Blood Flow in Artificial Organs and Cardiovascular Prostheses", eds JC Barbenel, AC Fisher, JDS Gaylor, WJ Angerson, CD Sheldon, Clarendon Press, Oxford, pp82-88.

Martin TRP, Black MM (1976), Problems of in-vitro testing of heart valve replacements. Proc ESAO 3:131-138.

Martin TRP, Tindale WB, Van Noort R, Black MM (1981), In vitro heart valve evaluation: fact or fantasy ? Trans Am Soc Artif Organs XXVII:475-479.

Martin TRP, van Noort R, Black MM, Morgon J (1980), Accelerated fatigue testing of biological tissue heart valves. Proc ESAO 7:315-319.

Mavrilas D, Missirlis Y (1991), An approach to the optimization of preparation of bioprosthetic heart valves. J Biomechanics 24:331-339.

Mayne ASD, Christie GW, Smaill BH, Hunter PJ, Barratt-Boyes BG (1989), An assessment of the mechanical properties of leaflets from four second-generation porcine bioprostheses with biaxial testing techniques. J Thorac Cardiovasc Surg 98:170-180.

Mercer JL, Benedicty M, Bahnson HT (1973), The geometry and construction of the aortic leaflet. J Thorac Cardiovasc Surg 65:511-518.

Middleman S (1977), Fundamentals of polymer processing. McGraw-Hill Book Company, New York.

Missirlis YF, Armeniades CD (1976), Stress analysis of the aortic valve during diastole: important parameters. J Biomechanics 9:477-480.

Missirlis YF, Chong M (1978), Aortic valve mechanics-part 1: Material properties of natural porcine aortic valves. J Bioengineering 2:287-300.

Mohnhaupt A, Affeld K, Mohnhaupt R, Bücherl ES (1975), A comparative performance analysis of heart valve prostheses. Proc ESAO 2:39-45.

Mohri H, Hessel EA, Nelson RJ, Anderson HN, Dillard DH, Merendino KA (1973), Design and durability test of Silastic trileaflet aortic valve prostheses. J Thorac Cardiovasc Surg 65:576-582.

Murgo JP, Giolma JP, Altobelli SA (1977), Physiologic signal acquisition and processing for human hemodynamic research in a clinical cardiac-catheterization laboratory. Proc IEEE 65:696-702.

Nardi G, Cicconardi S, Pietrabissa R, Lazzoni M, Migliaresi C, Giusti P (1982), Development and testing of a new prosthetic heart valve, in "Polymers in medicine. Biomedical and pharmacological applications", eds E Chiellini, P Giusti, pp349-357.

Nerem RM, Rumberger JA, Gross DR, Hamlin RL, Geiger GL (1974), Hot-film anemometer velocity measurements of arterial blood flow in horses. Circ Res 34:193-203.

Nerem RM, Seed WA (1972), An in vivo study of aortic flow disturbances. Cardiovascular Research 6:1-14.

Nichols WW, Conti RC, Walker WE, Milnor WR (1977), Input impedance of the systemic circulation in man. Circ Res 40:451-458.

Nistal F, García-Martínez V, Arbe E, Fernàndez D, Artiñano E, Mazorra F, Gallo I (1990), In vivo experimental assessment of polytetrafluoroethylene trileaflet heart valve prosthesis. J Thorac Cardiovasc Surg 99:1074-1081.

Nugent A, Scotten LN, Walker DK, Brownlee RT (1984), Accelerated fatigue testing of heart valves: a preliminary database. Proc ACEMB 37:149.

Nygaard H, Giersiepen M, Hasenkam JM, Westphal D, Paulsen PK, Reul H (1990), Estimation of turbulent shear stresses in pulsatile flow immediately downstream of two artificial aortic valves in vitro. J Biomechanics 23:1231-1238.

Olin C (1971), Pulsatile flow studies of prosthetic aortic valves. Scand J Thorac Cardiovasc Surg 5:1-12.

Patel DJ, Mason DT, Ross J, Braunwald E (1965), Harmonic

analysis of pressure pulses obtained from the heart and great vessels of man. Am Heart J 69:785-794.

Paulsen PK, Hasenkam JM (1983), Three-dimensional visualization of velocity profiles in the ascending aorta in dogs, measured with a hot-film anemometer. J Biomechanics 16:201-210.

Paulsen PK, Hasenkam JM, Stodkilde-Jorgensen H, Albrechtsen O (1988a), Three-dimensional visualization of velocity profiles in the ascending aorta in humans. Int J Artif Org 11:277-292.

Paulsen PK, Nygaard H, Hasenkam JM, Gormsen J, Stodkilde-Jorgensen H, Albrechtsen O (1988b), Analysis of velocity in the ascending aorta in humans. Int J Artif Org 11:293-302.

Pasipoularides A, Murgo JP, Bird JJ, Craig WE (1984), Fluid dynamics of aortic stenosis: mechanisms for the presence of subvalvular pressure gradients. Am J Physiol 246 (Heart Circ Physiol 15):H542-H550.

Peskin CS (1982), The fluid dynamics of heart valves: Experimental, theoretical, and computational methods. Ann Rev Fluid Mech 14:235-259.

Phillips WM, Snyder A, Alchas P, Rosenberg G, Pierce WS (1980), Pulsatile prosthetic valve flows. Trans Am Soc Artif Intern Organs 26:43-49.

Rainer WG, Christopher RA, Sadler TR, Hilgenberg AD (1978), Dynamic behaviour of prosthetic aortic tissue valves as viewed by high-speed cinematography. Ann Thorac Surg 28:274-280.

Reul H (1983), In-vitro evaluation of artificial heart valves, in "Advances in Cardiovascular Physics", vol 5, part IV, Karger, Basel, pp16-30.

Reul H, Giersiepen M, Knott E (1986), Laboratory testing of prosthetic heart valves, in "Heart Valve Engineering", Mech Eng Publ Ltd, for IME, pp3-13.

Reul H, Giersiepen M, Schindehütte H, Effert S, Rau G (1985), Comparative in vitro evaluation of porcine and pericardial bioprostheses. Z Kardiol 74(Supp 7):1-10.

Reul H, Schoenmackers J, Starke W (1972), Loss of pressure, energy and performance at simulated stenoses in pulsatile quasiphysiological flow. Med & Biol Eng 10:711-718.

Reul H, Talukder N, Müller EW (1981), Fluid mechanics of the natural mitral valve. J Biomechanics 14:361-372.

Rivas MA, Shapiro AH (1956), On the theory of discharge coefficients for rounded-entrance flowmeters and venturis. Trans ASME 78:489-497.

Robel SB (1972), Structural mechanics of aortic valve, in "Prosthetic Replacement of the Aortic Valve", eds LR Sauvage, RF Viggers, K Berger, SB Robel, PN Sawyer, & SJ Wood, Charles C Thomas, Illinois, pp3-37.

Roe BB (1989), A compression-molded leaflet prosthetic valve. Ann Thorac Surg 48:S26-S27.

Roe BB (1991), "Extinct" cardiac valve prostheses, in "Replacement Cardiac Valves", eds E Bodnar & RWM Frater, Pergamon Press Inc, New York, pp307-332.

Roschke EJ (1973), An engineer's view of prosthetic heart valve performance. Biomat Med Dev Art Org 1:249-290.

Rossow MP, Gould PL, Clark RE (1978), A simple method for estimating stresses in natural and prosthetic heart valves. Biomat Med Dev Art Org 6:277-290.

Rousseau EPM, van Steenhoven AA, Janssen (1988), A mechanical analysis of the closed Hancock heart valve prosthesis. J Biomechanics 21:545-562.

Russell FB, Lederman DM, Singh PI, Cumming RD, Morgan RA, Levine FH, Austen WG, Buckley MJ (1980), Development of seamless tri-leaflet valves. Trans Am Soc Artif Intern Organs 26:66-71.

Sabbah HN, Hamid MS, Stein PD (1985), Estimation of mechanical stresses on closed cusps of porcine bioprosthetic valves: effects of stiffening, focal calcium and focal thinning. Am J Cardiol 55:1091-1096.

Sabbah HN, Hamid MS, Stein PD (1986), Mechanical stresses on closed cusps of porcine bioprosthetic valves: Correlation with sites of calcification. Ann Thorac Surg 42:93-96.

Sabbah HN, Stein PD (1979), Contribution of semilunar leaflets to turbulent blood flow. Biorheology 16:101-108.

Sauren AAHJ, Kuijpers W, van Steenhoven AA, Veldpaus FE (1980), Aortic valve histology and its relation with mechanics- Preliminary report. J Biomechanics 13:97-104.

Sauren AAHJ, van Hout MC, van Steenhoven AA, Veldpaus FE, Janssen JD (1983), The mechanical properties of porcine aortic valve tissues. J Biomechanics 16:327-337.

Schoen FJ, Levy RJ (1991), Calcification of bioprosthetic heart valves, in "Replacement Cardiac Valves", eds E

Bodnar & RWM Frater, Pergamon Press Inc, New York, pp125-148.

Schoephoerster RT, Chandran KB (1989), Effect of systolic flow rate on the prediction of effective prosthetic valve orifice area. J Biomechanics 22:705-715.

Schoephoerster RT, Chandran KB (1990), Numerical simulation of blood flow past mitral valve prostheses in a simplified two-dimensional left ventricle, in "1990 Advances in Bioengineering", ed SA Goldstein, ASME, New York, pp131-134.

Schoephoerster RT, Chandran KB (1991), Velocity and turbulence measurements past mitral valve prostheses in a model left ventricle. J Biomechanics 24:549-562.

Schramm D, Müller-Mohnssen H, Baldauf W, Meisner H (1982), Fresh human aortic and artificial heart valves studied in vitro using ultramicroscope anemometry. Further results. Thorac Cardiovasc Surgeon 30:273-280.

Scotten LN, Racca RG, Nugent AH, Walker DK, Brownlee RT (1981), New tilting disc cardiac valve prostheses. In vitro comparison of their hydrodynamic performance in the mitral position. J Thorac Cardiovasc Surg 82:136-146.

Scotten LN, Walker DK, Brownlee RT (1979), Construction and evaluation of a hydromechanical simulation facility for the assessment of mitral valve prostheses. J Med Eng Technol 3:11-18.

Scotten LN, Walker DK, Smith DW, Brownlee RT (1983), A versatile pump for simulating physiological fluid flows. AAMI Proc 18:108.

Seed WA, Wood NB (1971), Velocity patterns in the aorta. Cardiovascular Research 5:319-330.

Stein PD, Munter WA (1971), New functional concept of valvular mechanics in normal and diseased aortic valves. Circulation 44:101-108.

Stein PD, Sabbah HN (1976), Turbulent blood flow in the ascending aorta of humans with normal and diseased aortic valves. Circ Res 39:58-65.

Stein PD, Sabbah HN (1990), Turbulent blood flow and its relation to cardiovascular pathophysiology, in "McDonald's Blood Flow in Arteries", 3rd edition, eds WW Nichols, MF O'Rourke, Edward Arnold, London, pp54-76.

Stein PD, Sabbah HN, Anbe DT (1979), Comparison of disturbances of flow in the main pulmonary artery and ascending aorta of man. Biorheology 16:357-362.

Stevenson DM, Yoganathan AP, Williams FP (1985), Numerical simulation of steady turbulent flow through trileaflet aortic heart valves-II. Results on five models. J Biomechanics 18:909-926.

Swanson WM (1984a), Comparison of in vitro valve pressure drop results from different investigators. Medical Instrumentation 18:115-117.

Swanson WM (1984b), Relative performance of prosthetic heart valves based on power measurements. Medical Instrumentation 18:318-325.

Swanson WM, Clark RE (1973), Aortic valve leaflet motion during systole. Circ Res 32:42-48.

Swanson WM, Clark RE (1974), Dimensions and geometric relationships of the human aortic valve as a function of pressure. Circ Res 35:871-882.

Swanson WM, Clark RE (1977a), A simple cardiovascular system simulator: design and performance. J Bioeng 1:135-145.

Swanson WM, Clark RE (1977b), Cardiovascular system simulation requirements. J Bioeng 1:121-133.

Tadmor Z, Gogos CG (1979), Principles of polymer processing. Wiley-Interscience, New York.

Talukder N, Reul H, Müller EW (1977), Fluid mechanics of the natural aortic valve. Inserm-Euromech 92, Cardiovascular and pulmonary dynamics 71:335-350.

Taylor DEM, Wade JD (1973), Pattern of blood flow within the heart: a stable system. Cardiovascular Research 7:14-21.

Thomson FJ, Barratt-Boyes BG (1977), The glutaraldehyde-treated heterograft valve. Some engineering observations. J Thorac Cardiovasc Surg 74:317-321.

Thubrikar MJ, Aouad J, Nolan SP (1986), Patterns of calcific deposits in operatively excised stenotic or purely regurgitant aortic valves and their relation to mechanical stress. Am J Cardiol 58:304-308.

Thubrikar M, Bosher PL, Nolan SP (1979), The mechanism of opening of the aortic valve. J Thorac Cardiovasc Surg 77:863-870.

Thubrikar M, Harry R, Nolan SP (1977), Normal aortic valve function in dogs. Am J Cardiol 40:563-568.

Thubrikar MJ, Nolan SP (1990), Principles for the design

of a tri-leaflet valve, in "Surgery for Heart Valve Disease", ed E Bodnar, ICR Publishers, London, pp280-287.

Thubrikar M, Piepgrass WC, Deck JD, Nolan SP (1980), Stresses of natural versus prosthetic aortic valve leaflets in vivo. Ann Thorac Surg 30:230-239.

Thubrikar M, Piepgrass WC, Shaner TW, Nolan SP (1981), The design of the normal aortic valve. Am J Physiol 241 (Heart circ physiol 10):H795-H801.

Tillmann W, Reul H, Herold M, Bruss K-H, van Glise J (1984), In-vitro wall shear measurements at aortic valve prostheses. J Biomechanics 17:263-279.

Tindale WB, Black MM, Martin TRP (1982), In vitro evaluation of prosthetic heart valves: anomalies and limitations. Clin Phys Physiol Meas 3:115-130.

Tindale WB, Trowbridge EA (1983), Evaluation in vitro of prosthetic heart valves: pulsatile flow through a compliant aorta. Life Support Systems 1:173-185.

Tindale WB, Trowbridge EA (1986), Modification of the Gorlin equation for use with heart valve substitutes. Cardiovascular Research 20:458-465.

Trowbridge EA, Crofts CE (1987), Pericardial heterograft valves: An assessment of leaflet stresses and their implications for heart valve design. J Biomed Eng 9:345-355.

Trowbridge EA, Lawford PV, Crofts CE, Roberts KM (1988), Pericardial heterografts: Why do these valves fail ?, J Thorac Cardiovasc Surg 95:577-585.

Tsutsui T, Maeta H, Sakai A, Okamura K, Ijima H, Mitsui T, Hori M, Hojoh M (1985), A mesh reinforced polyurethane trileaflet cardiac valve prosthesis. Jpn J Artif Organs 14:1273-1276.

Ubago JL, Figueroa A, Colman T, Ochoteco A, Duran CG (1980), Hemodynamic factors that affect calculated orifice areas in the mitral Hancock xenograft valve. Circulation 61:388-394.

van Steenhoven AA, van Dongen MEH (1979), Model studies of the closing behaviour of the aortic valve. J Fluid Mech 90:21-32.

van Steenhoven AA, van Duppen ThJAG, Cauwenberg JWG, van Renterghem RJ (1982), In vitro closing behaviour of Björk-Shiley, St Jude and Hancock heart valve prostheses in relation to the in vivo recorded aortic valve closure. J Biomechanics 15:841-848.

van Steenhoven AA, Veenstra PC (1982), The effect of some hemodynamic factors on the behaviour of the aortic valve. J Biomechanics 15:941-950.

van Steenhoven AA, Verlaan CWJ, Veenstra PC, Reneman RS (1981), In vivo cinematographic analysis of behaviour of the aortic valve. Am J Physiol 240 (Heart circ physiol 9):H286-H292.

Vesely I, Boughner D (1989), Analysis of the bending behaviour of porcine xenograft leaflets and of natural aortic valve material: Bending stiffness, neutral axis and shear measurements. J Biomechanics 22:655-671.

Vesely I, Boughner D, Song T (1988), Tissue buckling as a mechanism of bioprosthetic valve failure. Ann Thorac Surg 46:302-308.

Vesely I, Noseworthy R (1992), Micromechanics of the fibrosa and the ventricularis in aortic valve leaflets. J Biomechanics 25:101-113.

Viggers RF (1972), Hydraulics of the aortic valve, in "Prosthetic replacement of the aortic valve", eds LR Sauvage, RF Viggers, K Berger, SB Robel, PN Sawyer, SJ Wood, Charles C Thomas, Illinois, pp38-80.

Viggers RF, Robel SB, Sauvage LR (1967), A hydraulic figure-of-merit for heart valve prostheses. J Biomed Mater Res 1:103-112.

Walburn FJ, Sabbah HN, Stein PD (1985), Turbulent stresses in the region of a Hancock porcine bioprosthetic aortic valve. J Biomech Engng 107:200-205.

Walker DK, Scotten LN, Brownlee RT (1979), In vitro comparison of observed and calculated mitral valve areas. Artificial Organs 3:365-369.

Walker DK, Scotten LN, Brownlee RT (1984), New generation heart valves. Their in vitro function in the mitral position. J Thorac Cardiovasc Surg 88:573-582.

Walker DK, Scotten LN, Modi VJ, Brownlee RT (1980), In vitro assessment of mitral valve prostheses. J Thorac Cardiovasc Surg 79:680-688.

Walker DK, Scotten LN, Racca RG, Brownlee RT (1983), Acquisition and analysis of data obtained from the in vitro testing of replacement heart valves. AAMI Proc 18:129.

Westerhof N, Elzinga G, Sipkema P (1971), An artificial arterial system for pumping hearts. J Appl Physiol 31:776-781.

Wheatley DJ (1986). Heart valves, in "Encyclopedia of Physics in Medicine and Biology", ed TF McAinsh, Pergamon Press, Oxford, pp379-384.

Wheatley DJ, Fisher J, Reece IJ, Spyt T, Breeze P (1987), Primary tissue failure in pericardial heart valves. J Thorac Cardiovasc Surg 94:367-374.

Wieting DW, Hall CW, Liotta D, De Bakey ME (1969), Dynamic flow behaviour of artificial heart valves, in "Prosthetic heart valves", ed LA Brewer, Charles C Thomas, Illinois, pp34-49.

Wijsmuller EG, Yu LS, Yuan B, Bishop ND, Kolff WJ (1990), Development of a new inflow valve for a 20cc semisoft ventricle: preliminary results. Int J Artif Organs 13:503-508.

Wisman CB, Pierce WS, Donachy JH, Pae WE, Myers JL, Prophet GA (1982), A polyurethane trileaflet cardiac valve prosthesis: in vitro and in vivo studies. Trans Am Soc Artif Intern Organs 28:164-168.

Woo Y-R, Williams FP, Yoganathan AP (1983), Steady and pulsatile flow studies on a trileaflet heart valve prosthesis. Scand J Thorac Cardiovasc Surg 17:227-236.

Woo Y-R, Yoganathan AP (1986), In vitro pulsatile flow velocity and shear stress measurements in the vicinity of mechanical mitral valve prostheses. J Biomechanics 19:39-51.

Wouters LHG, Rousseau EPM, van Steenhoven AA, German AL (1986), Development of artificial leaflets for heart valve prostheses, in "Polymers in Medicine and Surgery", The Plastics and Rubber Institute, Holland, pp22/1-22/9.

Wright JTM (1979), Hydrodynamic evaluation of tissue valves, in "Tissue Heart Valves", ed MI Ionescu, Butterworths, London, pp29-87.

Wright JTM, Temple LJ (1977), A flow visualization study of prosthetic aortic and mitral heart valves in a model of the aorta and left heart. Engineering in Medicine 6:31-45.

Yearwood TL, Chandran KB (1984), Physiological pulsatile flow experiments in a model of the human aortic arch. J Biomechanics 15:683-704.

Yellin EL (1983), Mitral valve motion, intracardiac dynamics and flow pattern modelling: Physiology and pathophysiology, in "Advances in Cardiovascular Physics", vol 5, part I, Karger, Basel, pp137-161.

Yellin EL (1966), Laminar-turbulent transition process in pulsatile flow. Circ Res 19:791-804.

Yellin EL, Peskin CS (1975), Large amplitude pulsatile water flow across an orifice. Dynamic Systems, Measurement and Control. Trans ASME 97:92-95.

Yoganathan AP, Corcoran WH, Harrison EC (1979), Pressure drops across prosthetic aortic heart valves under steady and pulsatile flow - in vitro measurements. J Biomechanics 12:153-164.

Yoganathan AP, Corcoran WH, Harrison EC, Carl JR (1978), The Björk-Shiley aortic prosthesis: flow characteristics, thrombus formation and tissue overgrowth. Circulation 58:70-76.

Yoganathan AP, Strand DM, Woo Y-R, Stevenson DM (1984), An on-line method for evaluation of the pressure drop and regurgitative characteristics of prosthetic heart valves. Medical Instrumentation 18:109-113.

Yoganathan AP, Woo Y-R, Sung H-W, Williams FP, Franch RH, Jones M (1986), In vitro hemodynamic characteristics of tissue bioprostheses in the aortic position. J Thorac Cardiovasc Surg 92:198-209.

Yoganathan AP, Woo Y-R, Williams FP, Stevenson DM, Franch RH, Harrison EC (1983), In vitro fluid dynamic characteristics of Ionescu-Shiley and Carpentier-Edwards tissue bioprostheses. Artificial Organs 7:459-469.

Young DF (1979), Fluid mechanics of arterial stenoses. J Biomech Engng 101:157-175.

Yu LS, Drevjin R, Kolff WJ (1987), Experimental analysis of mechanical failure of polyurethane trileaflet valve. Proc 40th ACEMB, pp117.

Yu LS, Yuan B, Bishop D, Topaz S, van Griensven J, Hofma S, Swier P, Klinkmann J, Kolff J, Kolff WJ (1989), New polyurethane valves in new soft artificial hearts. Trans Am Soc Artif Intern Organs 35:301-304.

# Appendix 1.

## Example of a calculations file from PULSEDUP

```
**************************************************

File name  :  C:\PULSEDUP\D_TO_A\GP02C.DOC
Acquired   :  28/8/1992
Glasgow_pericardial_27mm_mitral_test_conditions_C
**************************************************

Mean Period = 750.0 milliseconds
Standard Deviation =   0.0 milliseconds

i.e.  80.0  cycles per minute
      Data acquired over 26  cycles

Mean standard deviations on each channel  :
 ( Note:  resolution of ADC = 10 / 4096 = 0.0024 volts  )

   Channel 1 : Aortic Pressure          0.0694  volts
   Channel 2 : Atrial Pressure          0.0495  volts
   Channel 3 : Ventricular Pressure     0.0324  volts
   Channel 4 : Differential Pressure    0.1256  volts
   Channel 5 : Flow                     0.0569  volts
   Channel 6 : Pump Displacement        0.0035  volts
   Channel 7 : Pump Velocity            0.0070  volts

Times for events over 1 cycle  :

   1. Start of forward flow =  0 ms
   2. Start of forward pressure =  10 ms
   3. End of forward pressure =  400 ms
   4. End of forward flow =  450 ms
   5. Start of leakage flow =  530 ms
      Pump displacement zero ( +ve to -ve ) = -590 ms


 Flow
 ----
                    Forward          Regurgitant          Leakage
                     Flow               Flow               Flow

 Duration (ms)       450                80                 220

 Volume (ml)          78.47             -3.58              -1.02
```

## Effective Orifice Areas

Calculated from :

EOA = RMS flow / ( sqrt ( mean pressure ) * 51.6 )

| | Mean pressure (mm Hg) | Mean flow (ml/s) | RMS flow (ml/s) | EOA (cm2) |
|---|---|---|---|---|
| F-F | 5.33 | 174.40 | 186.91 | 1.57 |
| P-P | 7.44 | 189.49 | 197.59 | 1.40 |
| P-F | 6.23 | 178.21 | 189.02 | 1.47 |
| F-P | 6.39 | 184.92 | 195.11 | 1.50 |

Peak Forward Pressure = 13.23 mm Hg
Peak Forward Flow = 262.72 ml per second
EOA at maxima = 1.40 cm squared

## Energies over 1 cycle

Calculated by integrating:

( pressure difference * flow ) w.r.t. time

| Interval | Duration ( ms ) | Flow ( ml ) | Energy ( mJ ) |
|---|---|---|---|
| 1. -> 2. | 10 | 0.06 | -0.10 |
| 2. -> 3. | 390 | 74.63 | 75.80 |
| 3. -> 4. | 50 | 4.51 | 0.44 |
| 4. -> 5. | 80 | -3.58 | -94.72 |
| 5. -> 1. | 220 | -1.02 | -16.17 |

## Appendix 2.

Computer program (Turbo Pascal 5.0) to calculate coordinate points on valve leaflet surface, for input into CAD/CAM system.

```
PROGRAM Ell_Rev;

{
To find surface of intersection between:
     a) cylinder: radius 14
                  centered on (0,0,0)
                  along z axis
     b) ellipsoid:
           sqr((x-14)/14) + sqr(y/14) + sqr(z/16) = 1
}


VAR theta, delta : integer;
    d2r, x, y, z, inc, theta_r, c :real;
    f : text;

BEGIN

  d2r:= pi / 180;
assign(f,'out_file.DOC');  rewrite(f);

x:= 14 * cos(d2r*60);
y:= 14 * sin(d2r*60);
z:= 1 - ((sqr(x-14)+sqr(y))/sqr(14));
if (z <> 0) then z:= -1 * 16 * sqrt(z);
writeln(f,x:1:5,' ',y:1:5,' ',z:1:5);
writeln(f,x:1:5,' ',(-1*y):1:5,' ',z:1:5);

{ Intersection of circle, ellipsoid and y=xtan60,
  in any z plane
  i.e. endpoints at top of stent post                }

theta:= 60;

while (theta > 0) do

begin
   if (theta>55) or (theta<=5) then delta:= 2
   else delta:= 10;
   theta:= theta - delta;
   theta_r:= d2r * theta;
   x:= 14 * cos(theta_r);
   y:= 14 * sin(theta_r);
   z:= 1 - ((sqr(x-14)+sqr(y))/sqr(14));
```

```
  if (z <> 0)  then z:= -1 * 16 * sqrt(z);
  writeln(f,x:1:5,' ',y:1:5,' ',z:1:5);
  writeln(f,x:1:5,' ',(-1*y):1:5,' ',z:1:5);

{ Intersection of ellipsoid, circle and y=xtan(theta),
  for fixed theta and circle in any z plane          }

  if (theta>55) then inc:= delta else inc:= 10;
  c:= 1 - sqr(y/14);
  while ((-14*sqrt(c-sqr((z+(inc/10))/16)))+14) >
        y/sqrt(3) do
  begin
     z:= z + (inc/10);
     x:= (-14 * (sqrt(1-sqr(y/14)-sqr(z/16)))) + 14;
     writeln(f,x:1:5,' ',y:1:5,' ',z:1:5);
     writeln(f,x:1:5,' ',(-1*y):1:5,' ',z:1:5);
  end;

{ For fixed theta & y, increment z upwards along
  surface of ellipsoid  until y=xtan60 is reached }

  x:= y / sqrt(3);
  z:= 1 - ((sqr(x-14)+sqr(y))/sqr(14));
  if (z<>0) then z:= -1 * 16 * sqrt(z);
  writeln(f,x:1:5,' ',y:1:5,' ',z:1:5);
  writeln(f,x:1:5,' ',(-1*y):1:5,' ',z:1:5);

{ Intersection of ellipsoid and y=xtan60 in any z
  plane, for y fixed                                 }

  end;     { while theta > 0 do }

  close(f);

END.
```

Isometric view of the points generated:

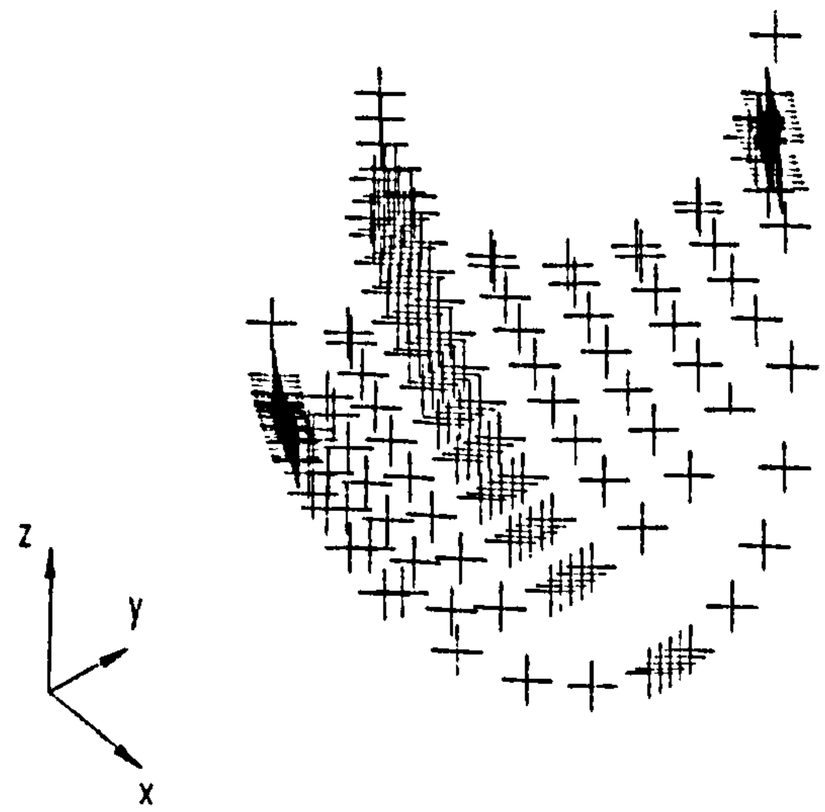

## Appendix 3.

Example of the toolpath code used by the Deckel FP 4NC milling machine.

```
&%01                                              { program number 1 }

%
(&%01/000000)                                          { file header }
N0100 F100.                          { feed rate 100 mm per minute }
N0102 S+2000                  { spindle speed 2000 rpm clockwise }
N0104 M08                                               { coolant on }
N0106 G00 X+7.800 Y-7.477     { G00: rapid traverse rate }
N0108 G00 Z+.000
N0110 G01 Z-4.800                    { G01: linear interpolation }
N0112 G01 X+7.760 Y-7.465 Z-4.774
N0114 G01 X+7.684 Y-7.440 Z-4.734
N0116 G01 X+7.728 Y-7.454 Z-4.758
N0118 G01 X+7.787 Y-7.479 Z-4.778
N0120 G01 X+7.700 Y-7.442 Z-4.747
N0122 G01 X+7.732 Y-7.455 Z-4.760
N0124 G01 X+7.773 Y-7.476 Z-4.767
N0126 G01 X+7.661 Y-7.422 Z-4.745
N0128 G01 X+7.784 Y-7.482 Z-4.769
N0130 G01 X+7.931 Y-7.570 Z-4.784
N0132 G01 X+7.799 Y-7.490 Z-4.771
 .
 .
 .
 .
 .
 .
 .
 .
 .
 .
 .
 .
 .
 .
 .
 .
 .
 .
 .
 .
 .
 .
 .
 .
```

```
.
.
.
N2142 G01 X+7.723 Y+7.457 Z-4.745
N2144 G01 X+7.533 Y+7.344 Z-4.765
N2146 G01 X+9.443 Y+9.819 Z-4.967
N2148 G01 X+9.380 Y+11.727 Z-5.500
N2150 G01 X+9.263 Y+12.036 Z-5.611
N2152 G01 X+9.109 Y+12.341 Z-5.719
N2154 G01 X+8.922 Y+12.630 Z-5.818
N2156 G01 X+8.714 Y+12.890 Z-5.904
N2158 G01 X+8.602 Y+13.010 Z-5.937
N2160 G00 Z+.000
N2161 M0                                    { program stop }

N2162 G55 W120.0 I0.0 J0.0
                          { rotate 120 degrees about z axis }
N2163 L2 N0106 N2162
            { repeat from line N0106 to line N2162 twice }

N2164 G53          { return to original coordinate system }
N2165 M09                                     { coolant off }
N2166 G00
N2167 M30                                   { end of program }

?
0000
```

## Appendix 4.

Computer program (Turbo Pascal 5.0) to generate toolpath for female leaflet surface on IBM valve design, using 10mm ball-nosed cutter.

```
PROGRAM FS_2NC;

{
Hyperbola:  sqr( (x - H_offset)/a ) - sqr( y/b ) = 1

Ellipse:

   sqr( (x - E_offset)/Maj_Ax ) + sqr( z/Min_Ax ) = 1

Hyperbola asyptotes remain constant: b / a = tan 60
}


CONST   H_offset = -5.370;
        E_offset = 22.332;
        Maj_Ax = 26.882;
        Min_Ax = 20.424;
        radius = 15.7;
        z_off = 19.62;

        { z: tool offset = 5 , machine offset = 14.62 }

VAR     f : text;
        d2r,x,y,z,a,b,grad,Aq,Bq,Cq,Root_q,check : real;
        count_y,count_z,line : integer;


BEGIN

   d2r:= pi / 180;
   grad:= sqrt(3);                                  { tan 60 }
   assign(f,'FS_2NC.DOC');    rewrite(f);
   line:= 1000;

   writeln(f,'(&%00/000000)');                  { file header }
   writeln(f,'N10 G54');                      { initialisation }
   writeln(f,'N100 G0 X0 Y0 H1');
   writeln(f,'N102 S1000');    { spindle speed 1000 rpm }
   writeln(f,'N104 M03');                        { coolant on }
   writeln(f,'N106 G01 Z0.000 F100');   { feed rate 100
                                          mm per minute }

for count_z:= 1 to 10 do
begin
   z:=  3 + ( count_z / 4 );
```

```
                    { z increment 0.25  :  -3.25  -> -5.5 }

a:= E_offset - H_offset -
     ( Maj_Ax * sqrt( 1 - sqr(z/Min_Ax) ));
b:= a * grad;
Aq:= sqr(b) + sqr(a);
Bq:= -2 * sqr(b) * H_offset;
Cq:= sqr( b * H_offset ) - sqr( a * b ) -
     sqr( radius * a );
Root_q:= sqrt( sqr(Bq) - ( 4 * Aq * Cq ) );
x:= ( (-1 * Bq) + Root_q ) / ( 2 * Aq );
check:= sqr(radius) - sqr(x);
if (check >= 0) then
begin
   y:= -1 * sqrt(check);
   if ( count_z mod 2 ) = 1 then y:= -1 * y;
   line:= line + 2;
   writeln(f,'N',line,' ','X',x:1:3,' ','Y',
           y:1:3,' ','Z',(z-z_off):1:3);
end;

for count_y:= -54 to -15 do
begin
   y:= count_y / 3;

                    { y increment 0.33 :  -18 -> -5 }

   x:= H_offset + ( a * sqrt( 1 + sqr(y/b) ));
   if (( sqr(x) + sqr(y) ) < sqr( radius - 0.3) )
   then
   begin
      line:= line + 2;
      if ( count_z mod 2 ) = 1 then y:= -1 * y;
      writeln(f,'N',line,' ','X',x:1:3,
              ' ','Y',y:1:3);
   end;
end;

for count_y:= -24 to 24 do
begin
   y:= count_y / 5;

                    { y increment 0.2  : -4.8 -> 4.8 }

   x:= H_offset + ( a * sqrt( 1 + sqr(y/b) ));
   if (( sqr(x) + sqr(y) ) < sqr( radius - 0.3) )
   then
   begin
      line:= line + 2;
      if ( count_z mod 2 ) = 1 then y:= -1 * y;
      writeln(f,'N',line,' ','X',x:1:3,
              ' ','Y',y:1:3);
   end;
end;
```

```
for count_y:= 15 to 54 do
begin
   y:= count_y / 3;

                              { y increment 0.33 : 5 -> 18 }

   x:= H_offset + ( a * sqrt( 1 + sqr(y/b) ));
   if (( sqr(x) + sqr(y) ) < sqr( radius - 0.3) )
   then
   begin
      line:= line + 2;
      if ( count_z mod 2 ) = 1 then y:= -1 * y;
      writeln(f,'N',line,' ','X',x:1:3,
                ' ','Y',y:1:3);
   end;
end;

Aq:= sqr(b) + sqr(a);
Bq:= -2 * sqr(b) * H_offset;
Cq:= sqr( b * H_offset ) - sqr( a * b ) -
     sqr( radius * a );
Root_q:= sqrt( sqr(Bq) - ( 4 * Aq * Cq ) );
x:= ( (-1 * Bq) + Root_q ) / ( 2 * Aq );
check:= sqr(radius) - sqr(x);
if ( check >= 0 ) then
begin
   y:= sqrt(check);
   line:= line + 2;
   if ( count_z mod 2 ) = 1 then y:= -1 * y;
   writeln(f,'N',line,' ','X',x:1:3,' ','Y',y:1:3);
   end;

end;                                  ( for count_z:= 1 to 10 }


writeln(f,'N9000 G00 Z0.000');
writeln(f,'N9002 M02');                    { end of program }


close(f);

END.
```